MATHEMATICAL ASPECTS OF SALT TRANSPORT IN POROUS MEDIA

PROEFSCHRIFT

ter verkrijging van de graad van doctor
aan de Technische Universiteit Delft,
op gezag van de Rector Magnificus Prof.dr.ir. J. Blaauwendraad,
in het openbaar te verdedigen ten overstaan van een commissie,
door het College voor Promoties aangewezen,
op maandag 9 februari 1998 te 16.00 uur

door

RUDOLF JOHANNES SCHOTTING
hbo ingenieur in de technische natuurkunde

geboren te Rotterdam

Dit proefschrift is goedgekeurd door de promotor:
Prof.dr.ir. C.J. van Duijn.

CWI

Centrum voor Wiskunde en Informatica

'Gravity cannot be held responsible for people falling in love'

Albert Einstein

Aan
mijn ouders
en natuurlijk aan
Kitty
en onze kinderen
Sanne en David.

Contents

1

Chapter 1

Introduction

Groundwater is the water that occurs below the surface of the earth, where it occupies all or part of the void spaces in a geological formation. Its availability in large quantities plays a crucial role in the development of densely populated and industrialized regions.

Worldwide there is a growing concern about the quality of groundwater, which is affected by natural factors and human activities. Examples of the latter are disposal of industrial waste to natural waters, irrigation return flows containing salt and fertilizers, and silting of man-made reservoirs.

Groundwater pollution control has been recognized as an important environmental issue. The chemical composition of groundwater, in particular near drinking water reservoirs, is continuously and intensively being monitored and in the past decades many advanced and dedicated techniques have been developed to avoid or reduce contamination of soil-groundwater systems. Needless to say that mathematical modeling and computer simulations play an essential role in the prediction of the extend of contamination events and in the design of clean-up strategies.

An increasing threat to groundwater systems is contamination by salt[1] This type of 'natural' pollution occurs, for instance, when salt seawater intrudes into coastal aquifers. These aquifers play an important role as resources for fresh (drinking) water, in particular in heavily urbanized areas, see Bear & Verruijt [13]. Under natural undisturbed conditions, a coastal aquifer is in a state of equilibrium, with a transition zone between fresh groundwater and seawater. To meet the drinking water demand, fresh water is being pumped from the aquifer. The hydraulic gradients that result from this induce a flow of saline water landward and thus movement of the transition zone until a new state of equilibrium is reached. This process is called seawater intrusion or encroachment. The earliest analysis of the nature of the processes involved were carried out independently by Ghyben [28] and Herzberg [39] around the turn of the century. They considered a homogeneous, unconfined coastal aquifer with an abrupt transition or interface separating the fresh and salt groundwater. Moreover, they assumed the following simple hydrostatic conditions in both fluids: at each point of the interface, the weight of a column fresh water (density ρ_f) extending from the interface to the water table is balanced by the weight of a column salt water

---

[1]Sodium and chlorine predominate in seawater; together they form more than 85 percent by weight of the total amount of dissolved salts. The total amount of the dissolved salts may vary from place to place and from time to time, due to evaporation or dilution (rain, snow, rivers, melting icebergs), but its relative chemical composition is remarkably constant, see e.g. Sverdrup et.al. [34]. The total volume of the oceans and seas, covering 71 percent of the Earth's surface, is approximately $1.37 \cdot 10^9$ km^3 and the average total concentration of salt in seawater amounts to 36 kg/m^3, which corresponds to an average seawater density of 1025 kg/m^3. The total amount of salt is therefore roughly $5.0 \cdot 10^{19}$ kg. Dried and spread over the whole Earth, this would produce a layer of 45 m thickness.

(density ρ_s) extending from the interface to sea level. Hence: $\rho_s g z_s = \rho_f g(z_s + z_f)$ or:

$$z_s = \frac{\rho_f}{\rho_s - \rho_f} z,$$
(1.0.1)

which is referred to as the Ghyben-Herzberg relation. Here, z_f denotes the distance between the phreatic surface and sea level and z_s the distance between sea level and the interface. Typical density values are: $\rho_f = 1000$ kg/m^3 and $\rho_s = 1025$ kg/m^3, hence $z_s = 40 z_f$. The latter implies that if we lower the water table by $\Delta z_f = 1$ m, the fresh-salt interface will rise by $\Delta z_s = 40$ m! This example, taken from the book by Freeze & Cherry [27], clearly illustrates the sensitivity of the position of the interface to changes in the height of the water table.

A more realistic case was studied by Hubbert [45], who considered a similar problem, but now with steady-state outflow of fresh water into the sea. He was able to determine the position of the interface for any given water table configuration by a graphical flow-net analysis. Henry [38] was the first author to present a mathematical solution for a steady-state case that includes dispersion. In fact, this solution is one of the very few explicit solutions known for dispersive salt water intrusion problems. Due to the complex nature of the governing equations, many authors resort to numerical methods to solve seawater intrusion problems, see e.g. Pinder & Cooper [68], Segol & Pinder [74], Baumann & Moser [4], Kashef [48], Holzbecher & Baumann [40], Bear & Dagan [10].

Summarizing we can state that the dynamics of the zone of contact between fresh water and seawater, either considered as a sharp interface or as a dispersive mixing zone, plays a key role in understanding and managing practical seawater intrusion problems.

Much higher salt concentrations are found in groundwater near of salt domes. Salt domes or evaporites are mostly formed from minerals that precipitated under hot arid conditions in seas and large saline lakes. The resulting beds of evaporite minerals can be very thick and extensive. The Permian salts of the Deaware Basin (USA), for instance, extend over 300,000 km^2, while in Texas (USA) salt deposits up to 3500 m thick are present (Roxburgh [70]). Salt domes have long been considered as prime candidates for high level (nuclear) waste (HLW) disposal (see IAEA [44]). This is due to their low water content, high thermal conductivity and ability to act in a plastic manner which makes them self-sealing should fractures ocur. Amongst other places in Western Europe salt domes are being examined for the purpose of HLW disposal near Gorleben in Germany and in the Mors area of Denmark.

Risk assessment studies for salt rock repositories usually pose two questions: does the repository scenario imply unacceptable environmental consequences, and if so, can they be eliminated or reduced to acceptable limits by changing the design of the repository in some way (Barr et. al. [5]). In his study, Roxburgh [70] concludes that transportation by groundwater potentially represents the greatest single threat to the integrity of a HLW rock repository. Hence a thorough and basic understanding of groundwater flow and salt transport processes in the vicinity of salt domes is of vital importance in risk assessment studies.

Salt can also enter a groundwater system through the process of crystal dissolution. Salt (or other contaminants) is sometimes present as a thin layer of mineral (crystalline or amorphous) phase on the soil particles of an aquifer. The formation of this layer is in general due to a precipitation reaction. When fresh water intrudes such an aquifer, salt is going to participate in a dissolution reaction. This reaction is often not in equilibrium, but is kinetically controlled, see e.g. Rubin [71] and Willis & Rubin [83].

To quantify the above discussed phenomena, we first need to describe them in terms of a mathematical model. Bear & Verruijt [13] define a (mathematical) model as *a simplified version of the real (here groundwater) system that approximately simulates the excitation-response relations of the latter.* In general, it is not possible to include all aspects of a real system into a mathematical model. A set of simplifying assumptions has to be imposed, such that the model still expresses basic and relevant features of the real system. This step in the modeling process is not always straightforward and often subject to debate.

The quality and practical relevance of modeling results are primarily determined by the degree of simplification in the model.

This thesis focusses on mathematical aspects of salt transport in porous media. Analytical, semi-analytical and numerical techniques are developed and utilized to gain better understanding of the transport processes, the governing model equations and its relevant transport parameters. Chapters 2,3 and 4 deal with the mathematical analysis of problems related to HLW disposal in salt rock formations. In Chapters 2 and 3, we investigate the effect of volume changes due to the presence of (extremely) high salt concentrations in groundwater.

The relation between high salt concentration gradients and the dispersive behavior of salt in hydrodynamically stable displacement experiments is considered in Chapter 4. A large number of laboratory experiments (Ben Salah [14], Bues et.al. [17], Bringham et. al. [15], Kempers [52], [51] (gives an overview), Slobod & Howlett [75], Hassanizadeh & Leijnse [35], Hassanizadeh et.al. [36], Moser [61]) indicate that the dispersion coefficient decreases as the difference between the salt concentrations of the resident and the displacing fluids increases. This phenomenon is not simulated by the classical dispersion theory, which utilizes Fick's law as dispersive mass flux equation. However, a nonlinear dispersion theory, as suggested by Hassanizadeh and Leijnse [35], provides satisfactory agreement between measurements (breakthrough curves) and modeling results, in both low and high concentration gradient regimes.

In Chapter 5, we present a numerical study of interface problems related to salt water intrusion. In many practical situations, the width of the transition zone between fresh and salt groundwater is small as compared to the horizontal and vertical extensions of the aquifer. This allows us to approximate the diffusive/dispersive mixing zone by a sharp interface: the fluid density is discontinuous at the interface separating the fluids. This assumption simplifies the governing equations and leads in mathematical terms to so-called free boundary problems.

Finally, in Chapter 6, we study crystal dissolution in flows through porous media. We consider a model for transport of solutes participating in a dissolution reaction, in general not in equilibrium. The dissolving solid is initially present as a thin layer covering the grains of the porous medium in part of the flow domain. In the absence of diffusion/dispersion and under the assumption of a constant flow rate, two fronts will emerge as time proceeds: the water or salinity front which travels with the (constant) fluid velocity and a dissolution front, separating the domain where the solid concentration is identical zero and the domain where the solid concentration is positive. The speed of this front is in general not constant. It is determined by the nature of the non-equilibrium dissolution reaction and its rate constants.

1.1 Basic equations

Fluid flow in the void spaces of a porous medium is described by the Navier-Stokes equations, subject to appropriate boundary and initial conditions. Solving these equations in the fluid domain is unpractical because of the enormous complexity of the flow geometry. Even if one could determine a solution for an idealized domain, still the question remains how to relate

measured field quantities (usually volume averaged) to micro-scale modeling results. To over-come these difficulties, a continuum theory for flow in porous media has been established. In this continuum or macro-scale approach, averaged micro-scale details, reappear in the form of macro-scale coefficients. The development of micro-scale averaging techniques have received a lot of attention in the porous media literature. Amongst many others we mention Whitaker [79], [80], [81], Bear & Bachmat [8], [9], Bear [6], Gray [29], Hassanizadeh & Gray [30], [31], [32], Marle [59] and Zijl [87]. In the seventies mathematicians have developed an averaging tech-nique called homogenization. This technique was developed for partial differential equations with (highly) oscillatory coefficients and has proven to be very powerful. See for instance Tartar [77] (Darcy's law), Keller [50] (Darcy's law), Hornung et. al. [41] (reactive transport of solutes), Hornung & Jäger [42] (dispersion and chemical reactions), Hornung [43] (miscible displacement in unsaturated soils), Mikelić & Aganović [60], Bhattacharaya [3] (solute dispersion) and Ene & Polisevski [26] (thermal flow).

The macro-scale equations (in terms of volume averaged and measurable quantities) for salt transport in porous media are based on two fundamental principles: mass conservation (of both fluid and salt) and momentum conservation of the fluid.

1.1.1 Conservation of mass

The fluid mass balance equation in a nondeformable porous medium reads

$$n\frac{\partial \rho}{\partial t} + \text{div}\,(\rho \mathbf{q}) = 0, \tag{1.1.2}$$

where n [-] denotes the effective porosity of the porous medium, ρ [kg/m^3] the fluid density, and $\mathbf{q}$ [m^3/(m^{2}s)] the specific discharge or Darcy velocity vector. Source and sink terms are omited in (1.1.2). The interstitial or fluid velocity vector $\mathbf{v}$ [m/s] is given by

$$\mathbf{v} = \frac{\mathbf{q}}{n} \tag{1.1.3}$$

Equation (1.1.2) is also known as the continuity equation. In case of a homogeneous and incom-pressible fluid, i.e. grad $\rho = 0$ and $\partial\rho/\partial t = 0$, equation (1.1.2) reduces to

$$\text{div}\,\mathbf{q} = 0. \tag{1.1.4}$$

The salt mass balance is given by

$$n\frac{\partial \rho\omega}{\partial t} + \text{div}\,(\rho\omega\mathbf{q} + \mathbf{J}) = 0, \tag{1.1.5}$$

where $\mathbf{J}$ denotes the dispersive mass flux vector and ω the salt mass fraction. If salt partic-ipates in a dissolution/precipitation reaction, additional terms in (1.1.5) are required, as well as additional (rate) equations. This will be discussed separately in Section 1.5. The salt mass fraction ω [kg/kg] is defined as the salt mass concentration c [kg/m^3] divided by the fluid density ρ [kg/m^3]. In analogy to diffusive mass transport, the dispersive mass flux $\mathbf{J}$ is often assumed to have the form of Fick's law,

$$\mathbf{J} = -\rho D \text{grad}\omega, \tag{1.1.6}$$

which indicates a linear proportionality between dispersive mass flux and the salt mass fraction gradient. In (1.1.6), D denotes a velocity dependent second rank symmetric tensor, generally

referred to as dispersion matrix. In fact, the analogy between Fick's law and the dispersive mass flux equation is a working hypothesis, motivated by experimental and theoretical dispersion research which started some decades ago. For an overview we refer to Bear [6]. We note that expression (1.1.6) can only be justified for relatively low salt concentrations. An alternative expression for brine transport will be presented in Section 1.3 (and in Chapter 4).

Several physical phenomena can affect the fluid volume, and thereby its density. These are: thermal expansion, pressure compressibility and volume changes due to high salt content. This implies that the fluid density is a function of (absolute) temperature T, fluid pressure p and salt mass fraction ω (or salt concentration c). The empirical relation between these variables is given by the equation of state

$$\rho = \rho(T, p, \omega) = \rho_0 e^{\beta_T(T-T_0) + \beta_p(p-p_0) + \gamma\omega}, \qquad (1.1.7)$$

where $\rho_0 = \rho(T_0, p_0, 0)$ (a reference density), and where β_T and β_p respectively denote the thermal expansion and the compressibility coefficient. For salt (NaCl) dissolved in fresh water, the coefficient γ is approximately $\gamma = \ln(2)$. Under isothermal conditions, and disregarding fluid volume changes due to small pressure variations, the equation of state reduces to

$$\rho(\omega) = \rho_f e^{\gamma\omega}, \qquad (1.1.8)$$

where ρ_f denotes the density of fresh water.

1.1.2 Conservation of momentum

The fluid momentum balance equation in a nondeformable medium and in the absence of inertial effects, is given by

$$\mathbf{q} = -\frac{\kappa}{\mu}(\text{grad } p + \rho g \mathbf{e}_z), \qquad (1.1.9)$$

where p [N/m^2] denotes fluid pressure, κ [m^2] the intrinsic permeability tensor, μ [kg/(sm)] the dynamic viscosity, g [m/s^2] the acceleration of gravity, and $\mathbf{e}_z$ the unit vector in the vertical positive z-direction. Equation (1.1.9) expresses a balance between the driving forces due to gravity and fluid pressure gradients, i.e. $-(\text{grad } p + \rho \mathbf{g})$, and the flow resistance force at the fluid-solid interfaces (drag forces), expressed by $(\mu/\kappa)\mathbf{q}$. The latter is only correct for flows at low Reynolds-numbers (laminar flow). The range of validity of equation (1.1.9) is approximately Re$<$ 10, which is satisfied in most practical groundwater problems. The momentum balance equation (1.1.9) is generally referred to as Darcy's law.

A flow field satisfying curl $\mathbf{q} = 0$ is called irrotational. The driving force per unit volume $(\text{grad } p + \rho g \mathbf{e}_z)$ is irrotational if the fluid density is a function of the vertical coordinate z only. Then the pressure gradient is the only driving force causing fluid flow. If the fluid density depends on the horizontal coordinates (x, y) as well, Darcy's law (1.1.9) gives (taking the curl)

$$\text{curl}\left(\frac{\mu}{\kappa}\mathbf{q}\right) = -g\,\mathbf{e}_z \times \text{grad } \rho \neq 0. \qquad (1.1.10)$$

Since the vector product $\mathbf{e}_z \times \text{grad } \rho$ evaluates to $(-\partial\rho/\partial y, +\partial\rho/\partial x)$, equation (1.1.10) indicates that horizontal density gradients induce rotational fluid flow.

Remark:
The Helmholz-Hodge decomposition theorem states that any sufficiently vector fie ld $\mathbf{w}$ on a bounded domain Ω can be uniquely decomposed into the form

$$\mathbf{w} = \mathbf{q} + \text{grad } p, \qquad (1.1.11)$$

where $\mathbf{q}$ has zero divergence (a so called solenoidal vector field) and is parallel to $\partial\Omega$, i.e. div $\mathbf{q} = 0$ and $\mathbf{q \cdot n}$ on $\partial\Omega$. The gradient field grad$p$ is irrotational since curl(grad p) $= 0$. Solenoidal and irrotational fields are orthogonal because

$$\int_\Omega \mathbf{q} \cdot \operatorname{grad} p \, dV = 0. \qquad (1.1.12)$$

1.2 Brine transport: volume effects

The subject of brine transport in porous media is typically related to risk assessment studies for HLW storage in subsurface salt domes and received a lot of attention in the hydrological literature in the last (two) decades. Many (dedicated) numerical codes have been developed to simulate fluid flow, transport of salt (brine) and (simultaneous) transport of dissolved chemicals and/or radionuclides, see e.g. Kröhn & Zielke [55], Voss & Souza [85], Oldenburg & Pruess [64] and Kolditz et. al. [54].

The equations describing brine transport are the continuity equation for the fluid (1.1.2), the mass balance equation for salt (1.1.5) combined with an equation for the dispersive mass flux (e.g. Fick's law (1.1.6)), Darcy's law (1.1.9) and the particular form of the equation of state (1.1.8). If we introduce the material derivative

$$\frac{D}{Dt} = \frac{\partial}{\partial t} + \frac{\mathbf{q}}{n} \cdot \operatorname{grad} \qquad (1.2.13)$$

in the continuity equation (1.1.2) we obtain

$$\frac{n}{\rho}\frac{D\rho}{Dt} + \operatorname{div} \mathbf{q} = 0. \qquad (1.2.14)$$

This expression shows that density variations may affect the divergence or local volume of the fluid, which in turn can cause additional (enhanced) movement of the fluid. Our main goal is to investigate this effect and we shall use analytical techniques to make it explicit. Although no pressure dependence in (1.1.8) is assumed, we shall use the term 'compressibility effect' in relation to fluid volume changes caused by concentration gradients. This is inspired by the fact that all phenomena affecting the local volume result in a flow field which is not divergence free.

The complex nature of the brine equations, i.e. nonlinear coupling between the density distribution and velocity field due to both gravity (free convection or rotational flow due to horizontal density gradients) and local fluid volume changes (caused by high density gradients), implies that the availability of exact or semi-exact solutions for numerical code verification is rather poor. A series of benchmark problems has been defined by the international HYDRO-COIN [49] project. These benchmarks are utilized for cross-verification of numerical codes, see e.g Kolditz et. al. [54]. Both phenomena causing enhanced fluid flow are considered in the proposed benchmark problems. Therefore, it is hard to distinguish between these phenomena, both qualitative and quantitative.

To study the effect of compressibility induced flow, we define three model problems that typically relate to transport of brines in the vicinity of a salt dome: (i) The salt dome problem: flow of fresh water along the surface of a salt dome, (ii) The mixing problem: mixing of parallel fluid layers in a porous medium (fresh water and brine) and (iii) The column problem: brine displacing fresh water in an infinitely long porous column. Both the salt dome problem and the mixing problem are studied in Chapters 2 and 3 of this thesis. The column problem is studied in Chapter 3.

As will be shown in Chapters 2 and 3, each of the above problems can be described in terms of a coupled set of (scaled) partial differential equations in one space dimension. The resulting equations are

$$\frac{\partial \rho}{\partial t} + \frac{\partial}{\partial z}(\rho q) + \frac{1}{\varepsilon}\frac{\partial q}{\partial z} = 0, \qquad (1.2.15)$$

and

$$\frac{\partial \rho}{\partial t} + q\frac{\partial \rho}{\partial z} - \frac{\partial^2 \rho}{\partial z^2} = 0. \qquad (1.2.16)$$

All variables in (1.2.15), (1.2.16) are dimensionless and the z-coordinate does not necessarily coincide with the vertical axis. The scaling is different for each problem and imposed by the flow geometry and hydrology of each individual problem. The parameter ε in (1.2.15) denotes the relative density difference, which is defined as

$$\varepsilon = \frac{\rho_s - \rho_f}{\rho_f}, \qquad (1.2.17)$$

where ρ_f is the density of fresh water and ρ_s is the density of salt water.

To illustrate the contents of Chapters 2 and 3 we discuss here the salt dome problem. In that case, equations (1.2.15) and (1.2.16) have to be solved for $z > 0$, subject to the scaled boundary/initial conditions

$$\rho(z,0) = 0 \ \text{ for } \ z > 0, \qquad (1.2.18)$$

$$\rho(0,t) = 1 \ \text{ for } \ t > 0, \qquad (1.2.19)$$

and

$$q = -\varepsilon K(\varepsilon)\frac{\partial \rho}{\partial z}(0,t) \ \text{ for } \ t > 0 \qquad (1.2.20)$$

where $K(\varepsilon)$ is a constant, see Van Duijn et. al. [23]. The particular form of the specific discharge boundary at the salt rock boundary is due to Hassanizadeh & Leijnse [33].

Due to the nonlinear coupling between (1.2.15) and (1.2.16), it is not possible to find explicit, closed form solutions of these problems. Nevertheless, their special structure enables us to obtain much information concerning the qualitative behavior of the solutions and to obtain accurate approximations. The key idea in Chapter 2 is to look for self-similar solutions, which reduce (1.2.15), (1.2.16) to a set of coupled ordinary differential equations, subject to boundary conditions originating from (1.2.18), (1.2.20). In fact, this coupled set of ordinary differential equations can be combined into a single nonlinear third order equation. To tackle this directly is not straightforward. Therefore, several other transformations are proposed to reduce the problem to a well-known boundary value problem. This procedure provides detailed information about qualitative properties of solutions.

The key idea in Chapter 3 is to reduce the coupled system (1.2.15)-(1.2.16) to a single second order nonlinear diffusion equation by applying a so-called Von Mises transformation, see e.g. Von Mises & Friedrichs [63]. The resulting diffusion problems that arise from this transformation are well known and received a lot of attention in the mathematical oriented literature. The special choice of the boundary and initial conditions in the example problems (see above) implies that the corresponding nonlinear diffusion problems are solvable in terms of, again, a similarity solution. With the Von Mises transformation as intermediate step, these similarity solutions are natural to the problem and straight forward to find. Moreover, we know that they represent the large time behavior of the corresponding flow problem with more general (i.e. non-constant) boundary/initial data: see e.g. Van Duijn & Peletier [67]) or the book by Barenblatt ([1]).

1.2.1   Similarity solutions

The dimensionless system (1.2.15)-(1.2.16) allows a similarity solution of the form

$$\eta = \frac{z}{\sqrt{t}},\tag{1.2.21}$$

and

$$\rho(z,t) = f(\eta) \ \text{ and } \ q(z,t) = \frac{1}{\sqrt{t}}g(\eta),\tag{1.2.22}$$

where f and g satisfy the coupled set of ordinary differential equations

$$(fg)' + \frac{1}{\varepsilon}g' - \frac{1}{2}\eta f' = 0,\tag{1.2.23}$$

$$f'(g - \frac{1}{2}\eta) = f''\tag{1.2.24}$$

for $\eta > 0$. Here the primes denote differentiation with respect to η. To have a uniform notation in the introduction, we introduce here f and g for the similarity variables, which differs from the notation used in Chapter 2. The boundary conditions for the salt dome problem are

$$f(0) = 1, \ \ f(+\infty) = 0 \ \text{ and } \ g(0) = -\varepsilon K(\varepsilon)f'(0).\tag{1.2.25}$$

It can be shown that solutions of problem (1.2.23)-(1.2.25) satisfy

  (i) $f'(\eta) < 0$ for all $0 < \eta < +\infty$,

  (ii) there exists $\eta_0 > 0$ such that $f''(\eta) < 0$ for $\eta < \eta_0$ and $f''(\eta) > 0$ for $\eta > \eta_0$,

  (iii) $g(\eta_0) = \frac{1}{2}\eta_0$ and $g'(\eta) > 0$ for $\eta < \eta_0$ and $g'(\eta) < 0$ for $\eta > \eta_0$,

  (iv) $f'(\eta) \to 0$ if $\eta \to \infty$,

see Van Duijn et. al. [23]. This implies that the brine concentration decreases strictly with z and is concave below the plane $z = \eta_0\sqrt{t}$ and convex above it. The z−component of the specific discharge has a maximum at $z = \eta_0\sqrt{t}$ of magnitude $q(\eta_0\sqrt{t}, t) = 1/2\eta_0/\sqrt{t}$.

   In the limit $\varepsilon \to 0$ equations (1.2.23) and (1.2.24) reduce to

$$f'' + \frac{1}{2}\eta f' = 0 \ \text{ for } \ \eta > 0,\tag{1.2.26}$$

while $g(\eta) = 0$. Equation (1.2.26) subject to the boundary conditions on f has an explicit solution, given by

$$f = \text{erfc}\left(\frac{\eta}{2}\right) \ \text{ for } \ \eta > 0.\tag{1.2.27}$$

This solution is referred to as the Boussinesq limit of the salt dome problem. Figures 1.a. and 1.b. show solutions of (1.2.23)-(1.2.24) subject to (1.2.25) for $\varepsilon = 0.2$ and the corresponding Boussinesq limit ($\varepsilon = 0.0$).

   Although $\varepsilon = 0.2$ corresponds to almost saturated brine, the difference between the f-curve for $\varepsilon = 0.2$ and the Boussinesq solution is $\approx 5\%$. A comparison in terms of the similarity variables is convenient because the result is uniformly valid for all $t > 0$. Moreover, the similarity solution provides an upper bound for the magnitude of the volume effects. This is due to the choice of the discontinuity of ρ at $z = 0$, $t = 0$, see (1.2.18). In most practical situations, the initial condition on ρ will be smooth and therefore the volume effects less noticeable.
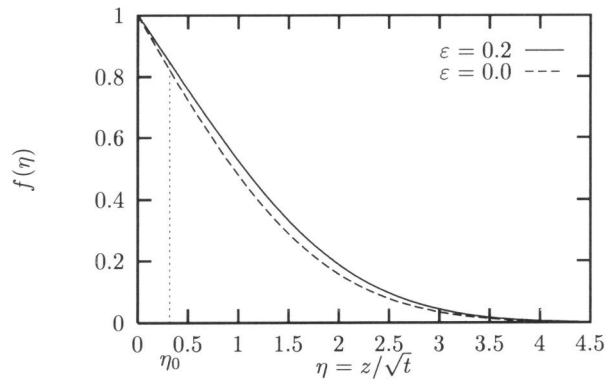
Figure 1.a. The similarity solution $f(\eta)$ for $\varepsilon = 0.0$ (Boussinesq limit) and $\varepsilon = 0.2$.
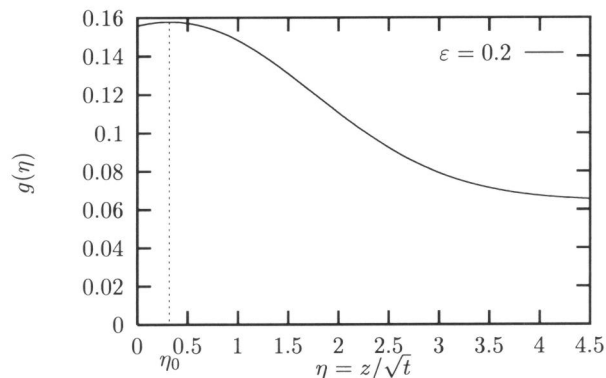
Figure 1.b. The similarity solution $g(\eta)$ $(= q(z,t)\sqrt{t})$ for $\varepsilon = 0.2$. The Boussinesq limit is $g(\eta) = 0$.

The induced discharge is perpendicular to the salt rock boundary and causes additional movement of salt.

In Chapter 2, we also consider the brine induced flow of radionuclides. Then we need to consider the additional scaled equation

$$\frac{\partial \bar{\omega}_c}{\partial t} + q \frac{\partial \bar{\omega}_c}{\partial z} - \frac{\theta}{(\varepsilon\rho + 1)} \frac{\partial}{\partial z} \left((\varepsilon\rho + 1) \frac{\partial \bar{\omega}_c}{\partial z} \right) = 0. \tag{1.2.28}$$

in which we eliminated the decay term by setting $\omega_c(z,t) = \bar{\omega}_c(z,t)e^{-\lambda t}$. Here, ω_c denotes the scaled tracer mass fraction, relative to the fluid (brine) density. The parameter θ is defined as the ratio between the dispersivity of the tracer divided by the dispersivity of brine. The boundary and initial conditions are

$$\begin{aligned} \bar{\omega}_c(0,t) &= 1 \quad \text{for all} \quad t > 0 \\ \bar{\omega}_c(z,0) &= 0 \quad \text{for all} \quad z > 0 \end{aligned} \tag{1.2.29}$$

This problem corresponds to the continuous release of radionuclides (tracers) at the salt rock boundary with scaled mass fraction $\bar{\omega}_c(0,t) = 1$. The radionuclides are transported by dispersion/diffusion and the convection induced by the density gradients of the brine. Since

$q(z,t) = g(\eta)/\sqrt{t}$ and $\rho(z,t) = f(\eta)$, we note that (1.2.28)-(1.2.29) has a self similar solution $\bar{\omega}_c(z,t) = w(\eta)$, where w is a solution of the linear boundary value problem

$$\begin{cases} w'(g - \dfrac{\eta}{2}) - \dfrac{\theta}{(\varepsilon f + 1)} \left((\varepsilon f + 1)w' \right)' = 0 \\ w(0) = 1 \\ w(\infty) = 0 \end{cases}$$
(1.2.30)

To solve this problem we first eliminate g using (1.2.16) and integrate the resulting equation. This leads to

$$w(\eta) = 1 - \frac{\displaystyle\int_0^\eta \left(\frac{f'(\xi)}{f'(0)}\right)^{\frac{1}{\theta}} \frac{(1+\varepsilon)}{\varepsilon f(\xi) + 1}\, d\xi}{\displaystyle\int_0^\infty \left(\frac{f'(\xi)}{f'(0)}\right)^{\frac{1}{\theta}} \frac{(1+\varepsilon)}{\varepsilon f(\xi) + 1}\, d\xi} = 1 - \frac{\displaystyle\int_0^\eta \frac{|f'(\xi)|^{\frac{1}{\theta}}}{\varepsilon f(\xi) + 1}\, d\xi}{\displaystyle\int_0^\infty \frac{|f'(\xi)|^{\frac{1}{\theta}}}{\varepsilon f(\xi) + 1}\, d\xi},$$
(1.2.31)

where f is the solution of (1.2.23)-(1.2.25), for a given value of ε. The corresponding scaled radionuclide concentration is

$$\bar{c}(\eta) = w(\eta) \frac{\varepsilon f(\eta) + 1}{\varepsilon + 1}.$$
(1.2.32)

Only for special values of θ the integral (1.2.31) evaluates to an exact closed form expression.

In the limit $\theta \to 0$, i.e. no tracer dispersion, the solution of (1.2.30) reduces to

$$w(\eta) = \begin{cases} 1 & \text{for} \quad 0 < \eta < \eta_0 \\ 0 & \text{for} \qquad \eta > \eta_0 \end{cases}$$
(1.2.33)

and thus

$$\bar{c}(\eta) = \begin{cases} \dfrac{\varepsilon f(\eta) + 1}{\varepsilon + 1} & \text{for} \quad 0 < \eta < \eta_0 \\ 0 & \text{for} \qquad \eta > \eta_0 \end{cases}$$
(1.2.34)

As a consequence a radionuclide front emerges which moves with speed $g(\eta_0)/\sqrt{t}$, where $g(\eta_0)$ = $\max((g(\eta)) = \eta_0/2$, see property (iii) above. The position of the front in the (z,t)-plane is given by $s(t) = 2g(\eta_0)\sqrt{t} = \eta_0\sqrt{t}$, which is equivalent to the path of a tracer particle released at $t = 0$ in $z = 0$, i.e. at the beginning of the brine transport process. Hence in the limit $\theta \to 0$, the movement of the tracer is caused by the compressibility or volue effect only. The scaled tracer concentration $\bar{c}$ is plotted for different values of the parameter θ in Figure 2. This picture clearly shows convergence towards the front solution as $\theta \to 0$.
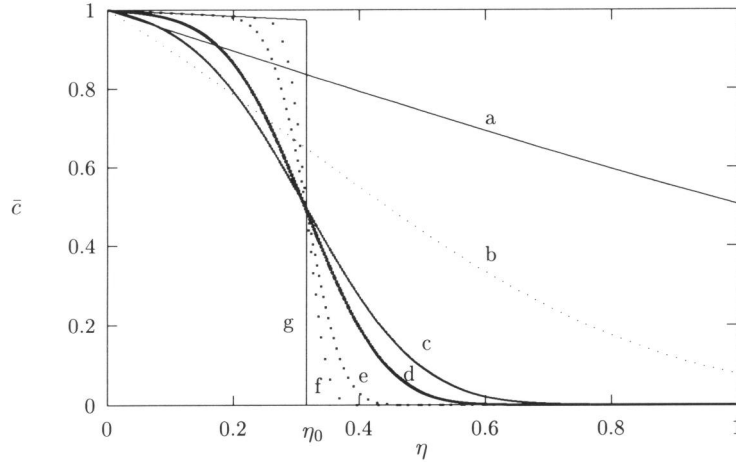
Figure 2. The scaled radionuclide concentration $\bar{c}(\eta)$ for $\varepsilon = 0.2$ and different val ues of θ: a. $\theta = 1.0$, b. $\theta = 0.1$, c. $\theta = 0.01$, d. $\theta = 0.005$, e. $\theta = 0.001$, f. $\theta = 0.0003$, g. $\theta = 0.0$ (the front solution).

1.2.2 The Von Mises transformation

To reduce system (1.2.15)-(1.2.16) to a single, nonlinear diffusion equation we apply a coordinate transformation which is a variant of the Von Mises transformation, see e.g. Mises & Friedrichs [63]. First we redefine the scaled density variable ρ by setting $u := \rho + 1/\varepsilon$. In this new variable, equations (1.2.15)-(1.2.16) become, for $z > 0$, $t > 0$,

$$\frac{\partial u}{\partial t} + \frac{\partial}{\partial z}(qu) = 0 \tag{1.2.35}$$

$$\frac{\partial u}{\partial t} + q\frac{\partial u}{\partial z} - \frac{\partial^2 u}{\partial z^2} = 0, \tag{1.2.36}$$

with

$$u(z, 0) = u_f \text{ for } z > 0, \tag{1.2.37}$$

and

$$u(0, t) = u_s \text{ and } q(0, t) = -\varepsilon K(\varepsilon)\frac{\partial u}{\partial z}(0, t) \text{ for } t > 0. \tag{1.2.38}$$

Here u_f and u_s are the scaled densities of fresh water and brine.

Considering the fluid balance equation (1.2.35) as the divergence operator in the (t, z)-plane, acting on the vector (u, uq), we introduce a modified stream function $\Psi = \Psi(z, t)$, which satisfies

$$u = \frac{\partial \Psi}{\partial z} \text{ and } uq = -\frac{\partial \Psi}{\partial t}. \tag{1.2.39}$$

We use this 'stream function' to replace z as independent variable. Thus instead of t and z we take

$$t = t \text{ and } \Psi = \int_{h(t)}^{z} u(s, t)\, ds, \tag{1.2.40}$$

as new variables, where $h(t)$ is a yet unknown function of time which will be determined later on from the boundary condition on q. It will be normalized such that $h(0) = 0$. The Von Mises transformation is

$$\hat{u} = \hat{u}(\Psi, t) = \hat{u}(\Psi(z,t), t) = u(z,t). \tag{1.2.41}$$

Under this transformation, equations (1.2.35)-(1.2.36) become

$$\frac{\partial \hat{u}}{\partial t} = \hat{u} \frac{\partial}{\partial \Psi} \left(\hat{u} \frac{\partial \hat{u}}{\partial \Psi} \right) \quad \text{with} \quad \Psi \in Q, \ t > 0, \tag{1.2.42}$$

where Q denotes the range of Ψ. The presence of the second boundary condition in (1.2.38) implies that the domain Q is time dependent and a priori unknown. It has to be determined as part of the problem. Using the second equation in (1.2.39) we obtain

$$\Psi(0,t) = -u_s \int_0^t q(0,\xi) \, d\xi = -\varepsilon K(\varepsilon) u_s \int_0^t \frac{\partial u}{\partial z}(0,\xi) \, d\xi. \tag{1.2.43}$$

Differentiating this expression and introduction of the Von Mises variables gives, with $\varphi(t) = \Psi(0,t)$,

$$\frac{d\varphi(t)}{dt} = \varepsilon K(\varepsilon) \, \hat{u}^2(\varphi(t), t) \frac{\partial \hat{u}}{\partial \Psi}(\varphi(t), t) = \varepsilon K(\varepsilon) \, u_s^2 \frac{\partial \hat{u}}{\partial \Psi}(\varphi(t), t) \quad \text{for} \ t > 0. \tag{1.2.44}$$

Integrating the first equation in (1.2.39) gives

$$\Psi(z,t) = \varphi(t) + \int_0^z u(s,t) \, ds. \tag{1.2.45}$$
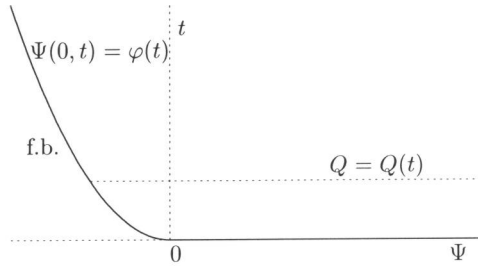
Figure 3. The (Ψ, t)-plane.

Hence

$$Q(t) = (\varphi(t), \infty) \quad \text{for} \ t \geq 0, \tag{1.2.46}$$

see Figure 3. Thus we have found that $\hat{u}(\Psi, t)$, if it exists, satisfies equation (1.2.42) on the time dependent domain $Q(t)$, subject to the boundary condition

$$\hat{u}(\varphi(t), t) = u_s \quad \text{for} \ t > 0, \tag{1.2.47}$$

and the initial condition

$$\hat{u}(\Psi, 0) = u_f \quad \text{for} \ \Psi > 0. \tag{1.2.48}$$

Condition (1.2.44) relates the speed of the boundary of the transformed domain to the spatial derivative of $\hat{u}$ at that boundary. The combination of equation (1.2.42), conditions (1.2.47), (1.2.48) and equation (1.2.44) is called a free boundary problem, with (1.2.44) being the free boundary equation. The special form of (1.2.44) is known in literature as the Stefan condition for the free boundary problem, see for instance Meirmanov [62].

Because conditions (1.2.47) and (1.2.48) are constant, a solution of this free boundary problem can be determined in terms of the similarity variables

$$\hat{u}(\Psi, t) = f(\eta) \ \text{ with } \ \eta = \frac{\Psi}{\sqrt{t}}. \tag{1.2.49}$$

Assuming in addition that the free boundary $\Psi = \varphi(t)$ has the form

$$\varphi(t) = a\sqrt{t}, \tag{1.2.50}$$

with a a priori unknown, the transformed problem for f becomes

$$\begin{cases} \dfrac{1}{2}\eta f' + f(ff')' = 0 \ \text{ for } \ \eta > a, \\[2mm] f(a) = u_s, \ \ f(+\infty) = u_f, \\[2mm] f'(a) = \dfrac{a}{2\varepsilon K(\varepsilon)f(a)^2}. \end{cases} \tag{1.2.51}$$

This problem is solved numerically, details are given in Chapter 3.

Having obtained a solution $f(\eta)$, and thereby $\hat{u} = \hat{u}(\Psi, t)$, we use (1.2.39) to return to the original variables in the (z, t)-plane. To this end, we integrate the first equation in (1.2.39), yielding

$$z = \int_0^{\Psi(z,t)} \frac{1}{\hat{u}(s,t)} \, ds + h(t) \ \text{ for } \ (z,t) \ \text{ for } \ z > 0, \ t > 0, \tag{1.2.52}$$

where $h(t)$ is the integration constant depending on t only, satisfying $h(0) = 0$ (which implies $\Psi(0, 0) = 0$).

To find $h(t)$ we differentiate (1.2.52) with respect to t and use the second equation in (1.2.39). This yields an expression for q, given by

$$q(z,t) = h'(t) - \int_0^{\Psi(z,t)} \frac{\hat{u}_t}{\hat{u}^2}(s,t) \, ds. \tag{1.2.53}$$

where $\hat{u}_t$ denotes the partial derivative of $\hat{u}$ with respect to t. We use the boundary condition on q in (1.2.53) to determine the function $h(t)$, yielding

$$h(t) = \int_0^t \left\{ q(0,\xi) + \int_0^{\varphi(\xi)} \frac{\hat{u}_t}{\hat{u}^2}(s,\xi) \, ds \right\} d\xi. \tag{1.2.54}$$

After combining expressions (1.2.52), (1.2.54) and (1.2.53), (1.2.54), and rewriting the result in terms of the similarity variables we obtain

$$z = z(\eta, t) = \sqrt{t} \int_a^\eta \frac{1}{f(s)} \, ds \ \text{ for } \ \eta > a, \ t > 0, \tag{1.2.55}$$

and

$$q = q(\eta, t) = \frac{1}{2\sqrt{t}} \left\{ -\frac{a}{f(a)} + \int_a^\eta \frac{sf'}{f^2} \, ds \right\} \ \text{ for } \ \eta > a, \ t > 0. \tag{1.2.56}$$

The solution $u = u(z, t)$ is obtained by forst inverting (1.2.52), which gives $\eta = \eta(z, t)$, and then substituting this in $f(\eta)$: i.e. $u(z, t) = f(\eta(z, t))$. Similarly we define $q(z, t) = q(\eta(z, t), t)$. In Chapter 3, we show that this solution is idential to the solution obtained by direct similarity transformation. Therefore, we refer to Figures 1.a. and 1.b. for a graphical representation of the solution in terms of the variable $z/\sqrt{t}$.

The Von Mises transformation provides a reduction of the governing balance equations which directly leads to a second-order nonlinear diffusion equation. The latter has been extensively studied in the mathematics literature. Much is known about the large time behavior of this equation for fairly general initial functions. In particular, sharp estimates were obtained for the rate at which the solutions converge towards the similarity profile, see e.g. Van Duijn & Peletier [67] for a related problem on $(-\infty, \infty)$. The example given above and the other examples in Chapter 3 are special because they allow similarity transformation. The result is a second-order ordinary differential equation which makes the analysis more tractable. If we do not use the Von Mises transformation as intermediate step, the result of the similarity transformation is a third-order ordinary differential equation, see again Chapter 3.

1.3 Brine transport: high concentration gradient dispersion

A stable displacement process in a vertical porous column is described by the one-dimensional version of equations (1.1.2), (1.1.5) and (1.1.8). At fufficiently low salt concentrations, the salt mass flux in equation (1.1.5) can be considered Fickian, as we are dealing with transport of tracers. In that case, for one-dimensional flows, the dispersion tensor in (see Bear [2]) (1.1.6) reduces to the dispersion coefficient

$$D = D(q) = D_m + \alpha_L q. \tag{1.3.57}$$

Here α_L [m] denotes the longitudinal dispersion length or dispersivity and D_m the molecular diffusion coefficient [m^2/s]. Hence, the parameter that solely characterizes the dispersive salt transport at low salt concentrations is α_L.

However, if the salt concentration of the displacing fluid is much higher than the concentration of the displaced fluid, equations (1.1.2), (1.1.5), (1.1.6) and (1.1.8) can still be used but the dispersion coefficient (1.3.57) has to be lowered by a factor which depends on the density difference between the fluids and on the average flow rate in the column. Hassanizadeh & Leijnse [35] observed a decrease of the tracer dispersion length ($\alpha_L = 0.09$ cm) by a factor three when the density difference between the displacing and resident fluids was increased from 1 to 175 kg/m^3 (for a constant flow rate). These results indicate that at the column scale linear Fick's law (1.1.6) does not hold when there exist high salt concentration gradients, and thereby high density gradients in the fluid phase.

This behavior can be explained as follows. The porous medium in the column is not perfectly homogeneous, and permeability and porosity may vary locally in space, which in turn causes local velocity variations in the fluid flow. Hydrodynamic dispersion is the macroscopic outcome of these velocity variations, In case of tracer density differences, the dispersion is not influenced by gravitational forces. When the density difference between the resident and displacing fluids becomes significant, the gravitational forces give rise to a reduction of the dispersion.

Instead of the linear Fick's law, Hassanizadeh & Leijnse [35] formulated a (macroscopic) nonlinear theory for high concentration dipersion in porous media which turns out to be in excellent agreement with with a variety of experimental results. They showed that Fick's law

has to be replaced by the nonlinear dispersive mass flux equation, given by

$$\mathbf{J}(\beta|J| + 1) = -D\rho\text{grad }\omega, \tag{1.3.58}$$

where $\beta = \beta(q)$ [m^2 s / kg] denotes a velocity dependent dispersion parameter, D the tracer dispersion coefficient (1.3.57), $\mathbf{J}$ [kg/(m^2 s)] the dispersive mass flux vector and $|J|$ [kg/(m^{2}s)] its magnitude. In the limit $J \to 0$, i.e. for very low (tracer) mass fluxes, (1.3.58) reduces to Fick's law. Note the resemblance between equation (1.3.58) and the Forchheimer equation for high velocity flow in porous media

$$\mathbf{q}(a|q| + 1) = -\frac{\kappa}{\mu}(\text{grad }p - \rho\mathbf{g}), \tag{1.3.59}$$

where a [s/m] denotes the Forchheimer coefficient, see e.g. [2].

Hassanizadeh et. al. [36] carried out hydrodynamically stable displacement experiments in a vertical column, homogeneously packed with glass beads. They varied the salt concentration difference between the resident and displacing fluid, from tracer values to almost saturated brine, while keeping the flow rate approximately constant. The longitudinal dispersion length was determined from low concentration (LC or tracer) experiments. A value of the dispersion parameter β could be obtained from the results of the high concentration (HC) experiments. The reader is referred to [35] for details concerning the experimental setup and the analysis of the results. Using the nonlinear theory, it is possible to simulate both LC and HC experiments with a unique set of experimentally determined parameters α_L and β.

1.3.1 Experimental results

A series of well-controlled experiments have been performed by Moser [61] in order to address a number of open questions related to brine transport. The purpose of the experiments was to determe the effect of large salt concentration differences and large absolute salt concentrations on dispersion and to investigate the combined effect of flow velocity and large concentration differences. To this end, four series of displacement experiments were carried out (see Table 1 through 4 in Chapter 4 for an overview):

- Fourteen tracer experiments where a low salt concentration solution was displaced by fluid with a sightly higher salt concentration. These are of LC-type.

- Seven HC-experiments were performed, where a low-concentration solution was displaced by a fluid with a high salt concentration. The concentration differences ranged from 2.8 kg/m^3 to 44.6 kg/m^3. The inflow rate for this series of experiments was kept to a constant value of $5.4 \cdot 10^{-4}$ m/s.

- Nine HC-experiments were performed for which the concentration difference between the resident and displacing fluids had a constant value of 63.4 kg/m^3, but the flow rate was varied from $1.0 \cdot 10^{-4}$ m/s to $2.3 \cdot 10^{-3}$ m/s.

- Four experiments where carried out wherin a high concentration solution (90 kg/m^3) was displaced with a yet higher concentration solution.

The experimental results are discussed in Chapter 4, and are summarized in Figure 4. Figure 4 shows the apparent dispersion coefficient relative to the molecular diffusion coefficient D_m as a function of the Peclet number. The latter is defined as

$$\text{Pe} = \frac{qd_{50}}{D_m}, \tag{1.3.60}$$

where $d_{50} = 5.0 \cdot 10^{-4}$ m denotes the middle particle diameter of the quartz sand used in the experiments.
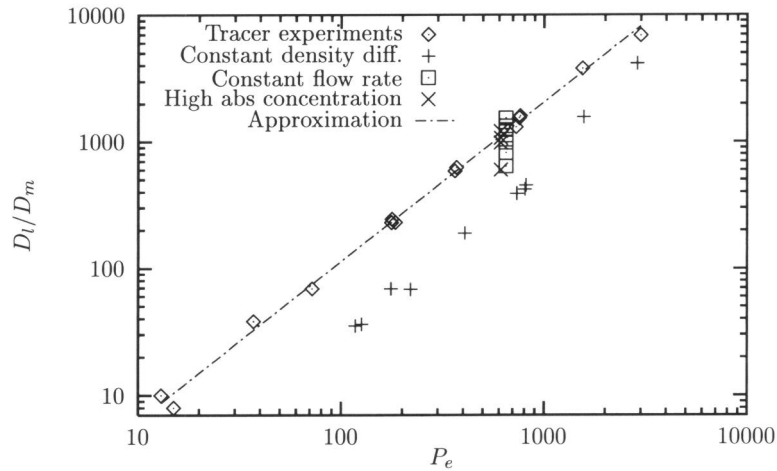
Figure 4 The relative apparent dispersion coefficient as a function of the Peclet number.

All apparent dispersion coefficients were determined by matching the explicit error-function solution of the linear one-dimensional convection-diffusion equation ($q = $ constant) to breakthrough curves obtained from the experiments, see [61] for details.

The LC tracer experiments are in excellent agreement with experimental data collected by Pfankuch [69]. The tracer dispersion coefficient is nearly proportional to the Peclet number, see the dashed line in Figure 4. This is in agreement with the classical expression (1.3.57). The results of the HC constant density difference experiments, i.e. all having the same density difference but different flow rates, indeed show a smaller value of the dispersion coefficient, when compared to the tracer experiments. The constant flow rate experiments, i.e. all having the same flow rate but different density differences, show the same tendency: if the density difference increases, the dispersion coefficient decreases.

An other important conclusion can be drawn from the data in Figure 4. The difference between the HC and tracer dispersion coefficients decreases as the Pe-number increases. This gives evidence that the HC dipersion coefficient β is velocity dependent.

The high absolute density experiments indicate that for the density difference in the tracer range, the tracer dispersion coefficient is recovered. This result explicitly shows that the (apparent) dispersion coefficient is independent of the absolute salt concentration of the fluids.
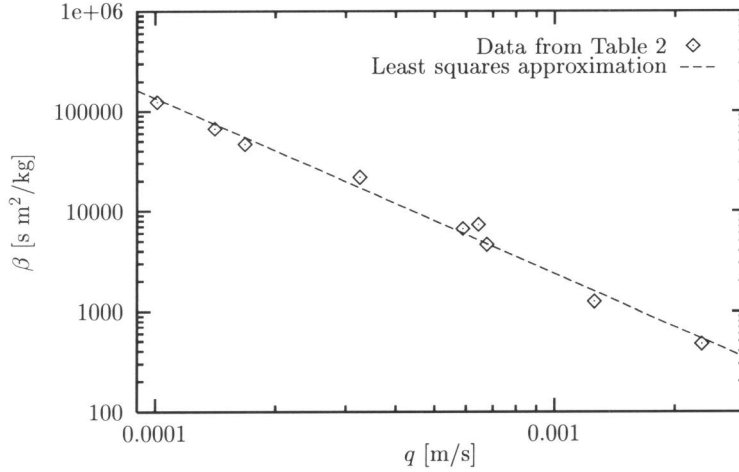
Figure 5. The parameter β as a function of q for the constant density difference experiments.

Once q, α_L, ε and n are known, the parameter β can be determined by matching numerical solutions of (1.1.2), (1.1.5), (1.1.8) and (1.3.58) (in one space dimension and subject to appropriate boundary/initial conditions) to the experimental data. The constant density difference HC experiments are used to determine the relation between the parameter β and the discharge q. The results are shown on a log-log scale in Figure 5. A least squares curve fitting yields an approximate expression for $\beta(q)$, given by

$$\beta(q) \approx \frac{0.0125}{q^{1.76}} \ \text{sm}^2/\text{kg} \ \text{ for } \ 9.0 \cdot 10^{-5} < q < 3.0 \cdot 10^{-3} \ \text{m/s}. \tag{1.3.61}$$

The dashed line in Figure 5 corresponds to expression (1.3.61). Note that the discharges in the experiments are relatively high when compared to groundwater discharges in the field, typically ranging from 0.0 m/s to $\approx 3.0 \cdot 10^{-5}$ m/s (i.e. 3.0 m/day).

1.3.2 Mathematical analysis and approximations

All experiments reported here have an essentially one-dimensional character. Only small variations of the measured quantities in the horizontal x- and y-directions have been observed. After appropriate scaling (see Chapter 4), equations (1.1.2), (1.1.5), (1.1.8) and (1.3.58) can be combined into

$$\frac{\partial \rho}{\partial t} + \frac{\partial}{\partial z}(q\rho) + \frac{1}{\varepsilon}\frac{\partial q}{\partial z} = 0, \tag{1.3.62}$$

and

$$\frac{\partial \rho}{\partial t} + q\frac{\partial \rho}{\partial z} + \gamma\frac{\partial}{\partial z}\left\{ -\frac{1}{2\beta_0(q)\varepsilon} + \frac{1}{2\beta_0(q)\varepsilon}\sqrt{1 - 4\beta_0(q)\varepsilon\frac{\theta}{\gamma}\frac{\partial \rho}{\partial z}} \right\} = 0, \tag{1.3.63}$$

for $-\infty z + \infty$ and $t > 0$. Here, θ is the scaled (tracer) dispersion coefficient and $\beta_0(q)$ is the scaled β-parameter. In writing (1.3.63) we assumed that $\partial \rho/\partial z < 0$, as in the experiments.

Without additional simplifications, equations (1.3.62), (1.3.63), subject to appropriate initial/boundary conditions, can only be solved numerically. If we assume that the effect of the density variations on the fluid flow is small, we may disregard equation (1.3.62) and use $q(z,t) = 1$ in the transport equation (1.3.63). Assuming moreover

$$\beta |J| >> 1 \qquad (1.3.64)$$

in the dispersive mass flux equation (1.3.58), an explicit solution can be constructed. A less explicit, but more quantitative analysis can be carried out for the system (1.3.62)-(1.3.63) if we assume again (1.3.64). In that case, we introduce Von Mises and similarity transformations, yielding an ordinary differential equation which is mathematically known and can easily be solved by relatively straightforward numerical techniques, see Chapter 4. A comparison of the different solutions is given and the results are used to analyze the experimental data.

The explicit solution Taking $q = 1$ and consequently $\beta_0(q) = \beta_0(1) = $ constant) in (1.3.63), and using assumption (1.3.64), which implies

$$-4\beta_0\varepsilon\frac{\theta}{\gamma}\frac{\partial\rho}{\partial z} >> 1, \qquad (1.3.65)$$

we find the reduced transport equation

$$\frac{\partial\rho}{\partial t} + \frac{\partial\rho}{\partial z} + \sqrt{\frac{\theta\gamma}{\beta_0\varepsilon}}\frac{\partial}{\partial z}\left\{\sqrt{-\frac{\partial\rho}{\partial z}}\right\} = 0. \qquad (1.3.66)$$

For piecewise constant initial data

$$\rho(z,0) = \rho_0(z) = \begin{cases} 1 & \text{for} \quad z < 0 \\ 0 & \text{for} \quad z > 0 \end{cases} \qquad (1.3.67)$$

equation (1.3.66) can be solved explicitly. The solution is

$$\rho(z,t) = \frac{1}{2}\left\{1 - \frac{\arctan\left(\sqrt{\frac{B}{C}}(z-t)t^{-\frac{2}{3}}\right)}{C\sqrt{BC}} - \frac{(z-t)t^{-\frac{2}{3}}}{C(B(z-t)^2t^{-\frac{4}{3}}+C)}\right\}, \qquad (1.3.68)$$

for $-\infty < z < +\infty$, $t > 0$, where

$$B = \frac{1}{3}\sqrt{\frac{\beta_0\varepsilon}{(\theta\gamma)}} \quad \text{and} \quad C = C_2 = \left(\frac{3\pi^2}{4}\right)^{\frac{1}{3}}\left(\frac{\theta\gamma}{\beta_0\varepsilon}\right)^{\frac{1}{6}}. \qquad (1.3.69)$$

We matched the approximate solution (1.3.68) with breakthrough curves of the constant flow rate experiments to determine the value of the unscaled $\beta(q)$. In addition, we matched numerical solutions of the full problem with the same breakthrough data. The results are summarized in Figure 6. As to be expected, matching the full numerical solution to the experimental HC breakthrough data yields a nearly constant β-value.
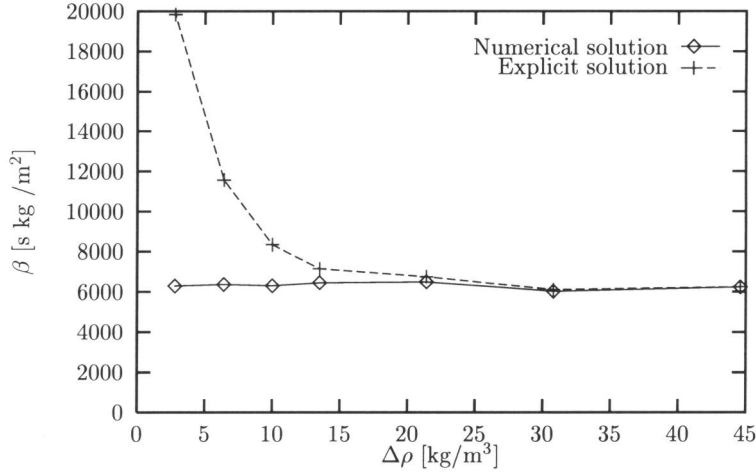
Figure 6. Comparison of β-values obtained by fitting the numerical and the explicit solution to breakthrough curves of the constant flow rate experiments.

Note that the explicit solution provides accurate β-values for the range $\Delta\rho > 25$ kg/m^3.

The semi-explicit solution If we drop the constant flow rate approximation but maintain assumption (1.3.65), the resulting equations are (1.3.62) and (1.3.66). The initial condition on ρ is given by (1.3.67) and the boundary condition on q by $q(-\infty, t) = 1$, i.e. $q(-\infty, t) = q_0$ unscaled. In addition we assume that the local discharge variations due to the volume effect are small enough to justify the approximations $\beta(q) = \beta(q_0)$ and $D(q) = D(q_0)$. To solve the problem we use the Von Mises transformation (1.2.39), (1.2.40) and (1.2.41) to reduce system (1.3.62), (1.3.66) to a single nonlinear diffusion equation. The latter allows similarity transformation and the final result is a semi-explicit solution $(\rho(z,t), q(z,t))$. For details on the solution procedure we refer to Chapter 4.

The difference between the explicit solution (1.3.68) and the semi-explicit solution is small, even for high ε-values. The discharge $q = q(z, t)$ exhibits a maximum which coincides with the position of the inflection point of the density profile in the column . The (scaled) decay of this maximum is given by

$$q_{max} = 1 + t^{-\frac{1}{3}}G \ \text{ for } \ t > 0, \tag{1.3.70}$$

and its position by

$$z_{max} = t + \frac{3}{2}t^{\frac{2}{3}}G \ \text{ for } \ t > 0, \tag{1.3.71}$$

where $G \approx 5.7736 \cdot 10^{-2}$. See Chapter 4 for details. Note that occurrence of the terms containing the constant G in (1.3.70) and (1.3.71) is only due to the volume effects. By setting $G = 0$ we recover the $q = $ constant situation. In Chapter 3 we consider compressible flow in an infinitely long column, using linear Fick's law as dispersive mass flux equation. In that case, q_{max} exhibits $t^{-\frac{1}{2}}$-decay.

We used expressions (1.3.70),(1.3.71) to quantify the volume effects and found that they can be disregarded in all experiments considered. The enhanced displacement of salt is not noticeable within the accuracy of the experimental setup.

The numerical solution The above assumptions that β and the dispersion coefficient D are independent of the local discharge variations <u>within</u> each experiment is also maintained to obtain a numerical solution of the full problem. This implies that (1.3.63) reduces to

$$\frac{\partial \rho}{\partial t} + q \frac{\partial \rho}{\partial z} + \frac{\gamma}{2\beta_0 \varepsilon} \frac{\partial}{\partial z} \sqrt{1 - 4\beta_0 \varepsilon \frac{\theta}{\gamma} \frac{\partial \rho}{\partial z}} = 0, \qquad (1.3.72)$$

for $\partial \rho / \partial z < 0$. The full problem, i.e. (1.3.62), (1.3.72) subject to (1.3.67) and $q(-L, t) = 1$, is solved numerically on a sufficiently large domain $z \in [-L, L]$, using standard finite difference methods. The initial condition on ρ, i.e. (1.3.67), is approximated by a piecewise linear approximation of a steep error function.

The numerical solutions of the full problem were used to check the validity of the explicit and semi-explicit solutions, and to determine β-values from the experimental breakthrough curves.

1.3.3 Summary of the main results

The LC experiments satisfy the classical equations and are in agreement with tracer experiment reported in literature. The experiments reported here confirm the validity of the nonlinear dispersion theory. The dispersion parameter β depends on the flow rate, but it is independent of the density difference. The absolute salt concentration does not affect the apparent dispersivity. The analysis of the nonlinear equations shows that for relatively low density differences and at the short time scale of the experiments, the nonlinear term in (1.3.58) predominates the dispersive behaviour. The volume effects can be disregarded in all experiments considered.

1.4 The fresh-salt interface in heterogeneous media

In most practical sea water intrusion problems, the horizontal and vertical extensions of the aquifer are large when compared to the width of the diffusive/dispersive mixing zone. This motivates to assume the existence of an interface between the fluids: when crossing the interface the specific weight changes abruptly from one value to the other value.

The implications of the existence of an interface between fresh and salt groundwater have been studied by De Josselin De Jong [47]. In that case, the horizontal density gradients across the interface are singular and the interface becomes a surface source (in three space dimensions) or a line source (in a vertical cross section) of vorticity. The flow of the separate fluids is rotation free, while the rotation of the total flow is produced by the (singular) vorticity distribution along the interface. As a consequence, the velocity component normal to the interface is continuous, while the component tangential to the interface exhibits a discontinuity across the interface: the shear flow.

In a later paper, De Josselin De Jong [46], derived a nonlinear diffusion-type equation to approximate density-driven flow in a vertical cross section of horizontally extended aquifers confined by two impermeable layers. The derivation is based on the Dupuit assumption, i.e. the horizontal component of the specific discharge is constant in each fluid and jumps at the interface. The advantage of this approach is that the two-dimensional flow problem reduces to a one-dimensional initial value problem in terms of the interface height. Solutions of this approximate equation give insight in the time evolution and flow properties of the full problem, in particular with respect to the large time behavior, i.e. for relatively flat interfaces.

Following the original work of De Josselin De Jong [47], Chan Hong et.al. [18] studied the movement of the interface between fresh and salt groundwater numerically. They formulate

the problem in terms of an elliptic (Poisson) equation for the stream function describing the flow and a hyperbolic equation for the time evolution of the interface. The parameterization of the interface is of the form $z = u(x, t)$, where respectively x and z denote the horizontal and vertical coordinate of a point located at the interface. The elliptic problem is solved using a finite element method (moving mesh) while the interface motion equation is solved explicitly in time, by means of a predictor-corrector method. Chan Hong et. al. [18] compare numerical results with solutions of simplified problems, based on the Dupuit approximation with respect to the horizontal flow. Only homogeneous flow domains are considered.

We focus on the transient behavior of an interface in heterogeneous aquifers, including those cases where it is not possible to parameterize the interface according to $z = u(x, t)$ or $x = u(z, t)$. We modified the existing finite element code [18] to allow for heterogeneous intrinsic permeability distributions in the flow domain and developed a front tracking method, to compute the discrete time evolution of the interface. The latter is inspired by ideas developed in Dupaix et. al. [21] and Scheid [72]. Points along the discretized interface are displaced by computing an approximate normal direction and an approximate normal velocity from the stream function along the interface.

1.4.1 The stream function equation

We consider flow of an incompressible fluid of variable specific weight γ and constant viscosity μ, in a rectangular domain with variable intrinsic permeability κ. The flow domain is given by the strip $\Omega = I \times (0, h)$, where I denotes the interval $(-R, R)$ with $R > 0$, such that $R >> h$ ($h > 0$). The strip represents a vertical cross section of a horizontally extended aquifer, bounded from above and below by impermeable layers.

We assume incompressibility of the fluids, implying (1.1.4). At the boundary $\partial\Omega$ we assume a no-flow condition, i.e.

$$\mathbf{q} \cdot \mathbf{n} = 0 \qquad \text{on } \partial\Omega, \tag{1.4.1}$$

where $\mathbf{n}$ denotes the outward normal unit vector on $\partial\Omega$. By taking the two-dimensional curl of equation (1.1.9), we obtain

$$\text{curl}\left(\frac{\mu}{\kappa}\mathbf{q}\right) + \text{curl}\left(\gamma\mathbf{e}_z\right) = 0 \qquad \text{in } \Omega. \tag{1.4.2}$$

Here the curl of a vector function $\mathbf{a} = (a_x, a_z)$ must be understood in the sense that curl $\mathbf{a} := \partial a_x / \partial z - \partial a_z / \partial x$. Since the flow satisfies equation (1.1.4) we can introduce a stream function ψ such that

$$\mathbf{q} = \text{curl } \psi = \left(-\frac{\partial\psi}{\partial z}, \frac{\partial\psi}{\partial x}\right). \tag{1.4.3}$$

Substitution this expression in (1.4.2) yields

$$\text{div}\left(\frac{\mu}{\kappa}\nabla\psi\right) = -\frac{\partial\gamma}{\partial x} \qquad \text{in } \Omega. \tag{1.4.4}$$

This equation has to be interpreted in the weak sense, see Van Duijn & De Josselin De Jong [22] for details. The no-flow condition (1.4.1) implies that ψ is constant at $\partial\Omega$. The value of ψ on $\partial\Omega$ can be chosen arbitrarily. For convenience we set:

$$\psi = 0 \qquad \text{on } \partial\Omega. \tag{1.4.5}$$

Next, we introduce the interface approximation: the interface, denoted by $\Gamma(t)$, separates fresh groundwater, with specific weight γ_f, and salt groundwater, with specific weight γ_s, where $0 < \gamma_f < \gamma_s$. This implies that γ is discontinuous at the interface and thereby the right-hand side of 1.4.4 a singularity. Consequences of the latter are summarized Chapter 5. Thus, given an interface at a certain time $t \geq 0$, the solution of (1.4.4) subject to (1.4.5), determines the stream function distribution in flow domain Ω, and by (1.4.3) the corresponding discharge $\mathbf{q}$.

The heterogeneities considered are discontinuities in intrinsic permeability. We confine ourselves to the special case of piecewise constant permeability distributions: a vertical heterogeneity given by

$$\kappa = (\kappa_2 - \kappa_1)H(x) + \kappa_1 \text{ for } x \in I, \tag{1.4.6}$$

and a horizontal heterogeneity given by

$$\kappa = (\kappa_1 - \kappa_2)H(z - h/2) + \kappa_2 \text{ for } z \in [0, h], \tag{1.4.7}$$

where H denotes the Heaviside function: $H(\xi) = 1$ for $\xi > 0$ and $H(\xi) = 0$ for $\xi < 0$.

1.4.2   Time evolution of the interface

In order to allow for more general interface shapes, we do not parameterize the interface explicitly, as in e.g. Chan Hong et. al. [18] or [46]. Given a solution $\psi = \psi(x, z, t)$ of problem (1.4.4)-(1.4.5), the normal component of the velocity at the interface $\Gamma(t)$ satisfies

$$V_n = \frac{1}{\varepsilon}\mathbf{q} \cdot \mathbf{n} = \frac{1}{\varepsilon}\text{curl } \psi \cdot \mathbf{n} \qquad \text{at } \Gamma(t), \tag{1.4.8}$$

where $\mathbf{n}$ denotes the normal unit vector at $\Gamma(t)$, pointing into the fresh water region and ε the porosity of the porous medium. The latter is assumed to be constant. Evaluation of (1.4.8) yields

$$V_n = \frac{1}{\varepsilon}\frac{\partial \psi}{\partial s} \qquad \text{at } \Gamma(t), \tag{1.4.9}$$

where $\partial/\partial s$ denotes the tangential direction along the interface.

When the interface shape allows parametrization of the form $z = u(x, t)$ in Ω, the interface motion equation can be written as

$$\frac{\partial u}{\partial t} = \frac{1}{\varepsilon}\frac{\partial}{\partial x}\{\psi(x, u(x, t), t)\} \qquad \text{in } I \times \mathbf{R}^+. \tag{1.4.10}$$

This particular form is due to Chan Hong et. al. [18]. Suppose that an interface touches the domain boundaries at $z = 0$ and $z = h$. Let the corresponding x-coordinates be given by $S_1(t)$ (toe) and $S_2(t)$ (top). It was also shown in [18] that $S_1(t)$ and $S_2(t)$ satisfy the differential equations

$$\dot{S}_1(t) = -\frac{1}{\varepsilon}\lim_{x \to S_1(t)} \frac{\psi(x, u(x, t), t)}{u(x, t)} \text{ and } \dot{S}_2(t) = \frac{1}{\varepsilon}\lim_{x \to S_2(t)} \frac{\psi(x, u(x, t), t)}{h - u(x, t)}. \tag{1.4.11}$$

We use these expressions to compute the velocity of the top and toe under the assumption that the interface can be parameterized in a small neighborhood of the lower and upper domain boundaries.

After appropriate scaling, see Chapter 5, equations (1.4.4) and (1.4.8), subject to boundary and initial conditions, lead to the problem of finding the stream function $\psi = \psi(x, z, t)$ and $\Gamma(t)$

satisfying:

$$(P) \begin{cases} -\text{div}\left(\frac{1}{\kappa}\nabla\psi\right) = \frac{\partial}{\partial x}\left(\gamma(x,z,t)\right) & \text{in } \Omega \times \mathbf{R}^+, \\ \psi = 0 & \text{on } \partial\Omega \times \mathbf{R}^+, \\ V_n = \frac{\partial\psi}{\partial s} & \text{on } \Gamma(t), \ t \in \mathbf{R}^+, \\ \Gamma(t=0) = \Gamma_0. \end{cases} \tag{1.4.12}$$

1.4.3 The numerical method

The numerical procedure consists of three steps. We first solve the elliptic problem for the stream function, for a given interface $\Gamma(t^k)$ at time level $t = t^k$, see also [18]. To this end, domain Ω is decomposed in the subdomains Ω_f^k and Ω_s^k, being respectively the domains of fresh and salt water. The triangularization of the subdomains is constructed such that the piecewise linear approximation of Γ^k always coincides with sides of triangles in Ω_f^k and Ω_s^k. The FEM meshes are generated using the mesh generator of the SEPRAN finite element package, which is developed at Delft University of Technology. Next, we compute an approximation of the normal component of the velocity at the interface. Finally we apply a discrete front tracking method to obtain an approximation of the position of the interface at the new time level $t = t^{k+1}$. For details we refer to Chapter 5.

In order to gain confidence in the front tracking method, we compared front tracking solutions with solutions based on the procedure proposed in [18]. They use the explicit $S^{\alpha,\beta}$-scheme of Leyrat & Peyret [57] to discretize the interface motion equation (1.4.10). In case of a linear initial interface (initial slope $\pi/4$) in a homogeneous domain, the maximum relative difference between computed interface positions, using both methods, is $\approx 0.06\%$. Moreover, we observe convergence of the speed of propagation of the top and toe of the interface, towards a similarity solution of the corresponding approximate Dupuit problem, see e.g. [86]. The latter describes the large-time behavior of the full problem.

1.4.4 The interface crossing a discontinuity in permeability

When a fresh-salt interface intersects a discontinuity in permeability, it is possible to derive a simple expression for the shape of the interface in an infinitesimal small neighborhood of the intersection point, provided the interface is non-singular. By the latter, we mean that the velocities at the interface are finite and compatible. The derivation is based on the two-fluid interface conditions in a homogeneous porous medium combined with the flow conditions of a homogeneous fluid at a discontinuity in permeability, see Chapter 5.

Consider a straight line through the origin of the (x, z)-plane, under inclination angle β with the horizontal x-axis, being a vertical cross section of the plane separating two regions with permeability κ_1 (upper region) and κ_2 (lower region). An interface, separating two fluids with specific weight γ_f (upper fluid) and γ_s (lower fluid), intersects this line at the origin. The inclination angle of the interface with the horizontal in the region $x > 0$ is denoted by α_1, while the angle between the interface and the negative x-axis in the region $x < 0$, is given by α_2. We assume for the moment that $\alpha_1 \neq \alpha_2 \neq \beta$, implying that the interface and the discontinuity in permeability divide the (x, z)-plane in four distinct regions. Then, α_1, α_2, β and the permeability

ratio κ_1/κ_2 have to satisfy

$$\tan(\alpha_1) = \frac{\tan(\alpha_2)\left(1 + \frac{\kappa_1}{\kappa_2}\tan^2(\beta)\right) - \left(1 - \frac{\kappa_1}{\kappa_2}\right)\tan(\beta)}{\left(\frac{\kappa_1}{\kappa_2} + \tan^2(\beta)\right) - \tan(\alpha_2)\tan(\beta)\left(1 - \frac{\kappa_1}{\kappa_2}\right)}. \tag{1.4.13}$$

A similar relation has been found by Bear & Shapiro [12], expressing the angles of intersection α_1 and α_2 in terms of β and the fresh and salt water fluxes in the intersection point. Note that the fluid density difference does not appear in (1.4.13). Equation (1.4.13) gives an exact relation between the angles of intersection and the permeability ratio, and therefor it is an indispensable tool for computer code verification.

1.4.5   A vertical discontinuity in permeability

The full interface problem (1.4.12) can be reduced to a simplified problem using the Dupuit approximation. Under this assumption, interface motion equation (1.4.10) reduces to (after appropriate scaling)

$$\frac{\partial u}{\partial t} = \frac{\partial}{\partial x}\left\{\kappa\, u(1-u)\frac{\partial u/\partial x}{1 + (\partial u/\partial x)^2}\right\} \quad \text{for } (x,t) \in \mathbf{R} \times \mathbf{R}^+, \tag{1.4.14}$$

subject to the initial condition $u(x,0) = u_0(x)$, see De Josselin De Jong [46]. For homogeneous aquifers, κ is constant. For the special case of a vertical discontinuity in permeability, the scaled coefficient κ is given by

$$\kappa = \kappa(x) = \begin{cases} \kappa_1 & \text{for } x < 0 \\ \kappa_2 & \text{for } x > 0 \end{cases} \tag{1.4.15}$$

Under the assumption that $\partial u/\partial x \ll 1$, i.e. in case of a (very) flat interface, equation (1.4.14) reduces to

$$\frac{\partial u}{\partial t} = \frac{\partial}{\partial x}\left\{\kappa(x)u(1-u)\frac{\partial u}{\partial x}\right\} \quad \text{for } (x,t) \in \mathbf{R} \times \mathbf{R}^+. \tag{1.4.16}$$

If the initial interface is given by

$$u(x,0) = u_0(x) = \begin{cases} 1 & \text{for } x > 0 \\ 0 & \text{for } x < 0 \end{cases} \tag{1.4.17}$$

then (1.4.16), (1.4.15) allows a similarity solution of the form $u(x,t) = f(\eta)$ with $\eta = x/\sqrt{t}$, where the function f is a solution of the boundary value problem

$$\frac{1}{2}\eta f' + (\kappa(\eta)\, f(1-f)f')' = 0 \quad \text{for } \eta \in \mathbf{R}, \tag{1.4.18}$$

where the primes denote differentiation with respect to η, subject to

$$f(-\infty) = 0 \quad \text{and} \quad f(+\infty) = 1. \tag{1.4.19}$$

After additional transformations, we solve this problem using a shooting procedure in the subdomains $\eta > 0$ and $\eta < 0$. The resulting Dupuit similarity solution approximates the large time behavior of the full problem in case of a vertical discontinuity in permeability.
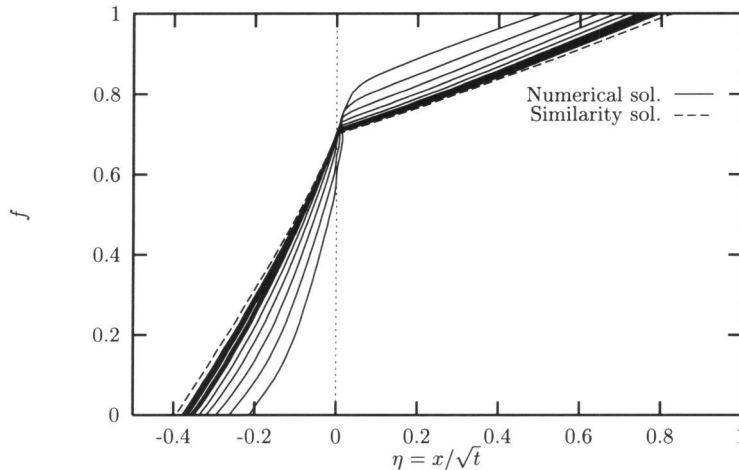
Figure 7. The numerical solution in terms of the similarity variable η and the corresponding Dupuit similarity solution for $\kappa_1/\kappa_2 = 0.1261$.

In Figure 7 we plotted numerical solutions of the full problem for $\kappa_1/\kappa_2 = 0.1261$ in terms of the similarity variable $\eta = x/\sqrt{t}$. The corresponding Dupuit similarity solution is represented by the dashed line in Figure 7. At the short time scale of the numerical simulations, the Dupuit assumption is not satisfied. Moreover, large deviations between expression (1.4.13) and the computed angles of intersection at the discontinuity in permeability are found. The latter is due to the singular initial interface, implying very high initial fluid velocities. As time proceeds, the numerical solution converges towards a similarity profile which is very close to the approximate Dupuit solution, see Figure 7. The numerical similarity profile satisfies expression (1.4.13) up to a small error.

1.4.6 A horizontal discontinuity in permeability

Next we consider a horizontal heterogeneity, consisting of two parallel layers of equal thickness with different permeability κ_1 (upper layer) and κ_2 (lower layer), under the assumption that $\kappa_1 < \kappa_2$. Again, the initial interface is vertical at $x = 0$, such that the region $x < 0$ is occupied by fresh water and the region $x > 0$ by salt water. In this more complicated case it is not possible to obtain a similarity solution of a simplified problem based on the Dupuit approximation.

For $t > 0$, a hydrodynamically unstable zone develops in the vicinity of the discontinuity in permeability, where fresh water is overlain by salt water. The horizontal width of this zone grows in time. Under natural (field) conditions, small local variations in permeability perturb the interface in this zone, and fresh-salt fingers can occur. These fingers grow in time. A normal-mode linear stability analysis shows that fingers of any width or 'wave length' > 0 can develop, see e.g. List [58]. The distribution of observed wave lengths in the fingering pattern depends on the nature of the perturbation mechanism of the interface, for instance the local (small scale) heterogeneous permeability field.

When we consider fresh and salt groundwater as miscible fluids and allow for diffusion/dispersion, stability analysis showes that there exists a (minimum) critical wave length λ_0 in the fingering pattern. The value of λ_0 is related to the value of the diffusion/dispersion coefficient D. This implies that fingers with width smaller that the critical wave length are dissipated by diffusion

and/or dispersion and decay in time. In case of the interface approximation, i.e. in the limit $D \to 0$, we have, at least in theory, $\lambda_0 = 0$.

The computed time evolution of an initially vertical interface exhibits the development of fresh-salt fingers in the vicinity of the horizontal discontinuity in permeability, see Figure 8. To ensure numerical stability, the (variable) time step is chosen such that the CFL condition CFL= 0.2 is satisfied at any time level. The onset of the instabilities in the physically unstable zone is caused by the discrete approximation of the interface: small numerical and discretization errors perturb the unstable interface at any time level which triggers the growth of the fresh-salt fingers.
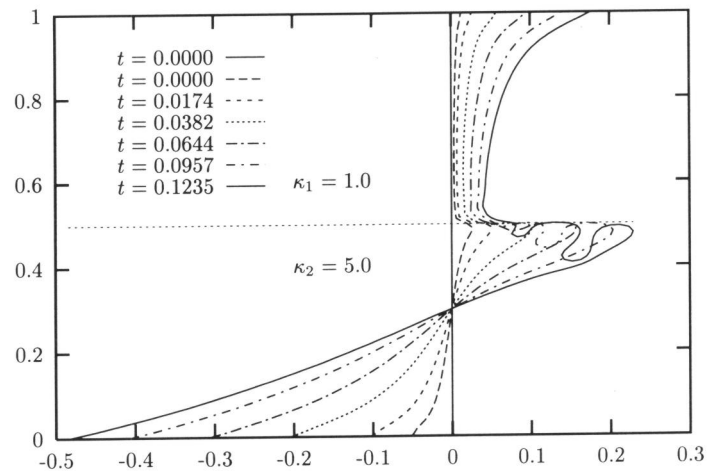
Figure 8. Time evolution of an initially vertical interface.

The width of the fingers that grow in time is directly related to the coarseness of the discretization of the interface. The minimum finger width at the onset of an instability is approximately 6 interface piecewise linears. If we refine the mesh by a factor 2, the width of the fingers that grow is also reduced by a factor 2, while the fingers start to develop earlier. The computations break down whenever adjacent parts of the interface coincide. This is a consequence of the fact that the moving mesh procedure is based on the decomposition of the flow domain in two distinct subdomains, separated by the interface.
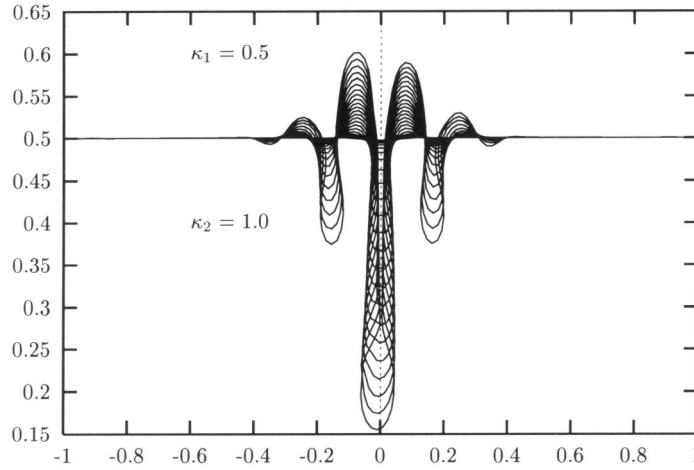
Figure 9. Time evolution of an initially horizontal interface that coincides with the discontinuity in permeability, and which is perturbed at (0.0,0.5) by −0.006.

In Figure 9 we show the computed time evolution of an initially horizontal interface that coincides with the discontinuity in permeability at $z = 0.5$, and which is perturbed at $(0.0, 0.5)$ by -0.006. If do not perturb the interface, nothing happens, as to be expected. The perturbation triggers the instabilities and fingers start to grow. Note that the piecewise linears of the interface approximation are clearly visible. Mesh refinement at the interface does not yield a more smooth interface, but leads to smaller fingers. The asymmetry of the fingering pattern with respect to the vertical axis is caused by the asymmetry in the mesh generation.

The examples given above show that the finger widths that occur in the computations are selected by the numerical method, and not by any physical mechanism. The absence of diffusion/dispersion implies this immediately. Therefor, the practical use of interface models for simulation of instabilities is limited. Moreover, the instabilities or fingers create a mixing zone of fresh and salt groundwater which is in some sense in contradiction with the basic interface approximation: strictly miscible fluids are treated as immiscible.

1.5   Crystal dissolution

When transported solutes, e.g. salts, participate in a dissolution-precipitation reaction, under certain conditions, two distinct zones may develop: one containing a mineral phase (crystalline or amorphous) which is present as a thin layer on the grains of the porous medium, and one in which the mineral phase is completely dissolved. The boundary separating these zones is referred to as the dissolution (or precipitation) front, and is a typical example of a free boundary. In general, the dissolution front moves with a (constant or nonconstant) velocity which is less than the velocity of the fluid (or salinity) front.

Rubin [71] studied this problem in terms of a classically formulated initial-boundary value problem, i.e. with the explicit appearance of the dissolution front as a free boundary. The mathematical implications of this model are studied by Pawell & Krannick [65]

1.5.1   The mathematical model

We consider as solutes two species M_1 and M_2, for example ions, say M_1 being a cation and M_2 an anion. In addition, we assume a crystalline solid $\bar{M}_{12}$ to be present as a (very) thin layer at the surface of the grains of the porous medium. The latter allows to assume a constant water content Θ (= porosity), i.e. independent of the presence of the solid phase $\bar{M}_{12}$. M_1 and $M-2$ may precipitate at the grain surfaces to form $\bar{M}_{12}$, while $\bar{M}_{12}$ may dissolve to form M_1, M_2. The stoichiometry of such a reaction is given by

$$\bar{M}_{12} \rightleftharpoons nM_1 + mM_2, \tag{1.5.20}$$

where n, m denote positive numbers. If the participating species are ions, then n is the valence of M_2 and is m the valence M_1, implying electroneutrality of the fluid. Let the molar concentration of M_i ($i = 1, 2$) relative to the water volume be given by c_i (mM/cm^3), and let the molar concentration of $\bar{M}_{12}$ relative to the mass of the porous skeleton be given by c_{12} (mM/g). We only consider the physically realistic situation $c_1, c_2, c_{12} \geq 0$.

Under the assumption that the solid phase is spatially immobile, conservation of the corresponding total masses leads to a coupled set of partial differential equations:

$$\frac{\partial}{\partial t} \left(\Theta c_1 + n\rho c_{12} \right) - \mathrm{div}\left(\Theta D \mathrm{grad}\, c_1 - \mathbf{q}c_1 \right) = 0 \tag{1.5.21}$$

$$\frac{\partial}{\partial t} \left(\Theta c_2 + m\rho c_{12} \right) - \mathrm{div}\left(\Theta D \mathrm{grad}\, c_2 - \mathbf{q}c_2 \right) = 0 \tag{1.5.22}$$

where ρ denotes the bulk density (g/cm^3), D is the diffusion/dispersion tensor (cm^2/s) and $\mathbf{q}$ (cm/s) is the specific discharge vector. If we define

$$c := mc_1 - nc_2, \tag{1.5.23}$$

then the mass balance equations (1.5.21), (1.5.22) imply conservation of the quantity c

$$\frac{\partial}{\partial t} \left(\Theta c \right) - \mathrm{div}\left(\Theta D \mathrm{grad}\, c - \mathbf{q}c \right) = 0. \tag{1.5.24}$$

For the special case of an ionic binary reaction, c may be interpreted as follows: the valence of M_1 is $m\nu$ and the valence of M_2 is $n\nu$, where ν denotes a positive integer. If M_1 is a cation and M_2 an anion, then νc denotes the total positive electric charge of the fluid. With appropriate boundary and initial conditions, equation (1.5.24) can be solved (at least numerically) and thereby we consider $c = c(\mathbf{x}, t)$ as a known quantity. This allows to reduce the number of unknowns by one, by setting

$$c_2 = \frac{1}{n}(mc_1 - c). \tag{1.5.25}$$

The positivity requirement of a solution of equations (1.5.21), (1.5.22), i.e. $c_1 \geq 0, c_2 \geq 0$, implies

$$c_1 \geq \left(\frac{c}{m} \right)_+, \tag{1.5.26}$$

where $u_+ = u$ for $u \geq 0$ and $u_+ = 0$ for $u < 0$.

The dissolution/precipitation reaction is assumed to satisfy the rate equation

$$\rho \frac{\partial c_{12}}{\partial t} = \Theta k^{\star}(r_p - r_d), \tag{1.5.27}$$

where r_d and r_p (mM/cm^3) respectively denote the dissolution and precipitation rates relative to the water volume and k^* (s^{-1}) is a rate parameter. At equilibrium, i.e. in the limit $k^* \to \infty$, equation (1.5.27) reduces, at least formally, to

$$r_d = r_p. \tag{1.5.28}$$

With respect to r_d and r_p we make the following general remarks, see e.g. Snoeyink & Jenkins [76] or Walton [78]:

- the activity of the solid is a positive constant k_d

$$r_d = k_d \quad \text{provided} \quad c_{12} > 0 \tag{1.5.29}$$

- the precipitation rate is given by the mass action law, i.e.

$$r_p = k_p \, r(c_1, c_2), \tag{1.5.30}$$

where the function r is a smooth nonnegative nonlinearity (for $c_1, c_2 \geq 0$). An example is the thermodynamically ideal mass action law:

$$r(c_1, c_2) = c_1^n c_2^m \tag{1.5.31}$$

Thus, if $c_{12} > 0$, then in the non-equilibrium case we have

$$\rho \frac{\partial c_{12}}{\partial t} = \Theta k^* \left(k_p r(c_1, c_2) - k_d \right), \tag{1.5.32}$$

and consequently in case of equilibrium we have

$$r(c_1, c_2) = K \left(:= \frac{k_d}{k_p} \right). \tag{1.5.33}$$

Notice that (1.5.33) can be obtained either by setting $\partial c_{12} / \partial t = 0$ in (1.5.32) or by letting $k = \infty$ in (1.5.32). The condition $r(c_1, c_2) = K$ is referred to as saturation, $r(c_1, c_2) < K$ is undersaturation and $r(c_1, c_2) > K$ is oversaturation. Using (1.5.25), these inequalities can be written in c_1 alone, provided c is given. The concentration c_1 is called the solubility concentration if $r(c_1, 1/n(mc_1 - c)) = K$. Notice that, if $c_{12} = 0$, the concentrations c_1, c_2 are no longer determined. In order to include the case $c_{1,2} = 0$, we need to extend the definition of the dissolution rate, such that the equilibrium description (1.5.28) is able to satisfy all possible equilibrium states. Hence, for arbitrary $c_{12} \geq 0$ we require

$$\begin{aligned} &0 \leq r(c_1, c_2) \leq K &&\text{(either saturation or undersaturation)} \\ &c_{12} > 0 \Rightarrow r(c_1, c_2) = K &&\text{(saturation)} \\ &r(c_1, c_2) < K \Rightarrow c_{12} = 0 &&\text{(undersaturation, no solid present)} \end{aligned} \tag{1.5.34}$$

which is equivalent to (in a more compact notation)

$$\begin{aligned} &0 \leq r(c_1, c_2) \leq K, \quad c_{12} \geq 0 \\ &(K - r(c_1, c_2))c_{12} = 0 \end{aligned} \tag{1.5.35}$$

We can bring this in the form of (1.5.28) by writing

$$0 \in k_p r(c_1, c_2) - k_d H(c_{12}) \quad (\Leftrightarrow r(c_1, c_2) \in K H(c_{12})), \tag{1.5.36}$$

where H denotes the set-valued Heaviside graph, i.e. defined by

$$H(c_{12}) = \begin{cases} 1 & \text{for} \quad c_{12} > 0 \\ [0,1] & \text{for} \quad c_{12} = 0 \\ 0 & \text{for} \quad c_{12} < 0 \end{cases} \tag{1.5.37}$$

In particular, this description includes the well-known equilibrium solubility product

$$\text{if } c_{12} > 0, \text{ then } r(c_1, c_2) = K. \tag{1.5.38}$$

Moreover, for any possible choice of $H(0) = \alpha$, where $\alpha \in [0,1]$, (1.5.37) fixes $r(c_1, c_2) = \alpha K$ for $c_{12} = 0$.

When considering non-equilibrium we also have to allow for oversaturation and if $c_{12} = 0$, i.e. no solid phase present, precipitation can only occur in case of oversaturation. Guided by this and relation (1.5.36), Knabner et. al. [53]) propose the following non-equilibrium rate description

$$\rho \frac{\partial c_{12}}{\partial t} \in \Theta k^*(k_p r(c_1, c_2) - k_d H(c_{12})) \tag{1.5.39}$$

or equivalently

$$\rho \frac{\partial c_{12}}{\partial t} = \Theta k^*(k_p r(c_1, c_2) - k_d w), \tag{1.5.40}$$

where $w \in H(c_{12})$ which means

$$0 \leq w \leq 1 \text{ and } w = 1 \text{ for } c_{12} > 0. \tag{1.5.41}$$

Notice that this description includes the precipitation rate of (1.5.30) and the dissolution rate (1.5.29) for $c_{12} > 0$, but for c_{12}, an artificial dissolution rate $k_d w \leq k_d$ is allowed for in order to be compatible with the equilibrium conditions (1.5.34)/(1.5.36).

For convenience, we introduce the scaled variables:

$$u := c_1, \quad v := \frac{n\rho}{\Theta} c_{12}, \quad q := \frac{q}{\Theta}, \quad k := nk^* k_p \text{ and } K := \frac{k_d}{k_p} \tag{1.5.42}$$

and define the function g

$$g(c_1; c) := r\left(c_1, \frac{1}{n}(mc_1 - c)\right) = u^n \left(\frac{1}{n}(mu - c)\right)^m, \tag{1.5.43}$$

where we substituted (1.5.31) and used (1.5.25) to eliminate c_2. Substitution of (1.5.42) and (1.5.43) in equations (1.5.21), (1.5.24) and (1.5.40) (in a spatially one-dimensional domain) yields

$$\frac{\partial}{\partial t}(u + v) + q\frac{\partial u}{\partial x} - D\frac{\partial^2 u}{\partial x^2} = 0 \tag{1.5.44}$$

$$\frac{\partial v}{\partial t} = k\{g(u; c) - wK\} \tag{1.5.45}$$

$$0 \leq w(x, t) \leq 1, \text{ and } w(x, t) = 1 \text{ if } v(x, t) > 0 \tag{1.5.46}$$

for $-\infty < x < +\infty$, $t > 0$. The function c, i.e. the (scaled) excess (positive) charge distribution, satisfies the linear convection-diffusion equation

$$\frac{\partial c}{\partial t} + q\frac{\partial c}{\partial x} - D\frac{\partial^2 c}{\partial x^2} = 0 \tag{1.5.47}$$

for $-\infty < x < +\infty$, $t > 0$. Equations (1.5.44), (1.5.45) and (1.5.47) have to be supplemented by appropriate boundary/initial conditions. This will give the function c explicitly for all cases considered here.

This observation helps us to distinguish between two principal observations with respect to the initial conditions. Consider the (scaled) piecewise constant initial states:

$$u(x,0), v(x,0), c(x,0) = \begin{cases} u^*, v^*, c^* & \text{for} \quad x < 0 \\ u_*, v_*, c_* & \text{for} \quad x > 0 \end{cases} \tag{1.5.48}$$

These initial states implicitly define the boundary conditions at $x = -\infty$ and $x = +\infty$. Two distinct situations can be considered: a homogeneous charge distribution, i.e.

$$c^* = c_*, \quad \text{and therefore} \quad c(x,t) = c = \text{ constant}, \tag{1.5.49}$$

or a non-constant charge distribution

$$c^* \neq c_*. \tag{1.5.50}$$

In case of (1.5.49), the boundary(/initial) conditions are compatible in the sense that the displacing fluid has the same ionic composition as the resident fluid. Knabner et.al. [53] and Van Duijn & Knabner [25] proved that a homogeneous charge distribution is a necessary condition for the existence of traveling wave solutions of (1.5.44)-(1.5.47), and moreover, that the solutes have to participate in a dissolution reaction. In case of (1.5.50), the ionic composition of the invading fluid differs from the composition of the resident fluid, implying incompatible boundary(/initial) conditions.

We are particularly interested in solutions of (1.5.44)-(1.5.47) subject to (1.5.48), (1.5.50) in the presence of a dissolution front, i.e. a curve in the (x,t)-plane separating the region where $v = 0$ from the region where $v > 0$. To ensure that a dissolution front exists for all $t \geq 0$, we need that

$$v^* = 0 \quad \text{and} \quad v_* > 0. \tag{1.5.51}$$

By requiring (1.5.51), we assume the initial states to be in chemical equilibrium, i.e.

$$\left(\frac{c}{m}\right)_+ \leq u^* \leq u_S(c^*) \quad \text{and} \quad u_* = u_S(c_*), \tag{1.5.52}$$

where u_S is the scaled solubility concentration for a given value of c.

When advective transport dominates dispersive transport, it is reasonable to let $D \to 0$ in (1.5.44) and (1.5.47). This assumption neglects only certain smoothing effects, and therefore it emphasizes the influence of the chemical reactions in the solutions. Then, the initial value problem (1.5.44)-(1.5.47) reduces to

$$\frac{\partial}{\partial t}(u + v) + q\frac{\partial u}{\partial x} = 0 \tag{1.5.53}$$

$$\frac{\partial v}{\partial t} = k\{g(u;c) - wK\} \tag{1.5.54}$$

$$0 \leq w \leq 1 \quad \text{and} \quad w(x,t) = 1 \quad \text{if} \quad v(x,t) > 0 \tag{1.5.55}$$

$$\frac{\partial c}{\partial t} + q\frac{\partial c}{\partial x} = 0 \tag{1.5.56}$$

for $-\infty < x < +\infty$, $t > 0$, subject to (1.5.48). This hyperbolic initial value problem is known as a Riemann problem. We consider the analytical and numerical construction of solutions of this problem by means of the method of characteristics. The latter allows a nearly explicit solution, which provides both detailed quantitative and qualitative information about the structure of solutions.

The solution of equation (1.5.56) can be found directly, without a priori knowledge of the solutions u, v and w. It is given by the piston flow profile

$$c(x,t) = c_0(x - qt) = \begin{cases} c^* & \text{for} \quad x < qt \\ c_* & \text{for} \quad x > qt \end{cases} \tag{1.5.57}$$

where we assume that $c^* > c_*$, and consequently by virtue of (1.5.43), $u_S(c^*) > u_S(c_*)$ holds true.

1.5.2 Equilibrium

In the case of chemical equilibrium we replace the first order equation (1.5.54) by the equilibrium reaction

$$g(u;c) = wK, \tag{1.5.58}$$

which is equivalent to setting $k = \infty$ in equation (1.5.54). In that case, the Riemann problem reduces to

$$\frac{\partial}{\partial t}(u + v) + q\frac{\partial u}{\partial x} = 0 \tag{1.5.59}$$

$$g(u;c) = wK, \quad 0 \le w \le 1 \ \text{ and } \ w(x,t) = 1 \ \text{ if } \ v(x,t) > 0, \tag{1.5.60}$$

for $-\infty < x < +\infty$, $t > 0$, subject to (1.5.48). This simple case is well known in the chemical engineering literature and is a special case of Bryant et. al. [16]. We consider it for reference purposes.

With respect to the construction of solutions, two important observations can be made. The first one relates to (1.5.58) and states that if $v(x,t) > 0$ then $w = 1$, and thereby $g(u(x,t), c(x,t)) = K$. In addition, if $x > qt$ then $u(x,t) = u_S(c_*) = u_*$ and if $x < qt$ then $u(x,t) = u_S(c^*)$. The second one is the Rankine-Hugoniot shock condition for solutions of (1.5.59). This condition says that discontinuities (or shocks) in solutions of (1.5.59) propagate with speed

$$\text{speed} = \frac{[u]}{[u + v]}, \tag{1.5.61}$$

where the quantities between brackets denote the size of the jump discontinuity in u and v across the location of the shock.

If we now assume the existence of a dissolution front $x = s(t)$ such that

$$v(x,t) = \begin{cases} 0 & \text{for} \quad x < s(t) \\ > 0 & \text{for} \quad x > s(t) \end{cases} \tag{1.5.62}$$

then we expect on physical grounds that $s(t) \leq qt$ for $t > 0$. A straight forward mathematical reasoning, see Chapter 6, yields the same result, and moreover, the Rankine-Hugoniot condition leads to the important inequality

$$0 \leq \dot{s}(t) \leq q \ \text{ for } \ t > 0. \tag{1.5.63}$$

The ordering of the fronts and (1.5.60) imply

$$u(x,t) = \begin{cases} \leq u_S(c^*) & \text{for } -\infty < x < s(t) \\ u_S(c^*) & \text{for } s(t) < x < qt \\ u_S(c_*) & \text{for } qt < x < +\infty \end{cases} \tag{1.5.64}$$

The dissolution follows from (1.5.61): $s(t) = at$, where

$$a = \frac{u_S(c^*) - u^*}{u_S(c^*) - u^* + v_*} q \ \ (< q). \tag{1.5.65}$$

Across the salinity front, i.e. $x = qt$, v is constant, which is consistent with (1.5.61). A sketch of the level sets of concentrations in the (x,t)-plane is given in Figure 10.
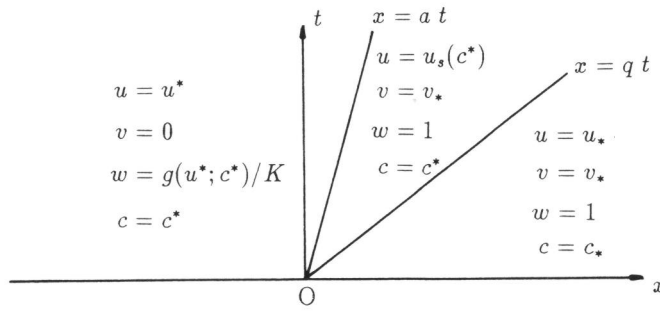
Figure 10. Level sets of concentrations at equilibrium.

1.5.3   Non-equilibrium

When the dissolution reaction is not at equilibrium, the first order reaction equation (1.5.54) has to be incorporated. This leads to a much more involved analysis. The object is again to find the location of the dissolution front $x = s(t)$ and the corresponding concentration profiles of $u(x,t)$ and $v(x,t)$. Therefore, we are going to consider the problem

$$\left. \begin{aligned} \frac{\partial u}{\partial t} + q\frac{\partial u}{\partial x} &= k\{K - g(u;c^*)\} \\ \frac{\partial v}{\partial t} &= k\{g(u;c^*) - K\} \end{aligned} \right\} \text{ for } s(t) < x < qt, \ t > 0 \tag{1.5.66}$$

such that

$$u(s(t),t) = u^*, \ \ v(s(t),t) = 0 \ \text{ and } \ v(qt,t) = v_*. \tag{1.5.67}$$

Note that, due to (1.5.61) the solid concentration v is continuous at $x = qt$, while the fluid concentration u is possibly discontinuous at the salinity front.

We solve the u-equation of (1.5.66) by the method of characteristics (MOC). The characteristics in the domain $\{(x, t) : s(t) < x < qt,\ t > 0\}$ are straight lines with slope q with respect to the t-axis. The characteristic through an arbitrary point (y, τ), i.e. the curve $x = y + q(t - \tau)$, intersects the dissolution front in a point $(s(t_0), t_0)$, which satisfies

$$s(t_0) = y + q(t_0 - \tau). \tag{1.5.68}$$

This intersection point is unique due to $\dot{s}(t) \leq q$. Integration of (1.5.66) along the characteristic
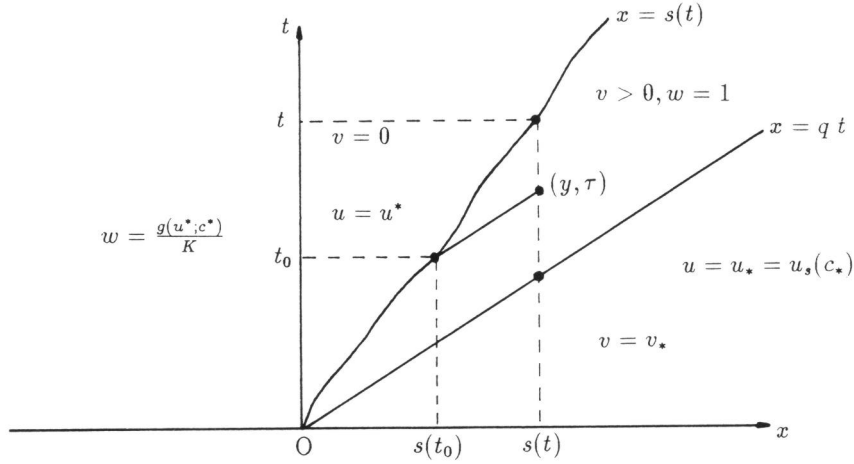
Figure 11. Dissolution front in the (x, t)-plane.

and using the boundary condition on u, i.e. (1.5.67), yields

$$\int_{u^*}^{u(y, \tau)} \frac{1}{k\{K - g(z; c^*)\}}\, dz = \tau - t_0(y, \tau) = \frac{y - s(t_0(y, \tau))}{q}. \tag{1.5.69}$$

If we set $y = s(t)$ for $t > 0$, then (1.5.69) takes the form

$$\int_{u^*}^{u(s(t), \tau)} \frac{1}{k\{K - g(z; c^*)\}}\, dz = \frac{s(t) - s(t_0)}{q} \quad \text{where } t_0 = t_0(s(t), \tau), \tag{1.5.70}$$

which implies

$$k\{K - g(u(s(t), \tau); c^*)\} = F(s(t) - s(t_0)) \quad \text{for } \frac{s(t)}{q} < \tau < t. \tag{1.5.71}$$

Here, the function F is a known function, determined by the rate function g, given by (1.5.43).

Next we integrate the v-equation of (1.5.66) and use the boundary condition on v (1.5.67), yielding

$$\int_{\frac{s(t)}{q}}^{t} F(s(t) - s(t_0))\, d\tau = v_* \quad \text{for } t \geq t_*, \tag{1.5.72}$$

where $t_* = \inf\{t > 0 : s(t) > 0\}$ and denotes a waiting time. The waiting time is a natural consequence of (1.5.72): letting $t \downarrow 0$ in (1.5.72) would make the left hand side of the integral zero while at the right hand side $v_* > 0$. The introduction of t_*, such that

$$s(t) = \begin{cases} 0 & \text{for} \quad 0 \le t \le t_* \\ > 0 & \text{for} \quad t > t_* \end{cases} \tag{1.5.73}$$

resolves this problem. By letting $t \downarrow t_*$ in (1.5.720 we conclude

$$t_* F(0) = v_*, \tag{1.5.74}$$

and combination of (1.5.69) and (1.5.71) yields for the waiting time

$$t_* = \frac{v_*}{F(0)} = \frac{v_*}{k\{K - g(u^*; c^*)\}}. \tag{1.5.75}$$

Note that if u^* equals the solubility concentration then $t_* = \infty$, which implies that the dissolution front remains stagnant.

Next we rewrite the integral (1.5.72) in terms of t_0 and do this by using (1.5.68). The result is

$$\int_0^t F(s(t) - s(t_0))\, dt_0 = v_* + \frac{1}{q}\int_0^{s(t)} F(z)\, dz, \tag{1.5.76}$$

where the left hand side can be rewritten by introducing the waiting time:

$$\int_0^t F(s(t) - s(t_0))\, dt_0 == t_* F(s(t)) + \int_{t_*}^t F(s(t) - s(t_0)) dt_0. \tag{1.5.77}$$

To summarize, we have obtained an integral equation from which the location of the dissolution front can be determined. The precise formulation is:

Let the waiting time be given by (1.5.75). Then find the function $s(t)$, satisfying (1.5.73) and the dissolution front equation (DFE)

$$(DFE) \begin{cases} \int_{t_*}^t F(s(t) - s(t_0))\, dt_0 = B(s(t)) \quad \text{for} \quad t \ge t_* \quad \text{where} \\ B(s(t)) := t_*\{F(0) - F(s(t))\} + \frac{1}{q}\int_0^{s(t)} F(z)\, dz. \end{cases} \tag{1.5.78}$$

Only in very special cases (DFE) can be solved in terms of an exact solution. In general we have to rely on numerical techniques to solve (DFE). An example of such a method is given in Chapter 6. There we show that (DFE) can be transformed into a standard linear Volterra integral equation of the first kind, from which many characteristic properties of the function $s(t)$ can be derived. Once $s(t)$ is known we go back to equation (1.5.69) and definition (1.5.71) to determine $u(x, t)$. The solid concentration $v(x, t)$ then follows from integration of (1.5.72).

Figure 12 shows the dissolution front in the (x, t)-plane for the nonlinear case $n = m = 1$. The corresponding breakthrough curves for u and the time evolution of the solid concentration v are respectively depicted in Figures 13 and 14. The numbers used in the computations are: $c_* = 0$, $c^* = u^* = 2.0 \cdot 10^{-4}$. In this case the solubility concentration is given by $u_S(c) = c/2 + 1/2\sqrt{c^2 + 4K}, i.e. u_S(c^* > u_S(c_*)$ and because $c_* = 0$ we have $K = u_*^2$. The waiting time turns out to be $t_* = 7108.0$ s. Notice in Figure 12 that indeed $\dot{s}(t) < q$. A qualitative comparison between the results of Willis & Rubin [83] and our results will be given in Chapter 6. However, a quantitative comparison is not possible because they allow for diffusion in their model and consider only equilibrium reactions.
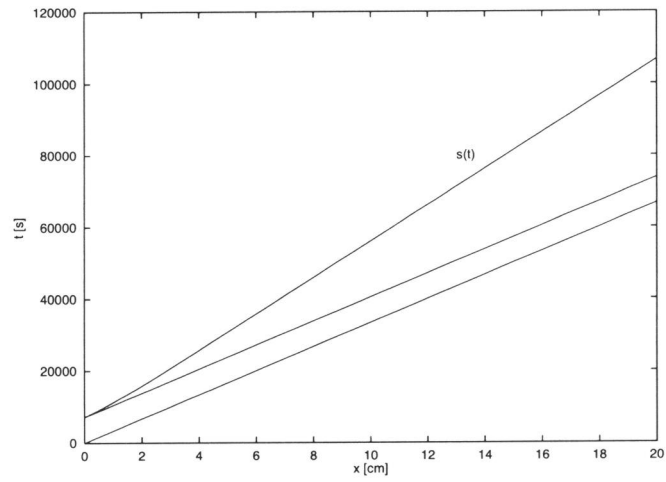
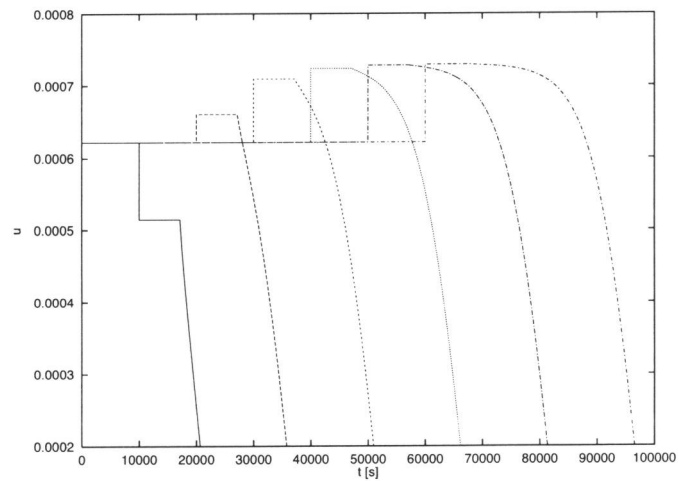Figure 12. Dissolution front in the (x, t)-plane for the nonlinear case $n = m = 1$.

Figure 13. Breakthrough curves of the fluid concentration at different positions. The observation points are: $x = 3.0, 6.0, .., 18.0$ cm. See Figure 12.
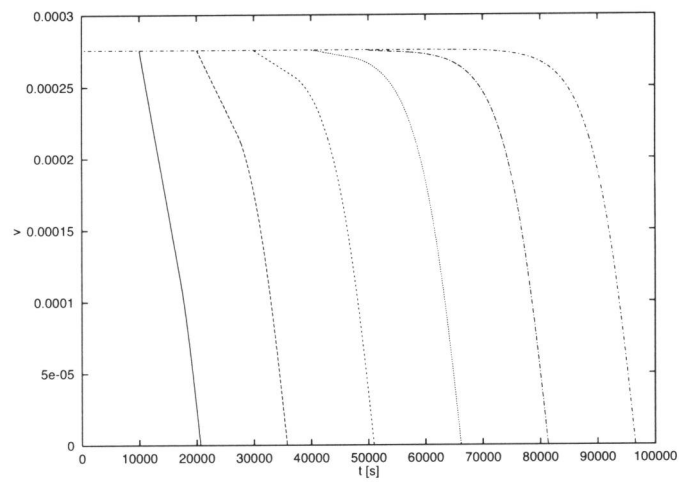
Figure 14. Time evolution of the solid concentration at different positions. The observation points are: $x = 3.0, 6.0, .., 18.0$ cm. See Figure 12.

Bibliography

[1] Barenblatt, G.I., Scaling, self-similarity and intermediate asymptotics, Cambridge Univ. Press (1996).

[2] Bear, J., Dynamics of fluids in porous media, Elsevier, New York, 1972

[3] Bhattacharya, R.N. & Gupta, V.K., A theoretical explanation of solute dispersion in saturated porous media at the Darcy scale, Water Res. Res. **10** (1983), p.p. 938-944.

[4] Baumann, R. & Moser. H., Modellierung der Meerwasserinvasion im Delta arider un semi-arider Gebiete am Beispiel des Nildeltas, Z. dt. geol. Ges. **143** (1992), p.p 316-324.

[5] Bar, G.E., Bingham, F.W. & Tierney, M.S., The use and misuse of scenarios in waste-disposal studies, Radionuclide release scenarios for geologic repositories, OECD, Paris (1981).

[6] Bear,J, Dynamics of fluids in porous media, Elsevier, New York (1972).

[7] Bear, J., Hydraulics of Groundwater, McGraw-Hill Book Company (1979)

[8] Bear, J. & Bachmat, Y., Transport phenomena in porous media - Basic equations, in J. Bear & M.Y. Corapcioglu (eds.), Fundamentals of transport phenomena in porous media, Martinus Nijhoff, Dordrecht (1984), p.p. 3-61.

[9] Bear, J. & Bachmat, Y., On the equivalence of areal and volumetric averages in transport phenomena, Adv. Water Resour. **6**(1), p.p. 59-62.

[10] Bear, J. & Dagan, G., The transition zone between fresh and salt water in a coastal aquifer, Prog. Rep. 2: A steady flow to an array of wells above the interface approximate (1963).

[11] Bear, J. & Dagan, G., Moving interface in coastal aquifers, Proc. ASCE **99**(HY4) (1964), p.p. 193-215.

[12] Bear, J. & Shapiro, A.M., On the shape of the non-steady interface intersecting discontinuities in permeability, Adv. Water Resources, Volume **7** (1984), pp. 106-112.

[13] Bear, J. & Verruijt, A., Modeling Groundwater Flow and Pollution, D. Reidel Publ. Comp., The Netherlands (1987).

[14] Ben-Salah, M.D. Influence des contrastes de viscosité et de densité sur le déplacement en milieu poreux de deux fluides miscibles, Revue de l'Institut Francais de Petrole (1965), 1237-1255.

[15] Bringham, W.E., Reed, P.W. & Dew, J.N., Experiments on mixing during miscible displacements in porous media, Soc. Petrol. Engng. J., March (1961), p.p. 1-8.

[16] Bryant, S.L., Schechter, R.S. & Lake, L.W., Mineral sequences in precipitation/dissolution waves, AIChE Journal **33** (1987), p.p. 1271-1287.

[17] Bues, M.A., Aachib, M. & Zilliox, L., Indence of heterogeneities on pollutant transport - density and viscosity contrasts of the liquid phase - structure of solid matrix, Contaminant transport in groundwater, ed. H.E. Kobus & W. Kinzelbach (1990), p.p. 251-257.

[18] Chan Hong, J.R., Van Duijn, C.J., Hilhorst, D. & Van Kester, J., The interface between fresh and salt groundwater : a numerical study, IMA J. of Appl. Math. (1989), 42, 299-316.

[19] Chorin, A.J. & Mardsden, J.E., A mathematical introduction to fluid mechanics, third e.d., Springer-Verlag (1992).

[20] Davis, S.N. & De Wiest, R.J.M., Hydrogeology, John Wiley ans Sons (1966).

[21] Dupaix, C., Hilhorst, D. & Scheid, J.F., On a dissolution-growth problem with surface tension : a numerical study, to appear.

[22] Vann Duijn, C.J. $ De Josselin De Jong, G., Free boundary problems in fresh-salt groundwater flow, In Summer School on Flow and Transport in Porous Media, Beijing, China, 8-26 August 1988, Editor: Xiao Shutie, World Scientific.

[23] Van Duijn, C.J, Peletier, L.A. & Schotting, R.J., On the analysis of brine transport in porous media, Europ. Journ. of Appl. Math. Vol **4** (19 93), 271-302.

[24] Van Duijn, C.J. & Floris, F.J.T., Mathematical analysis of the influence of power-law fluid rheology on a capillary diffusive zone, J. Pet. Sc. Eng. **7** (1992), p.p. 215-237.

[25] Knabner, P. & Van Duijn, C.J., Travelling wave behaviour of crystal dissolution in porous media flow, Euro. Jnl. Appl. Math., **8** (1997), p.p. 49-72.

[26] Ene, H.I. & Sanchez-Palencia, E., Equations et phénomenes de surface pour l'écoulement dans un modèle de milieu poreux, J. Mécan. **14** (1975), p.p. 73-108.

[27] Freeze, R. A. & Cherry, J.A., Groundwater, Prentice-Hall, Inc., USA (1979).

[28] Ghyben, W.B., Nota in verband met de voorgenomen putboring nabij Amsterdam, Tijdschrift van het Koninklijk Inst. van Ing. (1888).

[29] Gray, W.G.A., A derivation of the equations for multi-phase transport, Chem. Angr. Sci. **30** (1975), p.p. 229-233.

[30] Hassanizadeh, S.M. & Gray, W.G.A., General conservation equations for multi-phase systems: 1. averaging procedure, Adv. Water Resour. **2** (1979), p.p. 131-144.

[31] Hassanizadeh, S.M. & Gray, W.G.A., General conservation equations for multi-phase systems: 2. mass, momenta, energy and entropy equations, Adv. Water Resour. **2** (1979), p.p.191-203.

[32] Hassanizadeh, S.M. & Gray, W.G.A., General conservation equations for multi-phase systems: 3. constitutive theory for porous media flow, Adv. Water Resour. **3** (1980), p.p. 25-40.

[33] Hassanizadeh S.M. & Leijnse, A., On the modeling of brine transport in porous media, Water Resour. Res., **24** (1988), pp. 321-330.

[34] Sverdrup, H.U., Johnson, M.W. & Fleming, R.H., The Oceans (1942)

[35] Hassanizadeh, S.M. & Leijnse, Anton, A non-linear theory of high-concentration-gradient dispersion in porous media, Adv. Water Resour. ,Vol. **18** (1995), pp. 203-215

[36] Hassanizadeh, S.M., Leijnse, A., De Vries, W.J. & Stapper, R.A.M., Experimental study of brine transport in porous media, Report 728514005, RIVM, Bilthoven, The Netherlands, 1990.

[37] Hassanizadeh, S.M., Derivation of basic equations of mass transpo rt in porous media. Part 1. Macroscopic balance laws, Adv. Water Resour. **9** (1986), p.p. 196-206

[38] Henry, H.R., Salt water intrusion into coastal aquifers, Intern. Assoc. Sci. Hydrol, Publ 52 (1960), p.p. 478-487.

[39] Herzberg, A., Die Wasserversorgung einiger Nordseebader, J. Gasbeleucht. Wasserversorg **44** (1901), p.p. 815-819.

[40] Holzbecher, E. & Baumann, R., Numerical simulations of seawater intrusion into the Nile Delta aquifer, Computational Methods in Water Resources X, A. Peters et.al. (eds.), Kluwer Acad. Publ. the Netherlands (1994), p.p. 1001-1018.

[41] Hornung, U., Jäger, W. & Mikelić, A., Reactive transport through an array of cells with semi-permeable membranes,

[42] Hornung, U. & Jäger, W., Diffusion, convection, adsorption and reaction of chemicals in porous media, J. Diff. Equat. **92** (1991), p.p. 199-225.

[43] Hornung, U., Homogenization of miscible displacement in unsaturated soils, G. Dal Maso, G.F. Dell'Antonio (eds.), Composite media and homogenization theory, Progress in nonlinear differential equations and their applications, Birkhäuser, Boston (1991), 143-153.

[44] IAEA, Site selection factors for repositories of solid high-level and alpha-bearing wastes in geological formations, Techn. Rep. No 177 (1977), IAEA, Vienna.

[45] Hubbert, M.K., The theory of groundwater motion, J. Geol. **48** (1940), p.p. 785-944.

[46] De Josselin De Jong, G., The simultaneous flow of fresh water in aquifers of large horizontal extension determined by shear flow and vortex theory, Proceedings Euromech. **143** (1981) (eds A. Verruijt & F.B. J. Barends), Balkema Rotterdam, pp. 132-149.

[47] De Josselin De Jong, G., Singularity distributions for the analysis of multiple flow through porous media, J. Geophys. Res. **65** (1960), p.p. 3739-3758.

[48] Kashef, A., Saltwater intrusion in the Nile Delta, Groundwater **21**(2) (1983), p.p. 160-167.

[49] HYDROCOIN, Swedish Nuclear Inspectorate, An international proje ct for studying groundwater hydrology modeling strategies, Level 1 Final Report: Verification of groundwater flow ,odels, Case 5. Swedish Nucl. Insp., Stockholm (1986)

[50] Keller, J.B., Darcy's law for flow in porous media and the two-space method, R.L. Sternberg (ed.) Nonlinear partial differential equations in engineering and applied sciences, Dekker (1980), p.p. 429-443.

[51] Kempers, L.J.T.M., Effects of fluid properties on hydrodynami c dispersion: comparison of analytical models to numerical simulations, Proc. 1s t SPE/IMA Europ. Conf. Mathematics of Oil Recovery, Cambridge, UK, 25-27 July 19 89.

[52] Kempers, L.J.T.M., Dispersive mixing in stable and unstable m iscible displacements, PhD thesis Delft University of Technology, The Netherland s, 1991.

[53] Knabner, P, Van Duijn, C.J. & Hengst, S., An analysis of crystal dissolution fronts in flows through porous media. Part 1: Compatible boundary conditions, Adv. in Water Resour., **18**(3) (1995), p.p.171-185.

[54] Kolditz, O., Ratke, R., Diersch, H.G. and Zielke, W., Coupled groundwater flow and transport: 1. Verification of variable density flow and transport models, Adv. Water Resour. **21**(1) (1998), p.p. 27-46

[55] Kröhn, K.P., & Zielke, W, FE-Simulation von Transportvorgängen im klüftigen Gestein., Deutsche Gewässerkundliche Mitteilungen **35**(3-4) (1991), p.p. 82-88

[56] Landau, H.G., Heat conduction in a melting solid, Q. Appl. Math . **7** (1950), 81-94

[57] Lerat, A. & Peyret, R., Sur le chois de schémas aux différences finies du second ordere fournissant des profiles de choc sans oscillations. C.R. Acad. Sci. Paris **277** (1973), pp. 363-366.

[58] List, E.J., The stability and mixing of a density-stratified horizontal flow in a porous medium, Rep. KH-R-11, Calif. Inst. of Technology, Pasadena (1965).

[59] Marle, C.M., On macroscopic equations governing multi-phase flow with diffusion and chemical reactions in porous media, Int. J. Eng. Sci. **20** (1982), p.p. 643-662.

[60] Mikelić, A. & Aganović, I. , Homogenization of stationary flow of miscible fluids in a domain with a grained boundary, SIAM J. Math. Anal. **19** (1988), p.p. 287-294.

[61] Moser, H, Einfluss der Salzkonzentration auf die hydrodynamische Dispersion im porösen Medium, Mitteilung Nr. 128, Technische Universität Berlin (Ph.D. thesis), 1995.

[62] Meirmanov, A.M., The stefan problem, De Gruyter expositions in mathematics, Berlin-New York (1992).

[63] Mises, R. Von & K.O. Friedrichs, Fluid dynamics, Applied mathem atics series 5, Springer, New York (1977), 171

[64] Oldenburg, C.M. & Pruess, K., Dispersive transport dynamics in a strongly coupled groundwater-brine flow system, Wat. Resour. Res. **31** (2) (1995), p.p. 289-302

[65] Pawell,A. & Krannich, K.D., Dissolution effects arising in transport in porous media which affect a chemical equilibrium. (Unpublished)

[66] Pedersen, A. & Lindstrom, J., Selection of release scenarios for a Danish waste repository in a salt dome, Radionuclide release scenarios for geologic repositories, Proceedings of the NEA Workshop, Paris, 8-12 September 1980.

[67] Peletier, L.A. $ Van Duijn, C.J., Asymptotic behaviour of solutions of nonlinear diffusion equations, Arch. Ration al Mech. Anal. **65** (1977), p.p. 363-377.

[68] Pinder, G.F. & Cooper, H.H., A numerical technique for calculating the transient position of the salt water front, Water Resour. Res. **6** (1970), p.p. 875-882.

[69] Pfannkuch, H. O., Contribution á l'étude des déplacements de fluides miscibles dans un milieu poreux, Revue de l'Institut Francais du Pétrole, Vol. **18** (1963), pp. 215-270.

[70] Roxburgh, I.S., Geology of high-level nuclear waste disposal: An introduction, Chapman and Hall London New York (1987).

[71] Rubin, J, Transport of reacting solutes in porous media: Relation between mathematical nature of problem formulation and chemical nature of reactions, Water Resour. Res. **19** (1983), p.p. 1231-1252.

[72] Scheid, J.F., Etude théorique et numérique de l'évolution morphologiq ue d'interfaces, Ph.D. thesis, Orsay 1994.

[73] Scheidegger, A.E., The physics of flow through porous media, 2nd ed., Univ. of Toronto Press (1960).

[74] Segol, G. & Pinder, G.F., Transient simulation od salt water intrusion in southeastern Florida, Water Resour. Res. **12** (1976), p.p. 65-70.

[75] Slobold, R.L. & Howlett, W.E., Effects of gravity segregation in laboratory studies of miscible displacement in vertical unconsolidated porous media, Soc. Petrol. Engng. J., March (1964), p.p. 1-8.

[76] Snoeyink, V.L. $ Jenkins, D., Water Chemistry, John Wiley, New York USA (1980).

[77] Tartar, L., Incompressible fluid flow in a porous medium - convergence of the homogenization process, E. Sanchez-Palencia (eds.), Non-homogeneous media and vibration theory, Lecture notes in physics **127** Springer, Berlin (1980), p.p. 368-377.

[78] Walton, A.G., The formation and properties of precipitates, Wiley Interscience, New York USA (1967).

[79] Whitaker, S., Flow in porous media I: A theoretical derivation of Darcy's law, Transp. Porous Media, **1** (1986), p.p. 3-25.

[80] Whitaker, S., Flow in porous media II: The governing equations for immiscible, two-phase flow, Transp. Porous Media, **1** (1986), p.p. 105-125.

[81] Whitaker, S., Flow in porous media III: Deformable media, Transp. Porous Media, **1** (1986), p.p. 127-154.

[82] De Wiest, R.J.M., Geohydrology, John Wiley and Sons (1965).

[83] Willis C. & Rubin, J., Transport of reacting solutes subject to a moving dissolution boundary: Numerical methods and solutions, Water Resour. Res. **23**(8) (1987), p.p. 1561-1574.

[84] Vita-Finzi, C., Rates of holocenic folding in the coastal Zagros near Bandar Abbas, Iran, Nature **278** (1979), p.p. 632-633.

[85] Voss, C.I. & Souza, W.R., Variable density flow and solute trans port simulation of regional aquifers containing a narrow freshwater-saltwater transition zone. W ater Resour. Res. **23**(10) (1987), p.p. 1851-1866.

[86] Zhang, H.F., Nonlinear degenerate diffusion problems, PhD thesis, Delft University of Technology, The Netherlands.

[87] Zijl, W. & Nawalaney, M., Natural groundwater flow, Lewis Publishers USA (1993).

Chapter 2

Brine transport: similarity solutions

2.1 Introduction

Recently *Hassanizadeh and Leijnse, [1988] [1990] [1995]* revisited the theory of brine transport in porous media, designed numerical codes and did experiments in the laboratory. They raised the question whether (semi-) analytical solutions of the governing equations could be obtained under certain boundary and initial conditions. This question initiated our mathematical study and the results are published in the mathematics literature *[Van Duijn et.al.,1992]*. Because the subject of brine transport is still of current interest in the hydrological literature and the availability of analytical work in this field is poor, we decided to make the mathematical results more accessible for non-mathematicians and wrote this paper. The material has been extended with new results and the emphasis is now on the construction of semi-explicit self similar solutions.

Brine is water containing a high concentration of salt. In an almost saturated brine the *mass fraction* (ω), which is defined as the mass concentration of the salt over the density of the brine, can reach 0.26. This corresponds to a brine density of approximately 1200 kg/m^3. For sea water $\omega = 0.04$ corresponding to a fluid density of 1025 kg/m^3. Mass fraction and density are related by an equation of state, which has been empirically determined. Brines are found in surface waters, such as the Dead Sea, and in groundwater near salt domes *[Glasbergen, 1981]*. These are geological structures in the subsurface consisting of vertical cylinders of salt, a kilometer or more in diameter, embedded in horizontal or inclined strata. Salt domes are potential places for storage of nuclear waste *[Roxburgh, 1987]*, and it is of practical importance to know the flow of the groundwater around them.

Any model for fluid flow and salt transport in a porous medium must contain the mass balance equations for the fluid and the salt, and Darcy's law. The specific model we propose to study uses the complete fluid balance equation *[Hassanizadeh & Leijnse, 1988]*

$$\phi \frac{\partial \rho}{\partial t} + \text{div} \left(\rho \mathbf{q} \right) = 0, \qquad (2.1.1)$$

where ϕ denotes the porosity of the medium, ρ the fluid density and $\mathbf{q}$ the specific discharge vector. Introducing the material derivative

$$\frac{D}{Dt} = \frac{\partial}{\partial t} + \frac{\mathbf{q}}{\phi} \cdot \text{grad}, \qquad (2.1.2)$$

in the balance equation yields

$$\frac{\phi}{\rho} \frac{D\rho}{Dt} + \text{div} \mathbf{q} = 0. \qquad (2.1.3)$$

49

This expression shows that density variations may affect the compressibility of the fluid, which in turn can cause an additional movement of the fluid. To make this effect explicit is one of the goals of this study.

In this paper we intend to employ mainly analytical techniques. Therefor we are forced to restrict ourselves in the choice of flow problems. Inspired by earlier work of *de Josseling de Jong & van Duijn [1986]* we shall analyze two simplified cases denoted by Problem I and Problem II. Problem I describes the mixing of fresh water and brine, originally separated and parallel flowing, due to transversal dispersion. Problem II relates to the flow of groundwater along the surface of a salt dome. A sketch of the corresponding initial and boundary conditions is given in Figure 1. In Problem I the flow domain is unbounded above and below. Initially, say at $t = 0$,

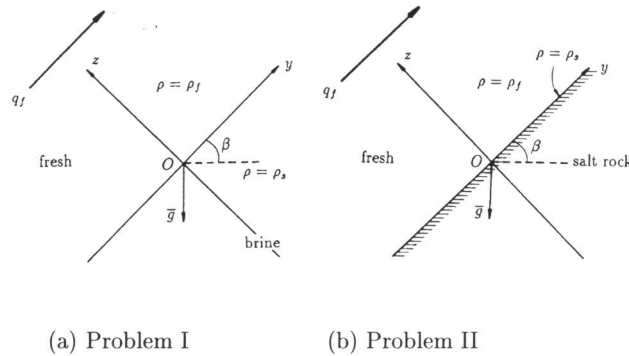(a) Problem I   (b) Problem II

Fig 1. Initial and boundary conditions

the region above the plane $\{z = 0\}$ is filled with fresh water and the brine fills the region below it. In this case one has to specify the specific discharge either as $z \to +\infty$ or as $z \to -\infty$. Here we shall adopt the former, and fix $\mathbf{q} \to (q_f, 0)$ as $z \to +\infty$, where q_f is a given constant.

In Problem II the flow domain consists of the upper half space $\{z > 0\}$ and is bounded below by an impermeable salt rock. Again at $t = 0$, fresh water occupies the region $\{z > 0\}$ while the salt from the rock ensures that $\rho = \rho_s$ (mass density of saturated brine) along the boundary $\{z = 0\}$. Here we can only specify the y-component of the specific discharge at $z = +\infty$, because the z-component is determined by a second boundary condition, as explained in Section 3, at the surface of the rock. In both problems the y-coordinate ranges from $-\infty$ to $+\infty$.

These problems are chosen because they admit similarity. This means that the underlying partial differential equations can be reduced to ordinary differential equations by introducing an appropriate similarity variable ($z/\sqrt{t}$ in Figure 1). This makes the analysis tractable, yielding semi-explicit results. The mathematical justification of the results is given elsewhere [*Van Duijn et.al., 1992*]. As a consequence of the analysis we can quantify the effect of the additional brine transport due to the fluid compressibility for Problem I and II, where in particular the latter is relevant to understand the flow near salt domes.

Among recent papers focusing on brine transport we mention [*Oldenburg and Pruess,1995; Carey et al.,1995; Herbert et al.,1988; Hassanizadeh and Leijnse, 1995*]. Numerical codes [*Hassanizadeh and Leijnse,1990 and 1988*] are developed to simulate flow of groundwater containing high salt concentrations. In general it is hard to compare numerical results with experimental

data because the availability of brine experiments is poor. However our analytical results can be used to verify the accuracy of numerical codes [*HYDROCOIN, 1986, Hassanizadeh, 1990*]. *Herbert et.al. [1988]* stresses the importance of analytical work on this subject.

Hassanizadeh and Leijnse [1995] reported on column tests of brine displacing fresh water in a porous medium. They showed that the dispersivity of brine decreases when the relative density difference between brine and fresh water increases and resolved this problem by introducing a nonlinear form of Fick's law. *Carey et al.[1995]* suggest a density dependent diffusivity/dispersivity. Although these results are interesting we shall confine ourselves to the classical formulation of Fick's and Darcy's law in this paper.

In Section 2 we formulate the mathematical model in general terms and in Section 3 we define the two specific problems (I and II). Dimensionless variables are introduced in Section 4. In Section 5 we discuss properties and construction of self similar solutions. Numerical procedures and results are given in Section 6 while asymptotic results for small relative density difference, yielding approximately div(**q**) = 0, can be found in Section 7. The simultaneous transport of brine and dissolved radionuclides is the subject of Section 8. In Section 9 we discuss the results and Section 10 contains the conclusions.

2.2 The mathematical model

Since this paper focuses on analytical aspects of subsurface brine transport, we shall impose simplifying restrictions on the properties of the porous medium and flow. With respect to the porous medium we assume that it is homogeneous and isotropic, characterized by a constant porosity ϕ and intrinsic permeability κ. With respect to the flow we shall consider the two specific cases which are introduced in Section 1 and about the fluid, with density ρ and salt mass fraction ω, we assume that the dynamic viscosity μ does not depend on ω and is constant. Assuming a Fickian type of dispersion/diffusion term in the salt mass flux and restricting ourselves to the conventional form of the momentum balance equation, we obtain the following equations for transport of brine [*Hassanizadeh & Leijnse, 1986*]:

Mass balance of the fluid

$$\phi\frac{\partial \rho}{\partial t} + \text{div}(\rho\mathbf{q}) = 0; \tag{2.2.1}$$

Mass balance of the salt

$$\phi\frac{\partial \rho\omega}{\partial t} + \text{div}(\rho\omega\mathbf{q} - D\rho\text{grad}\omega) = 0; \tag{2.2.2}$$

Darcy's law

$$\frac{\mu}{\kappa}\mathbf{q} + \text{grad}p - \rho\mathbf{g} = 0; \tag{2.2.3}$$

Equation of state

$$\rho = \rho_f e^{\gamma\omega}. \tag{2.2.4}$$

Here $\mathbf{q} = (q_y, q_z)$ denotes the specific discharge, p the fluid pressure and $\mathbf{g} = (g_y, g_z)$ the acceleration of gravity. In the equation of state, where we disregard the effect of pressure variations on the fluid density, ρ_f is the density of the fresh water and γ is a constant ($\gamma = 0.6923 \approx \ln 2$)

obtained by curve fitting using a table from *Weast [1982]*. Following *Bear [1972]*, we use for the hydrodynamic dispersion tensor $D = (D_{ij})$ the expression

$$D_{ij} = \{\alpha_T|\mathbf{q}| + \phi D_{\mathrm{mol}}\}\delta_{ij} + (\alpha_L - \alpha_T)q_iq_j/|\mathbf{q}|, \qquad (2.2.5)$$

where α_L and α_T are positive constants with $\alpha_L > \alpha_T$. They are called the longitudinal and transversal dispersion length, and describe the spreading of solutes due to mechanical dispersion caused by randomness of the structure of the porous material and heterogeneities. Further D_{mol} denotes the effective molecular diffusivity, which incorporates the effect of tortuosity. Finally, δ_{ij} denotes the Kronecker δ and $|\cdot|$ the Eucidian norm in $\mathbf{R}^2$. For mathematical reasons we use in most of this paper (except in Section 9) the approximation

$$D_{ij} = \phi D\delta_{ij} \qquad (2.2.6)$$

where D is a positive constant. If α_L and α_T are small (fine granular, homogeneous material), then this approximation is justified for $D = D_{mol}$. However, if the influence of the heterogeneities is significant, then D in (2.2.6) accounts for dispersion in an averaged sense.

2.3   The flow problems

The object of any study of brine transport is to determine the specific discharge and density (or mass fraction of salt) of the fluid as a function of position and time. We will investigate here two specific problems. In Problem I, see Figure 1(a), we consider an unbounded flow domain above and below the $z = 0$ plane. Initially, at time $t = 0$ say, the region above this plane is filled with fresh water (density ρ_f) and the region below it with brine (density ρ_s). Since $\rho_s > \rho_f$, this leads to a stable salt distribution for all $t > 0$. As a boundary condition we impose that at large distance above the $z = 0$ plane, the flow is known (and given) and points into the y-direction:

$$\mathbf{q} \to q_f\mathbf{e}_y \;\; \text{as} \;\; z \to +\infty, \;\; \text{for all} \;\; t \geq 0. \qquad (2.3.1)$$

where q_f is a given constant and $\mathbf{e}_y$ the unit vector in the positive y-direction.

Studies of brine distributions in aquifers have shown that the zone between brine and fresh water is relatively narrow, in particular when the fluids are stagnant. If this situation is perturbed by draining fresh water we end up with a situation that can be represented schematically by Problem I.

In Problem II the flow domain occupies the half space $\{z > 0\}$, see Figure 1(b). In formulating this problem we have assumed the initial situation where, due to regional effects, fresh groundwater flows along the top boundary of a salt dome. As a result salt will dissolve from it. The physico-chemical processes that take place at a salt rock boundary are complex and difficult to model. For instance, the dissolution of salt creates a cap (residue) rock layer along the top of the salt dome. Geological studies, e.g. *Bornemann et al. [1986]*, estimate the growth of this layer to be 0.04 mm/year. Following *Hassanizadeh & Leijnse [1988]* we disregard this movement and assume that the mass fraction remains at all times at the maximal salt mass fraction of the saturated brine along the fixed boundary, i.e.

$$\omega = \omega_s \;\; \text{at} \;\; z = 0, \;\; \text{for all} \;\; t \geq 0. \qquad (2.3.2)$$

Further, the flux of salt entering the flow domain induces a movement of water. This leads to the additional boundary condition, see again *Hassanizadeh & Leijnse [1988]*,

$$(\mathbf{q} + \frac{D}{(1 - \omega_s)}\mathrm{grad}\omega) \cdot \mathbf{n} = 0 \;\; \text{at} \;\; z = 0, \;\; \text{for all} \;\; t \geq 0, \qquad (2.3.3)$$

where $\mathbf{n}$ denotes the outward normal at the boundary $\{z = 0\}$. As initial concentration we have $\rho = \rho_f$ or $\omega = 0$ everywhere in the flow region. At large distance above the $\{z = 0\}$ plane we now impose only the y-component of the flow, since the z-component will be determined by the problem. Thus we set

$$q_y \to q_f \text{ as } z \to +\infty, \text{ for all } t \geq 0. \tag{2.3.4}$$

In both problems the y-coordinate ranges from $-\infty$ to $+\infty$. Therefore we may look for a density and specific discharge depending only on the z-coordinate and time, i.e.

$$\rho = \rho(z, t) \text{ and } \mathbf{q} = \mathbf{q}(z, t). \tag{2.3.5}$$

Following *de Josseling de Jong & van Duijn [1986]* we use (2.3.5) and Darcy's law (2.2.3) to obtain a linear algebraic relation between the fluid density and the y-component of the specific discharge. This relation can be found by first taking the curl of (2.2.3):

$$\frac{\partial}{\partial z}\{q_y - \frac{\kappa}{\mu}\rho g_y\} - \frac{\partial}{\partial y}\{q_z - \frac{\kappa}{\mu}\rho g_z\} = 0, \tag{2.3.6}$$

and by substituting (2.3.5) into this expression. The result is

$$q_y - \frac{\kappa}{\mu}\rho g_y = q_y + \frac{\kappa}{\mu}\rho g \sin\beta = \text{constant in space}, \tag{2.3.7}$$

where β is the inclination of the $z = 0$ plane. To determine the constant in (2.3.7) we use the behavior of q_y and ρ at $z = +\infty$:

$$q_y(\infty, t) = q_f \text{ and } \rho(\infty, t) = \rho_f \text{ for all } t > 0. \tag{2.3.8}$$

This yields the relation

$$q_y = q_f - \frac{\kappa}{\mu}(\rho - \rho_f)g \sin\beta. \tag{2.3.9}$$

Thus in order to determine the pair $(\rho, \mathbf{q})$ from the differential equations with initial and boundary conditions, there remains, by virtue of (2.3.9), only to determine ρ and q_z. Using (2.3.9), the equations for these quantities reduce to

$$\phi\frac{\partial\rho}{\partial t} + \frac{\partial}{\partial z}(\rho q_z) = 0 \tag{2.3.10}$$

and

$$\phi\frac{\partial\rho\omega}{\partial t} + \frac{\partial}{\partial z}(\rho\omega q_z - D\rho\frac{\partial\omega}{\partial z}) = 0. \tag{2.3.11}$$

Combining these equations yields

$$\phi\rho\frac{\partial\omega}{\partial t} + \rho q_z\frac{\partial\omega}{\partial z} = \frac{\partial}{\partial z}(\rho D\frac{\partial\omega}{\partial z}) \tag{2.3.12}$$

and with the equation of state (2.2.4) we obtain

$$\phi\frac{\partial\rho}{\partial t} + q_z\frac{\partial\rho}{\partial z} = D\frac{\partial^2\rho}{\partial z^2}. \tag{2.3.13}$$

We use the coupled system (2.3.10) and (2.3.13) in our analysis. To determine ρ and q_z from this system we need to impose the initial and boundary conditions. In Problem I we look for a solution in the domain $\{(z,t) : -\infty < z < +\infty, t > 0\}$ subject to the initial condition

$$\rho(z,0) = \begin{cases} \rho_f & \text{for } z > 0 \\ \rho_s & \text{for } z < 0. \end{cases} \tag{2.3.14}$$

and boundary condition (2.3.1) for the flow

$$q_z(+\infty, t) = 0 \ \text{ for all } \ t \geq 0 \tag{2.3.15}$$

We note that a condition on the flow such as (2.3.15) is natural for the problem. Combining equations (2.3.10) and (2.3.13) gives the ordinary differential equation

$$\rho \frac{\partial q_z}{\partial z} + D \frac{\partial^2 \rho}{\partial z^2} = 0. \tag{2.3.16}$$

Thus knowing ρ, an additional condition on q_z is needed to determine the solution. The specific choice is arbitrary. In fact one could construct a solution corresponding to any given $q_z(+\infty, t)$. We also observe at this point that equation (2.3.16), when writing it in the form

$$\text{div}\mathbf{q} = \frac{\partial q_z}{\partial z} = -\frac{1}{\rho}\text{div}(D\text{grad}\rho), \tag{2.3.17}$$

clearly demonstrates the coupling between brine transport by diffusion/dispersion, creating a non-zero divergence in the flow field and hence fluid transport by specific discharge. Density gradients imply fluid movement and vice versa.

Problem II is solved in the domain $\{(z,t) : z > 0, t > 0\}$ where we impose initially

$$\rho(z,0) = \rho_f \ \text{ for } \ z > 0 \tag{2.3.18}$$

and along the boundary, see expressions (2.3.2) and (2.3.3)

$$\rho(0,t) = \rho_{sm} := \rho_f e^{\gamma \omega_s}, \tag{2.3.19}$$

and

$$q_z(0,t) = -\frac{D}{\gamma \rho_{sm}(1-\omega_s)} \frac{\partial \rho}{\partial z}(0,t), \tag{2.3.20}$$

for all $t > 0$. Here ρ_{sm} denotes the density of saturated brine. Boundary condition (2.3.3) relates the specific discharge to the spatial derivative of the fluid density at the salt rock boundary. Although no water is being produced along the salt rock boundary, a non-zero discharge exists along that boundary due to volume effects caused by high salt concentration gradients in the fluid.

2.4   Dimensionless variables

Before discussing equation (2.3.10) and (2.3.13) we introduce the dimensionless variables

$$\rho^* = \frac{\rho - \rho_f}{\tilde{\rho}_s - \rho_f}, \quad q_z^* = \frac{q_z}{\frac{\kappa}{\mu}\rho_f g}, \quad z^* = \frac{\frac{\kappa}{\mu}\rho_f g}{D}z, \quad t^* = \frac{(\frac{\kappa}{\mu}\rho_f g)^2}{\phi D}t \tag{2.4.1}$$

and

$$\varepsilon = \frac{\tilde{\rho}_s - \rho_f}{\rho_f},$$

(2.4.2)

where $\tilde{\rho}_s = \rho_s$ in Problem I and $\tilde{\rho}_s = \rho_{sm}$ in Problem II. In terms of these new variables the equations become (dropping again the asteriks notation)

$$\frac{\partial \rho}{\partial t} + \frac{\partial}{\partial z}(\rho q_z) + \frac{1}{\varepsilon}\frac{\partial q_z}{\partial z} = 0$$

(2.4.3)

and

$$\frac{\partial \rho}{\partial t} + q_z \frac{\partial \rho}{\partial z} = \frac{\partial^2 \rho}{\partial z^2}.$$

(2.4.4)

The rescaled initial and boundary conditions in Problem I are

$$\rho(z, 0) = \begin{cases} 0 & \text{for } z > 0 \\ 1 & \text{for } z < 0 \end{cases}$$

(2.4.5)

and

$$q_z(+\infty, t) = 0 \quad \text{for all } t > 0.$$

(2.4.6)

In Problem II the scaling (2.4.1),(2.4.2) leads to

$$\rho(z, 0) = 0 \quad \text{for } z > 0,$$

(2.4.7)

$$\rho(0, t) = 1 \quad \text{for } t > 0$$

(2.4.8)

and

$$q_z(0, t) = -\varepsilon K(\varepsilon)\frac{\partial \rho}{\partial z}(0, t),$$

(2.4.9)

where K(ε) is given by:

$$K(\varepsilon) = \frac{\rho_f}{\rho_{sm}}\frac{1}{\gamma(1 - \omega_s)} = \frac{1}{(1 + \varepsilon)(\gamma - \log(1 + \varepsilon))}.$$

(2.4.10)

Note that the relative density difference lies in the interval

$$0 < \varepsilon < e^{\gamma \omega_s} - 1 \approx 2^{\omega_s} - 1 \approx 0.2$$

(2.4.11)

for $\omega_s = 0.26$.

2.5 Self-similar solutions

Due to the nonlinear coupling between equations (4.3) and (4.4) it is not possible to find explicit, closed-form solutions of Problems I and II. Nevertheless, their special structure enables us to obtain much information concerning the qualitative behavior of the solutions and to obtain accurate approximations.

The key idea is to look for self-similar solutions, which reduce (4.3),(4.4) to a set of coupled ordinary differential equations with boundary conditions originating from (4.5)-(4.9). The transformed problems were studied in detail by *van Duijn et al. [1992]*. They considered fundamental questions related to existence and uniqueness of solutions, as well as their qualitative behavior.

With respect to the latter, they showed certain monotonicity properties of solutions and their asymptotic behavior for $|z| \to \infty$ and for $\varepsilon \downarrow 0$. Some of these results will be discussed here and in Section 7.

The similarity transformations for Problems I and II are given by

$$\eta = \frac{z}{\sqrt{t}} \tag{2.5.1}$$

and

$$\rho(z,t) = u(\eta) \quad \text{and} \quad q_z(z,t) = \frac{1}{\sqrt{t}} v(\eta) \tag{2.5.2}$$

This results in the set of differential equations

$$(uv)' + \frac{1}{\varepsilon} v' - \frac{1}{2} \eta u' = 0 \tag{2.5.3}$$

$$u'v - \frac{1}{2} \eta u' = u'' \tag{2.5.4}$$

where the primes denote differentiation with respect to η. The independent variable η ranges from $-\infty$ to $+\infty$ in Problem I and from 0 to $+\infty$ in Problem II.

The following boundary conditions for $u(\eta)$ and $v(\eta)$ in Problem I result from (4.5),(4.6) and are found to be

$$u(-\infty) = 1 \quad \text{and} \quad u(+\infty) = 0 \tag{2.5.5}$$

and

$$v(+\infty) = 0. \tag{2.5.6}$$

For Problem II we find from (4.7)-(4.9)

$$u(0) = 1 \quad \text{and} \quad u(+\infty) = 0 \tag{2.5.7}$$

and

$$v(0) = -K(\varepsilon)\varepsilon u'(0). \tag{2.5.8}$$

Equations (2.5.3) and(2.5.4) can be combined into:

$$u'' + (\frac{1}{2}\eta - v)u' = 0, \tag{2.5.9}$$

$$v' = -\frac{u''}{u + \frac{1}{\varepsilon}}. \tag{2.5.10}$$

Let us first discuss Problem I. We start with the important observation that solutions (u, v) of equations (5.9),(5.10) on $\mathbf{R}$ are invariant under linear shifts. By this we mean the following. For any given $a \in \mathbf{R}$, let

$$\overline{\eta} = \eta - a, \quad \overline{u}(\overline{\eta}) = u(\eta) \quad \text{and} \quad \overline{v}(\overline{\eta}) = v(\eta) - \frac{1}{2}a. \tag{2.5.11}$$

Then if $(u(\eta), v(\eta))$ solves (2.5.9) and (2.5.10) for $-\infty < \eta < +\infty$, than so does $(\overline{u}(\overline{\eta}), \overline{v}(\overline{\eta}))$ if we replace η by $\overline{\eta}$ in (2.5.9). This means that if $(u(\eta), v(\eta))$ is a solution for which $v(\pm\infty)$ exists, then by shifting η over a suitable distance a, we can reach any limiting value of $v(\eta)$, either at $\eta = -\infty$ or at $\eta = +\infty$. If we choose $a = 2v(+\infty)$ in (2.5.11) we can ensure that condition (2.5.6) is satisfied. This invariance property will be used in both the mathematical and numerical procedures for solving Problem I.

Before discussing the construction of solutions, we recall some a priori properties which give an idea about the qualitative behavior of the solution. We proved that

(i) $u'(\eta) < 0$ for all $-\infty < \eta < +\infty$

(ii) there exists $\eta_0 > 0$ such that $u''(\eta) < 0$ for $\eta < \eta_0$ and $u''(\eta) > 0$ for $\eta > \eta_0$

(iii) $v(\eta_0) = \frac{1}{2}\eta_0$ and $v'(\eta) > 0$ for $\eta < \eta_0$ and $v'(\eta) < 0$ for $\eta > \eta_0$

(iv) $u'(\eta) \to 0$ if $|\eta| \to \infty$

The first assertion implies that the brine concentration increases strictly with depth and is concave below the plane $z = \eta_0\sqrt{t}$ and convex above it. Also the z-component of the specific discharge has a maximum at $z = \eta_0\sqrt{t}$ of magnitude $q_z(\eta_0\sqrt{t}, t) = \frac{1}{2}\eta_0/\sqrt{t}$. The number η_0 plays a prominent role in simultaneous transport of brine and radionuclides, which will be explained in Section 8.

Next we turn to the solution procedure. As a first observation we note that equations (5.9)-(5.11) can be combined into a single equation with η missing. This equation, having the form

$$\frac{1}{2} + \left(\frac{u''}{u'}\right)' = -\frac{u''}{u + \frac{1}{\varepsilon}} \quad \text{with} \quad -\infty < \eta < +\infty, \tag{2.5.12}$$

needs three conditions to be solved uniquely. Two conditions are given by (5.5). As a third condition we take, for instance,

$$u(0) = \frac{1}{2}. \tag{2.5.13}$$

We outline below how to obtain a unique solution satisfying (5.12), (5.5) and (5.13) and how to obtain from that solution a corresponding $v = v(\eta)$ so that the pair (u, v) satisfies equations (5.3) and (5.4). This function v will not satisfy condition (5.6). To achieve that condition one applies the linear shift (5.11) with $a = 2v(\infty)$.

Equation (2.5.12) is of third order, nonlinear and defined on an unbounded domain. To tackle it directly is therefor not straightforward. As so often in mathematics, we solve problems by combining and applying what we already know. Also in this case. We will transform equation (2.5.12) into a second order equation on a finite domain, yielding a boundary value problem which is well-known in the mathematical literature. This transformation is achieved by taking u as the independent variable, which is allowed by the monotonicity of u, and by taking u' as the new independent variable. Thus setting

$$\eta = \eta(u) \quad \text{and} \quad y(u) = -u'(\eta(u)). \tag{2.5.14}$$

we obtain

$$y\{(1 + \varepsilon u)y'\}' = -\frac{1}{2}(1 + \varepsilon u), \quad 0 < u < 1 \tag{2.5.15}$$

In view of property (iv) we obtain for y the boundary conditions

$$y(0) = 0 \quad \text{and} \quad y(1) = 0. \tag{2.5.16}$$

By setting further

$$s = \frac{\log(1 + \varepsilon u)}{\log(1 + \varepsilon)} \quad \text{and} \quad z(s) = \frac{\varepsilon}{\log(1 + \varepsilon)} y(u) \tag{2.5.17}$$

we obtain the problem

$$(I') \begin{cases} -zz'' = \frac{1}{2}e^{2s\log(1+\varepsilon)}, \quad z > 0 \quad \text{for} \quad 0 < s < 1 \\ \\ z(0) = z(1) = 0. \end{cases} \tag{2.5.18}$$

which is well-known and arises in the study of self-similar solutions of nonlinear diffusion equations, see for instance *Esteban et.al. [1988]*,*van Duijn & Peletier [1977]* and *van Duijn & Floris [1991]*. In the context of nonlinear diffusion one calls equation (5.18) the flux equation, because it specifies the flux in terms of the concentration. One sees immediately (since $z > 0$) that

$$z''(s) < 0 \quad \text{for} \quad 0 < s < 1. \tag{2.5.19}$$

Less straightforward are the proofs of the properties

$$\lim_{s \downarrow 0} z'(s) = +\infty \quad \text{and} \quad \lim_{s \uparrow 1} z'(s) = -\infty, \tag{2.5.20}$$

which can be found in *van Duijn & Floris [1991]*. Knowing that a solution $z = z(s)$ of Problem I' exists and is unique, and knowing much about its qualitative behavior, one finds $y = y(u)$ from (5.17). Finally, the solution $u = u(\eta)$ satisfying (5.12),(5.5) and (5.13) is implicitly defined by

$$\eta(u) = \int_u^{\frac{1}{2}} \frac{1}{y(s)}\, ds \tag{2.5.21}$$

which results from integrating (2.5.14). The corresponding $v = v(\eta)$ is given by

$$v(\eta) = \frac{1}{2}\eta - y'(u(\eta)) \quad \text{for} \quad -\infty < \eta < +\infty \tag{2.5.22}$$

which follows from (2.5.9) and (2.5.14).

Since Problem II is defined on the semi-infinite interval $0 < \eta < +\infty$, we loose invariance property (2.5.11). But the other properties (i)..(iv) remain the same, when taking $0 < \eta < +\infty$, yielding a similar qualitative picture of the solution. The solution procedure proceeds along the same lines. It leads to the transformed problem

$$(II') \begin{cases} -zz'' = \frac{1}{2}e^{2s\log(1+\varepsilon)}, \quad z > 0 \quad \text{for} \quad 0 < s < 1 \\[2mm] z(0) = 0, \quad z'(1) = -Lz(1), \end{cases} \tag{2.5.23}$$

where L is a constant given by

$$L = K(\varepsilon)(1+\varepsilon)\log(1+\varepsilon) = \frac{\log(1+\varepsilon)}{\gamma - \log(1+\varepsilon)}. \tag{2.5.24}$$

The boundary condition at $s = 1$ is a direct consequence of condition (5.8). To return to $u = u(\eta)$, we first use again (5.17) to obtain $y = y(u)$ and then

$$\eta = \int_{u(\eta)}^1 \frac{1}{y(s)} ds \quad \text{for} \quad 0 < \eta < +\infty. \tag{2.5.25}$$

The corresponding $v = v(\eta)$ is obtained from (2.5.22).

2.6 Numerical procedures and results

The mathematical analysis has provided us with qualitative information about the structure of the solutions of Problem I and II. This information can be used to develop procedures to obtain accurate numerical solutions.

Starting point for both problems is the third order equation (2.5.12). We write this equation as a system of first order equations by setting

$$p = u, \quad q = u' \quad \text{and} \quad r = v. \tag{2.6.1}$$

Substitution in (5.12) yields

$$(S) \begin{cases} p' &= q \\ q' &= q(r - \dfrac{1}{2}x) \\ r' &= -\dfrac{q(r - \frac{1}{2}x)}{p + \frac{1}{\varepsilon}}. \end{cases} \tag{2.6.2}$$

To solve this system we impose three conditions at $\eta = 0$:

$$p(0) = u(0) = p_0, \quad q(0) = u'(0) = q_0, \quad r(0) = v(0) = r_0, \tag{2.6.3}$$

where $p_0 = 1/2$ (Problem I) or $p_0 = 1$ (Problem II), and where q_0 and r_0 are a priori unknown. They have to be determined from the boundary conditions (2.5.5) (Problem I) or from (2.5.7), (2.5.8) (Problem II).

Concerning Problem I, one approach is to apply a shooting procedure in the regions $\{\eta < 0\}$ and $\{\eta > 0\}$. Taking for (S) the initial values $p_0 = 1/2$ and q_0, r_0 arbitrary, one solves the equations for $\{\eta < 0\}$ and $\{\eta > 0\}$. The idea is to choose p_0 and q_0 such that

$$p(-\infty) = u(-\infty) = 1 \quad \text{and} \quad p(+\infty) = u(+\infty) = 0. \tag{2.6.4}$$

However, this procedure is not at all trivial because there are two degrees of freedom in the problem. Moreover it would be time consuming to compute accurate values for q_0 and r_0 by trail and error such that the correct limiting behavior for u at $\eta = +/-\infty$ is achieved.

An alternative approach is to determine q_0 and r_0 directly from Problem (I') by noting that

$$p_0 = -y(\frac{1}{2}) = \frac{\log(1 + \varepsilon)}{\varepsilon} z \left(\frac{\log(1 + \frac{\varepsilon}{2})}{\log(1 + \varepsilon)} \right) \tag{2.6.5}$$

and, using (2.5.8),

$$r_0 = -y'(\frac{1}{2}) = \frac{1}{1 + \frac{\varepsilon}{2}} z' \left(\frac{\log(1 + \frac{\varepsilon}{2})}{\log(1 + \varepsilon)} \right). \tag{2.6.6}$$

We find approximate values of the shooting parameters q_0 and r_0 by solving (I') numerically. We omit the details of the computations. Next equations (S) are solved using a fourth order Runge-Kutta method in the regions $\{\eta < 0\}$ and $\{\eta > 0\}$, subject to p_0, q_0 and r_0. This gives the solution $(u(\eta), v(\eta))$ of (5.9) and (5.10) which satisfies $u(0) = \frac{1}{2}$. It also provides us with the value of $v(+\infty) = r(+\infty)$ which we need to obtain the correct shift $a = 2v(+\infty)$ to satisfy boundary condition (2.5.6).

In all cases considered, i.e. for all relevant values of ε, we verified the boundary conditions $u(+\infty) = 0$ and $u(-\infty) = 1$. Up to a small error term these values are taken on by the numerical approximations. This serves as an independent check for the accuracy of the numerical procedure for Problem (I').

Figures 2 and 3 give the results of the numerical approximations of the similarity solutions $u(\eta)$ and $v(\eta)$ for different values of the relative density difference ε.
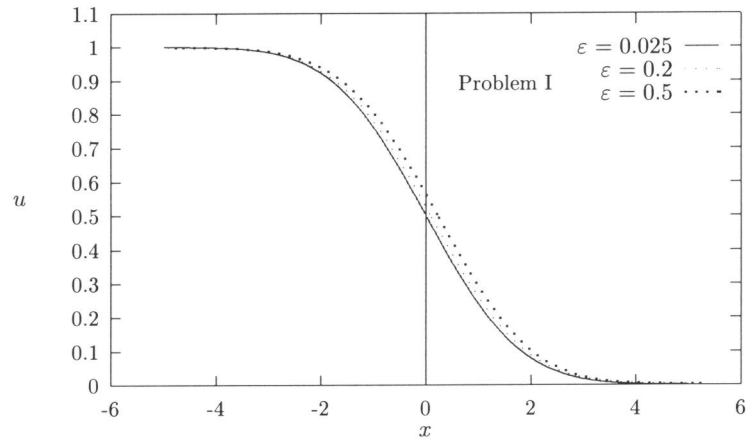
Figure 2. Numerical approximations of $u(\eta)$ for Problem I.
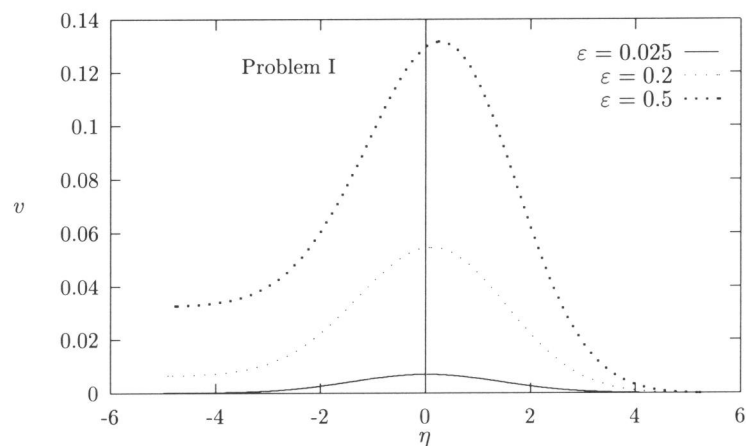
Figure 3. Numerical approximations of $v(\eta)$ for Problem I.

The value $\varepsilon = 0.025$ corresponds to sea water. This curve is hardly distinguishable from the curve for $\varepsilon = 0$ on the scale of Figure 2. The limit $\varepsilon \to 0$ is the so-called Boussinesq approximation or Boussinesq limit, see Section 7. The value $\varepsilon = 0.2$ corresponds with an almost saturated brine, while $\varepsilon = 0.5$ is chosen here to emphasize the effect. Observe that the numerical solutions satisfy the qualitative behavior discussed in Section 5.

Concerning Problem II we solve equations (S) for $\eta > 0$ subject to the initial conditions

$$\begin{aligned}
p(0) &= u(0) = 1, \\
q(0) &= u'(0) = q_0 < 0, \\
r(0) &= v(0) = -\varepsilon K(\varepsilon) q_0,
\end{aligned} \qquad (2.6.7)$$

where the last condition is a consequence of (2.5.8). This is a one-parameter shooting problem which is more straightforward and is solved without using Problem (II'). The object is to find

a approximate value of q_0 such that the boundary condition $u(+\infty)$ is satisfied. This can be achieved by starting the shooting procedure with an initial estimate for q_0 and check if the corresponding limiting behavior is satisfied at sufficiently large distance L from the origin. The problem is to determine an approximate value of q_0 such that the boundary condition $u(+\infty) = 0$ is satisfied. This can be achieved by starting the shooting procedure with an estimated value of q_0 and check if the corresponding limiting behavior is satisfied at a sufficiently large distance L from the origin. If $u(L) > \delta > 0$, where δ an a priori specified small error term, the estimated value of q_0 is decreased by a fixed amount Δq_0 and the shooting procedure is repeated. The step size Δq_0 remains fixed until, say after the n-the step, $u^n(L) < 0$. Now q_0^n is increased by the bisection of Δq_0, hence $q_0^{n+1} = q_0^0 - \Delta q_0(n - \frac{1}{2})$. If $u^{n+1}(L) > \delta$ or if $u^{n+1}(L) < 0$ we bistect the last alteration of q_0 again and obtain respectively : $q_0^{n+2} = q_0^0 - \Delta q_0(n - \frac{1}{4})$ or $q_0^{n+2} = q_0^0 - \Delta q_0(n - \frac{3}{4})$. This procedure is repeated until $0 \leq u(L) \leq \delta$. The number of steps depends on the quality of the initial guess of q_0 and the initial step size Δq_0.

Figure 4 shows the results of the iterative shooting procedure for the scaled density $u(\eta)$ for different ε-values. The corresponding scaled specific discharge distributions $v(\eta)$ are given in Figure 5. Notice that $v(0) \neq 0$. This is a consequence of boundary condition (5.8) at the salt rock/brine interface. Because u is a decreasing function we have $u'(0) < 0$, hence $v(0) > 0$, for all $\varepsilon > 0$.
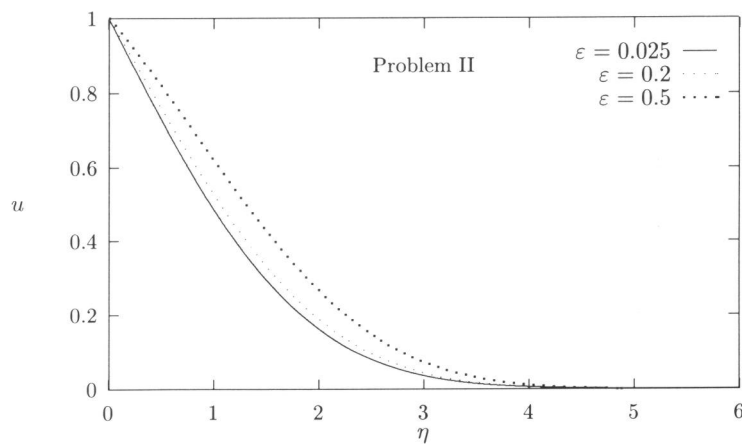
Figure 4. Numerical approximations of $u(\eta)$ for Problem II.
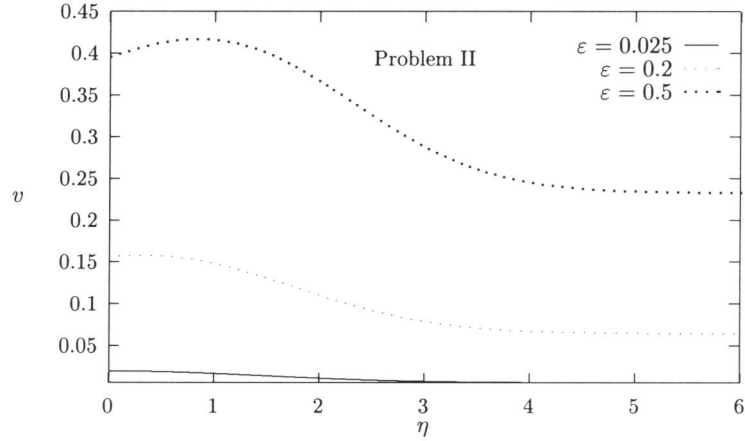
Figure 5. Numerical approximations of $v(\eta)$ for Problem II.

Figures 6 and 7 give the relative density $\rho(z,t) = u(z/\sqrt{t})$ and the unscaled specific discharge $q_z(z,t) = v(z/\sqrt{t})/\sqrt{t}$ at different time levels in the original variables. The other parameter values used in these examples are adopted from *Herbert et al. [1988]* and listed in Table 1.

Property	Value	Dimension
κ	10^{-12}	m^2
μ	10^{-3}	Pas
g	9.81	m/s^2
ϕ	0.3	–
ρ_f	1000	kg/m^3
D	10^{-9}	m^2/s

Table 1.
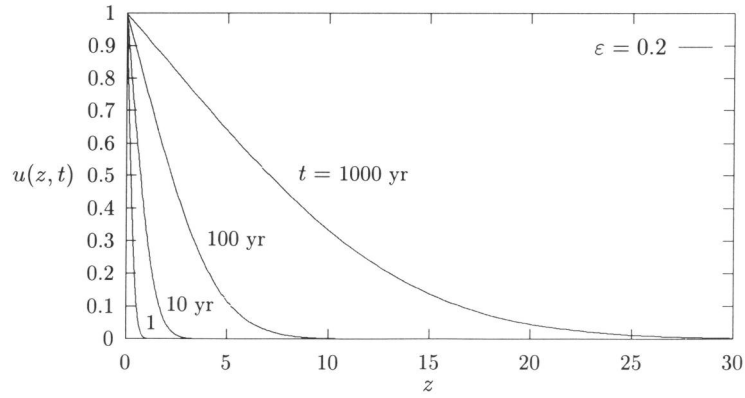
Figure 6. Brine density profiles at different times for $\varepsilon = 0.2$ in Problem II
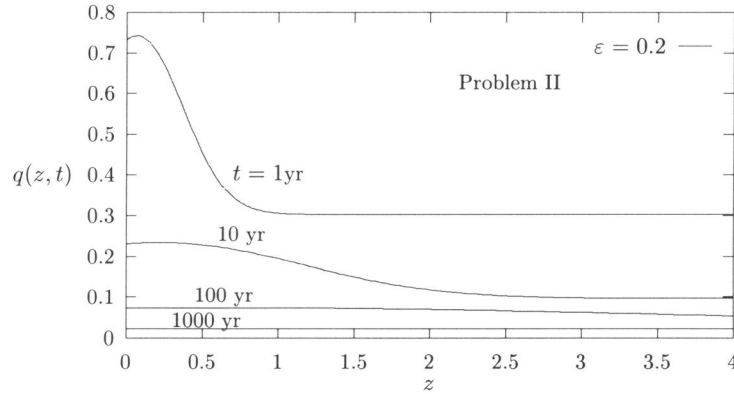
Figure 7. Specific discharge at different times for $\varepsilon = 0.2$ in Problem II.

Remark (Boundary Condition) If we impose, instead of (2.5.8), the condition $q_z(0,t) = 0$ for all $t > 0$ to express the assumption that the salt rock boundary is impervious, then the analysis yields $v(\eta) < v(0) = 0$ for all $\eta > 0$. An explanation for this behavior is that $q_z = 0$ at the boundary can only be maintained by a back flow coming from $+\infty$. We conclude that this is a physically unrealistic situation and that the no flow boundary is incompatible with the model discussed in this paper.

2.7 Approximate self similar solutions

In this section we give some results of a formal asymptotic analysis which can be found in detail in *van Duijn et al. [1992]*. The asymptotic analysis yields series expansions in terms of the relative density difference ε for the similarity solutions $(u(\eta), v(\eta))$ in both problems. When these expansions are truncated we obtain approximation formulas which can be of practical use to approximate $(u(\eta), v(\eta))$ up to a certain, known accuracy. To emphasize the dependence on ε, we denote the solutions by $(u_\varepsilon(\eta), v_\varepsilon(\eta))$. In the limit $\varepsilon \to 0$ the solutions $(u_\varepsilon, v_\varepsilon)$ converge to the corresponding Boussinesq limit (u_0, v_0) for both problems. For Problem I $v_0 = 0$, while the limit for u_0 is the solution of

$$B_I \begin{cases} u_0'' + \frac{1}{2}\eta u_0' = 0 \quad \text{for} \quad -\infty < \eta < +\infty \\ \\ u_0(-\infty) = 1 \quad \text{and} \quad u_0(+\infty) = 0 \end{cases} \tag{2.7.1}$$

and is given by

$$u_0(\eta) = \frac{1}{2}\text{erfc}(\frac{\eta}{2}). \tag{2.7.2}$$

If we integrate (6.2.21) over $(\eta, +\infty)$ and apply the boundary condition $v(+\infty) = 0$ we obtain

$$v(\eta) = -\varepsilon \frac{u'(\eta)}{(1 + \varepsilon u(\eta))} + \varepsilon^2 \int_\eta^{+\infty} \frac{(u'(s))^2}{(1 + \varepsilon u(s))^2} \, ds. \tag{2.7.3}$$

By (2.7.3) we have

$$\lim_{\varepsilon \to 0} \frac{v(\eta)}{\varepsilon} = -u_0'(\eta). \tag{2.7.4}$$

This expression can be used as a first order approximation of $v_\varepsilon(\eta)$. We can improve the quality of the approximation by adding more terms in the expansion

$$v_\varepsilon(\eta) = -u_0(\eta)\varepsilon + \{E_1(\eta) + o(1)\}\varepsilon^2 \tag{2.7.5}$$

where

$$E_1(\eta) = 2u_0(\eta)u_0'(\eta) - \frac{1}{2}u_0'(\eta) + \int_\eta^\infty \{u_0'(s)\}^2 \, ds. \tag{2.7.6}$$

The symbol $o(1)$[1] denotes the order symbol. A similar series expansion for $u_\varepsilon(\eta)$ can be derived

$$u_\varepsilon(\eta) = u_0(\eta) + \frac{1}{2}u_0(\eta)\{1 - u_0(\eta)\}\varepsilon + \{E_2(\eta) + o(1)\}\varepsilon^2, \tag{2.7.7}$$

where $E_2(\eta)$ is given by

$$E_2(\eta) = \int_\eta^\infty e^{-t^2/4} \int_0^t e^{s^2/4} f_\varepsilon(s) \, ds \, dt - A_\varepsilon \int_\eta^\infty e^{-t^2/4} \, dt. \tag{2.7.8}$$

In the latter expression $f_\varepsilon(\eta)$ and A_ε are

$$f_\varepsilon(\eta) = (1 - 3u_0(\eta))(u_0'(\eta))^2 - u_0'(\eta) \int_\eta^\infty \{u_0'(s)\}^2 \, ds \tag{2.7.9}$$

$$A_\varepsilon = \frac{1}{2\sqrt{\pi}} \int_{-\infty}^\infty e^{-t^2/4} \int_0^t e^{s^2/4} f_\varepsilon(s) \, ds \, dt. \tag{2.7.10}$$

Both series expansions are truncated after the ε^2 terms. A nice property of the approximate solutions u_ε and v_ε is that they are expressed in terms of the solution of the Boussinesq problem B_I and the small parameter ε only. Because $u_0(\eta)$ is known explicitly, u_ε and v_ε can be evaluated without great difficulty, for instance with the computer algebra package *Maple [1994]*.
In the Boussinesq limit for Problem II we have again $v_0 = 0$ while now u_0 is the solution of

$$B_{II} \left\{ \begin{array}{l} u_0'' + \frac{1}{2}\eta u_0' = 0 \ \ \text{for} \ \eta > 0 \\ u(0) = 1 \ \ \text{and} \ \ u(+\infty) = 0, \end{array} \right. \tag{2.7.11}$$

hence

$$u_0(\eta) = \text{erfc}(\frac{\eta}{2}). \tag{2.7.12}$$

The asymptotic expressions for Problem II are

$$v_\varepsilon(\eta) = \{\frac{(1 - \gamma)}{\sqrt{\pi}\gamma} - u_0'(\eta)\}\varepsilon + \{E_3(\eta) + o(1)\}\varepsilon^2 \tag{2.7.13}$$

---

[1]The expression $f(x) = o(\psi(x))$ for $x \to +\infty$ means that $f(x)/\psi(x)$ tends to zero when $x \to +\infty$. It can be read as: 'Something that tends to zero, multiplied by'.

and

$$u_\varepsilon(\eta) = u_0(\eta) - \{\frac{2(1-\gamma)}{\pi\gamma}\{u_0(\eta) + \sqrt{\pi}u_0'(\eta)\} + \frac{1}{2}u_0(\eta)\{1 - u_0(\eta)\}\}\varepsilon +$$
$$\{E_4(\eta) + o(1)\}\varepsilon^2 \qquad (2.7.14)$$

with

$$E_3(\eta) = \frac{\gamma^2 - \gamma + 1}{\sqrt{\pi}\gamma} + u_0'(\eta)\left(2u_0(\eta) - \frac{\gamma(\pi + 4) - 4}{2\gamma\pi}\right) - \frac{2(\gamma - 1)}{\gamma\sqrt{\pi}}u_0''(\eta) +$$
$$\int_\eta^{+\infty}\{u_0'(s)\}^2\,ds \qquad (2.7.15)$$

and

$$E_4(\eta) = A_\varepsilon \int_0^\eta e^{-t^2/4}\,dt - \int_0^\eta e^{-t^2/4}\int_0^t e^{s^2/4}f_\varepsilon(s)\,ds\,dt. \qquad (2.7.16)$$

The function $f_\varepsilon(\eta)$ and the constant A_ε are defined as

$$f_\varepsilon(\eta) = \left(\frac{1}{2}u_0(\eta)(1 - u_0(\eta)) + \frac{2(\gamma - 1)}{\gamma\pi}\left(u_0(\eta) + \sqrt{\pi}u_0'(\eta)\right)\right)\left(u_0'(\eta) - \frac{1-\gamma}{\gamma\sqrt{\pi}}\right) -$$
$$u_0'(\eta)E_3(\eta) \qquad (2.7.17)$$

and

$$A_\varepsilon = \frac{1}{\sqrt{\pi}}\int_0^\infty e^{-t^2/4}\int_0^t e^{s^2/4}f_\varepsilon(s)\,ds\,dt. \qquad (2.7.18)$$

2.8 Transport of radionuclides

In this section we consider the simultaneous transport of radionuclides, occurring in tracer concentrations, in the vicinity of a salt dome. We assume that the flow geometry is given by Problem II, resulting in one-dimensional (z-direction) transport. The equation to be solved is

$$\phi\frac{\partial\rho\omega_c}{\partial t} + \frac{\partial}{\partial z}\left(\rho\omega_c q_z - D_c\rho\frac{\partial\omega_c}{\partial z}\right) - \phi\lambda\rho\omega_c = 0, \qquad (2.8.1)$$

where ω_c denotes the mass fraction of a radionuclide, λ the decay constant and D_c its effective diffusivity/dispersivity. Note that $q_z = q_z(z, t)$ and $\rho = \rho(z, t)$ are solutions of Problem II. Further note that in general $D_c \neq D$, the diffusivity of the salt. We introduce the parameter θ, defined as

$$\theta = D_c/D, \qquad (2.8.2)$$

and apply the scaling rules (2.4.1) in (2.8.1). This ensures identical time scales for brine and radionuclide transport. The radionuclide mass fraction is scaled according to

$$\omega_c^* = \frac{\omega_c}{\omega_0}, \qquad (2.8.3)$$

where ω_0 denotes a reference mass fraction, e.g. the (radionuclide) mass fraction at the salt rock boundary. As a consequence of (2.4.1) we find

$$\lambda^* = \frac{\phi D}{(\frac{\kappa}{\mu}\rho_f g)^2}\lambda \qquad (2.8.4)$$

as the dimensionless decay constant. Combining (2.8.1) and (2.3.10), and applying (2.4.1), (2.8.2), (2.8.3) and (2.8.4), we obtain (omitting the asteriks again)

$$\frac{\partial \bar\omega_c}{\partial t} + q_z \frac{\partial \bar\omega_c}{\partial z} - \frac{\theta}{(\varepsilon\rho + 1)} \frac{\partial}{\partial z} \left((\varepsilon\rho + 1) \frac{\partial \bar\omega_c}{\partial z} \right) = 0. \tag{2.8.5}$$

in which we eliminated the decay term in the usual way, i.e. by setting $\omega_c(z,t) = \bar\omega_c(z,t)e^{-\lambda t}$. The boundary and initial conditions are

$$\begin{aligned} \bar\omega_c(0,t) &= 1 \quad \text{for all} \quad t > 0 \\ \bar\omega_c(z,0) &= 0 \quad \text{for all} \quad z > 0 \end{aligned} \tag{2.8.6}$$

Since $q_z(z,t) = v(\eta)/\sqrt{t}$ and $\rho(z,t) = u(\eta)$, we note that (2.8.5)-(2.8.6) has a self similar solution $\bar\omega_c(z,t) = f(\eta)$, where f is a solution of the linear boundary value problem

$$(BVP) \begin{cases} f'(v - \dfrac{\eta}{2}) - \dfrac{\theta}{(\varepsilon u + 1)} \left((\varepsilon u + 1)f' \right)' = 0 \\ f(0) = 1 \\ f(\infty) = 0 \end{cases} \tag{2.8.7}$$

To solve this problem we first eliminate v using (2.5.9) and next integrate the resulting equation. This leads to

$$f(\eta) = 1 - \frac{\displaystyle\int_0^\eta \left(\frac{u'(\xi)}{u'(0)} \right)^{\frac{1}{\theta}} \frac{(1+\varepsilon)}{\varepsilon u(\xi)+1} \, d\xi}{\displaystyle\int_0^\infty \left(\frac{u'(\xi)}{u'(0)} \right)^{\frac{1}{\theta}} \frac{(1+\varepsilon)}{\varepsilon u(\xi)+1} \, d\xi} = 1 - \frac{\displaystyle\int_0^\eta \frac{|u'(\xi)|^{\frac{1}{\theta}}}{\varepsilon u(\xi)+1} \, d\xi}{\displaystyle\int_0^\infty \frac{|u'(\xi)|^{\frac{1}{\theta}}}{\varepsilon u(\xi)+1} \, d\xi}, \tag{2.8.8}$$

where u is the solution of Problem II, for a given value of ε. The corresponding, scaled radionuclide concentration is

$$\bar c(\eta) = f(\eta) \frac{\varepsilon u(\eta) + 1}{\varepsilon + 1}. \tag{2.8.9}$$

For $\theta = 1$ we can evaluate (2.8.8) and obtain

$$\bar c(\eta) = \frac{\varepsilon u(\eta) + 1}{\varepsilon + 1} \left(1 - \frac{\log\left(\dfrac{\varepsilon u(\eta) +)}{\varepsilon + 1} \right)}{\log\left(\dfrac{1}{\varepsilon + 1} \right)} \right). \tag{2.8.10}$$
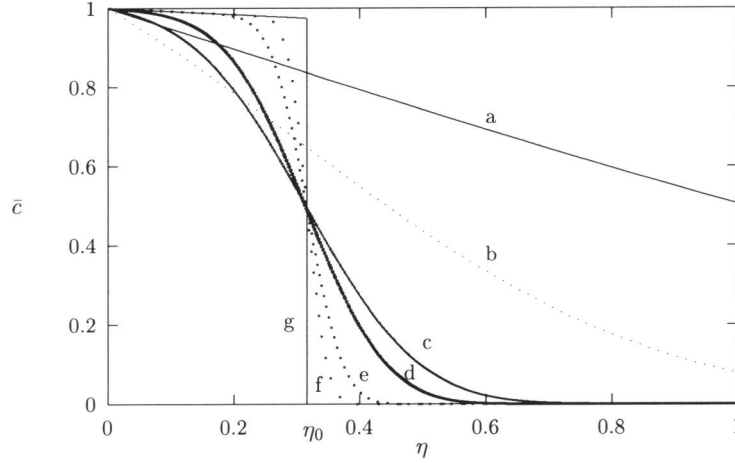
Figure 8. The scaled radionuclide concentration $\bar{c}(\eta)$ for $\varepsilon = 0.2$ and different values of θ: a. $\theta = 1.0$, b. $\theta = 0.1$, c. $\theta = 0.01$, d. $\theta = 0.005$, e. $\theta = 0.001$, f. $\theta = 0.0003$, g. $\theta = 0.0$.

Figure 8 shows the scaled concentration $\bar{c}$ for different values of θ and $\varepsilon = 0.2$. The results in this figure indicate that, as $\theta \to 0$, the concentration $\bar{c}$ has a discontinuity at $\eta = \eta_0 \approx 0.316$ with $\bar{c} = 0$ for $\eta > \eta_0$. This is a direct consequence of the limiting behavior of (BVP) as $\theta \to 0$: i.e.

$$\begin{cases} f'(v - \dfrac{\eta}{2}) = 0 & \text{for all } \eta > 0 \\ f(0) = 1, f(\infty) = 0 \end{cases} \tag{2.8.11}$$

which implies a piecewise constant solution

$$f(\eta) = \begin{cases} 1 & \text{for } 0 < \eta < \eta_0 \\ 0 & \text{for } \eta > \eta_0 \end{cases} \tag{2.8.12}$$

and thus

$$\bar{c}(\eta) = \begin{cases} \dfrac{\varepsilon u(\eta) + 1}{\varepsilon + 1} & \text{for } 0 < \eta < \eta_0 \\ 0 & \text{for } \eta > \eta_0 \end{cases} \tag{2.8.13}$$

As a consequence a radionuclide front emerges which moves with speed $v(\eta_0)/\sqrt{t}$, where $v(\eta_0)$ $= \max((v(\eta)) = \eta_0/2$, see property (iii) in Section 5. The position of the front in the (z, t)-plane is given by $s(t) = 2v(\eta_0)\sqrt{t} = \eta_0\sqrt{t}$, which is equivalent to the path of a tracer particle released at $t = 0$ in $z = 0$, i.e. at the beginning of the brine transport process. Hence in the limit $\theta \to 0$, the movement of the tracer is caused by the compressibility effect only.

2.9 Discussion

Self-similar solutions make the analysis tractable and (semi-)explicit results can be obtained. A crucial requirement for the applicability of similarity arguments is that both the governing equations *and* initial and/or boundary conditions be reducible to similarity form. Hence, only in special cases one may expect to find similarity solutions. Due to the piecewise initial density

data in Problem I and II we may consider the obtained similarity solutions as upper limits for the compressibility effect. Smooth initial data decrease the magnitude of the enhanced flow.

In analyzing Problems I and II we show explicitly the effect of enhanced groundwater flow due to compressibility of fluid caused by high salt concentration gradients. Characteristic for both problems is the occurrence of additional specific discharge in a direction perpendicular to the main groundwater direction. In both problems q_z is not influenced by gravity. The only quantity that depends on gravity is the specific discharge in the y-direction, parallel to the main flow q_f.

In this paper we only consider constant (molecular) diffusion. In a more realistic description a velocity dependent dispersion matrix has to be introduced into equation (2.2). Molecular diffusion underestimates the compressibility effects.

When transversal dispersion, due to the (regional) back ground flow q_y, dominates the dispersion/diffusion in the z-direction we arrive at a different situation. Under the assumption $|q_z| << |q_y|$ (2.2.5) reduces to

$$D \approx \phi D_{\mathrm{mol}} + \alpha_T |q_y| = \tag{2.9.1}$$

$$\phi D_{\mathrm{mol}} + \alpha_T |q_f - \frac{\kappa}{\mu}(\rho - \rho_f)g\sin\beta|, \tag{2.9.2}$$

yielding D as a function of ρ. The analysis of this case is quite different from what we discussed here and will be published elsewhere [Van Duijn & Schotting ,1996].

If $q_f >> \frac{\kappa}{\mu}(\rho_s - \rho_f)g\sin\beta$ we may replace (2.9.2) by

$$D \approx \phi D_{\mathrm{mol}} + \alpha_T |q_f|, \tag{2.9.3}$$

yielding a constant dispersivity which is in general much larger then the effective molecular diffusivity ϕD_{mol}. The number

$$P = \frac{\alpha_T |q_f|}{\phi D_{\mathrm{mol}}} \tag{2.9.4}$$

indicates the relative importance of (transversal) dispersion with respect to molecular diffusion. If $P < 1$ diffusion dominates dispersion. When $q_f = 100$ m/yr typical values of the dispersivity are: $D(\alpha_T = 0.1 \text{ m}) \approx 3.10^{-7}$ m^2/s and $D(\alpha_T = 1.0 \text{ m}) \approx 3.10^{-6}$ m^2/s. The corresponding P-numbers are: $\approx 10^3$ and $\approx 10^4$. It is obvious that such values of the dispersivity will enhance the compressibility effects in brine transport.

If we consider longitudinal dispersion of radionuclides in the z-direction (2.2.5) reduces to

$$D(q_z) = D_c + \alpha_L |q_z|, \tag{2.9.5}$$

remembering that $D_c = \phi D_{c-mol} = \theta D$. By virtue of the $1/\sqrt{t}$-decay of $q_z(z,t)$ one expects the longitudinal dispersion to dominate diffusion only on the short time scale in Problem II. A rough estimate of the order of magnitude of the time $\hat{t}$ after which diffusion becomes dominant can be given by using the approximation $q_z(z,t) \approx v_\varepsilon(0)/\sqrt{t}$ in

$$P = \frac{\alpha_L |q_z(z,t)|}{D_c} < 1, \tag{2.9.6}$$

hence

$$\hat{t} \approx \left(\frac{\alpha_L \varepsilon}{\gamma}\right)^2 \frac{\phi}{\pi\theta D}. \tag{2.9.7}$$

Typical values of $\hat{t}$ are (for $\theta = 1$): $\hat{t}(\alpha_l = 1 \text{ m}) \approx 0.9$ yr and $\hat{t}(\alpha_L = 10 \text{ m}) \approx 88$ yr, where as the typical time scale of brine transport processes is usually in the order of thousands of years. Hence at a very early stage of the brine transport process molecular diffusion starts to dominate longitudinal dispersion. Notice that $\hat{t}$ decreases when we replace the effective molecular diffusivity by a constant transversal diffusivity $\alpha_T q_f$, as discussed above.

2.10 Conclusions

1. Compressibilty effects in brine transport in porous media are small and have in most practical cases only little effect on the density distributions. We studied two specific brine problems and compared the solutions for $\varepsilon > 0$ with the corresponding Boussinesq solutions for $\varepsilon \to 0$, where ε denotes the relative density difference.

2. We found that high salt concentration gradients induce a convective flux, which is perpendicular to the main groundwater flow direction in the problems studied in this paper. The magnitude of this flux depends upon the relative density difference and the effective diffusivity/dispersivity of salt.

3. Taking only molecular diffusion into account underestimates the convective brine transport perpendicular to the main flow direction. For the problems studied in this paper it is more realistic to replace the molecular diffusivity by the transversal dispersivity due to the (regional) background flow. This increases the magnitude of q_z significantly and q_z can no longer be neglected as convective transport mechanism.

4. The similarity solutions presented are both of practical and theoretical use. First they provide us with detailed qualitative and quantitative information about the nature of compressibility effects. Secondly the solutions can be used to verify the accuracy of numerical codes designed to simulate brine transport.

5. The similarity solutions have the following properties: i) $u'(\eta) < 0$ for all $-\infty < \eta < +\infty$ (Problem I) and $0 \leq \eta < +\infty$ (Problem II), ii) there exists a number η_0 such that $u''(\eta) < 0$ for $\eta < \eta_0$ and $u''(\eta) > 0$ for $\eta > \eta_0$, iii) $v(\eta_0) = \eta_0/2$ and $v'(\eta) > 0$ for $\eta < \eta_0$ and $v(\eta) < 0$ for $\eta > \eta_0$. The number η_0 plays a prominent role in the simultaneous transport of radionuclides.

6. The results of the asymptotic analysis can be used to approximate the similarity solutions up to a given accurracy.

7. When considering simultaneous transport of brine and dissolved radionuclides we can construct an explicit solution for the radionuclide mass fraction expressed in terms of the solution of the underlying brine problem.

8. In the limit of vanishing radionuclide diffusion/dispersion a radionuclide front emerges in Problem II which travels with speed $v(\eta_0)/\sqrt{t}$. Hence, the movement of the radionuclide is caused by the compressibility effect only.

Bibliography

[1] Bear,J., Dynamics of fluids in porous media, Elsevier, New York,(1972)

[2] Bornemann,O & R. Fischbeck, Ablaugung und Hutgesteinsbildung am Salzstock Gorleben, Z. Geol. Ges., 137 (1986), 71-83

[3] Carey, A.E., S.W. Wheatcraft, R.J. Glass & J.P. O'Rourke, Non-fickian ionic diffusion across high concentration gradients, Water Res. Research , vol 31, 9 (1995) 2213-2218.

[4] Duijn, C.J. van & L.A. Peletier, A class of similarity solutions of nonlinear diffusion equations, Arch. Rational Mech. Anal. 65 (1977) 363-377.

[5] Duijn, C.J. van, L.A.Peletier & R.J.Schotting, On the analysis of brine transport in porous media, European. Journ. of Appl.Math.1992.

[6] Duijn, C.J. van & F.J.T Floris, Mathematical analysis of the influence of power law fluid rheology on a capillary diffusion zone, submitted to J. of Petr. Sc & Eng. (1992)

[7] Duijn, C.J.van, S.M.Gomez & Hongfei Zhang, On a class of similarity solutions of the equation $u_t = (|u|^{m-1}u_x)_x$ with $m > -1$, IMA Journal of Appl. Math.41 (1988) 147-163.

[8] Van Duijn, C.J. & R.J. Schotting, Brine transport in porous media: On the use of Von Mises and similarity solutions, submitted for publication (1996)

[9] Esteban, J.R., A. Rodriquez & J.L. Vazquez, A nonlinear heat equation with singular diffusivity, Commun. in Part. Diff. Eq., 13 (8) (1988), 985-1039.

[10] Glasbergen, P., Extreme Salt Concentrations in Deep Aquifers in the Netherlands, The Science of the Total Environment,21 (1981), 251-259

[11] Hassanizadeh, S.M. & T.Leijnse, On the modelling of brine transport in porous media, Water Resources Research 24(1988) 321-330

[12] Hassanizadeh, S.M., Experimental study of coupled flow and mass transport: a model validation exercise, ModelCARE 90: Calibration in Groundwater Modelling (Proceedings of the conference held in The Hague, September 1990, IAHS Publ. no. 195 (1990)

[13] Hassanizadeh, S.M. & T. Leijnse, A non-linear theory of high-concentration-gradient dispersion in porous media, Submitted and accepted for publication in Adv. Water Res. Research (1995)

[14] Herbert, A.W., C.P.Jackson & D.A.Lever, Coupled Groundwater Flow and Solute Transport With Fluid Density Strongly Dependent Upon Concentration, Water Res. Research 24(1988) 1781- 1795

71

[15] Josseling de Jong, G. de & C.J.van Duijn, Transverse dispersion from an originally sharp fresh-salt interface caused by shear flow, Journal of Hydrology **84** (1986) 147-163

[16] Maple, Version MapleV Release 3, Computer algebra package (software), Waterloo Maple Software, Canada (1994)

[17] Oldenburg, C.M. & K. Pruess, Dispersive transport dynamics in a strongly coupled groudwater-brine flow system, Water Res. Research 31(2) (1995), 289-302.

[18] Mises, R. von & K.O. Friedrichs, Fluid dynamics, Applied Mathematics Series 5, Springer, New York (1973), 171.

[19] Taylor, G., Dispersion of soluble matter in solvent flowing slowly through a tube, Proc. Roy. Soc. London (1953) 219, 186-203.

[20] Taylor, G., Conditions under which dispersion of a solute in a stream can be used to measure molecular diffusion, Proc. Roy, Soc. London (1954) 225, 473-477.

[21] Roxburgh, I.S., Geology of high-level nuclear waste disposal - An introduction, Chapman and Hall Ltd, London (1987)

[22] Swedish Nuclear Inspectorate HYDROCOIN, An international project for studying groundwater hydrology modeling strategies, Level 1 Final Report: Verification of groundwater flow models, Case 5, Swedish Nucl.Insp.,Stockholm (1986)

[23] Weast, R.C., Handbook of Chemistry and Physics, 63rd ed., CRC Press Boca Raton Fla.1982, p. D261

[24] Visser, W.A., Waste Disposal and Underground Waters, Geologie en Mijnbouw **53** (1974) 6, 249-256

Chapter 3

Brine transport: Von Mises transformations

3.1 Introduction

Brine transport in porous media is a process which is described by the fluid and salt mass balance equations, the fluid movement equation and an equation of state, relating the salt mass fraction to the fluid density, see e.g. Hassanizadeh & Leijnse [12]. This yields a mathematical model consisting of a system of coupled partial differential equations which has to be solved in the flow domain, subject to appropriate boundary and initial conditions.

In a heterogeneous, multi dimensional flow domain the model equations have to be solved numerically in order to determine the spreading of salt in the subsurface. However, under simplified and highly idealized conditions it is possible to reduce the partial differential equations by means of Von Mises and similarity transformations to a single ordinary differential equation, which can be solved by semi-analytical means. The purpose of this paper is to draw attention to such transformations. We shall work out three specific cases for which we give an interpretation of the results in the physical sense.

The idea behind the Von Mises transformation is to take the stream function of the flow as one of the unknowns and to reduce the partial differential equations to a single nonlinear diffusion equation. To illustrate this procedure we recall the example of a laminar, stationary and two-dimensional flow over a flat plate. Let U, V denote the velocity components in the x, y-direction and let the plate be situated along the positive $x-$axis. Following for instance, Chorin & Marsden [5] or Curle [9], one has to consider the Prandtl boundary layer equations

$$\begin{cases} \dfrac{\partial U}{\partial x} + \dfrac{\partial V}{\partial y} = 0 \\ U\dfrac{\partial U}{\partial x} + V\dfrac{\partial U}{\partial y} = \nu\dfrac{\partial^2 U}{\partial y^2} \end{cases} \tag{3.1.1}$$

for $(x, y) \in \mathbf{R}^+ \times \mathbf{R}^+$, subject to the boundary conditions

$$U(x, 0) = 0 \text{ for } x \in \mathbf{R}^+ \tag{3.1.2}$$

and

$$U(0, y) = U_0(y) \text{ for } y \in \mathbf{R}^+ \tag{3.1.3}$$

73

where U_0 is the velocity distribution at the leading edge of the plate. In (3.1.1), ν denotes the viscosity of the fluid. Assuming the existence of a stream function $\psi = \psi(x, y)$ satisfying

$$U = \frac{\partial \psi}{\partial y} \ \text{ and } \ V = -\frac{\partial \psi}{\partial x}, \tag{3.1.4}$$

one introduces the change of variables

$$x = x \ \text{ and } \ \psi = \psi(x, y) = \int_0^y U(x, s) \, ds \tag{3.1.5}$$

and the Von Mises transformation

$$\tilde{U}(x, \psi) = \tilde{U}(x, \psi(x, y)) = U(x, y). \tag{3.1.6}$$

Under this transformation we obtain for $\tilde{U}$ the nonlinear diffusion equation

$$\frac{\partial \tilde{U}}{\partial x} = \frac{\nu}{2} \frac{\partial^2 \tilde{U}^2}{\partial \psi^2} \ \text{ with } \ (x, \psi) \in \mathbf{R}^+ \times \mathbf{R}^+, \tag{3.1.7}$$

and the conditions

$$\tilde{U}(0, \psi) = \tilde{U}_0(\psi) := U_0(y) \ \text{ for } \ \psi \in \mathbf{R}^+, \tag{3.1.8}$$

and

$$\tilde{U}(x, 0) = 0 \ \text{ for } \ x \in \mathbf{R}^+. \tag{3.1.9}$$

Note that if U_0 is a positive constant, say $U_0(y) = U_0^* > 0$ for all $y > 0$, this initial-boundary value problem can be reduced to a boundary value problem for an ordinary differential equation in terms of the similarity variable $\psi/\sqrt{x}$. The solution of this boundary value problem describes the behavior of the solution of problem (3.1.7)-(3.1.9) for large values of x, provided $U_0(y) \to U_0^*$ as $y \to \infty$. Such convergence results are well known for nonlinear diffusion problems, see for example Van Duijn & Peletier [10], who studied the large time behavior of a uniformly parabolic version of problem (3.1.7)-(3.1.9) in terms of such a similarity solution.

Thus the combination of Von Mises and similarity transformations provides a straight forward way to establish the large time behaviour of the original system. With this in mind, we return to the transport of brine and consider as examples three time dependent problems that allow Von Mises and similarity transformations. These problems are: (i) Brine displacing fresh water in an infinitely long porous column, (ii) Flow of fresh water along a salt dome and (iii) Mixing of parallel layers of brine and fresh water. The flow geometry of (i) is one-dimensional while the flow domains of (ii) and (iii) are two dimensional. However, in all three problems the boundary conditions are chosen such that the resulting fluid and salt balance equations are one-dimensional. The unknowns are the density and the specific discharge.

Analogous to the Prandtl system one can reduce the two balance equations to a single nonlinear diffusion equation for the density. Here the fluid balance equation suggests the existence of a modified stream function which serves as the new independent Von Mises variable. Considering in addition a piecewise constant initial condition for the density a further reduction is possible in terms of a similarity variable. A boundary condition for the specific discharge is used in the (back) transformation to the original variables, yielding semi-analytical expressions in terms of the similarity solution. This is illustrated in Section 3.

Characteristic for the brine model is the nonlinear coupling between fluid density and specific discharge which is caused by gravity and salinity induced fluid volume changes. Gravity causes enhanced rotational flow in regions where horizontal density variations occur and local high density gradients induce volume changes in the fluid which in turn may cause enhanced fluid flow as well. Because the three example problems to be discussed are essentially one-dimensional, gravity will not play a role and only the second mechanism causes enhanced fluid flow.

Raats [25], [29] introduced a similar modified stream function, which he called 'parcel function', when studying one-dimensional transport of fluid and solutes in unsaturated soils. The fluid balance equation in unsaturated soils in one space dimension reads

$$\frac{\partial \theta}{\partial t} + \frac{\partial}{\partial z}(\theta v) = 0 \ \text{ for } \ (z,t) \in \mathbf{R} \times \mathbf{R}^+, \tag{3.1.10}$$

where θ denotes the volumetric water content and v the velocity of water. Analogous to (3.1.1) and (3.1.4) a function Ξ is introduced which satisfies

$$\theta = \frac{\partial \Xi}{\partial z} \ \text{ and } \ \theta v = -\frac{\partial \Xi}{\partial t}. \tag{3.1.11}$$

Integration of the total differential $d\Xi$ gives

$$\Xi(z,t) = \Xi(0,0) - \int_0^t \theta_0 v_0 \, d\tau + \int_0^z \theta \, d\xi, \tag{3.1.12}$$

which effectively labels all members of a collection of parcels of water. The function Ξ can be interpreted as a measure of soil water storage in a region or as the cumulative flux across a surface. Raats [26] does not consider coupling between fluid velocity and solute concentration in the solute mass balance equation. This assumption only is valid when the fluid density is not affected by of the solute concentration. In brine transport however the coupling between salt concentration and fluid density is an essential property.

This paper is organized as follows. In Section 2 we give the mathematical formulation of the brine model. In Section 3 we explain the details of the Von Mises transformation for one-dimensional problems and in Section 4 we study the application to the three examples with similarity, thus specifying the large time limit of three corresponding classes of problems. Finally, in Section 5, we present the conclusions.

3.2 The brine equations

A general study of the transport of brine through porous media was presented by Hassanizadeh & Leijnse [12]. Simplifying their formulation by taking Fick's law for the diffusive salt flux and the conventional form of Darcy's law for the fluid momentum equation we arrive at the following set of equations:

Mass balance equation for the fluid

$$n\frac{\partial \rho}{\partial t} + \text{div}\,(\rho \mathbf{q}) = 0, \tag{3.2.1}$$

where ρ denotes the density of the fluid, $\mathbf{q}$ the specific discharge vector and n the porosity of the porous medium.

Mass balance equation for the salt

$$n\frac{\partial (\rho \omega)}{\partial t} + \text{div}\,(\omega \rho \mathbf{q} - \rho I\!D \,\text{grad}\,\omega) = 0, \tag{3.2.2}$$

where ω denotes the mass fraction of the salt and $I\!\!D$ the hydrodynamic dispersion tensor. The mass fraction is defined as the concentration of the salt component divided by the density of the fluid.

Darcy's law

$$\frac{\mu}{\kappa}\mathbf{q} + \operatorname{grad} p - \rho\mathbf{g} = 0, \qquad (3.2.3)$$

where κ denotes the intrinsic permeability of the porous medium, μ the dynamic viscosity of the fluid and $\mathbf{g}$ the acceleration of gravity.

Equation of state

$$\rho = \rho_f e^{\gamma\omega}, \qquad (3.2.4)$$

where ρ_f denotes the density of fresh water and γ a constant:$\gamma \approx 0.6923 \approx \ln(2)$. In writing (2.2.4) we implicitly assumed that the density is a function of ω only (no pressure or thermal effects). In the subsequent analysis we also assume that the fluid viscosity is constant.

It is common practice to use for the hydrodynamic dispersion tensor $I\!\!D = (D_{ij})$ in (3.2.2) the expression, see for instance Bear [3],

$$D_{ij} = \{\alpha_T|\mathbf{q}| + nD_{\mathrm{mol}}\}\delta_{ij} + (\alpha_L - \alpha_T)q_iq_j/|\mathbf{q}|. \qquad (3.2.5)$$

Here α_L and α_T are the longitudinal and transversal dispersion lengths, and D_{mol} is the effective molecular diffusivity incorporating the effect of tortuosity. Further, δ_{ij} denotes the Kronecker δ and $|\cdot|$ the Euclidian norm in $\mathbf{R}^2$. However, for mathematical convenience we use in almost all of this paper the approximation

$$D_{ij} = nD\delta_{ij}, \qquad (3.2.6)$$

where D is a positive constant. If α_L and α_T are small (fine granular, homogeneous material), this approximation is justified for $D = D_{mol}$. However, if the influence of the heterogeneities is significant, then D in (3.2.6) accounts for dispersion in an averaged sense. Only when discussing the examples in Sections 4.2 and 4.3 we allow for some velocity dependence of D_{ij}, however different from (3.2.5).

As in Van Duijn et.al. [11] we first rewrite equations (3.2.1)- (2.2.4). Expansion of equation (3.2.2) gives

$$n\rho\frac{\partial\omega}{\partial t} + n\omega\frac{\partial\rho}{\partial t} + \omega\operatorname{div}(\rho\mathbf{q}) + \rho\mathbf{q}\cdot\operatorname{grad}\omega - \operatorname{div}(\rho I\!\!D\operatorname{grad}\omega) = 0 \qquad (3.2.7)$$

Multiplication of equation (3.2.1) by ω and subtracting the result from equation (3.2.7) results in

$$n\rho\frac{\partial\omega}{\partial t} + \rho\mathbf{q}\cdot\operatorname{grad}\omega - \operatorname{div}(\rho I\!\!D\operatorname{grad}\omega) = 0. \qquad (3.2.8)$$

Next we substitute the equation of state (3.2.4) in (3.2.8) and obtain

$$n\frac{\partial\rho}{\partial t} + \mathbf{q}\cdot\operatorname{grad}\rho - \operatorname{div}(I\!\!D\operatorname{grad}\rho) = 0, \qquad (3.2.9)$$

as a second equation for the unknowns ρ and $\mathbf{q}$. Note that equation(3.2.9) is no longer in divergence form and that the constant γ has vanished from the equations. The latter is due to

the exponential form of the equation of state. Hence, the resulting system of equations is

$$\begin{cases} n\dfrac{\partial \rho}{\partial t} + \operatorname{div}(\rho\mathbf{q}) = 0 \\[2mm] n\dfrac{\partial \rho}{\partial t} + \mathbf{q}\cdot\operatorname{grad}\rho - \operatorname{div}(I\!\!D\operatorname{grad}\rho) = 0 \end{cases} \tag{3.2.10}$$

In view of the applications in Section 4 we confine ourselves to the analysis of (3.2.10) in one space dimension. After appropriate scaling, imposed by the geometry and hydrology of each individual application in Section 4 and assuming (3.2.6) for the moment, we obtain the dimensionless system

$$\begin{cases} \dfrac{\partial u}{\partial t} + \dfrac{\partial}{\partial z}(qu) = 0 & (z,t)\in\Omega\times\mathbf{R}^+ \\[2mm] \dfrac{\partial u}{\partial t} + q\dfrac{\partial u}{\partial z} - \dfrac{\partial}{\partial z}\left(\dfrac{\partial u}{\partial z}\right) = 0 & (z,t)\in\Omega\times\mathbf{R}^+ \end{cases} \tag{3.2.11}$$

where Ω denotes the one-dimensional domain $\mathbf{R}$ or $\mathbf{R}^+$. Details of the scaling rules for each problem will be given in Section 4. Equations (3.2.11) can be combined to give

$$u\frac{\partial q}{\partial z} - \frac{\partial}{\partial z}\left(\frac{\partial u}{\partial z}\right) = 0 \quad (z,t)\in\Omega\times\mathbf{R}^+. \tag{3.2.12}$$

This expression shows that in order to solve (3.2.11) uniquely, one has to prescribe initial-boundary conditions for u and a single boundary condition for q. Specifically, if $\Omega = \mathbf{R}$ we consider (3.2.11) subject to the conditions

$$u(z,0) = u_0(z) \ \text{ for } \ z\in\mathbf{R} \tag{3.2.13}$$

and

$$q(-\infty,t) = q_0(t) \ \text{ for } \ t\in\mathbf{R}^+, \tag{3.2.14}$$

where u_0 and q_0 are the given, scaled initial density distribution and limiting discharge value.

If $\Omega = \mathbf{R}^+$, we consider (3.2.11) subject to initial condition

$$u(z,0) = u_f \ \text{ for } \ z\in\mathbf{R}^+, \tag{3.2.15}$$

and the boundary conditions

$$u(0,t) = u_s \ \text{ and } \ q(0,t) = q_0(t). \tag{3.2.16}$$

Here u_f and u_s are the scaled densities of fresh water and brine. Concerning the behavior of solutions of these problems we assume that for all $t\geq 0$:

$$u_f \leq u(z,t) \leq u_s \ \text{ for } \ z\in\Omega, \tag{3.2.17}$$

and

$$\lim_{z\to-\infty} u(z,t) = u_s \ (\text{if } \Omega = \mathbf{R}), \ \lim_{z\to+\infty} u(z,t) = u_f. \tag{3.2.18}$$

Remark: Introduction of the material derivative

$$\frac{D}{Dt} = \frac{\partial}{\partial t} + \frac{\mathbf{q}}{n} \cdot \text{grad} \tag{3.2.19}$$

in the fluid balance equation (3.2.1) results in

$$\frac{n}{\rho}\frac{D\rho}{Dt} + \text{div } \mathbf{q} = 0. \tag{3.2.20}$$

This expression shows that density variations may effect the divergence or local volume of the fluid, which in turn can cause additional movement of fluid. This effect will be investigated in the examples presented in Section 4.

3.3   Von Mises transformation

To reduce system (3.2.11) to a single, nonlinear diffusion equation we apply a coordinate transformation which is a variant of the Von Mises transformation, see e.g. Mises & Friedrichs [21]. Considering the fluid balance equation in (3.2.11) as the divergence operator in the (t, z)-plane, acting on the vector (u, uq), we introduce a modified stream function $\Psi = \Psi(z, t)$, which satisfies

$$u = \frac{\partial \Psi}{\partial z} \quad \text{and} \quad uq = -\frac{\partial \Psi}{\partial t}. \tag{3.3.1}$$

The new independent variables are

$$t = t \quad \text{and} \quad \Psi = \int_{h(t)}^{z} u(s, t)\, ds, \tag{3.3.2}$$

where $h(t)$ is a yet unknown function of time which will be determined later on from the boundary condition on q. It will be normalized such that $h(0) = 0$. The Von Mises transformation is

$$\hat{u} = \hat{u}(\Psi, t) = \hat{u}(\Psi(z, t), t) = u(z, t). \tag{3.3.3}$$

We use it to rewrite system (3.2.11) into the equation

$$\frac{\partial \hat{u}}{\partial t} = \hat{u}\frac{\partial}{\partial \Psi}\left(\hat{u}\frac{\partial \hat{u}}{\partial \Psi}\right) \quad \text{with} \quad \Psi \in Q, \ t \in \mathbf{R}^{+}. \tag{3.3.4}$$

Here Q denotes the range of Ψ.

First we consider the case $\Omega = \mathbf{R}$. Properties (3.2.17),(3.2.18) and definition (3.3.1) imply that Ψ is monotonically increasing in z with $\Psi(-\infty, t) = -\infty$ and $\Psi(+\infty, t) = +\infty$ for all $t > 0$. Hence $Q = \mathbf{R}$ in (3.3.4). To find the initial condition corresponding to (3.3.4) we need to transform the function u_0. To this end we consider (3.3.2) at $t = 0$:

$$\Psi = \int_{0}^{z} u_0(s)\, ds. \tag{3.3.5}$$

This expression defines the function $z = z(\Psi)$ for $-\infty < \Psi < +\infty$, which we use to obtain the transformed initial condition

$$\hat{u}(\Psi, 0) = u_0(z(\Psi)) \quad \text{for} \quad \Psi \in \mathbf{R}. \tag{3.3.6}$$

The initial value problem (3.3.4),(3.3.6) admits a similarity solution for piecewise constant initial data. If u_0 is given by

$$u_0(z) = \begin{cases} u_s & \text{for } z < 0 \\ u_f & \text{for } z > 0 \end{cases} \tag{3.3.7}$$

then the same is true for $\hat{u}(\Psi, 0)$: i.e.

$$\hat{u}(\Psi, 0) = \begin{cases} u_s & \text{for } \Psi < 0 \\ u_f & \text{for } \Psi > 0 \end{cases} \tag{3.3.8}$$

The corresponding solution is a similarity solution of the form $\hat{u}(\Psi, t) = f(\eta)$ with $\eta = \Psi/\sqrt{t}$.

Having obtained a solution $\hat{u} = \hat{u}(\Psi, t)$ we use (3.3.1) to return to the original variables. Integrating the first equation of (3.3.1) gives

$$z = \int_0^{\Psi(z,t)} \frac{1}{\hat{u}(s,t)} \, ds + h(t) \ \text{ for } \ (z,t) \in \mathbf{R} \times \mathbf{R}^+, \tag{3.3.9}$$

where $h(t)$ is an integration constant depending on t only, satisfying $h(0) = 0$ (which implies $\Psi(0,0) = 0$). If the function $h(t)$ were known, then (3.3.9) would define the modified stream function $\Psi = \Psi(z,t)$ and the solution in terms of the original variables would be given by

$$u(z,t) = \hat{u}(\Psi, t) \ \text{ for } \ (z,t) \in \mathbf{R} \times \mathbf{R}^+. \tag{3.3.10}$$

To find $h(t)$ we differentiate (3.3.9) with respect to t and use the second equation in (3.3.1). This yields an expression for q which is given by

$$q(z,t) = h'(t) - \int_0^{\Psi(z,t)} \frac{\hat{u}_t}{\hat{u}^2}(s,t) \, ds. \tag{3.3.11}$$

where $\hat{u}_t$ denotes the partial derivative of $\hat{u}$ with respect to t. Next we use the discharge boundary condition (3.2.14) to determine $h(t)$. Letting $z \to -\infty$ in (3.3.11) we find upon integration

$$h(t) = \int_0^t \left\{ q_0(\xi) - \int_{-\infty}^0 \frac{\hat{u}_t}{\hat{u}^2}(s,\xi) \, ds \right\} \, d\xi, \tag{3.3.12}$$

provided that this integral exists. Substituting (3.3.12) in (3.3.11) gives for the discharge the expression

$$q(z,t) = q_0(t) - \int_{-\infty}^{\Psi(z,t)} \frac{\hat{u}_t}{\hat{u}^2}(s,t) \, ds, \tag{3.3.13}$$

which completely determines the solution of the problem on $\mathbf{R}$.

Next we consider $\Omega = \mathbf{R}^+$. This case is more involved because the presence of the boundary at $z = 0$ which implies that the domain Q becomes time dependent. Using boundary condition (3.2.16) and integrating the second equation in (3.3.1) yields for $Q = Q(t)$

$$Q(t) = (\Psi(0,t), \infty) \ \text{ for } \ t \geq 0, \tag{3.3.14}$$

where

$$\Psi(0,t) = -u_s \int_0^t q_0(\xi) \, d\xi. \tag{3.3.15}$$

Let $\hat{u} = \hat{u}(\Psi, t)$ denote the solution of (3.3.4) subject to (3.3.6), now with $\Psi > 0$, and the boundary condition $\hat{u}(\Psi(0,t),t) = u_s$. Similarly to (3.3.12) we introduce

$$h(t) = \int_0^t \left\{ q_0(\xi) + \int_0^{\Psi(0,\xi)} \frac{\hat{u}_t}{\hat{u}^2}(s,\xi)\, ds \right\}\, d\xi, \tag{3.3.16}$$

and define $\Psi = \Psi(z,t)$ for $(z,t) \in \mathbf{R}^+ \times \mathbf{R}^+$ by

$$z = \int_0^{\Psi(z,t)} \frac{1}{\hat{u}(s,t)}\, ds + \int_0^t \left\{ q_0(\xi) + \int_0^{\Psi(0,\xi)} \frac{\hat{u}_t}{\hat{u}^2}(s,\xi)\, ds \right\}\, d\xi. \tag{3.3.17}$$

Then u is given by

$$u(z,t) = \hat{u}(\Psi(z,t),t) \tag{3.3.18}$$

and

$$q(z,t) = q_0(t) - \int_{\Psi(0,t)}^{\Psi(z,t)} \frac{\hat{u}_t}{\hat{u}^2}(s,\xi)\, ds. \tag{3.3.19}$$

If q_0 is not explicitly given but, as in the salt dome problem in Section 4.2, a function of $\partial u / \partial z$ at the boundary $z = 0$, then $\Psi(0,t)$ denotes a free boundary in the (Ψ, t)-plane. The position of the free boundary is a priori unknown and is part of the solution of the problem. When, as in Section 4.2, the discharge q_0 is given by

$$q_0(t) = -C\, \frac{\partial u}{\partial z}(0,t) \quad \text{for all } t > 0, \tag{3.3.20}$$

where C denotes a positive constant, then the following Stefan condition holds at the free boundary:

$$\frac{d\varphi(t)}{dt} = C\, \hat{u}^2(\varphi(t),t) \frac{\partial \hat{u}}{\partial \Psi}(\varphi(t),t) = C\, u_s^2 \frac{\partial \hat{u}}{\partial \Psi}(\varphi(t),t), \tag{3.3.21}$$

where $\varphi(t) := \Psi(0,t)$. This condition relates the speed of the free boundary in the (Ψ, t)-plane to the spatial derivative of $\hat{u}$ at the free boundary.

The nonlinear diffusion problems that arise from these transformations are well known and received much attention in the existing literature, for instance see the book of Crank [6] on the mathematics of diffusion or the book of Meirmanov [20] on the Stefan problem. Considering the role of similarity solutions as large time solutions of nonlinear diffusion problems we refer to the paper of Van Duijn & Peletier [10] and the book by Barenblatt on intermediate asymptotics [2].

The initial and boundary conditions of the flow problem discussed in the next section are chosen such that the corresponding nonlinear diffusion problems are solvable in terms of similarity solutions. With the Von Mises transformation as intermediate step such similarity solutions are natural to the problem and straight forward to find. Moreover, we know that they represent the large time behavior of the corresponding flow problem with more general (i.e. non-constant) boundary/initial data.

3.4   Applications

3.4.1   Flow in a porous column

In the first application we study brine transport in an infinitely long, one-dimensional porous column. From a practical point of view it would be more realistic to study a column with finite

length. But when the phenomenon to be studied occurs at a sufficiently large distance from the inlet and outlet of the column one expects only minor differences between the results for a finite and an infinite column. The column is in vertical position, directed along the z-axis, and gravity points downwards in the negative z-direction. The porous medium is saturated with fluid. The flow is in the positive z-direction, such that brine displaces fresh water in a stable manner. Initially the region $z > 0$ is filled with fresh water ($\rho = \rho_f$), and the region $z < 0$ with brine ($\rho = \rho_s$), such that the fluids are separated by a sharp transition at $z = 0$. At $z = -\infty$ the column is infiltrated with brine, with constant density ρ_s and constant specific discharge q_s. The mathematically relevant initial-boundary conditions for this problem are

$$q(-\infty, t) = q_s, \quad \text{with } t \in \mathbf{R}^+ \tag{3.4.1}$$

and

$$\rho(z,0) = \begin{cases} \rho_s & \text{for } z < 0 \\ \rho_f & \text{for } z > 0 \end{cases} \tag{3.4.2}$$

Note that the initial condition implies $\rho(-\infty, t) = \rho_s$ for $t > 0$, implying that indeed brine is injected into the column. Assuming the column to be filled with homogeneous, fine granular material we consider a constant dispersivity according to (2.2.6). This choice is also motivated by the fact that in this application the Von Mises transformation is not applicable for a velocity dependent dispersivity.

Next we introduce the dimensionless variables

$$u = \frac{1}{\varepsilon} + \frac{\rho - \rho_f}{\rho_s - \rho_f} \left(= \frac{\rho}{\rho_s - \rho_f} = \frac{1}{\varepsilon} \frac{\rho}{\rho_f} \right), \quad q^* = \frac{q}{q_s}, \quad t^* = t\frac{q_s^2}{nD}, \quad z^* = z\frac{q_s}{D}. \tag{3.4.3}$$

where ε is the relative density difference

$$\varepsilon = \frac{\rho_s - \rho_f}{\rho_f}. \tag{3.4.4}$$

Typical values of the relative density difference are: $\varepsilon \approx 0.025$ for sea water and $\varepsilon \approx 0.2$ for saturated brine; hence $(0 \leq)\varepsilon \leq 0.2$. Applying this scaling to (3.2.10) (in one space dimension), (3.4.1) and (3.4.2), and dropping the asterisks again in the notation, we obtain the mixed initial-boundary value problem

$$\begin{cases} \dfrac{\partial u}{\partial t} + \dfrac{\partial}{\partial z}(qu) = 0 \\ \dfrac{\partial u}{\partial t} + q\dfrac{\partial u}{\partial z} = \dfrac{\partial^2 u}{\partial z^2} \end{cases} \tag{3.4.5}$$

for $(z, t) \in \mathbf{R} \times \mathbf{R}^+$, with

$$q(-\infty, t) = 1 \quad \text{for } t \in \mathbf{R}^+, \tag{3.4.6}$$
$$\tag{3.4.7}$$

and

$$u(z,0) = \begin{cases} 1 + \frac{1}{\varepsilon} & \text{for } z < 0, \\ \frac{1}{\varepsilon} & \text{for } z > 0. \end{cases} \tag{3.4.8}$$

The Von Mises transformation (3.3.1)-(3.3.3) now gives the initial value problem

$$\begin{cases} \dfrac{\partial \hat{u}}{\partial t} = \hat{u}\dfrac{\partial}{\partial \Psi}\left(\hat{u}\dfrac{\partial \hat{u}}{\partial \Psi}\right) & \text{for } (\Psi, t) \in \mathbf{R} \times \mathbf{R}^+, \\ \tilde{u}(\Psi, 0) = \begin{cases} 1 + \frac{1}{\varepsilon} & \text{for } \Psi < 0, \\ \frac{1}{\varepsilon} & \text{for } \Psi > 0. \end{cases} \end{cases} \tag{3.4.9}$$

The special form of the initial condition implies similarity. Let

$$\eta = \frac{\Psi}{\sqrt{t}} \ \text{ and } \ \hat{u}(\Psi, t) = f(\eta),$$

(3.4.10)

then $f(\eta)$ should satisfy the boundary value problem

$$\frac{1}{2}\eta f' + f\{ff'\}' = 0 \ \text{ for } \ \eta \in \mathbf{R}$$

(3.4.11)

with

$$f(-\infty) = 1 + \frac{1}{\varepsilon} \ \text{ and } \ f(+\infty) = \frac{1}{\varepsilon}.$$

(3.4.12)

Here the primes denote differentiation with respect to η. No explicit solution to this boundary value problem is known. However, qualitatively the picture is quite complete: we know that there exists a unique C^∞ solution, strictly decreasing on $\mathbf{R}$, and much is known about the asymptotic behavior of $f(\eta)$ as $\eta \to \pm\infty$, see Van Duijn & Peletier [10], Atkinson & Peletier [1].

We will solve problem (3.4.11), (3.4.12) numerically. For this purpose it is convenient to transform the problem to one on a bounded domain, by considering a equation for the flux with f as independent variable. This transformation and the resulting flux equation have been studied in detail by Atkinson & Peletier [1], Van Duijn et.al [11] and Bouillet & Gomez [4]. Since f is strictly decreasing on $\mathbf{R}$ we can define the inverse

$$\eta = \sigma(f), \ \text{ with } \ \sigma = f^{-1},$$

(3.4.13)

and the flux function

$$w(f) := -ff'(\sigma(f)) \ \text{ for } \ \frac{1}{\varepsilon} \leq f \leq 1 + \frac{1}{\varepsilon}.$$

(3.4.14)

For w we find the boundary value problem

$$\begin{cases} -w\{fw'\}' = \dfrac{f}{2} \\ w(f) > 0 \\ w(\frac{1}{\varepsilon}) = w(1 + \frac{1}{\varepsilon}) = 0 \end{cases}$$

(3.4.15)

for $1/\varepsilon < f < 1 + 1/\varepsilon$, where now primes denote differentiation with respect to f. The sign of w implies that fw' is decreasing. We use this observation to determine $f = f(\eta)$ from the identity

$$\eta = 2fw'(f),$$

(3.4.16)

which also shows that w' changes sign at $f(0) = f_0 \in (1/\varepsilon, 1 + 1/\varepsilon)$ and that $\lim_{f \downarrow 1/\varepsilon} w'(f) = +\infty$ and $\lim_{f \uparrow 1 + 1/\varepsilon} w'(f) = -\infty$.

We solve (3.4.15) numerically by discretizing the derivatives central in f on a equidistant grid. The discretization of (3.4.15) leads to a set of nonlinear algebraic equations which we solve iteratively using a standard multi-dimensional Newton method. Once accurate numerical approximations of $w(f)$ and thereby of $w'(f)$ are obtained we compute $\sigma(f)$ directly using (3.4.16) and $f = f(\eta)$ by inverting the result. Figure 1 shows $w(f)$ and $f(\eta$ for $\varepsilon = 0.2$. The singular nature of w' at the boundary points is not visible in Figure 1. This is due to the asymptotic behavior of w', which is proportional to $\sqrt{\ln(1/w(f))}$ for $f \downarrow 1/\varepsilon$ and $f \uparrow 1 + 1/\varepsilon$, i.e. for $w(f) \downarrow 0$.
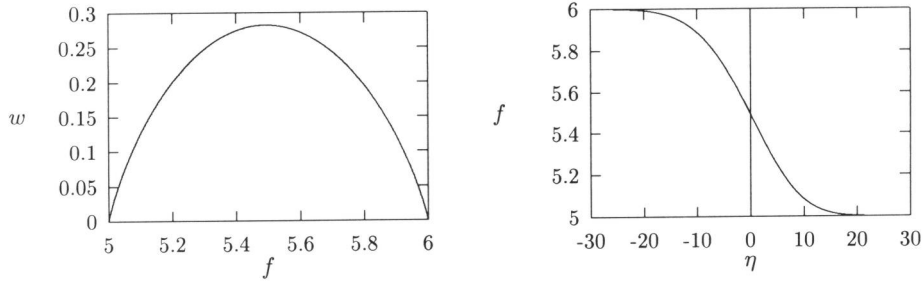
Figure 1. The functions $w(f)$ and $f(\eta)$ for $\varepsilon = 0.2$

Introduction of the similarity variables (3.4.10) in (3.3.13),(3.3.9) and (3.3.12) yields

$$q = q(\Psi, t) = 1 + \frac{1}{2\sqrt{t}} \int_{-\infty}^{\frac{\Psi}{\sqrt{t}}} \frac{s f'}{f^2} \, ds \quad \text{for all} \quad -\infty < \Psi < +\infty, t > 0, \qquad (3.4.17)$$

and

$$z = z(\Psi, t) = \sqrt{t} \int_0^{\frac{\Psi}{\sqrt{t}}} \frac{1}{f(s)} ds + t + \sqrt{t} \int_{-\infty}^0 \frac{s f'}{f^2} \, ds \quad \text{for all} \quad -\infty < \Psi < +\infty, t > 0. \quad (3.4.18)$$

This completes the construction of the solution of the column problem with piecewise constant initial data. The solution is given as parametric pairs $(z(\Psi, t), u(\Psi, t))$ and $(z(\Psi, t), q(\Psi, t))$. Figure 2 shows the results of $u = u(z, t)$ and $q = q(z, t)$ as function of z at fixed time levels, for $\varepsilon = 0.2$.

When using $v := (\rho - \rho_f)/(\rho_s - \rho_f)$ in the scaling (3.4.3), we arrive at the dimensionless system

$$\begin{cases} \dfrac{\partial v}{\partial t} + \dfrac{\partial}{\partial z}(qv) + \dfrac{1}{\varepsilon}\dfrac{\partial q}{\partial z} = 0 \\ \dfrac{\partial v}{\partial t} + q\dfrac{\partial v}{\partial z} - \dfrac{\partial}{\partial z}\left(\dfrac{\partial v}{\partial z}\right) = 0 \end{cases} \qquad (3.4.19)$$

for $(z, t) \in \mathbf{R} \times \mathbf{R}^+$. Note that the same result can be achieved by setting $u = v + 1/\varepsilon$ in (3.2.11). When passing to the limit $\varepsilon \to 0$ (3.4.19) reduces to

$$\begin{cases} \dfrac{\partial q}{\partial z} = 0 \\ \dfrac{\partial v}{\partial t} + q\dfrac{\partial v}{\partial z} - \dfrac{\partial}{\partial z}\left(\dfrac{\partial v}{\partial z}\right) = 0 \end{cases} \qquad (3.4.20)$$

for $(z, t) \in \mathbf{R} \times \mathbf{R}^+$, implying upon integration $q(z, t) = q_s$ and

$$v(z, t) = \frac{1}{2}\left(1 - \text{erf}\left(\frac{z - t}{2\sqrt{t}}\right)\right). \qquad (3.4.21)$$

A formal justification of this limit is given in Van Duijn et.al. [11]. We refer to (3.4.21) as the Boussinesq solution of the column problem.

The dashed line in the u-plot in Figure 2 corresponds to the Boussinesq solution (3.4.21) at $t = 1$. The difference between $(u(z, 1)$ and $v(z, 1)$ is small but noticeable, e.g. up to $\approx 5\%$ in this example. The results in Figure 2 clearly demonstrate the effect of a high concentration (or density) gradient on the fluid flow. At the short time scale of the problem, the deviation from the background flow ($q_s = 1$) is significant. As time proceeds, diffusion flattens the density

profile, which in turn causes decay of the specific discharge distribution towards its limiting value $q(z, \infty) = q_s = 1$.

At the short time scale of the problem $q(\infty, t)$ is negative which means that fluid enters the column at $z = +\infty$. After $t = \hat{t}$, defined by

$$\hat{t} = \frac{1}{4q_s^2} \left(\int_{-\infty}^{+\infty} \frac{sf'}{f^2} \, ds \right)^2 , \qquad (3.4.22)$$

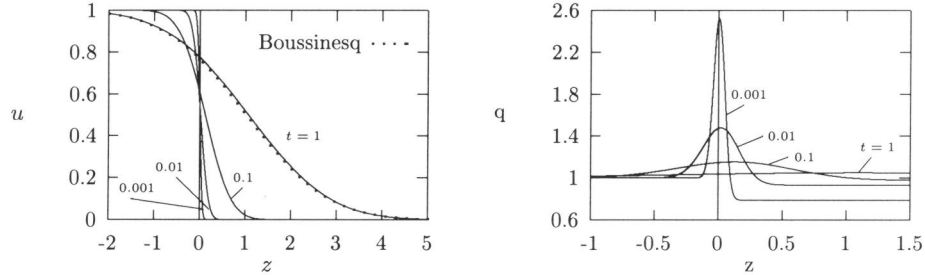$q(\infty, t)$ changes sign and outflow will occur at $z = +\infty$.

Figure 2. Scaled density and velocity profiles for column problem at $t = 0.001, 0.01, 0.1$ and 1.

Remark:

In his study of the laminar boundary layer equations, Crocco [7] introduced a transformation, in literature referred to as the Crocco transformation, which is related to the Von Mises transformation. Crocco takes the velocity in the x-direction and the x-coordinate as new independent variables and the viscous stress and enthalpy as dependent variables. For the case of zero pressure gradient, Crocco [8] proposed a solution procedure which resembles the solution procedure given in this paper. He also derives an equation which is similar to the differential equation in (3.4.15). For details we refer to Crocco's original paper [8] or to the book by Curle [9]

3.4.2   The salt dome problem

The salt dome problem models the flow of fresh groundwater along the surface of a salt rock; see Van Duijn et.al. [11] for a detailed description. A sketch of the flow geometry is given in Figure 3.
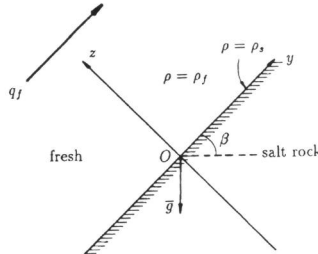

Figure 3. Flow geometry of the salt dome problem.

The flow domain consists of the upper half space $\{z > 0\}$ and is bounded below by an impermeable salt rock (= the salt dome) which has the inclination β with the horizontal plane.

Initially fresh water, $\rho = \rho_f$, is present in the flow domain which is maintained at a constant flow, $q_y = q_f$, far above and parallel to the salt rock boundary. Further, the presence of the salt rock ensures that $\rho = \rho_s$ along the boundary $\{z = 0\}$. Because ρ_f, ρ_s and q_f are constant and because the y-coordinate ranges from $-\infty$ to $+\infty$, we look for solutions with the dependence

$$\rho = \rho(z,t) \quad \text{and} \quad \mathbf{q} = \mathbf{q}(z,t), \tag{3.4.23}$$

satisfying

$$\rho(z,0) = \rho_f \quad \text{for } z \in \mathbf{R}^+, \tag{3.4.24}$$

$$\rho(0,t) = \rho_s \quad \text{for } t \in \mathbf{R}^+, \tag{3.4.25}$$

and

$$q_y(\infty,t) = q_f \quad \text{for } t \in \mathbf{R}^+. \tag{3.4.26}$$

Under assumption (3.4.23) we obtain a linear relation between the y-component of the specific discharge and the fluid density, see e.g. De Josseling De Jong & Van Duijn [16]. It is found by eliminating the pressure from Darcy's law. Taking the curl yields

$$\frac{\partial}{\partial z}\{q_y - \frac{\kappa}{\mu}\rho g_y\} - \frac{\partial}{\partial y}\{q_z - \frac{\kappa}{\mu}\rho g_z\} = 0, \tag{3.4.27}$$

which implies after integration

$$q_y + \frac{\kappa}{\mu}\rho g \sin\!\beta = \ \text{C}, \tag{3.4.28}$$

where C is a constant. Initial condition (3.4.24) implies

$$\rho(+\infty,t) = \rho_f \quad \text{for } t \in \mathbf{R}^+, \tag{3.4.29}$$

which we use, together with (3.4.26), to determine the constant C in (3.4.28). This yields in the linear relation

$$q_y = q_f - \frac{\kappa}{\mu}(\rho - \rho_f)g \, \sin\beta. \tag{3.4.30}$$

In this example we consider $I\!\!D$ to be velocity dependent. However, we cannot treat the full dispersion matrix, but we have to make the assumption that the flow in the y-direction dominates the induced flow (q_z): i.e. $|q_z| << |q_y|$. Then the dispersion tensor only has non-trivial diagonal elements, given by

$$\begin{cases} D_{zz} = \alpha_T|q_y| + nD_{\text{mol}} \\ D_{yy} = \alpha_L|q_y| + nD_{\text{mol}} \end{cases} \tag{3.4.31}$$

Because ρ satisfies (3.4.23), only D_{zz} appears in the model description. Note that D_{zz} combined with (3.4.30) gives

$$D_{zz} = \alpha_T|q_f - \frac{\kappa}{\mu}(\rho - \rho_f)g\sin\beta| + nD_{\text{mol}} := D(\rho). \tag{3.4.32}$$

The object is now to solve the balance equations (3.2.10) (in one space dimension, the z-direction), with the dispersivity given by (3.4.32) and subject to conditions (3.4.24),(3.4.25). As in the example treated in Section 4.1, we need an additional boundary condition forq_z, here along the

salt rock boundary. Following Hassanizadeh & Leijnse [12] we require for the specific discharge along the salt rock boundary

$$q_z(0,t) = -\frac{D(\rho_s)}{\gamma \rho_s \{1 - \omega_s\}} \frac{\partial \rho}{\partial z}(0,t) \text{ for } t \in \mathbf{R}^+. \tag{3.4.33}$$

Here ω_s denotes the salt mass fraction of saturated brine, i.e. $\rho_s = \rho_f e^{\gamma \omega_s}$. To put the equations in dimensionless form we introduce the variables

$$\mathbf{q}^* = \frac{\mathbf{q}}{\hat{q}}, \ z^* = \frac{z}{\alpha_T}, \ t^* = t\frac{\hat{q}}{n\alpha_T}, \ D^* = \frac{D}{\alpha_T \hat{q}}, \ \varepsilon = \frac{\rho_s - \rho_f}{\rho_f} \text{ and } u = \frac{1}{\varepsilon} + \frac{\rho - \rho_f}{\rho_s - \rho_f}, \tag{3.4.34}$$

where $\hat{q} = \frac{\kappa}{\mu}(\rho_s - \rho_f)g \sin\beta$. Dropping the asterisk notation, the dimensionless dispersivity is expressed as

$$D(u) = \lambda + |U - u|, \tag{3.4.35}$$

with

$$\lambda = \frac{nD_{\text{mol}}}{\alpha_T \hat{q}} \quad \text{and} \quad U = \frac{q_f}{\hat{q}} + \frac{1}{\varepsilon}, \tag{3.4.36}$$

and the scaled specific discharge component in the y-direction is given by

$$q_y = U - u. \tag{3.4.37}$$

The scaling proposed here differs from the one used in Section 4.1. It allows us to consider the limit of small molecular diffusion with respect to transversal dispersion, i.e. $\lambda = 0$, a mathematically interesting limit because it leads to degenerate diffusion at points where $u = U$. As a result we obtain the initial-boundary value problem

$$\begin{cases} \dfrac{\partial u}{\partial t} + \dfrac{\partial}{\partial z}(q_z u) = 0 \\ \dfrac{\partial u}{\partial t} + q_z \dfrac{\partial u}{\partial z} = \dfrac{\partial}{\partial z}\left\{ (\lambda + |U - u|)\dfrac{\partial u}{\partial z} \right\} \end{cases} \tag{3.4.38}$$

for $(z,t) \in \mathbf{R}^+ \times \mathbf{R}^+$, subject to

$$u(0,t) = 1 + \frac{1}{\varepsilon} \text{ for } t \in \mathbf{R}^+,$$
$$q_z(0,t) = -\varepsilon K(\varepsilon)\{\lambda + |U - u(0,t)|\}\frac{\partial u}{\partial z}(0,t) \text{ for } t \in \mathbf{R}^+, \tag{3.4.39}$$
$$u(z,0) = \frac{1}{\varepsilon} \text{ for } z \in \mathbf{R}^+,$$

where, through ρ_s and ω_s, K is a function of ε given by

$$K(\varepsilon) = \frac{1}{(1 + \varepsilon)(\gamma - \log(1 + \varepsilon))} \text{ for } 0 < \varepsilon < e^\gamma - 1. \tag{3.4.40}$$

The complete solution of the salt dome problem involves q_y, q_z and u. The pair (q_z, u) solves (3.4.38),(3.4.39), while q_y follows directly from (3.4.37), once u is known. To solve (3.4.38),(3.4.39) we apply the Von Mises transformation and obtain in the (Ψ, t)-plane the problem

$$\begin{cases} \dfrac{\partial \hat{u}}{\partial t} = \hat{u}\dfrac{\partial}{\partial \Psi}\left\{ (\lambda + |U - \hat{u}|)\hat{u}\dfrac{\partial \hat{u}}{\partial \Psi} \right\} & \text{for } \{(\Psi, t) : \varphi(t) < \Psi < +\infty, t > 0\} \\ \hat{u}(\Psi, 0) = \dfrac{1}{\varepsilon} & \text{for } \Psi > \varphi(0) \\ \hat{u}(\varphi(t), t) = 1 + \dfrac{1}{\varepsilon} & \text{for } t > 0 \end{cases} \tag{3.4.41}$$

Here the function $\varphi(t)$ denotes a free boundary in the (Ψ, t)-plane for which we need an additional condition. This condition is obtained by applying the Von Mises transformation to (3.4.39). It takes the from of a Stefan condition:

$$\frac{d\varphi}{dt}(0, t) = \frac{(1+\varepsilon)^2}{\varepsilon} K(\varepsilon)\{\lambda + |U - 1 - \frac{1}{\varepsilon}|\} \frac{\partial \hat{u}}{\partial \Psi}(\varphi(t), t) \text{ for } t \in \mathbf{R}^+. \tag{3.4.42}$$

This expression relates the salt mass flux at the salt rock boundary to the speed of the free boundary in the (Ψ, t)-plane. It is interesting to observe that the Von Mises transformation in the salt dome problem reduces to a nonlinear Stefan problem.

The free boundary problem (3.4.41), (3.4.42) too allows similarity of the form (3.4.10), with the free boundary given by

$$a = \frac{\varphi(t)}{\sqrt{t}} \text{ for } t \in \mathbf{R}^+. \tag{3.4.43}$$

The similarity solution $f = f(\eta)$, $\eta \geq a$, and the free boundary $\eta = a$ are found from the transformed ordinary differential equation problem:

$$\begin{aligned} &\tfrac{1}{2}\eta f' + f(\{\lambda + |U - f|\}ff')' = 0 \text{ for } \eta > a, \\ &f(a) = 1 + \frac{1}{\varepsilon}, \quad f(+\infty) = \frac{1}{\varepsilon} \end{aligned} \tag{3.4.44}$$

and

$$f'(a) = \frac{a}{2\varepsilon K(\varepsilon)\{\lambda + |U - f(a)|\}f^2(a)} \tag{3.4.45}$$

One can show that a solution of (3.4.44), (3.4.45) is strictly decreasing with respect to η. Consequently, from (3.4.45), we find $a < 0$.

As in Section 4.1 we solve the similarity problem by considering the corresponding flux equation. Setting, again,

$$w = \sigma(f) \text{ and } w = w(f) = -2\{\lambda + |U - f|\}ff'(\sigma(f)), \quad \frac{1}{\varepsilon} < f < 1 + \frac{1}{\varepsilon}, \tag{3.4.46}$$

we obtain for w the boundary value problem

$$w\{fw'\}' = -2\{\lambda + |U - f|\}f \text{ in } f \in (1/\varepsilon, 1 + 1/\varepsilon), \tag{3.4.47}$$

with

$$w(1 + \frac{1}{\varepsilon}) = -\frac{a}{(1+\varepsilon)K(\varepsilon)}, \quad w'(1 + \frac{1}{\varepsilon}) = \frac{\varepsilon a}{1+\varepsilon} < 0 \tag{3.4.48}$$

and

$$w(\frac{1}{\varepsilon}) = 0. \tag{3.4.49}$$

To solve this transformed w-problem we apply a shooting procedure: First, for a given $a < 0$, we solve the initial value problem (3.4.47), (3.4.48) for $f \in (1/\varepsilon, 1 + 1/\varepsilon)$ and then adjust a such that (3.4.49) is satisfied.

For two reasons it is more convenient to solve the w-problem in stead of the f-problem directly: (i) the domain is fixed and finite and (ii) the formulation allows to pass to the limit

$\lambda \to 0$ without (numerical) difficulty. To solve the initial value problem (3.4.47), (3.4.48) we apply a Runge-Kutta method with w and w' as primary unknowns.

Once the solution $f(\eta)$ is obtained we return to the original variables in the (z,t)-plane, using expressions (3.3.18), (3.3.17), (3.3.19) combined with the boundary condition (3.4.39) on q_z. Application of the Von Mises transformation in (3.4.39) yields

$$q_z(0,t) = q_0(t) = -\varepsilon K(\varepsilon)\{\lambda + |U - \hat{u}(\varphi(t),t)|\}\hat{u}(\varphi(t),t)\frac{\partial \hat{u}}{\partial \Psi}(\varphi(t),t). \qquad (3.4.50)$$

Introduction of the similarity variables in (3.4.50) and using (3.4.45) in the result gives

$$q_0 = -\frac{a}{2f(a)}. \qquad (3.4.51)$$

After rewriting (3.3.17) in terms of the similarity variables and substitution of (3.4.51), we obtain

$$z = \sqrt{t}\int_0^\eta \frac{1}{f(s)}\, ds + \int_0^t \frac{1}{2\sqrt{t}}\left\{-\frac{a}{f(a)} - \int_0^a \frac{\eta f'}{f^2}\, d\eta\right\} dt, \qquad (3.4.52)$$

implying

$$\xi := \frac{z}{\sqrt{t}} = \int_a^\eta \frac{1}{f(s)}\, ds \ \text{ for } \ \eta > a, \ t \in \mathbf{R}^+. \qquad (3.4.53)$$
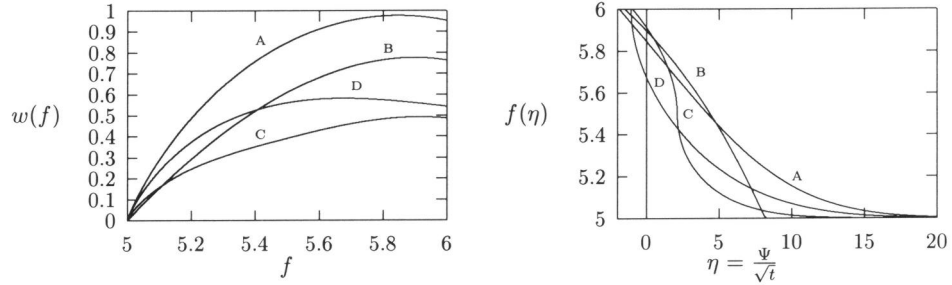

Figure 4. The solutions $w(f)$ and $f(\eta)$ for different λ and U values and $\varepsilon = 0.2$, see Table 1.

In a similar fashion, i.e. after combining (3.3.19), (3.4.10) and (3.4.51), we obtain

$$q_z = \frac{1}{2\sqrt{t}}\left\{-\frac{a}{f(a)} + \int_a^\eta \frac{sf'}{f^2}\, ds\right\} \ \text{ for } \ \eta > a, \ t \in \mathbf{R}^+. \qquad (3.4.54)$$

Note that equation (3.4.53) implies that $\eta\ (=\Psi/\sqrt{t})$ only depends on ξ, which we write as $\eta = \phi(\xi)$. Consequently

$$u(z,t) = \hat{u}(\Psi(z,t),t) = f(\eta) = f(\phi(\xi)) := r(\xi), \qquad (3.4.55)$$

and from (3.4.54)

$$q_z(z,t) = \frac{1}{2\sqrt{t}}\left\{-\frac{a}{f(a)} + \int_a^{\phi(\xi)} \frac{sf'}{f^2}\, ds\right\} := \frac{1}{\sqrt{t}}s(\xi). \qquad (3.4.56)$$

The identities (3.4.55) and (3.4.56) show the relation between solutions obtained with the Von Mises transformation and solutions that result from direct similarity transformation of the one-dimensional balance equations. Properties of the functions $r(\xi)$ and $s(\xi)$ have been extensively

studied in Van Duijn et.al. [11]. Parameter values for λ, U and computed values of a are given in Table 1. The labels A-D refer to the corresponding curves in Figures 4 and 5. Case A is computed with $D = \lambda = 1.0$, i.e. omiting the density dependent dispersivity term. The other three degenerate cases B-D are computed with $\lambda = 0$.

λ	U	a	Curve label
1.0	-	-1.866	A
0.0	5.0	-1.494	B
0.0	5.5	-0.952	C
0.0	6.0	-1.064	D

Table 1. Parameters and computed a-values.

Parameter	Value	Unit
κ	$1.0 \ 10^{-12}$	m^2
μ	$1.0 \ 10^{-3}$	kg/ms
ρ_s	1200	kg/m^3
ρ_f	1000	kg/m^3
ε	0.2	$-$
β	$\pi/4$	45^0
g	10.0	m/s^2
n	0.4	$-$
D_{mol}	$1.5 \ 10^{-9}$	m^2/s
α_T	0.5	m

$$(3.4.57)$$

Table 2. Parameter values.

In most practical situations, λ is small compared to the magnitude of the other dimensionless parameters. Table 2 lists a set of feasible geohydrological parameters in the vicinity of a salt dome, mainly adopted from Herbert et.al. [14]. Using the numbers from Table 1 we obtain $\hat{q} = 1.414 \ 10^{-6}$m/s ≈ 45 m/y and thereby $\lambda = 8.485 \ 10^{-4} \approx 10^{-3} (<< 1!)$.

Figure 4 shows numerical approximations of the solutions $w(f)$ and $f(\eta)$ for the parameter values listed in Table 1. Figure 5 shows the corresponding similarity solution $r(z/\sqrt{t})$ and the scaled specific discharge, plotted as $s(z/\sqrt{t}) = q_z\sqrt{t}$. We omit the plots of $u(z,t)$ and $q(z,t)$ for these cases.
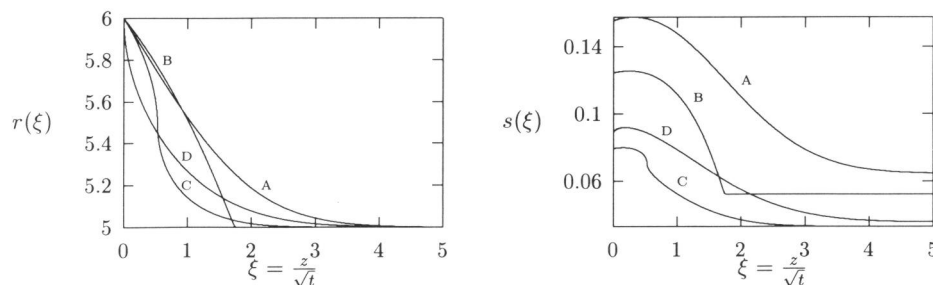
Figure 5. The similarity solutions $r(z/\sqrt{t})$ and $s(z/\sqrt{t})$ for different λ and U values and $\varepsilon = 0.2$, see Table 1.

In case of the non-degenerate example (A), both r and s are smooth, continuously differentiable functions. The degeneracy, i.e. $\lambda = 0$ and $u \to U$ in (3.4.35), causes singular behavior of the derivative r' (and thereby of u'). In case of the examples D and C, r' becomes infinite if $r(\xi) \to U$, where respectively $U = 6.0$ and $U = 5.5$. The corresponding scaled discharges s converge towards their limiting value as $\xi \to \infty$. The degenerate behavior of case B is different: at some point, say $\xi = \xi_0$, the function r attains the value of the (fresh water) boundary/initial condition $1/\varepsilon = 5.0 (= U)$ and remains constant for all $\xi > \xi_0$. Moreover, at $\xi = \xi_0$ r' exhibits a discontinuity, while $r' = 0$ for $\xi > \xi_0$. This point corresponds to an interface in the (z, t)−plane which moves with a finite speed of propagation. At the left hand side of the interface we have $u > 1/\varepsilon$, $u' < 0$, and on the right hand side $u = 1/\varepsilon$, $u' = 0$. The scaled discharge s (curve B) has a constant value for $\xi \geq \xi_0$. The discharges depicted in Figure 5 only result from the volume changes of the fluid due to the presense of (high) density gradients. Moreover, the induced flow is perpendicular to the main (or back ground) flow q_f.

3.4.3   Mixing of parallel fluid layers

Minor changes to the boundary and initial conditions in the salt dome problem lead to the problem of mixing of parallel flowing layers of fresh and salt water. De Josselin De Jong & Van Duijn [16] studied this problem for the incompressible case, i.e. div$(\mathbf{q}) = 0$ and Van Duijn et.al. [11] extended the analyses to the compressible case, when volume changes in the fluid occur. We consider the same flow geometry as is the salt dome problem, but replace the salt rock below the plane $\{z = 0\}$ by porous medium initially saturated with brine with density $\rho = \rho_s$. Equations (3.4.23)-(3.4.37) hold and the boundary conditions are

$$u(-\infty, t) = 1 + \frac{1}{\varepsilon}, \quad u(+\infty, t) = \frac{1}{\varepsilon} \quad \text{and} \quad q_z(-\infty, t) = 0 \qquad (3.4.58)$$

for $t \in \mathbf{R}^+$, while the initial conditions are given by

$$u(z, 0) = \begin{cases} 1 + \frac{1}{\varepsilon} & \text{for} \quad z < 0 \\ \frac{1}{\varepsilon} & \text{for} \quad z > 0 \end{cases} \qquad (3.4.59)$$

The choice of of the boundary condition $q_z(-\infty, t) = 0$ is arbitrary. When solving (3.2.11) subject to (3.4.58),(3.4.59) using Von Mises and similarity transformations we obtain (skipping all details)

$$\frac{z}{\sqrt{t}} = \int_0^\eta \frac{1}{f(\xi)} \, d\xi + \int_{-\infty}^0 \frac{\xi f'}{f^2} \, d\xi \qquad (3.4.60)$$

and

$$q_z = \frac{1}{2\sqrt{t}} \int_{-\infty}^\eta \frac{\xi f'}{f^2} \, d\xi, \qquad (3.4.61)$$

where f is the solution of the boundary value problem

$$\begin{cases} \frac{1}{2}\eta f' + f(\{\lambda + |U - f|\}ff')' = 0 \quad \text{for} \quad \eta \in \mathbf{R} \\ f(-\infty) = 1 + \frac{1}{\varepsilon} \\ f(+\infty) = \frac{1}{\varepsilon} \end{cases} \qquad (3.4.62)$$

Notice again the dependence of η on $z/\sqrt{t}$ in this example, which is due to the choice of the boundary condition $q_z(-\infty, t) = 0$. This implies that the problem also allows a transformation of type (3.5.1).

3.5 Discussion and conclusions

The Von Mises transformation provides a reduction of the governing balance equations to a single second-order nonlinear diffusion equation, which has been studied extensively in the mathematics literature. Much is known about the large time behavior of this equation for fairly general initial functions. In particular, sharp estimates were obtained for the rate at which the solutions converge to the self-similar profile, see e.g. Van Duijn & Peletier [10]. The examples given in Section 4 are special because they allow similarity transformation. The result is a second-order ordinary differential equation which makes the mathematical analysis more tractable.

When discussing the salt dome problem in Section 4, we observed that the similarity variable $\eta \ (= \Psi/\sqrt{t})$ only depends on $\xi \ (= z/\sqrt{t})$ (see (3.4.2)), which implies

$$\Psi(z,t) = \sqrt{t}\, \phi(\xi). \tag{3.5.1}$$

This is a well known transformation in the theory of boundary layers, usually derived through scaling arguments, see e.g. Chorin & Marsden [5]. Considering (3.3.1) and introducing (3.5.1) directly, we obtain

$$u = \frac{d\phi}{d\xi} := \phi' \ \text{ and } \ q_z = \frac{1}{2\sqrt{t}} \left(\frac{\xi\phi' - \phi}{\phi'} \right) \tag{3.5.2}$$

After substitution of (3.5.2) in (3.2.11) and using the boundary conditions, we obtain a third-order initial value problem:

$$\begin{cases} \dfrac{1}{2}\dfrac{\phi''\phi}{\phi'} + (\{\lambda + |U - \phi'|\}\phi'')' = 0 \ \text{ for } \ \xi > 0 \\ \phi(0) = \alpha \\ \phi'(0) = 1 + \dfrac{1}{\varepsilon} \\ \phi''(0) = \dfrac{1}{2(1+\varepsilon)K(\varepsilon)\{\lambda + |U - \phi'(0)|\}}\, \alpha \end{cases} \tag{3.5.3}$$

which reads: find α such that the boundary condition $\phi'(+\infty) = 1/\varepsilon$ is satisfied.

A similar transformation is possible in the column problem. From expression (3.4.18) we deduce that the similarity variable only depends on $(z - t)/\sqrt{t}$, implying

$$\Psi(z,t) = \sqrt{t}\, \theta(\zeta) \ \text{ with } \ \zeta = \left(\frac{z-t}{\sqrt{t}} \right). \tag{3.5.4}$$

The function θ satisfies the third order equation

$$2\theta'''\theta' + \theta\theta'' = 0. \tag{3.5.5}$$

However, the combination of Von Mises and similarity transformations as proposed in Sections 3 and 4 leads to a second-order ordinary differential equation, which is preferable to the third-order equation that results from the direct transformation (3.5.1).

Van Duijn et. al. [11] studied the one-dimensional balance equations by looking for self-similar solutions of the form

$$\rho(z,t) = u(\eta) \ \text{ and } \ q_z(z,t) = \frac{1}{\sqrt{t}}v(\eta), \tag{3.5.6}$$

where $\eta = z/\sqrt{t}$. This transformation also yields a third-order ordinary differential equation. The latter can be reduced to a second-order equation of the form

$$-pp'' = \frac{1}{2}e^{2cx}, \quad p > 0, \tag{3.5.7}$$

where $c = \log(1 + \varepsilon)$. Note that, if we divide equation (3.4.11) by f, introduce $x = \log(f)$ and define a flux function according to $p(x) := -e^{2x}dx/d\eta(\sigma(x))$, where $\sigma(x) = x^{-1}$, we obtain an equation which is identical to (3.5.7), but now with $c = 1$.

Due to the piecewise constant initial density functions, the examples discussed in Section 4 may be regarded as upper limits of the compressibility effect for a given value of ε. The induced specific discharge q_z is infinite at $t = 0$ and decays as $1/\sqrt{t}$ for $t > 0$ (see expressions (3.4.17), (3.4.54) and (3.4.61)). However, in most practical situations, the initial density data will be smooth, which implies that the enhanced discharge remains finite for all $t \geq 0$. Hence, in practice, the difference between Boussinesq solutions ($\mathrm{div}(\mathbf{q}) = 0$) and solutions of the balance equations for fluid and salt will be even smaller than predicted by the corresponding similarity solutions. The compressibility effect is noticeable only at the short time scale of the problems studied in Section 4 and has little impact on the density distributions. The fact that flow is induced in a direction perpendicular to the main groundwater flow direction might be of some practical importance, in particular in connection with transport of radionuclides, leaking from a salt dome repository.

The problem of brine transport is of utmost interest in the safety and risk assessment studies of high-level radioactive waste disposal in subsurface salt formations. With this practical application in mind, many (dedicated) numerical codes have been developed, see e.g. Pinder & Cooper [24], Voss & Souza [30], Kröhn & Zielke [18], Oldenburg & Pruess [22] and Kolditz et.al. [17]. The intricate character of the problem, i.e. nonlinear coupling between the velocity field and the fluid density distribution due to both gravity (free convection) and compressibility effects, implies that the availability of exact or semi-exact solutions of test problems is rather poor. In fact, only Henry's [13] semi-explicit solution of dispersive salt water intrusion in a confined aquifer, initially filled with fresh water, is frequently used as two-dimensional test problem for code verification. In order to test numerical simulators, a particular series of benchmark problems has been proposed by the international HYDROCOIN [15] project. These benchmarks are used for cross-verification of numerical models. Whereas the compressibility effect concerned, our semi-explicit results provide both accurate quantitative and qualitative information about solutions and therefor may contribute to numerical code verification.

Acknowledgement

Bibliography

[1] Atkinson, F.V. & Peletier, L.A., Similarity solutions of the nonlinear diffusion equation, Archs. Ration. Mech. Analysis **54** (1974), p.p. 373-392.

[2] Barenblatt, G.I., Scaling, self-similarity and intermediate asymptotics, Cambridge Univ. Press (1996).

[3] Bear, J., Dynamics of fluids in porous media, Elsevier, New York, 1972

[4] Bouillet, J.E. & S.M. Gomes, An equation with a singular nonlinearity related to diffusion problems in one dimension, Quart. Appl. Math. (1985), 395-402

[5] Chorin, A.J. & J.E. Marsden, A mathematical introduction to fluid mechanics, Springer-Verlag New York Inc, 3rd edition, 1992

[6] Crank,J, Free and moving boundary problems, Oxford University Press New York (1987)

[7] Crocco,L, Atti di Giudonia, **7** (1939)

[8] Crocco, L, Monografie Scientifiche di Aeronautica, **3** (1946)

[9] Curle, N., The laminar boundary layer equations, Oxford University Press, 1962

[10] Van Duijn, C.J. & Peletier, L.A., Asymptotic behaviour of solutions of nonlinear diffusion equations, Arch. Rational Mech. Anal. **65** (1977), p.p. 363-377

[11] Van Duijn, C.J, L.A. Peletier & R.J. Schotting, On the analysis of brine transport in porous media, Europ. Journ. of Appl. Math. Vol **4** (1993), 271-302

[12] Hassanizadeh, S.M. & T. Leijnse, On the modelling of brine transport in porous media, Water Res. Research **24** (1988), 321-330

[13] Henry, H.R., Interfaces between salt water and fresh water in coastal aquifers, US Geol. Surv. Water-Supply Paper 1613-C, Sea water in coastal aquifers (1964), p.p. 35-70

[14] Herbert, A.W., C.P. Jackson & D.A. Lever, Coupled groundwater flow and solute transport with fluid density strongly dependent upon concentration, Water Res. Research **24** (1988), 1781-1795

[15] HYDROCOIN, Swedish Nuclear Inspectorate, An international project for studying groundwater hydrology modeling strategies, Level 1 Final Report: Verification of groundwater flow ,odels, Case 5. Swedish Nucl. Insp., Stockholm (1986)

[16] Josselin de Jong, G. de & C.J. Van Duijn, Transverse dispersion from an originally sharp fresh-salt interface caused by shear flow, J. Hydrology **84** (1986), 55-79

93

[17] Kolditz, O., Ratke, R., Diersch, H.G. and Zielke, W., Coupled groundwater flow and transport: 1. Verification of variable density flow and transport models, Adv. Water Resour. **21**(1) (1998), p.p. 27-46

[18] Kröhn, K.P., & Zielke, W, FE-Simulation von Transportvorgängen im klüftigen Gestein., Deutsche Gewässerkundliche Mitteilungen **35**(3-4) (1991), p.p. 82-88

[19] Landau, H.G., Heat conduction in a melting solid, Q. Appl. Math. **7** (1950), 81-94

[20] Meirmanov, A.M., The stefan problem, De Gruyter expositions in mathematics, Berlin-New York (1992).

[21] Mises, R. Von & K.O. Friedrichs, Fluid dynamics, Applied mathematics series 5, Springer, New York (1977), 171

[22] Oldenburg, C.M. & Pruess, K., Dispersive transport dynamics in a strongly coupled groundwater-brine flow system, Wat. Resour. Res. **31**(2) (1995), p.p. 289-302

[23] Peletier, L.A. & C.J. van Duijn, A class of similarity solutions of the nonlinear diffusion equation, Nonl. Analysis, Theory, Methods and Applications, Vol. 1 **3**, 223-233

[24] Pinder, G.F. & Cooper, H.H., A numerical technique for c alculating the transient position of the salt water front, Water Resour. Res. bf 6 (1970), p.p. 875-882

[25] Raats, P.A.C., Convective transport of ideal tracers in unsaturated soils, in: Arnold, E.M., G.W. Gee and R.W. Nelson (eds.), Proceedings of the symposium on unsaturated flow and transport modelling, Seattle, Washington, (1982), 249-265

[26] Raats, P.A.C., Tracing parcels of water and solutes in unsaturated zones, in: Yaron, B, G. Dagan and J. Goldschmid (eds.), Pollutants in porous media: The unsaturated zone between soil surface and groundwater, Berlin, Springer (1984), 4-16

[27] Raats, P.A.C., Applications of the theory of mixtures in soil science, Math. Modelling **9** (1987), 849-856

[28] Roxburgh, I.S., Geology of high-level radioactive waste disposal, An Introduction,Chapman and Hall London New York (1987).

[29] Valk, C.F. de & P.A.C. Raats, Lumped models of convective solute transport in heterogeneous porous media: One-dimensional media, Water Res. Res, Vol. **31** (1995), 883-892

[30] Voss, C.I. & Souza, W.R., Variable density flow and solute transport simulation of regional aquifers containing a narrow freshwater-saltwater transition zone. Water Resour. Res. **23**(10) (1987), p.p. 1851-1866

Chapter 4

Brine transport: high concentration dispersion

4.1 Introduction

In recent years there has been a growing interest in the modelling of density-dependent flow and transport problems. Of particular interest have been the cases where high concentration differences in the system occur, e.g., in relation with the disposal of hazardous waste in salt formations. Some of the studies have been directed at developing numerical models capable of handling strong nonlinearities in the equations (see e.g. Leijnse [15], Kolditz et al. [14]; Oldenburg and Pruess [19]; for a list of such simulators see Kolditz et al. [14]).

Another group of studies have concentrated on the understanding of the physical processes and the validity of the basic equations used for the modelling of flow and transport. Examples are the works of Schincariol et. al. [24], Welty and Gelhar [27] and Wheatcraft [28] , Kempers [12], [13] and Hassanizadeh and Leijnse [6], [5].

Commonly, salt is considered to be nonadsorbing so that the basic equations governing high concentration (HC) transport in a rigid porous medium read:

$$n\frac{\partial \rho}{\partial t} + \text{div}\,(\rho \mathbf{q}) = 0 \qquad (4.1.1)$$

and

$$n\frac{\partial \rho\omega}{\partial t} + \text{div}\,(\rho\omega\mathbf{q} + \mathbf{J}) = 0, \qquad (4.1.2)$$

where n is porosity, ρ is fluid density, $\mathbf{q}$ is the specific discharge vector (or Darcy velocity), $\mathbf{J}$ is the dispersive mass flux vector and ω is the salt mass fraction, which is defined as the salt concentration divided by the fluid density. These are equations of mass balance and need to be supplemented with equations of momentum balance. Commonly, the classical Darcy's law and a linear Fickian dispersion equation are employed for this purpose. Hassanizadeh [8], [9] suggested that these equations may not be valid when high concentration gradients exist. This was later supported by one-dimensional displacement experiments (Hassanizadeh et al. [7]) . It was found that the dispersivity does not seem to be a property of the medium but may vary from experiment to experiment; it had to be decreased as the difference in concentration of the resident and displacing fluids increased. Hassanizadeh [7] showed that this effect could not be modelled by a dependence of dispersivity on salt concentration. Instead, he proposed the

following nonlinear extension of the Fickian dispersion equation

$$\mathbf{J}(\beta J + 1) = -\mathbf{D}\rho \text{ grad } \omega, \tag{4.1.3}$$

where β is the HC-coefficient and $\mathbf{D}$ is the well-know dispersion tensor given by:

$$\mathbf{D} = (nD_m + \alpha_T q)\mathbf{I} + (\alpha_L - \alpha_T)\mathbf{q}\mathbf{q}/q, \tag{4.1.4}$$

Here, D_m denotes the effective molecular diffusion coefficient (including tortuosity effects), α_L and α_T are the longitudinal and transversal dispersion lengths, , q is the magnitude of the specific discharge vector and $\mathbf{I}$ is the unit tensor. Hassanizadeh and Leijnse [5] have shown that the new relationship gives very good fits to their measured breakthrough curves. Their experiments, however, were limited in number and scope. A more extensive experimental study was later carried out by Moser [17] which included the effects of varying the flow velocity. This paper reports on two different but related studies. First, the one-dimensional equations of flow and transport are analyzed mathematically. An exact and explicit solution is obtained assuming a constant flow rate in the column and the dominance of the nonlinear dispersion term in (4.1.3). A semi-explicit solution, allowing local discharge variations due to high density differences, is given. Moreover, a numerical solution of the full set of equations is provided. The three solutions are compared and conclusions are drawn with regard to the relative significance of various terms, under different concentration gradients. Second, the experimental data of Moser [17] are analyzed and the validity of the nonlinear dispersion equation (4.1.3) is established. It is found that the HC-coefficient varies inversely with the flow velocity q.

4.2   Governing equations in one space dimension

Both experimetal and analytical studies reported here deal with HC solute transport in a one-dimensional domain. Therefore the governing equations presented in the previous section reduce to

$$n\frac{\partial \rho}{\partial t} + \frac{\partial}{\partial z}(\rho q) = 0, \tag{4.2.1}$$

where n denotes the porosity of the porous medium, ρ the fluid mass density, and $q = q(z,t)$ the specific discharge in the z-direction, and

$$n\frac{\partial \rho\omega}{\partial t} + \frac{\partial}{\partial z}\{\rho\omega q + J\} = 0 \tag{4.2.2}$$

where ω is the salt mass fraction and $J = J(z,t)$ the dispersive mass flux. Following Hassanizadeh & Leijnse [5], J is assumed to satisfy the nonlinear dispersion equation

$$J(\beta|J| + 1) = -D\rho\frac{\partial \omega}{\partial z}, \tag{4.2.3}$$

where β is a material coefficient which may depend on the flow velocity and D is the well-known one-dimensional dispersion coefficient, given by

$$D = nD_m + \alpha_L q. \tag{4.2.4}$$

Neglecting pressure effects and assuming isothermal conditions, the relation between density ρ and salt mass fraction ω is given by an equation of state

$$\rho = \rho_f e^{\gamma\omega}. \tag{4.2.5}$$

The constant γ in (4.2.5) is a curve fitting constant given by $\gamma = 0.6923 \approx \ln(2)$ and ρ_f is the (reference) density of fresh water. After combining (4.2.1) and (4.2.2) (see e.g. Van Duijn et.al, 1993) and substitution of (4.2.5) in the result, we obtain a set of three equations in terms of ρ, q and J:

$$n\frac{\partial \rho}{\partial t} + \frac{\partial}{\partial z}(\rho q) = 0, \qquad (4.2.6)$$

$$n\frac{\partial \rho}{\partial t} + q\frac{\partial \rho}{\partial z} + \gamma\frac{\partial}{\partial z}J = 0, \qquad (4.2.7)$$

and

$$J(\beta|J| + 1) = -D\frac{1}{\gamma}\frac{\partial \rho}{\partial z}. \qquad (4.2.8)$$

Next we introduce the following set of dimensionless variables:

$$z^* := z\frac{q_0}{D_0}, \quad t^* := t\frac{q_0^2}{nD_0}, \quad q^* := \frac{q}{q_0}, \quad J^* := J\frac{1}{\rho_f q_0} \text{ and } \rho := \frac{\rho - \rho_f}{\rho_s - \rho_f}. \qquad (4.2.9)$$

The relative density difference is defined as

$$\varepsilon = \frac{\rho_s - \rho_f}{\rho_f}. \qquad (4.2.10)$$

Moreover, we define a dimensionless parameter β_0^* such that

$$\beta_0^* = \beta q_0 \rho_f. \qquad (4.2.11)$$

For convenience we introduce a parameter θ, defined as the ratio

$$\theta = \frac{D}{D_0}. \qquad (4.2.12)$$

Here, D_0 and q_0 denote reference parameters, defined by the conditions of the experiments. Substitution of (4.2.9) and (4.2.10) in equations (4.2.6)-(4.2.8) yields (dropping the asterisks notation for convenience)

$$\frac{\partial \rho}{\partial t} + \frac{\partial}{\partial z}(q\rho) + \frac{1}{\varepsilon}\frac{\partial q}{\partial z} = 0, \qquad (4.2.13)$$

$$\frac{\partial \rho}{\partial t} + q\frac{\partial \rho}{\partial z} + \gamma\frac{\partial J}{\partial z} = 0, \qquad (4.2.14)$$

and

$$J(\beta_0\varepsilon|J| + 1) = -\frac{\theta}{\gamma}\frac{\partial \rho}{\partial z}. \qquad (4.2.15)$$

We assume that z is in the direction of decreasing density, such that $\partial\rho/\partial z < 0$. This implies $J > 0$ for all $(z,t) \in \mathbf{R} \times \mathbf{R}^+$. Under this assumption, (4.2.15) can be solved in terms of $\partial\rho/\partial z$, yielding

$$J = -\frac{1}{2\beta_0\varepsilon} + \frac{1}{2\beta_0\varepsilon}\sqrt{1 - 4\beta_0\varepsilon\frac{\theta}{\gamma}\frac{\partial \rho}{\partial z}} > 0 \qquad (4.2.16)$$

An implication of taking the full fluid mass balance (4.1.1) into account is that local density gradients cause enhanced flow in the column. During all our experiments, see Section 8, the inflow rate was kept constant. The scaled dispersion parameters β_0 and θ are velocity dependent. However, we disregard variations of these parameters due to the enhanced flow by assuming that β_0 and θ (and thereby the unscaled β and D) only depend on the mean or background flow in the column. Under this assumption, substitution of (4.2.16) in (4.2.14) gives

$$\frac{\partial \rho}{\partial t} + q \frac{\partial \rho}{\partial z} + \frac{\gamma}{2\beta_0 \varepsilon} \frac{\partial}{\partial z} \sqrt{1 - 4\beta_0 \varepsilon \frac{\theta}{\gamma} \frac{\partial \rho}{\partial z}} = 0. \tag{4.2.17}$$

Equations (4.2.13) and (4.2.17) are in 'standard' form. The analysis will be confined to this set of equations, subject to initial/boundary conditions imposed by the experiments.

As in Hassanizadeh & Leijnse [5], we introduce the notion of a (scaled) apparent dispersion coefficient θ_{app} defined by

$$J = -\theta_{\mathrm{app}} \frac{\partial \rho}{\partial z}. \tag{4.2.18}$$

Substitution of (4.2.18) in (4.2.16) and solving for θ_{app} yields

$$\frac{\theta_{\mathrm{app}}}{\theta} = \frac{2}{1 + \sqrt{1 - 4\beta_0 \varepsilon \frac{\theta}{\gamma} \frac{\partial \rho}{\partial z}}}. \tag{4.2.19}$$

Regardless of the choise of the reference dispersion coefficient D_0, the ratio $\theta_{\mathrm{app}}/\theta$ is equal to the ratio $\alpha_{L_{\mathrm{appa}}}/\alpha_L$, as defined in [5]. Notice that the apparent dispersion coefficient decreases when the gradient $-\partial \rho/\partial z$ increases for any $\beta_0, \varepsilon > 0$. In the limit $\partial \rho/\partial z \to 0$, which is in general the case for large times or when $\varepsilon \to 0$, we obtain the well known convection-diffusion equation

$$\frac{\partial \rho}{\partial t} + q \frac{\partial \rho}{\partial z} - \theta \frac{\partial^2 \rho}{\partial z^2} = 0. \tag{4.2.20}$$

4.3 Boundary and initial conditions

In order to keep the mathematical analysis as simple as possible we assume that the experimental column of finite length may be replaced by an infinitely long column. Effects due to the inlet boundary of a finite column usually vanish rapidly as time proceeds. This was explicitly shown by Ogata & Banks [18] for tracer transport in finite and semi-finite columns. The experimental column is initially filled with fresh water (ρ_f). At $t = 0$, brine (ρ_s) starts entering the column with uniform specific discharge q_s. The origin $z = 0$ coincides with the position of the inlet filter of the column. This implies the following scaled initial condition for the infinite column:

$$\rho(z, 0) = \rho_0(z) = \begin{cases} 1 & \text{for} \quad z < 0 \\ 0 & \text{for} \quad z > 0 \end{cases} \tag{4.3.1}$$

for $z \in \mathbf{R}$, while the boundary condition for the scaled specific discharge is given by

$$q(-\infty, t) = 1 \ \text{for} \ t > 0. \tag{4.3.2}$$

Subtraction of (4.2.14) and (4.2.13), and using (4.2.16), yields

$$\frac{\partial q}{\partial z} = \frac{\gamma \varepsilon}{\varepsilon \rho + 1} \frac{\partial J}{\partial z} = \frac{\varepsilon}{\varepsilon \rho + 1} \frac{\theta}{\sqrt{1 - 4\beta_0 \varepsilon \frac{\theta}{\gamma} \frac{\partial \rho}{\partial z}}} \frac{\partial^2 \rho}{\partial z^2}, \tag{4.3.3}$$

which indicates that (4.3.1) and (4.3.2) are sufficient conditions to obtain a unique solution. Moreover, this expression implies that density variations ($\varepsilon > 0$) affect the compressibility of the fluid, which in turn causes enhanced fluid flow. In the limit $\varepsilon \to 0$ the right hand side of (4.3.3) vanishes, implying $q = 1$ in the whole flow domain. The limit $\beta_0 \to 0$, i.e. constant diffusivity/dispersivity in Fick's law, has been studied in detail by Van Duijn et. al. [2], Van Duijn et. al. [3] and Van Duijn & Schotting [4], for various flow geometries. They showed that the compressibility effect due to local density variations is in general small, and even negligible in some cases.

4.4   The explicit solution

As a first step in our analysis, we make two approximations:

- The fluid mass balance equation (4.2.13) is disregarded by assuming a constant flow rate $q(z,t) = 1$ for all $(z,t) \in \mathbf{R} \times \mathbf{R}^+$ in the column. The implications of taking the full fluid mass balance equation, i.e. (4.2.13), into account are analyzed in the next section.

- In the nonlinear mass flux equation (4.2.16), the nonlinear term is assumed to dominate such that

$$-4\beta_0 \varepsilon \frac{\theta}{\gamma} \frac{\partial \rho}{\partial z} >> 1, \qquad (4.4.1)$$

This assumption is justified when there exists a sharp front with a large ε (which has been the case in experiments reported here).

As a result of these approximations, (4.2.17) reduces to

$$\frac{\partial \rho}{\partial t} + \frac{\partial \rho}{\partial z} + \sqrt{\frac{\theta \gamma}{\beta_0 \varepsilon}} \frac{\partial}{\partial z} \left\{ -\frac{\partial \rho}{\partial z} \right\}^{\frac{1}{2}} = 0. \qquad (4.4.2)$$

After differentiating (4.4.2) with respect to z and introduction of the variable

$$w = -\frac{\partial \rho}{\partial z}, \qquad (4.4.3)$$

we obtain

$$\frac{\partial w}{\partial t} + \frac{\partial w}{\partial z} = \sqrt{\frac{\theta \gamma}{\beta_0 \varepsilon}} \frac{\partial^2}{\partial z^2} w^{\frac{1}{2}}, \qquad (4.4.4)$$

subject to the initial condition

$$w(z,0) = w_0(z) = \delta(z) \quad \text{for} \ \ z \in \mathbf{R}, \qquad (4.4.5)$$

where $\delta(z)$ denotes the Dirac delta function. The solution satisfies the 'mass' conservation property

$$\int_{-\infty}^{+\infty} w(z,t) \, dz = \int_{-\infty}^{+\infty} w_0(z) \, dz = 1 \quad \text{for} \ \ t > 0. \qquad (4.4.6)$$

The latter follows immediately from (4.3.1). Because $q = 1 = $ constant, it is convenient to introduce a moving coordinate defined by

$$s = z - t, \qquad (4.4.7)$$

and the transformation

$$w(z,t) = v(s(z,t),t), \tag{4.4.8}$$

where $v(s,t)$ is the solution of the initial value problem

$$\frac{\partial v}{\partial t} = \sqrt{\frac{\theta\gamma}{\beta_0\varepsilon}} \frac{\partial^2}{\partial s^2} v^{\frac{1}{2}} \text{ for } (s,t) \in \mathbf{R} \times \mathbf{R}^+, \tag{4.4.9}$$

subject to

$$v(s,0) = v_0(s) = \delta(s) \text{ for } t > 0. \tag{4.4.10}$$

Next we introduce a similarity variable of the form

$$v(s,t) = t^\alpha f(\eta) \text{ with } \eta = st^{-\phi} \tag{4.4.11}$$

Substitution of (4.4.11) in the conservation integral (4.4.6) yields

$$t^{\alpha+\phi} \int_{-\infty}^{+\infty} f(\eta)\, d\eta = 1 \text{ for } t > 0, \tag{4.4.12}$$

implying

$$\alpha + \phi = 0 \text{ and } \int_{-\infty}^{+\infty} f(\eta)\, d\eta = 1. \tag{4.4.13}$$

After substitution of (4.4.11) in (4.4.9), and using (4.4.13) in the result, we obtain

$$\alpha = -\frac{2}{3} \text{ and } \phi = +\frac{2}{3}. \tag{4.4.14}$$

Thus, the function f has to satisfy the boundary value problem

$$\frac{2}{3}(\eta f)' + \sqrt{\frac{\theta\gamma}{\beta_0\varepsilon}} (f^{\frac{1}{2}})'' = 0 \text{ for } \eta \in \mathbf{R}, \tag{4.4.15}$$

where the primes denote differentiation with respect to η, subject to

$$f(\pm\infty) = 0. \tag{4.4.16}$$

Integration of (4.4.15) yields

$$\frac{2}{3}\eta f + \sqrt{\frac{\theta\gamma}{\beta_0\varepsilon}} (f^{\frac{1}{2}})' + C_1 = 0. \tag{4.4.17}$$

Then we use conditions (4.4.16) to obtain $C_1 = 0$. Integrating (4.4.17) once more gives

$$f(\eta) = \frac{1}{\left(\frac{1}{3}\sqrt{\frac{\beta_0\varepsilon}{\theta\gamma}}\eta^2 + C_2\right)^2}, \quad \text{with } C_2 = \left(\frac{3\pi^2}{4}\right)^{\frac{1}{3}} \left(\frac{\theta\gamma}{\beta_0\varepsilon}\right)^{\frac{1}{6}}, \tag{4.4.18}$$

where the value of the integration constant C_2 is determined using the conservation integral in (4.4.13). Back transformation to the original scaled density variable yields (skipping all details) yields

$$\rho(z, t) = -\int_0^\eta f(\xi) \, d\xi + C_3, \qquad (4.4.19)$$

where C_3 denotes an integration constant. Initial condition (4.3.1) implies: $\rho(-\infty, t) = 1$ and $\rho(+\infty, t) = 0$, which is used to obtain C_3. The final result, in the original scaled variables, is given by

$$\rho(z, t) = \frac{1}{2} \left\{ 1 - \frac{\arctan\left(\sqrt{\frac{B}{C}}(z-t)t^{-\frac{2}{3}}\right)}{C\sqrt{BC}} - \frac{(z-t)t^{-\frac{2}{3}}}{C(B(z-t)^2 t^{-\frac{4}{3}} + C)} \right\}, \qquad (4.4.20)$$

for $(z, t) \in \mathbf{R} \times \mathbf{R}^+$, where

$$B = \frac{1}{3}\sqrt{\frac{\beta_0 \varepsilon}{(\theta\gamma)}} \quad \text{and} \quad C = C_2 = \left(\frac{3\pi^2}{4}\right)^{\frac{1}{3}} \left(\frac{\theta\gamma}{\beta_0 \varepsilon}\right)^{\frac{1}{6}}. \qquad (4.4.21)$$

A comparison of (4.4.20) with experimental data will be given in Section 9.

4.5 A semi-explicit solution

In this analysis we drop the the constant flow rate assumption. Thus we solve (4.2.13) and (4.2.17), subject to the initial/boundary conditions (4.3.1) and (4.3.2), for $\varepsilon > 0$ and $\beta_0 > 0$. Assumption (4.4.1) is maintained. The idea is to apply a variant of the Von Mises transformation (see e.g. Von Mises & Friedrichs [16] and Van Duijn & Schotting [4]) in order to reduce the system (4.2.13), (4.2.17) to a single nonlinear diffusion equation. First, we introduce a new scaled density variable

$$u = \rho + \frac{1}{\varepsilon} \quad \text{for} \ \varepsilon > 0. \qquad (4.5.1)$$

Substitution of (4.5.1) in equations (4.2.13),(4.2.17) yields

$$\frac{\partial u}{\partial t} + \frac{\partial}{\partial z}(qu) = 0 \qquad (4.5.2)$$

and

$$\frac{\partial u}{\partial t} + q\frac{\partial u}{\partial z} + \frac{\theta\gamma}{\beta_0 \varepsilon}\frac{\partial}{\partial z}\left\{-\frac{\partial u}{\partial z}\right\}^{\frac{1}{2}} = 0. \qquad (4.5.3)$$

Hence, the initial/boundary conditions in the new variable are given by

$$u(z, 0) = u_0(z) = \begin{cases} 1 + \frac{1}{\varepsilon} & \text{for} \ z < 0 \\[2mm] \frac{1}{\varepsilon} & \text{for} \ z > 0 \end{cases} \qquad (4.5.4)$$

and

$$q(-\infty, t) = 1. \qquad (4.5.5)$$

Considering the fluid balance equation (4.5.2) as the divergence operator in the (t, z)-plane, acting on a vector (u, qu) we introduce a modified stream function $\Psi = \Psi(z, t)$, which satisfies

$$u = \frac{\partial \Psi}{\partial z} \quad \text{and} \quad qu = -\frac{\partial \Psi}{\partial t}. \tag{4.5.6}$$

The Von Mises variables are

$$t = t \quad \text{and} \quad \Psi = \int_{\varsigma(t)}^{z} u(\zeta, t) \, d\zeta, \tag{4.5.7}$$

where $\varsigma(t)$ is a yet unknown function of time, which will be determined from the boundary condition on q, i.e. 4.5.5, such that $\varsigma(0) = 0$. The Von Mises transformation is

$$u(z, t) = \hat{u}(\Psi(z, t), t) = \hat{u}(\Psi, t). \tag{4.5.8}$$

Under this transformation, the system of equations (4.2.13) and (4.2.17) reduces to single non-linear diffusion equation

$$\frac{\partial \hat{u}}{\partial t} + \sqrt{\frac{\theta \gamma}{\beta_0 \varepsilon}} \, \hat{u} \frac{\partial}{\partial \Psi} \left\{ -\hat{u} \frac{\partial \hat{u}}{\partial \Psi} \right\}^{\frac{1}{2}} = 0. \tag{4.5.9}$$

Multiplication of (4.5.9) by $\hat{u}$ and introduction of the new variable $\vartheta = \hat{u}^2$ yields

$$\frac{\partial \vartheta}{\partial t} + \sqrt{\frac{2\theta \gamma}{\beta_0 \varepsilon}} \, \vartheta \frac{\partial}{\partial \Psi} \left\{ -\frac{\partial \vartheta}{\partial \Psi} \right\}^{\frac{1}{2}} = 0, \tag{4.5.10}$$

subject to

$$\vartheta(\Psi, 0) = \vartheta_0(\Psi) = \begin{cases} (1 + \frac{1}{\varepsilon})^2 & \text{for} \quad \Psi < 0 \\[2mm] (\frac{1}{\varepsilon})^2 & \text{for} \quad \Psi > 0 \end{cases} \tag{4.5.11}$$

Next, we look for a similarity solution of the form

$$\vartheta(\Psi, t) = g(\eta) \quad \text{where} \quad \eta = \Psi t^{-\frac{2}{3}}. \tag{4.5.12}$$

The function $g(\eta)$ is the solution of the boundary value problem

$$\begin{cases} -\frac{2}{3} \eta g' + \sqrt{\frac{2\theta \gamma}{\beta_0 \varepsilon}} (\{-g'\}^{\frac{1}{2}})' = 0 \quad \text{for} \quad \eta \in \mathbf{R} \\[3mm] g(-\infty) = (1 + \frac{1}{\varepsilon})^2 \quad \text{and} \quad g(+\infty) = (\frac{1}{\varepsilon})^2 \end{cases} \tag{4.5.13}$$

Because it is not possible to obtain an exact solution of (4.5.13) we have to resort to a numerical method. Since g is strictly decreasing we may define the inverse of g and a flux variable according to

$$\eta = \eta(g) \quad \text{and} \quad h(g) = \{-g'\}^{\frac{1}{2}}, \tag{4.5.14}$$

implying

$$\eta = \frac{3}{2} \sqrt{\frac{2\theta \gamma}{\beta_0 \varepsilon}} g \frac{dh}{dg}, \tag{4.5.15}$$

and the boundary value problem

$$
\begin{cases}
h^2 \dfrac{d}{dg}\left(g\dfrac{dh}{dg}\right) = \dfrac{2}{3}\sqrt{\dfrac{\beta_0\varepsilon}{2\theta\gamma}} \ \ \text{for } g \in [(\tfrac{1}{\varepsilon})^2,(1+\tfrac{1}{\varepsilon})^2] \\[3mm]
h((1+\tfrac{1}{\varepsilon})^2) = 0 \ \text{ and } \ h((\tfrac{1}{\varepsilon})^2) = 0.
\end{cases}
\tag{4.5.16}
$$

We solve this boundary value problem by discretizing the equation on a equidistant grid and solve the resulting set of nonlinear algebraic equations iteratively by means of a standard multi-dimensional Newton method. This yields numerical approximations of h and thereby dh/dg. The latter is used in (4.5.15) to compute $g(\eta)$. Once an accurate approximation of the function $g(\eta)$ has been obtained we return to the original variables in the (z,t)-plane as follows. Integration of the first equation in (4.5.6) yields

$$
z = \int_0^{\psi(z,t)} \frac{1}{\hat{u}(s,t)}\,ds + \varsigma(t) \ \ \text{for } (z,t) \in \mathbf{R} \times \mathbf{R}^+.
\tag{4.5.17}
$$

Differentiating (4.5.17) with respect to t and using (4.5.6) and (4.5.8) in the result yields

$$
q = \varsigma'(t) - \int_0^{\Psi(z,t)} \frac{\hat{u}_t}{\hat{u}^2}(\xi,t)\,d\xi.
\tag{4.5.18}
$$

Next we use the boundary condition (4.5.5) to determine the function $\varsigma(t)$, yielding

$$
\varsigma(t) = \int_0^t \left\{ 1 - \int_{-\infty}^0 \frac{\hat{u}_t}{\hat{u}^2}(\xi,\tau)\,d\xi \right\}\,d\tau \ \ \text{for } t > 0.
\tag{4.5.19}
$$

Finally, after substitution of (4.5.19) in (4.5.17) and expressing $\hat{u}(\Psi,t)$ in terms of the similarity solution $g(\eta)$ we obtain

$$
z = t^{\frac{2}{3}}\int_0^{\eta} \frac{1}{g(\sigma)^{\frac{1}{2}}}\,d\sigma + t + \frac{1}{2}t^{\frac{2}{3}}\int_{-\infty}^0 \frac{\sigma g'}{g^{\frac{3}{2}}}\,d\sigma,
\tag{4.5.20}
$$

$$
\tag{4.5.21}
$$

and

$$
q = 1 + \frac{1}{3t^{\frac{1}{3}}}\int_{-\infty}^{\eta} \frac{\sigma g'}{g^{\frac{3}{2}}}\,d\sigma,
\tag{4.5.22}
$$

and

$$
u(z,t) = \hat{u}(\Psi,t) = \sqrt{g(\eta)} := \rho(z,t) + \frac{1}{\varepsilon}.
\tag{4.5.23}
$$

Van Duijn & Schotting [4] showed that in the linear Fickian case, i.e. $D = \text{constant}$ ($\beta_0 = 0$), the specific discharge distribution in an infinitely long porous column decays with $t^{-\frac{1}{2}}$, while here the specific discharge exhibits $t^{-\frac{1}{3}}$-decay.

4.6 A numerical solution of the full set of equations

Finally, for reference purposes, assumption (4.4.1) is also relaxed and the full set of equations (4.2.13)-(4.2.14), subject to (4.3.1) and (4.3.2), is solved numerically. This is achieved by solving

the reduced equations (4.2.17) and (4.3.3) with standard schemes. The Heaviside initial condition for u is approximated by a very steep error function on a fine equidistant grid. Equation (4.3.3) is discretized explicitly in space, providing a numerical approximation of the specific discharge distribution at that time level. A standard Crank-Nicholson scheme is used to discretize (4.2.17), yielding a numerical approximation of the density distribution at the new time level. The corresponding set of nonlinear algebraic equations is iteratively solved using a multidimensional Newton method. Once the density distribution at the new time level is known, we return to the discrete version of (4.3.3) to compute the specific discharge distribution at that time level, and so on.

4.7 Comparison of solutions

The explicit solution (4.4.20) is obtained under two simplifying assumptions , i.e. the explicit approximation (implying constant q in the column) and the assumption that $-4\beta_0\varepsilon\frac{\theta}{\gamma}\frac{\partial\rho}{\partial z} >> 1$. The latter is the only simplifying assumption needed to obtain the semi-explicit (Von Mises) solution , which incorporates the compressibility effect due to local density variations in the fluid. The numerical solution is based on the full set of equations, i.e. (4.2.13)-(4.2.15), subject to (4.3.1) and (4.3.2). The compressibility effect causes local deviations from this constant (background) velocity at points where $|\partial\rho/\partial z| > 0$, see e.g. (4.3.3) or expression (4.5.22), implying additional net displacement of the density front. The parameter controlling the magnitude of this effect is the relative density difference. Note that in view of (4.3.3), given a scaled density distribution $u(z,t)$, we may conclude $\partial q/\partial z|_{\beta_0=0} > \partial q/\partial z|_{\beta_0>0}$. Hence, the linear Fickian case, which corresponds to $\beta_0 = 0$, gives an upper bound for the magnitude of the enhanced flow.

At the short time scale we expect only little difference between the approximate solutions and the numerical solution. Figure 1 shows scaled density distributions at dimensionless times $t = 0, 0.25, 0.5, 0.75$ and 1.0. The parameters used to produce the graphs are: $\varepsilon = 0.2$, $q_0 = 3.209 \cdot 10^{-5}$ m/s, $\rho_f = 1000$ kg/m^3, $\theta = 1$, $\beta_0 = 1.0 \cdot 10^4$ m^2/kg/s, hence $\beta_0 = \beta q_0\rho_f \approx 320$. The corresponding scaled specific discharge distributions are given in Figure 2. In case of the semi-explicit solution, the decay of the maximum of the specific discharge distribution is given by

$$q_{\max} = 1 + t^{-\frac{1}{3}}G, \tag{4.7.24}$$

and

$$z_{\max} = t + \frac{3}{2}t^{\frac{2}{3}}G, \tag{4.7.25}$$

where $G = \frac{1}{3}\int_{-\infty}^{0} \sigma g'/g^{\frac{2}{3}} d\sigma \approx 5.7736 \cdot 10^{-2}$ for this parameter set. The additional displacement of the density front caused by the compressibility effect, is small but noticeable on the scale of Figure 1. The semi-explicit solution moves slightly faster than the corresponding numerical solution, which is due to the fact that assumption (4.4.1) leads to a higher apparent dispersivity in that case.

Figure 3 shows scaled density profiles for large times, i.e. $t = 0, 250, 500, 750$ and 1000. At this time scale the semi-explicit and explicit solutions are indistinguishable. As to be expected the approximate solutions become progressively inaccurate in regions where $\partial u/\partial z$ becomes small, i.e. the top and toe regions of the density profiles. The compressibility effect is no longer noticeable. The corresponding specific discharge distributions are given in Figure 4. At these times the enhanced flow is negligible, i.e less than 1 % of the scaled background flow.
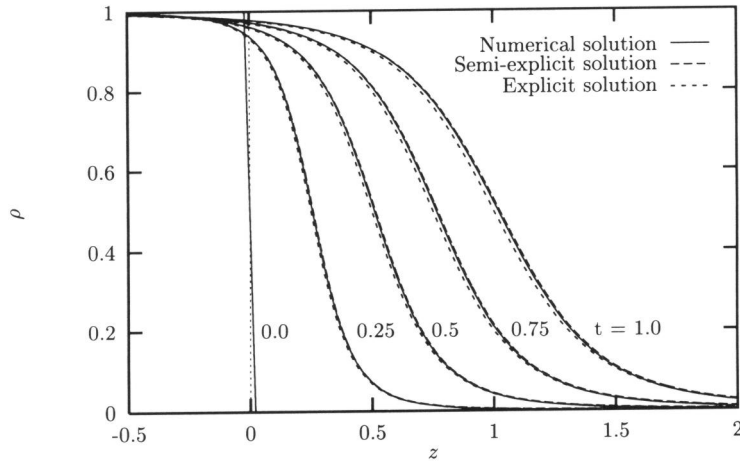
Figure 1. Comparison of solutions: density profiles at dimensionless times t=0, 0.25, 0.75 and 1.0 for $\varepsilon = 0.2$, $\theta = 1.0$ and $\beta_0 = 320$.
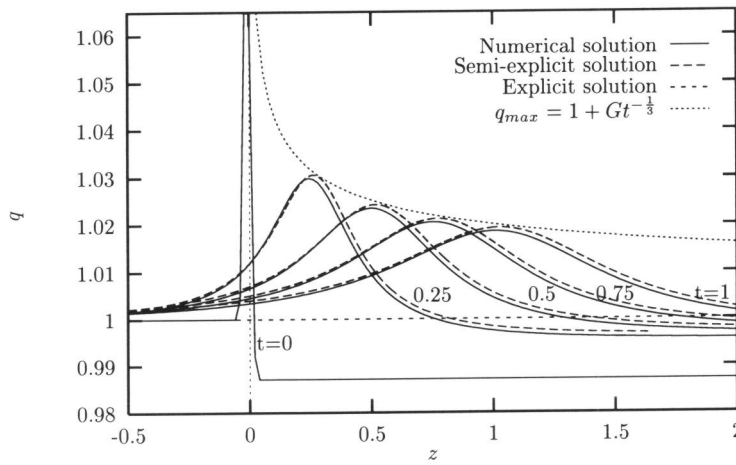

Figure 2. Comparison of solutions: specific discharge profiles at dimensionless times t=0, 0.25, 0.75 and 1.0 for $\varepsilon = 0.2$, $\theta = 1.0$ and $\beta_0 = 320$.
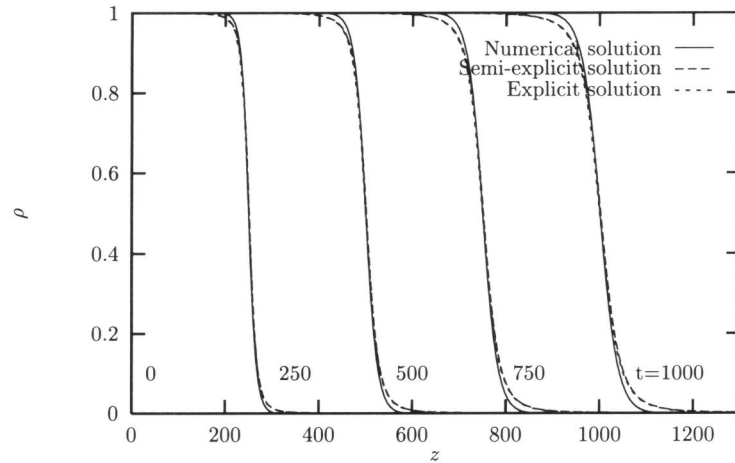
Figure 3. Comparison of solutions: density profiles at dimensionless times t=0, 250, 750 and 1000 for $\varepsilon = 0.2$, $\theta = 1.0$ and $\beta_0 = 320$.
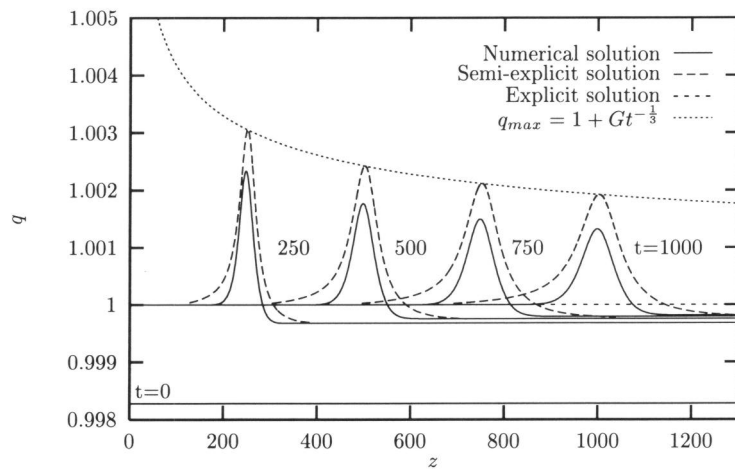
Figure 4. Comparison of solutions: specific discharge profiles at dimensionless times t=0, 250, 750 and 1000 for $\varepsilon = 0.2$, $\theta = 1.0$ and $\beta_0 = 320$.

4.8 Laboratory experiments

A series of well-controlled experiments have been performed in order to address a number of open questions related to brine transport. The experiments were aimed at determining the effects of large salt concentration differences as well as the absolute salt concentration on dispersion and to investigate the combined effect of flow velocity and large concentration differences. To this end, four series of displacement experiments were carried out (sse Table 1 through 4 for an overview):

- Fourteen tracer experiments where a low salt concentration solution was displaced by fluid with a sightly higher salt concentration (see Table 1). These are of tracer or LC-type.

- Seven HC experiments were performed, where a low-concentration solution was displaced by a fluid with a high salt concentration (see Table 3). The concentration differences ranged from 2.8 kg/m^3 to 44.6 kg/m^3. The inflow rate for this series of experiments was kept to a constant value of $5.4 \cdot 10^{-4}$ m/s.

- Nine HC experiments were performed for which the concentration difference between the resident and displacing fluids had a constant value of 63.4 kg/m^3, but the flow rate was varied from $1.0 \cdot 10^{-4}$ m/s to $2.3 \cdot 10^{-3}$ m/s (see Table 2).

- Four experiments where carried out wherein a high concentration solution (90 kg/m^3) was displaced with a yet higher concentration solution (see Table 4).

Here, a brief description of the experimental setup and methods is given. For more details, the interested reader should consult Moser [17].

4.8.1 The experimental setup

The column consisted of a 1500 mm long plexi-glass cylinder, with an internal diameter of 206 mm. The cylinder was filled with quartz sand with an middle particle diameter of $d_{50} = 0.5$ mm and a uniformity coefficient of $C_u = d_{60}/d_{10} \approx 1.9$. A soil having a uniformity coefficient $C_u < 2$, is considered uniform. The effective particle diameter, computed according to Beyer (see e.g. Langguth & Voigt [11]) is $d_e = 0.47$ mm. A sketch of the experimental setup is given in Figure 5. In order to obtain a homogeneously packed porous medium, the column
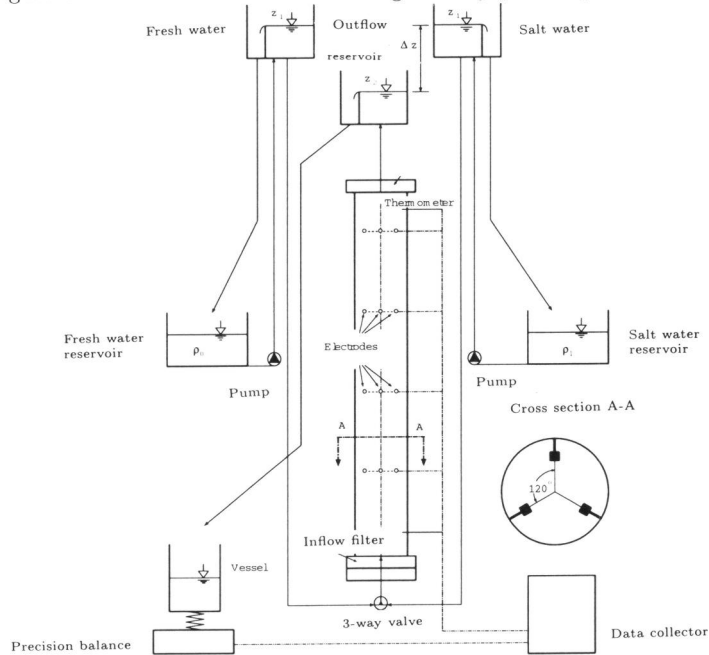

Figure 5. The experimental setup

was partially filled with water and subsequent layers (thickness $\approx$ 5 cm) were poured into
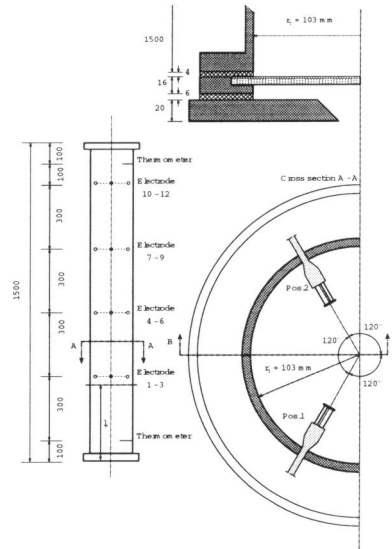
Figure 6. Details of the experimental setup

the column and each layer was packed by vibrating the column. The fluids were prepared by dissolving certain amounts of pure NaCl in distilled water. Both fresh and salt water circuits consisted of a storage reservoir, a pump and an overflow reservoir to ensure constant fluid pressure. The overflow reservoirs were connected to the inlet of the column by a three-way valve, which enabled instantaneous switching between the fresh and salt water circuit. The outlet of the column was also connected to an overflow reservoir whose level could be varied to create a desired pressure gradient over the porous medium. The outflowing fluid was collected in a vessel, which was mounted on an electronic precision balance. During the experiments, the amount of water in the collection vessel was recorded every 10 seconds. In case of the tracer experiments, a constant inflow rate could be obtained by fixing the distance between the water levels in the overflow reservoirs. However, when the density difference between the resident and displacing fluids was significant, the pressure gradient over the column would decease in time, causing a decrease of the flow rate. To overcome this problem, an adjustable valve was built into the salt water circuit. During high concentration experiments, this valve was gradually opened, such that the flow rate remained constant. The salt concentration was indirectly determined by measuring the electrical conductivity of the fluid in the porous medium. The electrodes consisted of three platinum/iridium wires, with a diameter of 1 mm and a length of 20 mm. The electrodes protruded into the porous medium, as shown in Figure 6. Each and every electrode was calibrated in-situ. A major disadvantage of relating the electrical conductivity to the salt concentration in a fluid is the fact that the sensitivity of conductivity measurements decreases as the salt concentration increases. Experiments showed that salt concentrations of 10 g/kg and 100 g/kg, could be reproduced within a relative error of respectively ±1% and ±2%. All displacement experiments were carried out at constant room temperature, i.e. 20° C ±1°. The temperature of the inflow and outflow fluid was constantly monitored.

4.8.2   The LC experiments

In the case of LG experiments, the salt mass fraction of the resident and invading fluids were, respectively, 1.0 g/kg and 4.0 g/kg. The only quantity that was varied between the twelve tracer experiments, was the flow rate. The molecular Peclet number, defined as

$$P_e = qd_{50}/D_m,$$ (4.8.1)

ranged from ≈ 10 to ≈ 3000, see Table 1. The dispersion coefficient was determined by analyzing the breakthrough curves, measured with electrodes 10, 11 and 12, i.e. at a distance of 130 cm from from the column inlet. electrode level in the top part of the column.

We used a least squares method to obtain an optimal fit between the analytical solution of the linear convention-diffusion equation (4.2.20) (constant flow rate), given by

$$\rho = \frac{1}{2}\left(1 - \text{erf}\left(\frac{L - qt/n}{2\sqrt{Dt}}\right)\right),$$ (4.8.2)

and the measured breakthrough curves. Here, L denotes the position of the electrode, q the specific discharge, n the porosity and D the fitting parameter. The porosity was determined from the measured flow rate and the breakthrough time of $c/c_0 = 0.5$. The obtained values of D and n are listed in Table 1. A comparison between the results of the tracer experiments and data from literature, collected by Pfannkuch [20], is given in Figure 7. The corresponding data can be found in Table 1.
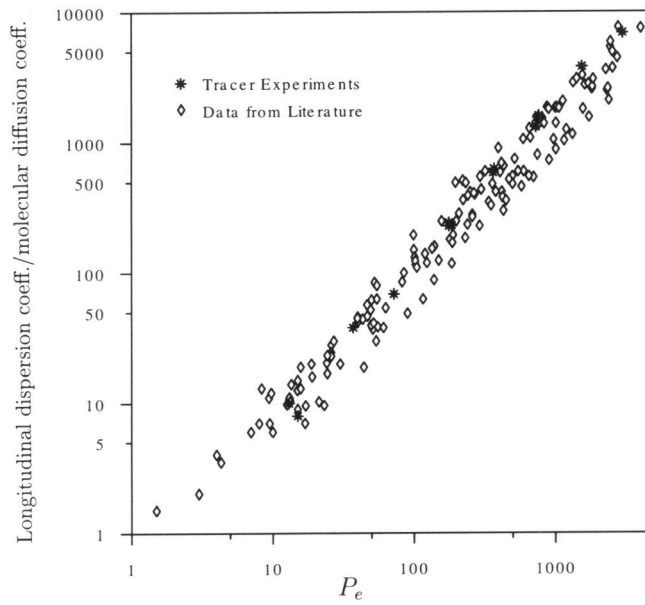

Figure 7. Comparison between data from literature and the results of the tracer experiments

Experiment number	Porosity	Specific discharge [mm/s]	Molecular Peclet numb.	Dispersion coefficient [mm²/s]
L10C04	0.382	0.010	13	0.01
L06C04	0.378	0.011	15	0.008
L07C04	0.408	0.029	37	0.038
L11C04	0.394	0.057	72	0.069
L09C04	0.403	0.143	177	0.229
L13C04	0.395	0.141	178	0.244
L04C04	0.403	0.149	185	0.230
L03C04	0.400	0.292	364	0.585
L14C04	0.397	0.294	370	0.626
L02C04	0.390	0.568	728	1.508
L15C04	0.391	0.592	757	1.543
L01C04	0.394	0.604	764	1.600
L16C04	0.385	1.189	1547	3.797
L12C04	0.387	2.312	2989	6.887

Table 1. Data of the tracer experiments.

4.8.3   HC experiments

In the second set of high concentration experiments the mass fractions of the resident and displacing fluids were respectively 6 g/kg and 100 g/kg, which amounts to $\Delta\rho = 63.7$ kg/m³ or $\varepsilon = 0.06$. The flow rate was varied such that the specific discharge ranged from ≈ 0.094 mm/s to ≈ 2.302 mm/s. The results are given in Table 2. All HC experiments showed a tailing phenomenon in the high concentration region of the breakthrough curves. This is probably caused by diffusion of salt into pores where the fluid is (almost) stagnant. The apparent values of the dispersion coefficient listed in Table 2 are only indicative and obtained by fitting the error function solution (4.8.2) to the measured breakthrough curves. Because of the asymmetry in the breakthrough curves, due to the tailing, we only used the first part of the breakthrough curve data, i.e. up to $c/c_0 = 0.5$, to determine an apparent value of the dispersion coefficient.

Experiment number	Specific discharge [mm/s]	Dispersion coefficient [mm²/s]
H09C100	2.302	4.153
H05C100	1.256	1.569
H01C100	0.653	0.452
H07C100	0.644	0.422
H02C100	0.588	0.389
H10C100	0.325	0.189
H03C100	0.176	0.068
H04C100	0.141	0.069
H06C100	0.101	0.036

Table 2. High concentration experiments: constant density difference ($\Delta\rho = 63.7$ kg/m³, M = 0.91) and different flow rates.

In the first set of high concentration experiments, the density difference was varied from $\Delta\rho \approx 3$ kg/m³ to $\Delta\rho \approx 45$ kg/m³, while the flow rate was fixed at a constant value, corresponding to a specific discharge of about 0.54 mm/s.

Experiment number	Density difference [kg/m³]	Dispersion coefficient [mm²/s]
H01C10	2.8	1.535
H01C15	6.4	1.331
H01C20	10.0	1.246
H01C25	13.5	1.023
H01C37	21.4	0.987
H01C50	30.8	0.816
H01C70	44.6	0.641

Table 3. High concentration experiments: constant flow rate ($q = 5.4 \cdot 10^{-4}$ m/s) and and various density differences.

Notice that experiments H01C10 and H01C15 are actually LC experiments. Table 3 clearly shows that the apparent dispersion coefficient decreases when the density difference between the fluids increases.

4.8.4 High absolute concentration experiments

The nonlinear dispersion theory indicates that the nonlinear effects depend on the fluid velocity and the magnitude of salt concentration gradients, but not on the absolute concentration levels of the resident and/or displacing fluids. To support this idea, a series of high absolute concentration experiments were carried out. The salt concentration of the resident fluid was 90 g/kg, while the concentration of the displacing fluid ranged from 100 g/kg to 150 g/kg, see Table 4. The specific discharge ranged from 0.45 mm/s to 0.52 mm/s. Experiment HH01C100 ($\Delta\rho = 7.4$ kg/m³) can be compared with experiment H01C15 ($\Delta\rho = 6.4$ kg/m³)in Table 3. Both are actually LC experiments and we notice that the dispersion coefficients have approximately the same value. The same holds for a comparison between HH01C100 and L02C04 in Table 1. These results indicate that the absolute salt concentration does not contribute to the nonlinear behavior of the dispersion coefficient.

Experiment number	Density difference [kg/m³]	Dispersion coefficient [mm²/s]
HH01C100	7.4	1.210
HH01C110	13.2	1.070
HH01C120	20.2	0.980
HH01C150	39.4	0.600

Table 4. High absolute concentration experiments.

Moreover, we observe in Table 4 the same tendency as in Table 3: the apparent dispersion coefficient decreases as the density difference increases. Experiment H01C70 in Table 3 gives almost the same results as experiment HH01C150 in Table 4, despite the fact that the salt concentration of the resident fluid in HH01C150 is a factor 15 higher, when compared to the initial salt concentration in H01C70.

4.9 Analysis of the experimental results

The results of the LC (tracer) experiments (Table 1) are plotted in Figure 8 in terms of the molecular Peclet number, defined in (4.8.1), and the ratio of the apparent longitudinal dispersion

coefficient and the molecular diffusion coefficient. A least squares curve fitting of the LC data points, as plotted in Figure 8, yields the relation

$$\frac{D_L}{D_m} = 0.35 \cdot P_e^{1.26} \quad \text{for} \;\; 10 < P_e < 3000. \tag{4.9.3}$$

Bear [1] gives a similar empirical expression which reads: $D_L/D_m = a \cdot P_e^m$, where $a \approx 0.5$ and $1 < m < 1.2$ in the range $6 < P_e < 200$. The latter is believed to be valid when the main spreading mechanism is caused by mechanical dispersion and transversal molecular diffusion, see [1]. In the range $200 < P_e < 10^4$, the mechanical dispersion is dominant, and the relation between D_L/D_m and P_e is supposed to be linear. However, when we fit the experimental data in the range $363 < P_e < 2989$ we still find some nonlinearity and the expression reads: $D_L/D_m = 0.57 \cdot P_e^1.18$. This relation indicates that the dispersivity $\alpha_L = nD/q$ is not really a constant but increases monotonically with the specific discharge q. This can be indeed confirmed by the data of the LC experiments given in Table 1. The average value of α_L is approximately 1 mm. This is twice the average particle diameter, as to be expected for a homogeneous porous medium, see e.g. Scheidegger [23].
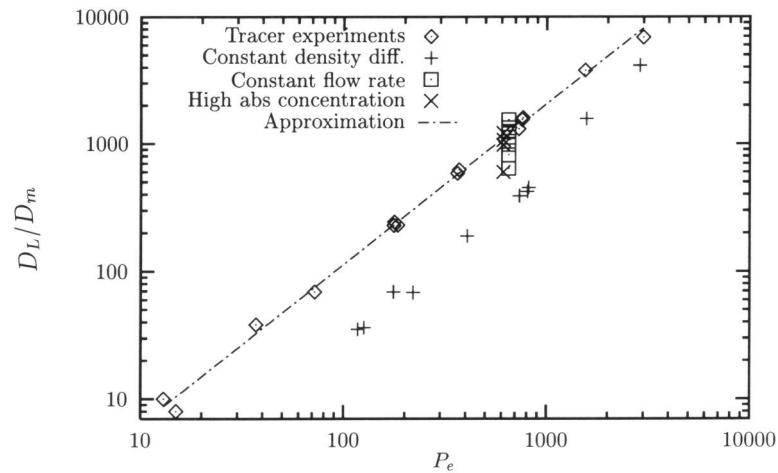

Figure 8. The ratio of the apparent dispersion coefficient and the molecular diffusion coefficient as a function of the molecular Peclet number.

Figure 8 shows the ratio of the longitudinal dispersion coefficient and the molecular diffusion coefficient as a function of the molecular Peclet number, for all experiments carried out in this study. Given a density difference of 63.7 kg/m^3, we observe a maximum reduction of the dispersion coefficient by a factor ≈ 3.4. This factor decreases gradually when the molecular Peclet number (actually flow rate) increases. This behavior can be explained as follows. The porous medium is not completely homogeneous and permeability and porosity may vary locally in space, which in turn causes local velocity variations in the fluid flow. Hydrodynamic dispersion is the macroscopic outcome of these varaiations. In case of tracer density differences, the dispersion is not influenced by gravitational forces. When the density difference between the resident and displacing fluids becomes significant, the gravitational forces give rise to a reduction of the dispersion. Local horizontal density gradients cause vortices (rotation) in the fluid motion, which in turn diminishes the longitudinal spreading due to hydrodynamical dispersion in the main flow

direction. The magnitude of the reduction of the dispersion depends upon the magnitudes of the average flow rate and the density difference.

A typical time scale associated with gravity stabilization of local velocity variations can be given by

$$t_g = \frac{\alpha\mu}{\kappa g \Delta\rho}. \qquad (4.9.4)$$

The time scale associated with the average flow in the column is

$$t_c = \frac{L}{q}. \qquad (4.9.5)$$

If t_c is large compared to t_g, then gravity will have enough time to reduce local velocity variations. Therefore, the ratio t_c/t_g is a measure for the significance of gravity effects. In fact, this ratio is identical to the Rayleigh number

$$R_a = \frac{t_c}{t_g} = \frac{\kappa g \Delta\rho L}{\mu \alpha_L q}. \qquad (4.9.6)$$

When using the Kozeny-Carman equation (see Bear [1]) to compute the intrinsic permeability of the porous medium, we obtain $\kappa \approx 2.0 \cdot 10^{-10}$ m^2. In case of the constant density difference experiments, the Rayleigh number ranges from $R_a = 1640$ ($P_e \approx 100$) to $R_a = 72$ ($P_e \approx 3000$). Here we used $\mu = 1.0 \cdot 10^{-3}$ kg/ms, $\Delta\rho = 63.7$ kg/m^3, $L = 1.3$ m, $\alpha_L = 1.0 \cdot 10^{-3}$m and $\kappa = 2.0 \cdot 10^{-10}$. Figure 8 shows indeed a decrease of the difference between the tracer dispersion coefficient and the HC dispersion coefficient for high Peclet numbers.

In any case, Figure 8 shows that dispersion coefficient as found in the classical Fickian equation is a nonlinear function of flow velocity and salt concentration differences. The nonlinear dispersion theory proposed in [5] is believed to account correctly for the density effects. Indeed, the experiments reported in [6], although limited in number and scope, give evidence that, for a certain flow rate, it is possible to determine a single value the parameter β, such that breakthrough curves of experiments with concentration differences ranging from 1.51 g/kg (tracer concentrations) to 232.43 g/kg can be simulated with a reasonable accuracy.

We computed an optimal value of β from the constant flow rate experiments, listed in Table 3, by fitting both the explicit solution and the full numerical solution to breakthrough curves. The results for $q = 5.4 \cdot 10^{-4}$ m/s are listed in Table 5. As to be expected, we obtain an almost constant value of β by fitting the numerical solution to the experimental data. The β-values, obtained with the explicit solution become progressively inaccurate for decreasing density differences. Both results are shown in Figure 9. When the displacing fluid is fresh water ($\rho_f \approx 1000$ kg/m^3), the explicit solution appears to be accurate for the range $\rho_s \approx 1025$ kg/m^3 (sea water) up to $\rho_s \approx 1300$ kg/m^3 (the saturation limit of NaCl in water). This emphasizes the applicabillity of the explicit solution, at least for this constant flow rate data set. A more general conclusion with respect to the validity of the explicit solution cannot be gained from the experimental results presented in this study.

Experiment number	density difference [kg/m³]	Dispersion coefficient [mm²/s]	β_{num} [s m²/kg]	β_{expl} [s m²/kg]
H01C70	44.6	0.641	6228	6240
H01C50	30.8	0.818	6013	6101
H01C37	21.4	0.987	6490	6749
H01C25	13.5	1.023	6447	7133
H01C20	10.0	1.246	6296	8333
H01C15	6.4	1.331	6366	11574
H01C10	2.8	1.535	6283	19841
$\beta_{average}$			6303	-

Table 5. Obtained β-values from the constant flow rate experiments ($q = 5.4 \cdot 10^{-4}$ m/s)
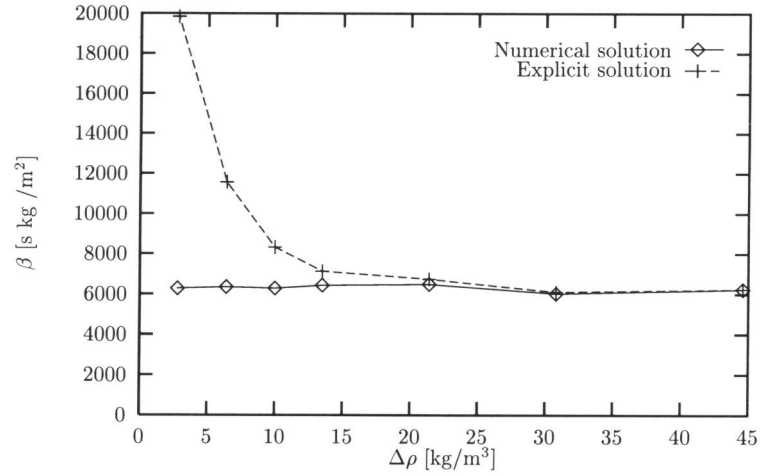
Figure 9 Comparison of β-values obtained by fitting the numerical and explicit solution to the breakthrough curves of the constant flow rate experiments

The breakthrough curves corresponding to the constant density difference experiments listed in Table 2, were analyzed in a similar fashion. The obtained β-values are plotted as a function of the specific discharge on a log-log scale in Figure 10. A least squares curve fitting yields an approximate expression for $\beta(q)$, given by

$$\beta(q) = \frac{0.0125}{q^{1.76}} \quad \text{for } 9.0 \cdot 10^{-5} < q < 3.0 \cdot 10^{-3} \text{ m/s.} \tag{4.9.7}$$

This indicates that the nonlinear effect decreases with increasing flow rate. This is in correspondence with our discussion of the Rayleigh number and the balance between gravitational and convective transport. Substitution of (4.9.7), (4.2.4) (disregarding molecular diffusion) in equation (4.2.8), and solving for J yields

$$J = \frac{q^n}{2A} \left\{ \sqrt{1 - 4\alpha_l A \gamma^{-1} q^{1-n} \frac{\partial \rho}{\partial z}} - 1 \right\}, \tag{4.9.8}$$

where $A = 0.0125$ and $n = 1.76$. This is the one-dimensional dispersive mass flux equation in terms of the original variables.
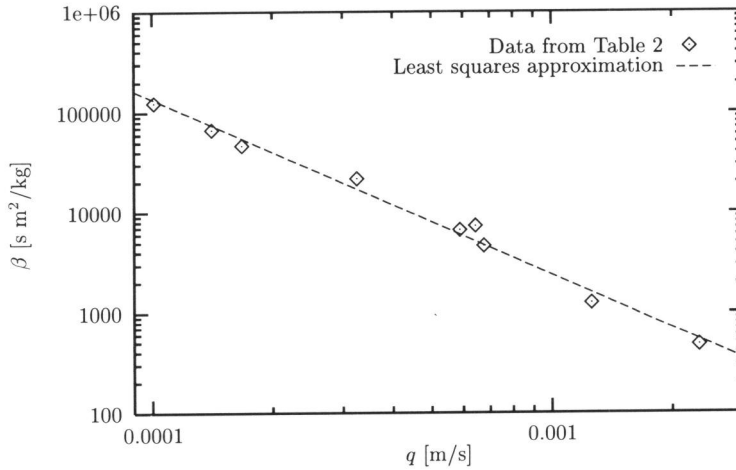
Figure 10. The parameter β as a function of q for the constant density difference experiments

4.10 Discussion

The experimental results presented in this study, confirm the validity of the nonlinear dispersive mass flux equation (4.2.3) and provide an empirical relationship for the HC dispersion coefficients in terms of the specific discharge. In the HC experiments, the specific discharge ranged from $q = 9.0 \cdot 10^{-5}$ m/s to $3.0 \cdot 10^{-3}$ m/s. These are relatively high when compared to groundwater discharges in the field, typically ranging from $3.0 \cdot 10^{-7}$ m/s (0.03 m/day) to $3.0 \cdot 10^{-5}$ m/s (3.0 m/day).

When we extrapolate expression (4.9.7) for $q > 3.0 \cdot 10^{-3}$ m/s, neglecting any high velocity effects, and pass to the (theoretical) limit $q \to +\infty$ we obtain $\beta(+\infty) \to 0$. This implies that the dispersive mass flux equation (4.2.3) reduces to Fick's law and HC experiments can be simulated using the tracer equations and the tracer dispersion coefficient. Extrapolation of (4.9.7) for $q < 9.0 \cdot 10^{-5}$ m/s, and passing to the limit $q \to 0$ yields $\beta(0) \to \infty$. This indicates that for low discharges (high Rayleigh numbers) the gravity effect, i.e. the nonlinear term in (4.1.3), completely dominates the dispersive behavior. From the physical point of view, both discharge limits are realistic in a qualitative sense. Additional experiments should be carried out to gain information about the behavior of $\beta(q)$ for discharges $q < 9.0 \cdot 10^{-5}$ m/s and $q > 3.0 \cdot 10^{-3}$ m/s. A particular interesting limit to study is the transition from pure diffusive transport to dispersion dominated transport under HC conditions.

Substitution of (4.9.8) in (4.2.1) and (4.2.2) yields a set of equations that no longer allows a Von Mises transformation. In fact, application of the Von Mises transformation is restricted to those cases where the longitudinal tracer dispersion coefficient D is constant, i.e. not a function of the local specific discharge, see [4]. A constant tracer dispersion coefficient may account for heterogeneities of the porous medium in an averaged sense, for instance by setting $D = \alpha_L q_0$, where q_0 denotes a background or mean specific discharge.

When using the latter, we can quantify the magnitude of the volume or compressibility effect in the experiments. To this end, we use the data of HC experiment H09C100 (see Table 3) and expressions (4.7.24) and (4.7.25). The breakthrough time of the 50%-level of the density

in experiment H09C100 is $t_{50\%} = 220$ s. The dimensionless breakthrough time is given by $t_{50\%}^* = 423$, see the scaling rules (4.2.9). Tracer experiment L12C04 was used to obtain values for D and n. At $t_{50\%}$, the relative magnitude of the maximum of the specific discharge with respect to the back ground flow q_0 can be determined from expression (4.7.24). This yields $(q_{max} - q_0)/q_0 \approx 0.8\%$. The additional relative displacement of the density front at $t_{50\%}$, given by (4.7.25), amounts to $\approx 1.2\%$. Both results indicate that volume effects can be disregarded. Such variations are not noticeable within the accuracy of the experiments.

The constant flow rate experiments show a significant reduction of the dispersion coefficient in case of an increasing density difference between the resident and displacing fluids. The tracer dispersion coefficient has to be lowered by a factor ≈ 2.4 (H01C70, $\Delta\rho = 44.6$ kg/m^3) in order to obtain a reasonable fit between the solution of the classical equations and the experimental data. Experiment H02C100, with approximately the same flow rate ($5.88 \cdot 10^{-4}$ m/s instead of $5.4 \cdot 10^{-4}$ m/s) and density difference 63.7 kg/m^3, exhibits a reduction by a factor ≈ 4. Figure 11 shows the scaled dispersion coefficient for the constant flow rate experiments (including H02C100) as a function of the density difference. The corresponding least squares approximation is given by $D_L/D_0 = 1.0158e^{-0.0212\Delta\rho}$, where $D_0 = 1.535 \cdot 10-6$ m^2/s.
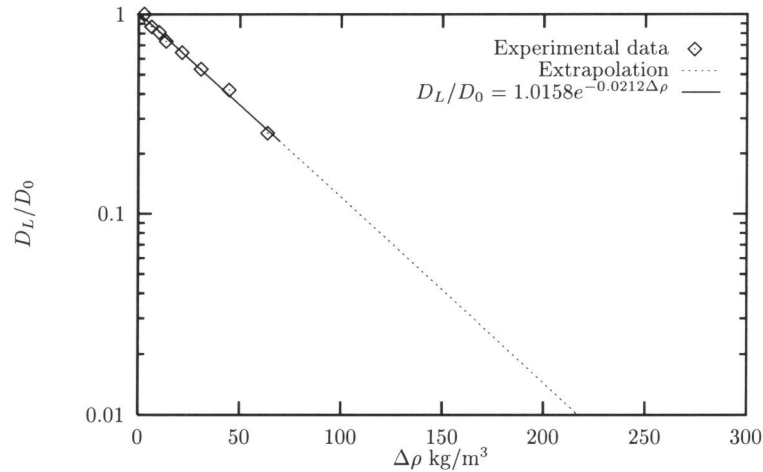

Figure 11. Scaled longitudinal dispersion coefficient as a function of the density difference for the constant flow rate experiments.

Extrapolation of the least squares approximation yields a reduction of the tracer dispersion coefficient by a factor > 100 for almost saturated brines. Whether this is extrapolation is realistic in the physical sense has to be determined experimentally in a future study.

An other question that needs to be addressed concerns the physical phenomenon that is assumed to cause the reduction of the apparent dispersion coefficient in HC transport of brines. Is the explanation that local horizontal density gradients at pore scale induce fluid rotation (vortices) such that the dispersion of salt is reduced when compared to the tracer dispersion correct? The latter is very likely, but cannot be proved at this time. Also, simple conceptual models for HC transport, gaining insight in the process and its governing equations, are still lacking. For tracer dispersion, such models, have proven to be very useful, see e.g. Taylor [25], [26], De Josselin De Jong [10], Saffman [21], [22].

If gravity is indeed responsible for the observed dispersion reduction in HC transport, then it is of fundamental importance to find the relation between the proposed nonlinear flux equation (4.2.3) and the induced flow due to local horizontal density gradients. The derivation of (4.2.3)

in [5] is formally correct, but is not directly linked to the physical phenomenon that causes the HC dispersion effect. Such a relation might be established by averaging the governing pore scale equations and/or by homogenization techniques. We leave these questions for a future study.

4.11 Conclusions

- This study concerns the mathematical and experimental analysis of brine dispersion in a saturated porous medium. Both low and high concentration experiments have been carried out. The LC (tracer) experiments presented in this paper are in excellent agreement with LC experiments reported in literature.

- The experiments show that for low concentration differences (even if the absolute salt concentration is high), the linear Fickian theory models the observed dispersion satisfactorily. In case of high concentration differences, the Fickian theory fails.

- All experiments reported here, both LC and HC, confirm the validity of the nonlinear HC dispersion theory given in [5].

- High absolute concentration experiments show that the HC dispersion coefficient is independent of the absolute salt concentration of fluids.

- The HC dispersion coefficient β is found to be independent of the salt concentration differences or gradients. It depends only on the flow rate. A relation between β and the specific discharge is established.

- An explicit solution for HC transport (assuming dominance of the nonlinearity in the salt flux equation and constant flow rate in the column) is given. This approximate solution can be used to simulate HC experiments in a wide range of density differences.

- A semi-explicit solution of the full set of governing equations (again assuming dominance of the nonlinearity in the salt flux equation) is obtained. Fluid volume changes due to high concentration gradients are taken into account. The results are used to quantify the volume effects in the HC experiments. It turns out that these effects can be disregarded for all experiments considered.

- The constant density HC experiments show a decrease of the difference between the tracer and the HC dispersion coefficients for increasing flow rates. This indicates that local (pore scale) horizontal density gradients might be responsible for the nonlinear HC dispersion effect. At high flow rates (large Peclet numbers) local gravity driven (stabilizing) flows become relatively un important (low Rayleigh numbers).

Bibliography

[1] Bear,J, Dynamics of fluids in porous media, Elsevier, New York, 1972.

[2] Van Duijn, C.J. , Peletier, L.A. & Schotting, R.J., On the analysis of brine transport in porous media, Euro. Jnl. of Appl. Mathematics, Vol **4** (1993), pp. 271-302.

[3] Van Duijn, C.J. , Peletier, L.A. & Schotting, R.J., Brine transport in porous media: self-similar solutions, CWI Report AM-R9616, November 1996.

[4] Van Duijn, C.J. & Schotting, R.J. , On the use of Von Mises transformation in brine transport in porous media, CWI Report in preparation 1997.

[5] Hassanizadeh, S.M. & Leijnse, Anton, A non-linerar theory of high-concentration-gradient dispersion in porous media, Adv. Water Resour. ,Vol. **18** (1995), pp. 203-215

[6] Hassanizadeh, S.M. & Leijnse, A., On the modelling of brine transport in porous media, Water Resour. Res., Vol. **24** (1988), pp. 321-330

[7] Hassanizadeh, S.M., Leijnse, A., De Vries, W.J. & Stapper, R.A.M., Experimental study of brine transport in porous media, Report 728514005, RIVM, Bilthoven, The Netherlands, 1990.

[8] Hassanizadeh, S.M., Derivation of basic equations of mass transport in porous media. Part 1. Macroscopic balance laws, Adv. Water Resour. **9** (1986), p.p. 196-206

[9] Hassanizadeh, S.M., Derivation of basic equations of mass transpo rt in porous media. Part 2. Generalized Darcy's and Fick's laws, Adv. Water Resour. **9** (1986), p.p. 207-222.

[10] De Josselin De Jong, G., Longitudinal and transverse diffusion in granular deposits, Trans. Amer. Geophys. Union **39** (1958), p.p. 67-74.

[11] Langguth, H.R. & Voigt, R., Hydrologische Methoden, Springer Verlag, Berlin (1980).

[12] Kempers, L.J.T.M., Effects of fluid properties on hydrodynamic dispersion: comparison of analytical models to numerical simulations, Proc. 1st SPE/IMA Europ. Conf. Mathematics of Oil Recovery, Cambridge, UK, 25-27 July 1989.

[13] Kempers, L.J.T.M., Dispersive mixing in stable and unstable miscible displacements, PhD thesis Delft University of Technology, The Netherlands, 1991.

[14] Kolditz, O., Ratke, R., Diersch, H.J. & Zielke, W., Coupled groundwater flow and transport: 1. Verification of density variable flow and transport models, Advances in Water Resources, in print, 1998.

[15] Leijnse, T., Three-dimensional modeling of coupled flow and transport in porous media, Ph.D. thesis, University of Notre Dame, Indiana, USA, 1992.

[16] Von Mises, R. & Friedrichs, K.O., Fluid dynamics, Applied Mathematics Series **5** (1973), Springer, New York, p. 171

[17] Moser, H, Einfluss der Salzkonzentration auf die hydrodynamische Dispersion im porösen Medium, Mitteilung Nr. 128, Technische Universität Berlin (Ph.D. thesis), 1995.

[18] Ogata, A. & Banks, R.B., A solution of the differential equation of longitudinal dispersion in porous media, U.S. Geological Survey, Professional paper 411-A (1961), Washington.

[19] Oldenburg, C.M. & Pruess, K., Disperive transport dynamics in a strongly coupled groundwater-brine flow system, Water Resources Research **31**(2) (1995), p.p. 289-302.

[20] Pfannkuch, H. O., Contribution á l'étude des déplacements de fluides miscibles dans un milieu poreux, Revue de l'Institut Francais du Pétrole, Vol. **18** (1963), pp. 215-270.

[21] Saffman, P.G., Dispersion due to molecular diffusion and macroscopic mixing in flow through a network of capillaries, J. Fluid Mech. No 2 **7** (1960), p.p. 194-208.

[22] Saffman, P.G., A theory of dispersion in a porous medium, J. Fluid Mech. No 3 **6** (1959), p.p. 321-349.

[23] Scheidegger, A.E., The physics of flow through porous media, 3rd edn, Univ. of Toronto Press, Toronto, Canada, 1974, p. 306.

[24] Schincariol, R.A. & Schwartz, F.W., An experimental investigation of variable density flow and mixing in homogeneous and heterogeneous media, Water Resources Research **26** (1990), p.p. 2317-2329.

[25] Taylor, G.I., Dispersion of soluble matter in solvent flowing slowly through a tube, Proc. Roy. Soc. A, No 1137 **219** (1953), p.p. 186-203.

[26] Taylor, G.I., The dispersion of matter in turbulent flow through a pipe, Proc. Roy. Soc. A. **223** (1954), p.p. 446-468.

[27] Welty, C. & Gelhar, L.W., Stochastic analysis of the effects of fluid density and viscosity variability on macro dispersion in heterogeneous porous media, Water Resources Research **27** (1991), p.p. 2061-2075.

[28] Wheatcraft, S.E., Carey, A.E., Glass, R.J. & O'Rourke, J.P., Non-Fickian ionic diffusion across high-concentration gradients, Water Resources Research **31** (1995), p.p. 2213-2218.

Chapter 5

The interface between fresh and salt groundwater

5.1 Introduction

Gravity induces a flow in a porous medium if horizontal density gradients are present. These horizontal gradients produce vorticity, which in turn causes (density-driven) fluid flow. This insight is mainly due to the work of Wooding [21], [22] and Elder [8].

Fresh and salt groundwater are essentially miscible fluids. When brought in contact in a porous medium, a mixing zone will develop, which is caused by molecular diffusion and hydrodynamical dispersion. The latter is additional mixing due to local velocity variations which are caused by local variations in permeability. In most practical situations the width of the transition zone is small compared to the extensions of the aquifer. This motivates to assume the existence of an interface between the fluids: the specific weight changes abruptly from one value to an other value. Thus in this approximation we treat the strictly miscible fluids as immiscible. In their mathematical formulation, interface models lead to so called free boundary problems.

The implications of the existence of an interface between fresh and salt groundwater have been studied by De Josselin De Jong [12]. In that case, the horizontal density gradients across the interface are singular and the interface becomes a surface source (in three space dimensions) or a line source (in a vertical cross section) of vorticity. The flow of the separate fluids is rotation free, while the rotation of the total flow is produced by the (singular) vorticity distribution along the interface. As a consequence, the velocity component normal to the interface is continuous and the velocity component tangential to the interface exhibits a discontinuity across the interface: the shear flow.

In a later paper, De Josselin De Jong [11], derived a nonlinear diffusion-type equation to approximate density-driven flow in a vertical cross section of horizontally extended aquifers confined by two impermeable layers. The derivation is based on the Dupuit assumption, i.e. the horizontal component of the specific discharge is constant in each fluid and jumps at the interface. The advantage of this approach is that the two-dimensional flow problem reduces to a one-dimensional initial value problem in terms of the interface height. Solutions of this approximate equation give insight in the time evolution and flow properties of the full problem, in particular with respect to the large time behavior, i.e. for relatively flat interfaces.

Following the original work of De Josselin De Jong [12], Chan Hong et.al. [6] studied the movement of the interface between fresh and salt groundwater by numerical means. They formulate the problem in terms of an elliptic (Poisson) equation for the stream function describing

the flow and a hyperbolic equation for the time evolution of the interface. The parameterization of the interface is of the form $z = u(x, t)$, where respectively x and z denote the horizontal and vertical coordinate of a point located at the interface. The elliptic problem is solved using a finite element method (moving mesh) while the interface motion equation is solved explicitly in time, by means of a predictor-corrector method. Chan Hong et. al. [6] compare numerical results with solutions of simplified problems, based on the Dupuit approximation with respect to the horizontal flow. Only homogeneous flow domains are considered.

We focus on the transient behavior of an interface in heterogeneous aquifers, including those cases where it is not possible to parameterize the interface according to $z = u(x, t)$ or $x = u(z, t)$. We modified the existing finite element code [6] to allow for heterogeneous intrinsic permeability distributions in the flow domain and developed a front tracking method, to compute the discrete time evolution of the interface. The latter is inspired by ideas developed in Dupaix et. al. [21] and Scheid [18]. Points along the discretized interface are displaced by computing an approximate normal direction and an approximate normal velocity from the stream function along the interface.

The heterogeneities considered are discontinuities in intrinsic permeability. In case of a vertical discontinuity in permeability, i.e. two adjacent regions with different piecewise constant permeability, we solve a related Dupuit problem in terms of a similarity solution. It turns out that the numerical solution converges towards a similarity solution as $t \to \infty$.

In case of two horizontal layers with different piecewise constant permeability, i.e a horizontal discontinuity, it is not possible to obtain a semi-explicit solution of a related Dupuit problem. Therefore it is difficult to validate the numerical solutions, even when the mass balance is conserved up to a small error. Moreover, if the initial interface is vertical, a hydrodynamically unstable zone will develop in the vicinity of the discontinuity in permeability, where the heavy fluid (salt ground water) is on top of the lighter one (fresh groundwater). Rayleigh-Taylor instabilities (fresh-salt fingers) are observed in the computational results, as soon as salt water is on top of fresh water.

A normal-mode linear stability analysis shows that instabilities (fresh-salt fingers) of any wave length λ (or wave number ω) can occur in the fingering pattern. List [58], studied the stability of the uniform horizontal motion of two miscible fluids of different density in a saturated, homogeneous porous medium, both theoretically (by means of a normal-mode linear stability analysis) and experimentally. List showed the existence of a critical wave length λ_0. Perturbations with wave length $\lambda < \lambda_0$ decay in time, while perturbations with $\lambda > \lambda_0$ grow. The number λ_0 is related to the dispersion coefficient D. In the limit $D \to 0$, i.e. in case of a fresh-salt interface, we obtain $\lambda_0 = 0$, implying that perturbations of any wave length will grow in time.

However, in the results of the interface computations we observe that only instabilities of a certain minimum wave length or finger width grow in time. The latter is determined by the coarseness of the (piecewise linear) discretization of the interface.

In addition, we consider a problem in a homogeneous flow domain. Van Duijn & Philip [17] studied bounds on the behavior of slumping brine mounds. Two modifications of the approximate Dupuit interface motion equation, see De Josselin De Jong [11], are applied to the slumping of finite two-dimensional brine mounds. Both modifications lead to simple similarity solutions. One gives upper bounds on the time-scales of the process and the other lower bounds. We check the validity of these approximate bounds against a numerical solution of the full problem. The results are in excellent agreement with the predictions in [17].

The organization is as follows. In Section 2 we give the governing flow equations and give the boundary and initial conditions. A description of the numerical procedure is given in Section 3.

In Section 4 we compare computed results with two approximate problems in a homogeneous flow domain, that are based on the Dupuit assumption. The first problem concerns the time evolution of a rotation linear interface. We compare the results obtained with the front tracking scheme, with the predictor-corrector scheme (as proposed in [6]) and with the corresponding Dupuit approximation. This problem is included mainly to gain confidence in the front tracking method. The second homogeneous problem concerns the slumping of brine mounds. We verify numerically the bounds on the time scale of the slumping process of decaying brine mounds [17]. In Section 5 a general expression is derived for the shape of the interface in an infinitesimal small neighborhood of a discontinuity in intrinsic permeability. This expression is used for verification of the numerical results. The special case of a vertical discontinuity in permeability is considered in Section 6. We derive an approximate Dupuit similarity solution and compare it with the large time behavior of numerical solutions of the full problem. A horizontal discontinuity in permeability is considered in Section 7. Special attention is given to the growth of Rayleigh-Taylor instabilities that occur in the vicinity of the discontinuity in permeability. Section 8 contains the conclusions and some discussion.

5.2   The model

The governing equations are the continuity equation for incompressible fluids and Darcy's law, i.e. the momentum balance equation. These equations can be combined into a single Poison equation for the stream function, which describes the flow induced by the difference in specific weight of the fluids. From the solution of the stream function equation, i.e. for a given specific weight distribution at a certain time level, we determine the normal component of the velocity at the interface. The result is used to displace the interface in time.

5.2.1   The stream function equation

We consider flow of an incompressible fluid of variable specific weight γ and constant viscosity μ, in a rectangular domain with variable intrinsic permeability κ. The flow domain is given by the strip $\Omega = I \times (0, h)$, where I denotes the interval $(-R, R)$ with $R > 0$, such that $R >> h$ ($h > 0$). The strip represents a vertical cross section of a horizontally extended aquifer, bounded from above and below by impermeable layers.

Let $\mathbf{q}$ denote the specific discharge vector, p the fluid pressure and $\mathbf{e}_z$ the unit vector pointing in the positive (upward) z-direction. The fluid movement is governed by Darcy's law, i.e.

$$\frac{\mu}{\kappa}\mathbf{q} + \nabla p + \gamma \mathbf{e}_z = 0 \qquad \text{in } \Omega \qquad (5.2.1)$$

and the continuity equation given by

$$\text{div } \mathbf{q} = 0 \qquad \text{in } \Omega. \qquad (5.2.2)$$

The latter expresses expresses the incompressibility of the fluid. At the boundary $\partial\Omega$ we assume a no-flow condition, i.e.

$$\mathbf{q} \cdot \mathbf{n} = 0 \qquad \text{on } \partial\Omega, \qquad (5.2.3)$$

where $\mathbf{n}$ denotes the outward normal unit vector on $\partial\Omega$. By taking the two-dimensional curl of equation (5.2.1), we obtain

$$\text{curl} \left(\frac{\mu}{\kappa}\mathbf{q} \right) + \text{curl} \left(\gamma \mathbf{e}_z \right) = 0 \qquad \text{in } \Omega. \qquad (5.2.4)$$

Here the curl of a vector function $\mathbf{a} = (a_x, a_z)$ must be understood in the sense that curl $\mathbf{a} := \partial a_x / \partial z - \partial a_z / \partial x$. Since the flow satisfies equation (5.2.2) we can introduce a stream function ψ such that

$$\mathbf{q} = \text{curl } \psi = \left(-\frac{\partial \psi}{\partial z}, \frac{\partial \psi}{\partial x} \right). \tag{5.2.5}$$

Substitution this expression in (5.2.4) yields

$$\text{div} \left(\frac{\mu}{\kappa} \nabla \psi \right) = -\frac{\partial \gamma}{\partial x} \qquad \text{in } \Omega. \tag{5.2.6}$$

This equation has to be interpreted in the weak sense, see Van Duijn & De Josselin De Jong [22] for details. The no-flow condition (5.2.3) implies that ψ is constant at $\partial \Omega$. The value of ψ on $\partial \Omega$ can be chosen arbitrarily. For convenience we set:

$$\psi = 0 \qquad \text{on } \partial \Omega. \tag{5.2.7}$$

Next, we introduce the interface approximation: the interface $\Gamma(t)$ separates fresh groundwater, with specific weight γ_f, and salt groundwater, with specific weight γ_s, where $0 < \gamma_f < \gamma_s$. This implies that γ is discontinuous at the interface and thereby the right-hand side of 5.2.6 a singularity. Consequences of the latter are summarized in Section 2.2. Thus, given an interface at a certain time $t \geq 0$, the solution of (5.2.6) subject to (5.2.7), determines the stream function distribution in flow domain Ω, and by (5.2.5) the corresponding discharge $\mathbf{q}$.

The heterogeneities considered in this paper are discontinuities in intrinsic permeability. We confine ourselves to the special case of piecewise constant permeability distributions: a vertical heterogeneity given by

$$\kappa = (\kappa_2 - \kappa_1) H(x) + \kappa_1 \text{ for } x \in I, \tag{5.2.8}$$

and a horizontal heterogeneity given by

$$\kappa = (\kappa_1 - \kappa_2) H(z - h/2) + \kappa_2 \text{ for } z \in [0, h], \tag{5.2.9}$$

where H denotes the Heaviside function: $H(\xi) = 1$ for $\xi > 0$ and $H(\xi) = 0$ for $\xi < 0$.

5.2.2   Properties of the stream function

Properties of the of the stream function, and thereby the induced discharge field, can be derived from problem (5.2.6)-(5.2.7), see e.g. [22], [6], [11]. In particular, we are interested in conditions on the stream function and the corresponding discharges at the interface and at discontinuities in permeability. Combining these conditions enables us to derive a fundamental expression for the behavior of an interface crossing a discontinuity in permeability, see Section 5.

Without loss of generality, we assume that the interface can be parameterized according to $z = u(x, t)$ in a small neighborhood of the discontinuity in permeability. Then the fluid domain Ω can be decomposed in 4 regions $\Omega_{i,j}$ for $i = 1, 2$ and $j = f, s$. Here $\Omega_{i,f}$ (respectively $\Omega_{i,s}$) denotes the domain occupied by fresh water (respectively salt water) in the region where $\kappa(x, z) = \kappa_i$, for $i = 1, 2$. Let Γ_i denote the part of the interface Γ in the region where $\kappa(x, z) = \kappa_i$ for $i = 1, 2$ and let Σ_j denote the boundary between the region where $\kappa = \kappa_1$ and that of $\kappa = \kappa_2$ in the part of the domain where $\gamma = \gamma_j$ for $j = f, s$, see Figure 1 for the case of a horizontal heterogeneity. Then let $\mathbf{n}$ (respectively $\mathbf{s}$) denote the outward normal unit vector (respectively
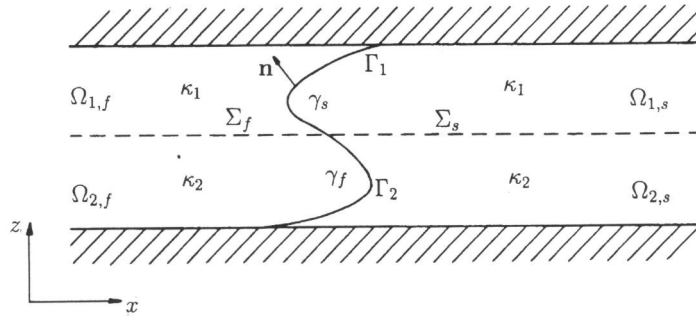
Figure 1. The interface in a confined aquifer: definition of the domains.

the tangential unit vector) to the boundary $\partial\Omega_{i,j}$ of $\Omega_{i,j}$. In case of sufficiently smooth interface $\Gamma(t)$, problem (5.2.6)-(5.2.7) in terms of ψ, can be written as a set problems on the subdomains $\Omega_{i,j}$ for $i = 1, 2$ and $j = f, s$, with conditions at the interface. It can be shown that a solution $\psi(x, z, t)$ of (5.2.6)-(5.2.7) satisfies the following basic properties: for $i = 1, 2$ and $j = f, s$ we have

$$(a) \quad -\Delta\psi_{i,j} = 0 \qquad\qquad\qquad\qquad \text{in } \Omega_{i,j}$$

$$\left.\begin{aligned}
(b) &\quad \psi_{i,f} = \psi_{i,s} \\
(c) &\quad \frac{\partial\psi_{i,f}}{\partial n} - \frac{\partial\psi_{i,s}}{\partial n} = -\frac{\kappa_i}{\mu}\left(\gamma_s - \gamma_f\right)n_x
\end{aligned}\right\} \text{ on } \Gamma_i$$

$$(5.2.10)$$

$$\left.\begin{aligned}
(d) &\quad \psi_{1,j} = \psi_{2,j} \\
(e) &\quad \kappa_2\frac{\partial\psi_{1,j}}{\partial n} - \kappa_1\frac{\partial\psi_{2,j}}{\partial n} = 0
\end{aligned}\right\} \text{ on } \Sigma_j$$

$$(f) \quad \psi = 0 \qquad\qquad\qquad\qquad \text{on } \partial\Omega_{i,j}$$

Here n_x denotes the x-component of the unit vector normal to the interface. Conditions (b) and (d) express the continuity of the stream function at Γ_i and Σ_j, implying $\partial\psi_{i,f}/\partial s = \partial\psi_{i,s}/\partial s$ for $i = 1, 2$, i.e. continuity of the discharge component normal to Γ_i, and $\partial\psi_{1,j}/\partial s = \partial\psi_{2,j}/\partial s$ for $j = f, s$, i.e. continuity of the discharge component normal to Σ_j. Expression (c) is the shear flow along the interface: the discharge tangential to the interface in discontinuous when crossing the interface. The discharge tangential to the discontinuity in permeability also exhibits a jump and satisfies (g). De Josselin De Jong [11]) arrived at the same result for the homogeneous case using physical arguments.

5.2.3   Time evolution of the interface

In order to allow for more general interface shapes, we do not parameterize the interface explicitly, as in e.g. Chan Hong et. al. [6] or [11]. Given a solution $\psi = \psi(x, z, t)$ of problem (5.2.6)-(5.2.7), the normal component of the velocity at the interface $\Gamma(t)$ satisfies

$$V_n = \frac{1}{\varepsilon} \mathbf{q} \cdot \mathbf{n} = \frac{1}{\varepsilon} \mathrm{curl}\, \psi \cdot \mathbf{n} \qquad \text{at}\ \ \Gamma(t), \tag{5.2.11}$$

where $\mathbf{n}$ denotes the normal unit vector at $\Gamma(t)$, pointing into the fresh water region and ε the porosity of the porous medium. The latter is assumed to be constant. Evaluation of (5.2.11) yields

$$V_n = \frac{1}{\varepsilon} \frac{\partial \psi}{\partial s} \qquad \text{at}\ \ \Gamma(t), \tag{5.2.12}$$

where $\partial/\partial s$ denotes the tangential direction along the interface.

Remark:

When the interface shape allows parametrization of the form $z = u(x, t)$ in Ω, the interface motion equation can be written as

$$\frac{\partial u}{\partial t} = \frac{1}{\varepsilon} \frac{\partial}{\partial x} \left\{ \psi\left(x, u(x, t), t\right) \right\} \qquad \text{in}\ I \times \mathbb{R}^+. \tag{5.2.13}$$

This particular form is due to Chan Hong et. al. [6]. Suppose that an interface touches the domain boundaries at $z = 0$ and $z = h$. Let the corresponding x-coordinates be given by $S_1(t)$ (toe) and $S_2(t)$ (top). It was also shown in [6] that $S_1(t)$ and $S_2(t)$ satisfy the differential equations

$$\dot{S}_1(t) = -\frac{1}{\varepsilon} \lim_{x \to S_1(t)} \frac{\psi\left(x, u(x, t), t\right)}{u(x, t)} \ \ \text{and}\ \ \dot{S}_2(t) = \frac{1}{\varepsilon} \lim_{x \to S_2(t)} \frac{\psi\left(x, u(x, t), t\right)}{h - u(x, t)}. \tag{5.2.14}$$

We use these expressions to compute the velocity of the top and toe under the assumption that the interface can be parameterized in a small neighborhood of the lower and upper domain boundaries.

The variables are redefined according to

$$x := \frac{x}{h}, \quad z := \frac{z}{h}, \quad \kappa := \frac{\kappa}{\kappa_0} \quad t := t\frac{(\gamma_s - \gamma_f)\kappa_0}{\varepsilon \mu h}, \tag{5.2.15}$$

and

$$\psi := \psi \frac{\mu}{(\gamma_s - \gamma_f)\kappa_0 h}, \quad \Gamma := \frac{\Gamma}{h}, \tag{5.2.16}$$

where κ_0 denotes a reference permeability. Then equations (5.2.6) and (5.2.11), subject to boundary and initial conditions, lead to the problem of finding the stream function $\psi = \psi(x, z, t)$ and $\Gamma(t)$ satisfying:

$$(P) \begin{cases} -\mathrm{div}\left(\frac{1}{\kappa}\nabla\psi\right) = \frac{\partial}{\partial x}\left(\gamma(x, z, t)\right) & \text{in}\ \Omega \times \mathbb{R}^+, \\[2mm] \psi = 0 & \text{on}\ \partial\Omega \times \mathbb{R}^+, \\[2mm] V_n = \frac{\partial\psi}{\partial s} & \text{on}\ \Gamma(t),\ t \in \mathbb{R}^+, \\[2mm] \Gamma(t = 0) = \Gamma_0. \end{cases} \tag{5.2.17}$$

In dimensionless form, the equations for the velocities of the top and toe of the interface, are given by

$$\dot{S}_1(t) = -\lim_{x \to S_1(t)} \frac{\psi(x, u(x,t), t)}{u(x,t)} \quad \text{and} \quad \dot{S}_2(t) = \lim_{x \to S_2(t)} \frac{\psi(x, u(x,t), t)}{1 - u(x,t)}, \tag{5.2.18}$$

where we redefined u according to $u := u/h$.

5.3 The numerical method

In this section we give a numerical algorithm for solving Problem (P). The procedure consists of three steps. We first solve the elliptic problem for the stream function, for a given interface Γ at time level t, see also [6]. Next, we compute an approximation of the normal component of the velocity at the interface. Finally we apply a discrete front tracking method to obtain an approximation of the position of the interface at the new time level.

5.3.1 Discretization of the stream function equation

Let $\gamma^k(x, z)$ and Γ^k be respectively the specific weight and the interface at time t^k. The stream function ψ is determined by the solution of problem

$$(P_\psi^k) \begin{cases} -\text{div}\left(\frac{1}{\kappa}\nabla\psi\right) = \frac{\partial}{\partial x}\left(\gamma^k(x, z)\right), & \text{for } (x, z) \in \Omega, \\ \psi = 0, & \text{on } \partial\Omega. \end{cases} \tag{5.3.1}$$

We solve (P_ψ^k) using a finite element method. The weak formulation of (P_ψ^k) is obtained by multiplying equation (5.3.1) by a test function $v \in H_0^1(\Omega)$ and integration by parts:

$$\int_\Omega \frac{1}{\kappa}\nabla\psi . \nabla v = \int_\Omega \gamma^k(x, z)\frac{\partial v}{\partial x}, \quad \text{for all } v \in H_0^1(\Omega). \tag{5.3.2}$$

We decompose domain Ω at time t^k into two subdomains Ω_f^k and Ω_s^k, being respectively the subdomain of fresh water and salt water. Moreover, we assume that the interface Γ^k between Ω_f^k and Ω_s^k is smooth enough. After integration by parts of the right-hand side of (5.3.2) we obtain the following weak formulation of Problem (P_ψ^k)

Find $\psi \in H_0^1(\Omega)$ such that

$$\int_\Omega \frac{1}{\kappa}\nabla\psi . \nabla v = (\gamma_f - \gamma_s)\int_{\Gamma^k} v \, n_x \, d\sigma, \quad \text{for all } v \in H_0^1(\Omega), \tag{5.3.3}$$

where n_x denotes the x-component of the unit vector normal to the interface Γ^k, pointing into Ω_f^k.

Let $\mathcal{T}_h$ be a triangularization of $\overline{\Omega}$. If we apply the finite element method with piecewise linear basis functions, then the discretized problem is given by:

Find $\psi_h \in V_h$ such that

$$\int_\Omega \frac{1}{\kappa}\nabla\psi_h \cdot \nabla v_h = (\gamma_f - \gamma_s)\int_{\Gamma_h^k} v_h \, n_{h,x} \, d\sigma, \quad \text{for all } v \in V_h, \tag{5.3.4}$$

where $V_h = \left\{ v_h \in C(\overline{\Omega}) \mid \forall T \in \mathcal{T}_h, \ v_h \text{ is linear on } T \text{ and } v_h = 0 \text{ on } T \right\}$. Here, Γ_h^k is a piecewise linear approximation of Γ^k, while n_h denotes an approximation of the unit vector normal to Γ^k.

Let $(\phi_i)_{i=1,...,N}$ be the piecewise linear basis function of V_h. We decompose ψ_h on this basis, i.e.

$$\psi_h(x,z) = \sum_{i=1}^{N} \psi_i \phi_i(x,z) \ \text{ for } \ (x,z) \in \Omega. \tag{5.3.5}$$

Then Problem (5.3.4) is equivalent to

$$\sum_{i=1}^{N} \psi_i \int_{\Omega} \frac{1}{\kappa} \nabla \phi_i . \nabla \phi_j = (\gamma_f - \gamma_s) \int_{\Gamma_h^k} \phi_j n_{h,x} d\sigma, \quad \text{for all } j = 1, ..., N. \tag{5.3.6}$$

Following [6], we apply a moving mesh method which enables to generate a new triangularization of Ω at each time step. Let $\Omega_{h,f}^k$ denote the fresh water domain and $\Omega_{h,s}^k$ the salt water domain. These domains are separated by the piecewise linear approximation of interface Γ_h^k. The triangularization of $\Omega_{h,f}^k$ and $\Omega_{h,s}^k$ is respectively $\tau_{h,f}^k$ and $\tau_{h,s}^k$. These are constructed such that Γ_h^k always coincides with sides of triangles of $\tau_{h,f}^k$ and $\tau_{h,s}^k$. We refine the mesh in the neighborhood of Γ_h^k. The meshes are generated, using the mesh generator of the SEPRAN finite element package, which is developed at Delft University of Technology.

5.3.2 Discretization of the interface motion: front tracking

Let ψ^k be the stream function at time level $t^k = k\Delta t$, where Δt denotes the time step and $k = 0, 1, ..K$. Then the normal component of the velocity of a point at the interface is given by

$$V_n^k = \frac{\partial \psi^k}{\partial s^k} = \nabla \psi^k \cdot \mathbf{s}^k$$

where $\mathbf{s}^k$ denotes the unit vector tangential to Γ^k. Since $V_n^k = \frac{\partial \Gamma}{\partial t}(k\Delta t) \cdot \mathbf{n}(k\Delta t)$, we compute the interface position at time level $t^{k+1} = (k+1)\Delta t$ explicitly in time using

$$\Gamma^{k+1} \cdot \mathbf{n}(k\Delta t) = \Gamma^k \cdot \mathbf{n}(k\Delta t) + \Delta t \ V_n.$$

Let Γ_h^k be defined by a set of nodal points $(P_i^k)_{i=1,...,I}$, hence

$$\Gamma_h^k = \left\{ \left[P_i^k P_{i+1}^k \right], i = 1, ..., I-1, \ P_1^k \text{ and } P_I^k \in \partial\Omega \right\}.$$

The displacement of each nodal point is given by

$$\overrightarrow{P_i^k P_i^{k+1}} = \Delta t \ V_{n,i}^k \approx \Delta t \ D_i^k \cdot \mathbf{s}_i^k, \ \text{ for } i = 2, ..., I-1$$

where $V_{n,i}^k$ denotes the approximation of $V_n(P_i^k)$ and D_i^k the approximation of $\nabla \psi^k(P_i^k)$. The unit vector at point P_i^k given by by the approximation

$$\mathbf{s}_i^k = \frac{\overrightarrow{P_{i-1}^k P_{i+1}^k}}{\| \overrightarrow{P_{i-1}^k P_{i+1}^k} \|}. \tag{5.3.7}$$

Since

$$\psi^k(P_{i-1}^k) \approx \psi^k(P_i^k) + \overrightarrow{P_i^k P_{i-1}^k} \cdot \nabla \psi^k(P_i^k) \ \text{ and } \ \psi^k(P_{i+1}^k) \approx \psi^k(P_i^k) + \overrightarrow{P_i^k P_{i+1}^k} \cdot \nabla \psi^k(P_i^k) \tag{5.3.8}$$

we have

$$\frac{\overrightarrow{P_{i-1}^k P_{i+1}^k}}{\| \overrightarrow{P_{i-1}^k P_{i+1}^k} \|} \cdot \nabla \psi^k(P_i^k) \simeq \frac{\psi^k(P_{i+1}^k) - \psi^k(P_{i-1}^k)}{\| \overrightarrow{P_{i-1}^k P_{i+1}^k} \|}.$$

This motivates to choose

$$V_{n,i}^k = D_i^k \cdot \mathbf{s}_i^k = \frac{\psi^k(P_{i+1}^k) - \psi^k(P_{i-1}^k)}{\| \overrightarrow{P_{i-1}^k P_{i+1}^k} \|}.$$

Then the displacement is given by

$$\overrightarrow{P_i^k P_i^{k+1}} = \Delta t \, \frac{\psi^k(P_{i+1}^k) - \psi^k(P_{i-1}^k)}{\| \overrightarrow{P_{i-1}^k P_{i+1}^k} \|}, \quad \text{for } i = 1, ..., I-1. \tag{5.3.9}$$

Formula (5.3.9) is only used if point P_i^k belongs to Ω. In addition, we solve equations (5.2.18) to determine the two points P_1^{k+1} and P_I^{k+1} of Γ_h^{k+1}, which belong to the boundary $\partial \Omega$. Again we use an explicit scheme to compute the displacement of the top and toe, yielding respectively

$$\overrightarrow{P_1^k P_1^{k+1}} = -\Delta t \, \frac{\psi^k(P_2^k)}{z(P_2^k)} \ \text{ and } \ \overrightarrow{P_I^k P_I^{k+1}} = \Delta t \, \frac{\psi^k(P_{I-1}^k)}{1 - z(P_{I-1}^k)}, \tag{5.3.10}$$

where $z(P)$ denotes the z-coordinate of point P.

To ensure stability of the numerical time integration we chose the time step such that the Courant-Friedrichs-Lewy (CFL) condition

$$\text{CFL} = C^k \frac{\Delta t}{l^k} \leq 1, \tag{5.3.11}$$

is satisfied at every time level k. Here, the constant C is given by

$$C^k = \max_{(x_i^k, z_i^k) \in \Gamma_h^k} \left\{ |\mathbf{q}(x_i^k, z_i^k)| \right\} = \max_{(x_i^k, z_i^k) \in \Gamma_h^k} \left\{ |q_x(x_i^k, z_i^k)|, |q_z(x_i^k, z_i^k)| \right\}, \tag{5.3.12}$$

and l^k denotes the minimum distance between two adjacent nodal points at the piecewise linear interface. For all practical purposes we chose CFL $= 0.2$.

5.4 The homogeneous case

The homogeneous case, i.e. when $\kappa_1 = \kappa_2 = \kappa$ in Ω, has been studied extensively by Chan Hong et.al. [6]. They parameterize the height of the interface and use the explicit $S^{\alpha,\beta}$-scheme of Lerat & Peyret [13] to discretize the hyperbolic interface motion equation (5.2.13). The parameters α, β are chosen such that they attain "optimal" values, with respect to the discretization of (5.2.13), see e.g. Wilders [20]. In addition they use a Runge-Kutta method to compute the displacement of the top and toe of the interface. For completeness and to gain confidence in the front tracking procedure proposed in this paper, we compare our numerical results with two distinct (semi) analytical similarity solutions of simplified problems: the rotating linear interface and slumping of brine mounds.

The full problem (5.2.17) can be reduced to a simplified problem, under the so called Dupuit approximation, yielding a nonlinear diffusion equation for the parameterized height of the interface. In this approximation, one assumes that the horizontal component of the specific discharge vector is constant in each fluid, and jumps at the interface. In view of $q_x = -\partial\Psi/\partial z$, this is equivalent to saying that the stream function is linear in z in each fluid. Numerical experiments, have shown that this is a reasonable approximation, as long as the inclination angle of the interface with the horizontal is less than $\pi/4$, provided the porous medium is homogeneous, see e.g. Chan-Hong et. al. [6]. Under the Dupuit approximation, interface motion equation (5.2.13) reduces to (after scaling according to (5.2.15), (5.2.16))

$$\frac{\partial u}{\partial t} = \frac{\partial}{\partial x}\left\{\kappa\, u(1-u)\frac{\partial u/\partial x}{1+(\partial u/\partial x)^2}\right\} \quad \text{for } (x,t) \in \mathbf{R} \times \mathbf{R}^+, \tag{5.4.1}$$

subject to the initial condition $u(x,0) = u_0(x)$, while the stream function is given by

$$\Psi(u,x,t) = \kappa\, u(1-u)\frac{\partial u/\partial x}{1+(\partial u/\partial x)^2}. \tag{5.4.2}$$

For homogeneous aquifers, κ is constant. Therefore, its appearance in equation 5.4.1 is not essential, but only there to keep the scaling uniform throughout the paper. These particular forms are due to De Josselin de Jong [11]. Note that (5.4.1) is only valid under the assumption that the interface extends through the full depth of the aquifer, hence $u \in [0,1]$. Equation is degenerate parabolic: at points where $u = 0$, 1 or $\partial u/\partial x = -1, +1$, the coefficient of the second-order derivative vanishes.

5.4.1   Comparison with the rotating line solution

The Dupuit equation (5.4.1) allows a similarity solution of the form

$$u_s(x,t) = \xi(\eta) \quad \text{with } \eta = xg(t), \tag{5.4.3}$$

where the function ξ is given by

$$\xi(\eta) = \begin{cases} 0 & -\infty < \eta \le -\frac{1}{2} \\ \eta + \frac{1}{2} & -\frac{1}{2} < \eta < +\frac{1}{2} \\ 1 & +\frac{1}{2} \le \eta < +\infty \end{cases} \tag{5.4.4}$$

and where the function $g(t)$ is the solution of the initial value problem

$$\frac{dg}{dt} = -2\frac{g^3}{1+g^2} \quad \text{for } t > 0, \tag{5.4.5}$$

subject to $g(0) = g_0$, see Zhang [23]. For $g_0 \in [-1,1]$ the similarity solution of (5.4.1) has the character of a rotating linear interface. It defines two interface curves in the (x,t)-plane: for $\eta = -1/2$ the movement of the toe is given by $(-1/(2g(t)),t)$ and for $\eta = +1/2$ the movement of the top is given by $(+1/(2g(t)),t)$. The similarity solution represents the large time behavior of equation (5.4.1). Van Duijn & Hilhorst [10] and Bertsch et al. [5] proved that an arbitrary initial interface converges towards u_s at $t \to \infty$. Chan Hong et. al. [6] demonstrated numerically similar behavior of the full problem. A highly irregular initial interface tends towards to a rotating linear interface as $t \to \infty$. Let the initial condition for u in problem (5.2.17)-(5.2.17)
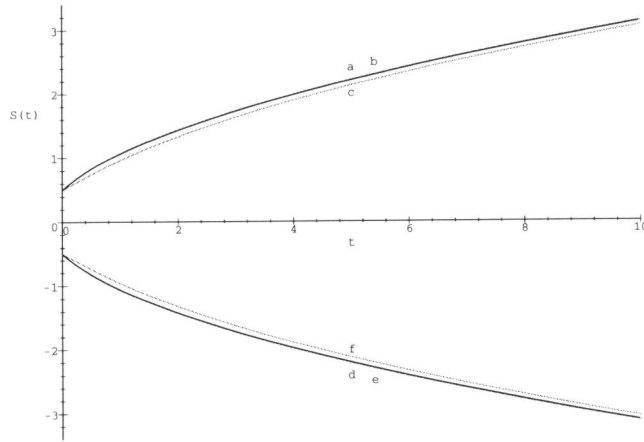
Figure 2. Comparison of the time evolution of the top and toe: (a) and (f) front tracking
method, (b) and (e) $S^{\alpha,\beta}$-scheme, (c) and (f) the Dupuit similarity solution.

be given by

$$u_0(x) = \begin{cases} 0 & -1 \leq x \leq -\frac{1}{2} \\ x + \frac{1}{2} & -\frac{1}{2} < x < +\frac{1}{2} \\ 1 & +\frac{1}{2} \leq x \leq +1 \end{cases} \tag{5.4.6}$$

which corresponds to $g(0) = 1$ for the rotating line solution. In Figure 2 we compare the
movement of the top and toe of the interface in the (x,t)-plane, for three different solutions:
the (semi) explicit rotating line solution, a numerical solution based on the $S^{\alpha,\beta}$-scheme and a
numerical solution based on the front tracking method. Note that both numerical solutions are
indistinguishable on the scale of Figure 2: the maximum relative difference is $\approx 0.06\%$. With
respect to the speed of propagation $\dot{S}(t)$ of the top and toe of the interface we observe in Figure
2 convergence of the numerical solutions (a,b,d and e) towards the similarity solution (c and f).
The numerically computed positions of the top and toe converge 'up to a constant' towards the
Dupuit similarity solution.

5.4.2 Bounds on the time scale of slumping brine mounds

Equation (5.4.1) only applies to special configurations with fresh-salt interfaces extending through
the full depth of an aquifer confined top and bottom by impermeable horizontal boundaries.
When the initial interface shape takes the form of a two-dimensional brine mound of finite

volume, Van Duijn & Philip [17] in their analytical study show that (5.4.1) may be replaced by

$$\frac{\partial u}{\partial t} = \frac{\partial}{\partial x} \left(u \frac{\partial x}{\partial x} \right) \quad \text{for} \ (x, t) \in \mathbf{R} \times \mathbf{R}^+, \tag{5.4.7}$$

under the assumption that $(\partial u / \partial x)^2 << 1$ and $u << 1$. This equation has a parabolic similarity solution, given by

$$u(x,t) = \begin{cases} \left(\dfrac{3a^2}{32(t+T)} \right)^{\frac{1}{3}} - \dfrac{x^2}{6(t+T)} & \text{for} \quad |x| \le \left(\dfrac{9a(t+T)}{2} \right)^{\frac{1}{3}} \\[4mm] 0 & \text{for} \quad |x| > \left(\dfrac{9a(t+T)}{2} \right)^{\frac{1}{3}} \end{cases} \tag{5.4.8}$$

where the constant T is defined by

$$T = \frac{3a^2}{32(u(0,0))^3}. \tag{5.4.9}$$

This solution describes nonlinear diffusion of an instantaneous source of strength a, released at $t = 0$, and has been obtained independently by Barenblatt [1] and Pattle [15]. Van Duijn & Philip [17] show that this solution gives a lower bound on the time scale of slumping brine mounds.
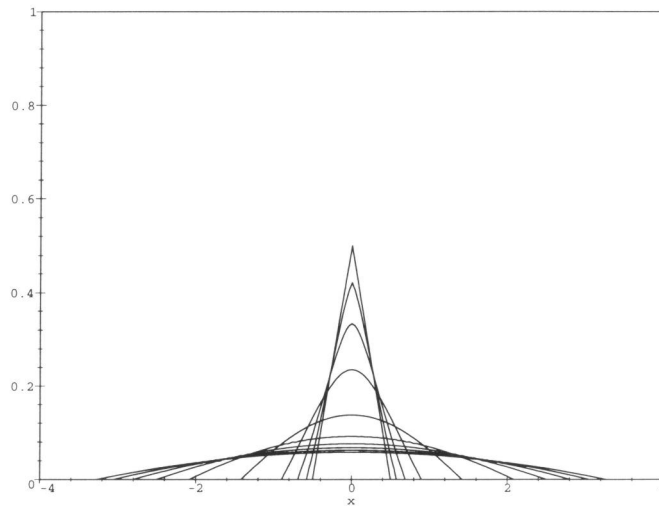
Figure 3.a. Computed time evolution of a decaying brine mound.
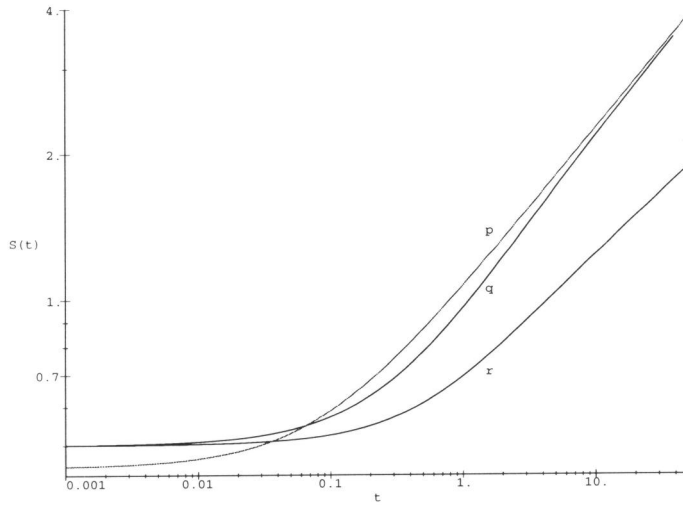
Figure 3.b. Time evolution of the toe: Lower bound on the time scale (p), i.e. parabolic solution, the numerical solution (q) and upper bound (r), i.e. triangular solution.

Moreover, they derive an approximate interface motion equation that gives a upper bound on the time scale of the slumping slumping process. Equation (5.4.1) is modified to restrict the fluid motion to the region $0 \leq z \leq g(t)^{-1}$, yielding

$$\frac{\partial u}{\partial t} = \frac{\partial}{\partial x} \left\{ u(g^{-1} - u) \frac{\partial u/\partial x}{1 + (\partial u/\partial x)^2} \right\}, \tag{5.4.10}$$

where $g(t)$ is a priori unknown and emerges as a part of the similarity solution of the problem. In writing (5.4.10), one implicitly assumes that fluid above the plane $\{z = g(t)\}$ is at rest. A triangular brine mound preserves mass and produces similarity when the horizontal dimensions increase by the factor $g(t)$ and vertical dimensions decrease by the factor $1/g(t)$. The function $g(t)$ is implicitly given by

$$t = \ln\left(\frac{g}{g_0}\right) + \frac{a^2}{4}(g^4 - g_0^4), \tag{5.4.11}$$

where $g_0 = g(0)$. For the details we refer to [17]. The gravitational potential energy is proportional to the elevation of the mound centre of gravity above its base. This quantity is used to match the triangular ($\triangle$) and parabolic ($\cap$) similarity solutions appropriately. One easily verifies that

$$\bar{z}_{\triangle}(t) = \frac{1}{3g(t)} \quad \text{and} \quad \bar{z}_{\cap}(t) = \left(\frac{3a^2}{500}\right)^{\frac{1}{3}} \frac{1}{(t+T)^{\frac{1}{3}}}. \tag{5.4.12}$$

Matching these expressions at $t = 0$ yields

$$u_\cap(0,0) = \left(\frac{125}{144}\right)^{\frac{1}{3}} \frac{1}{g(0)} \quad \text{and} \quad T = \frac{27}{250}a^2 g(0)^{\frac{1}{3}}. \tag{5.4.13}$$

The time course of the semi-width of the mound at its base, i.e. the position of the mound toe $S(t)$ at the right-hand side, for respectively the triangular and parabolic solution are given by

$$S_\triangle(t) = ag = \frac{a}{3\bar{z}_\triangle(t)} \quad \text{and} \quad S_\cap(t) = \left(\frac{9a(t+T)}{2}\right)^{\frac{1}{3}} = \frac{3a}{10\bar{z}_\cap(t)}. \tag{5.4.14}$$

The upper bound on the time scale (i.e. a lower bound on the displacement scale) is given by $t(S_\triangle)$ and the lower bound by $t(S_\cap)$. The computed time evolution of a brine mound, initially given by

$$u_0(x) = \begin{cases} \frac{1}{2} - x & \text{for} & 0 \leq x \leq \frac{1}{2} \\ \frac{1}{2} + x & \text{for} & -\frac{1}{2} \leq x < 0 \\ 0 & \text{for} & |x| > \frac{1}{2} \end{cases} \tag{5.4.15}$$

is shown in Figure 3.a. In Figure 3.b. we compare the bounds on the time scale obtained by Van Duijn & Philip [17] with a numerical solution of the full problem. Observe that the behavior of the numerical solution is closer to the upper bound ($\triangle$) at the (very) short time scale, while it approaches the lower bound ($\cap$) at large t. This is exactly the behavior that was predicted in [17].

5.5   An interface crossing a discontinuity in permeability

When a fresh-salt interface intersects a discontinuity in permeability, it is possible to derive a simple expression for the shape of the interface in an infinitesimal small neighborhood of the intersection point, provided the interface is non-singular. The derivation is based on the two-fluid interface conditions in a homogeneous porous medium combined with the flow conditions of a homogeneous fluid at a discontinuity in permeability. First we consider a linear interface
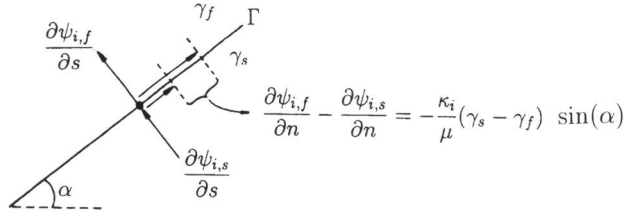

Figure 4. The shear flow at the interface.

Γ, under an inclination angle α with the horizontal, separating two fluids with specific weights

γ_f (upper fluid) and γ_s (lower fluid). At the interface, the normal components of the specific discharge are continuous, i.e.

$$\frac{\partial \psi_{i,f}}{\partial s} = \frac{\partial \psi_{i,s}}{\partial s} \text{ for } i = 1, 2 \tag{5.5.1}$$

while the tangential components of the specific discharge satisfy the shear flow relation, given by

$$\frac{\partial \psi_{i,f}}{\partial n} - \frac{\partial \psi_{i,s}}{\partial n} = -\frac{\kappa_i}{\mu} (\gamma_s - \gamma_f) \sin(\alpha) \text{ for } i = 1, 2, \tag{5.5.2}$$

see Figure 4. Then the corresponding relations between the x- and z-components of the specific discharge are given by

$$-\frac{\partial \psi_{i,f}}{\partial z} + \frac{\partial \psi_{i,s}}{\partial z} = \frac{\kappa_i}{\mu} (\gamma_s - \gamma_f) \sin(\alpha) \cos(\alpha) \text{ for } i = 1, 2, \tag{5.5.3}$$

and

$$\frac{\partial \psi_{i,f}}{\partial x} - \frac{\partial \psi_{i,s}}{\partial x} = \frac{\kappa}{\mu} (\gamma_s - \gamma_f) \sin^2(\alpha) \text{ for } i = 1, 2. \tag{5.5.4}$$

Next we consider flow of a homogeneous fluid in the vicinity of a discontinuity in permeability Σ, separating two regions with different intrinsic permeability: κ_1 (upper region) and κ_2 (lower region). The inclination angle between the discontinuity and the horizontal is given by β. Again we require continuity of the specific discharge components normal to the discontinuity in κ, hence

$$\frac{\partial \psi_{1,j}}{\partial s} = \frac{\partial \psi_{2,j}}{\partial s} \text{ for } j = f, s, \tag{5.5.5}$$

while the tangential discharge components at the discontinuity satisfy

$$\kappa_2 \frac{\partial \psi_{1,j}}{\partial n} - \kappa_1 \frac{\partial \psi_{2,j}}{\partial n} = 0 \text{ for } j = f, s, \tag{5.5.6}$$

see Figure 5. Consequently the relations between the x- and y-components of the specific discharge are given by

$$\tan(\beta) \left(-\frac{\partial \psi_{1,j}}{\partial z} + \frac{\partial \psi_{2,j}}{\partial z} \right) = \left(\frac{\partial \psi_{1,j}}{\partial x} - \frac{\partial \psi_{2,j}}{\partial x} \right) \text{ for } j = f, s, \tag{5.5.7}$$

and

$$\kappa_1 \frac{\partial \psi_{2,j}}{\partial z} - \kappa_2 \frac{\partial \psi_{1,j}}{\partial z} = \left(\kappa_1 \frac{\partial \psi_{2,j}}{\partial x} - \kappa_2 \frac{\partial \psi_{1j}}{\partial x} \right) \tan(\beta) \text{ for } j = f, s. \tag{5.5.8}$$

Expressions (5.5.3), (5.5.4) and (5.5.7), (5.5.8) can be combined in the following way. Consider a straight line through the origin of the (x, z)-plane, under inclination angle β with the horizontal x-axis, being a vertical cross section of the plane separating two regions with permeability κ_1 (upper region) and κ_2 (lower region). A sharp interface, separating two fluids with specific weight γ_f (upper fluid) and γ_s (lower fluid), intersects this line in the origin. The inclination angle of the interface with the horizontal in the region $x > 0$ is denoted by α_1, while the angle between the interface and the negative x-axis, i.e. in the region $x < 0$, is given by α_2. We assume for the moment that $\alpha_1 \neq \alpha_2 \neq \beta$, implying that interface and discontinuity in permeability
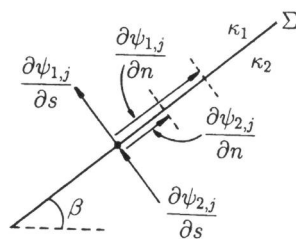
Figure 5. The discharge components at a discontinuity in permeability.

divide the (x, z)-plane in four distinct regions. Provided the interface is non-singular (finite and compatible velocities), the discharge components in an infinitesimal small neighborhood of the origin, between adjacent regions, have to satisfy (5.5.3), (5.5.4) or (5.5.7), (5.5.8). Hence, given the x- and z-discharge components in one of the regions, we can compute all corresponding discharges in the other regions. After some elementary algebra we obtain

$$\tan(\alpha_1) = \frac{\tan(\alpha_2)\left(1 + \frac{\kappa_1}{\kappa_2}\tan^2(\beta)\right) - \left(1 - \frac{\kappa_1}{\kappa_2}\right)\tan(\beta)}{\left(\frac{\kappa_1}{\kappa_2} + \tan^2(\beta)\right) - \tan(\alpha_2)\tan(\beta)\left(1 - \frac{\kappa_1}{\kappa_2}\right)}. \tag{5.5.9}$$

A similar relation has been found by Bear & Shapiro [3], expressing the angles of intersection α_1 and α_2 in terms of β and the fresh and salt water fluxes in the intersection point. Note that the fluid density difference does not appear in (5.5.9).

In the limit $\kappa_1/\kappa_2 \to 1$, i.e. a homogeneous porous medium, (5.5.9) yields $\alpha_1 = \alpha_2$, as to be expected. In case of a horizontal discontinuity in permeability, i.e. in the limit $\beta \to 0$, we obtain

$$\tan(\alpha_1) = \frac{\kappa_2}{\kappa_1}\tan\alpha_2 \tag{5.5.10}$$

while for a vertical discontinuity in permeability, i.e. in the limit $\beta \to \pi/2$, expression (5.5.9) reduces to

$$\tan(\alpha_1) = \frac{\kappa_1}{\kappa_2}\tan(\alpha_2). \tag{5.5.11}$$

The case $\beta = 0$, i.e. expression (5.5.10), implies that if $\alpha_1 \to \pi/2$ then $\alpha_2 \to \pi/2$. Equation (5.5.9) gives an exact relation between the angles of intersection and therefor it is an indispensable tool for computer code verification. Moreover it gains insight in the (transient) behavior of an interface intersecting a discontinuity in permeability.

5.6 Vertical discontinuity in permeability: the Dupuit approximation

For the special case of a vertical discontinuity in permeability, the scaled coefficient κ is given by

$$\kappa = \kappa(x) = \begin{cases} \kappa_1 & \text{for} \quad x < 0 \\[2mm] \kappa_2 & \text{for} \quad x > 0 \end{cases} \tag{5.6.1}$$

Under the assumption that $\partial u/\partial x \ll 1$, i.e. in case of a (very) flat interface, equation (5.4.1) reduces to

$$\frac{\partial u}{\partial t} = \frac{\partial}{\partial x} \left\{ \kappa(x) u (1 - u) \frac{\partial u}{\partial x} \right\} \quad \text{for} \quad (x, t) \in \mathbf{R} \times \mathbf{R}^+ xi, \tag{5.6.2}$$

while the stream function is given by

$$\Psi(u, x, t) = \kappa(x) u (1 - u) \partial u / \partial x \tag{5.6.3}$$

Continuity of the stream function at the discontinuity in κ at $x = 0$ requires

$$\lim_{x \downarrow 0} \Psi(u(x, t), x, t) = \lim_{x \uparrow 0} \Psi(u(x, t), x, t) \quad \text{for} \, t > 0. \tag{5.6.4}$$

In this limit (5.6.3) yields

$$\frac{\partial u}{\partial x}(0^+, t) = \left(\frac{\kappa_1}{\kappa_2} \right) \frac{\partial u}{\partial x}(0^-, t) \quad \text{or} \quad \tan(\alpha_1) = \left(\frac{\kappa_1}{\kappa_2} \right) \tan(\alpha_2). \tag{5.6.5}$$

This is identical to the exact expression (5.5.11). Note that the latter does not hold when $(\partial u \partial x)^2$ is not disregarded in (5.4.1).

Let the initial interface be given by

$$u(x, 0) = u_0(x) = \begin{cases} 1 & \text{for} \quad x > 0 \\ 0 & \text{for} \quad x < 0 \end{cases} \tag{5.6.6}$$

Then, problem (5.6.2)-(5.6.6) allows a similarity transformation of the form

$$u(x, t) = f(\eta) \quad \text{with} \quad \eta = \frac{x}{\sqrt{t}}, \tag{5.6.7}$$

where the function f is a solution of the boundary value problem

$$\frac{1}{2} \eta f' + (\kappa(\eta) \, f (1 - f) f')' = 0 \quad \text{for} \ \eta \in \mathbf{R}, \tag{5.6.8}$$

where the primes denote differentiation with respect to η, subject to

$$f(-\infty) = 0 \quad \text{and} \quad f(+\infty) = 1. \tag{5.6.9}$$

The solution of this problem exhibits a jump in the derivative at $\eta = 0$. To eliminate this discontinuity we introduce a new variable according to

$$s(\eta) = \int_0^\eta \frac{1}{\kappa(\xi)} \, d\xi \quad \text{for} \ \eta \in \mathbf{R}. \tag{5.6.10}$$

Because $\kappa(x)$ is piecewise constant, we may write

$$s(\eta) = \left\{ \begin{array}{ll} \eta/\kappa_1 & \text{for} \quad \eta < 0 \\ \eta/\kappa_2 & \text{for} \quad \eta > 0 \end{array} \right. \quad \text{or} \quad \kappa(s) = \left\{ \begin{array}{ll} \kappa_1 & \text{for} \quad s < 0 \\ \kappa_2 & \text{for} \quad s > 0 \end{array} \right. \tag{5.6.11}$$

Substitution of (5.6.11) in (5.6.8) yields

$$\frac{1}{2}s\kappa_2 f' + (f(1-f)f')' = 0 \text{ for } s > 0, \tag{5.6.12}$$

$$\frac{1}{2}s\kappa_1 f' + (f(1-f)f')' = 0 \text{ for } s < 0, \tag{5.6.13}$$

where the primes denote differentiation with respect to s. Now, the derivative f' is continuous at $s = 0$. Finally we introduce an additional transformation, in order to obtain the ratio κ_1/κ_2 as a single parameter in (5.6.12)-(5.6.13). Let

$$\xi = s\sqrt{\kappa_2} \text{ for } s \in \mathbf{R}, \tag{5.6.14}$$

then (5.6.12), (5.6.13) reduce to

$$\frac{1}{2}\xi f' + (f(1-f)f')' = 0 \text{ for } \xi > 0, \tag{5.6.15}$$

$$\frac{1}{2}\left(\frac{\kappa_1}{\kappa_2}\right)\xi f' + (f(1-f)f')' = 0 \text{ for } \xi < 0, \tag{5.6.16}$$

where now the primes denote differentiation with respect to ξ.

We solve boundary value problem (5.6.15), (5.6.16) subject to (5.6.9) numerically, using a shooting procedure in the sub-domains $\xi > 0$ and $\xi < 0$. The numerical integration is established with a standard adaptive step size Runge-Kutta method. First we solve (5.6.15) subject to $f(0) = f_0$ and $f'(0) = \alpha$, in the domain $\xi > 0$, where α denotes a shooting parameter. The value of α is determined experimentally, such that the numerical approximation of $f(\xi)$ satisfies the boundary condition $f(+\infty) = 1$. Next we solve (5.6.16) subject to f_0 and $f'_0 = \alpha$ (α known), in the domain $\xi < 0$. In order to satisfy the boundary condition $f(-\infty) = 0$, we adjust the value of the ratio κ_1/κ_2 accordingly in (5.6.16). Equations (5.6.15), (5.6.16) imply that f_0, which corresponds to the (stationary) height of the interface at $x = 0$ for any $t > 0$, depends on the ratio κ_1/κ_2 only. Figure 6 shows the numerical results for $f_0 = f_0(\kappa_1/\kappa_2)$.
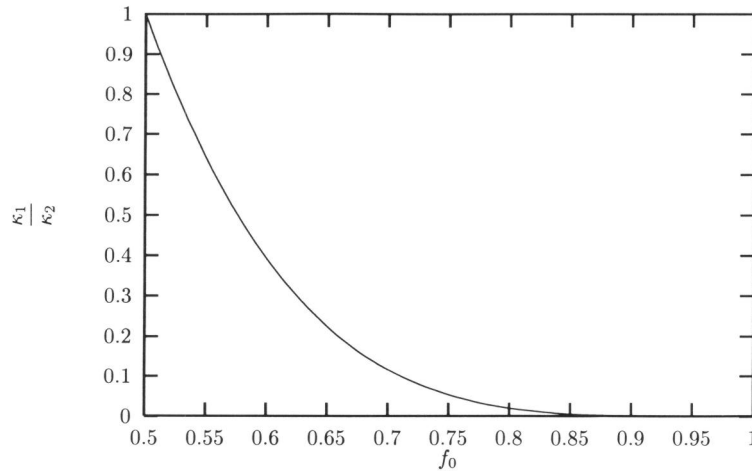

Figure 6. The relation between f_0 and κ_1/κ_2, for $0.5 < f_0 < 1.0$

When $\kappa_1/\kappa_2 = 1$, equations (5.6.12)-(5.6.13) reduce to (5.6.15), but now for $\xi \in \mathbf{R}$. The latter has an exact solution of the form of a rotating line, given by

$$f(\xi) = \begin{cases} 1 & \text{for} & \xi > 0 \\ \frac{1}{2}(1+\xi) & \text{for} & -1 \leq \xi \leq +1 \\ 0 & \text{for} & \xi < -1 \end{cases} \qquad (5.6.17)$$

see Philip [16]. Figure 7 shows numerical approximations of the similarity solution $f(\xi)$ for different values of the ratio κ_1/κ_2. Figure 8 gives an example of the time evolution of the interface $u(x,t)$ for $\kappa_1/\kappa_2 = 0.1261$ and $f_0 = u(0,t) = 0.7$.
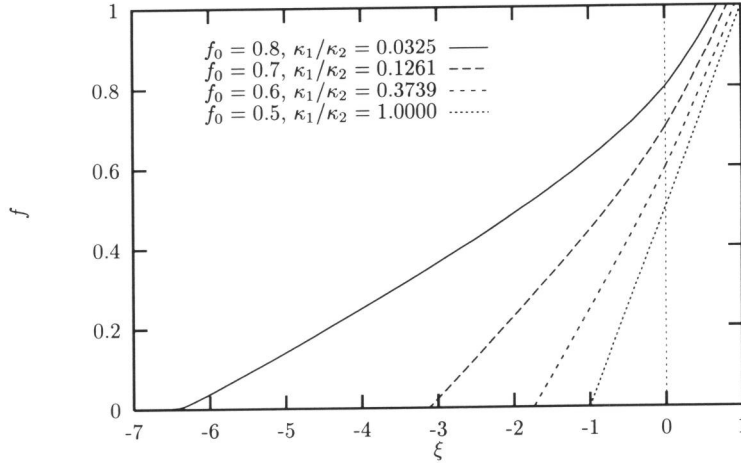
Figure 7. The similarity solution $f(\xi)$ for different values of f_0 and corresponding κ_1/κ_2-values
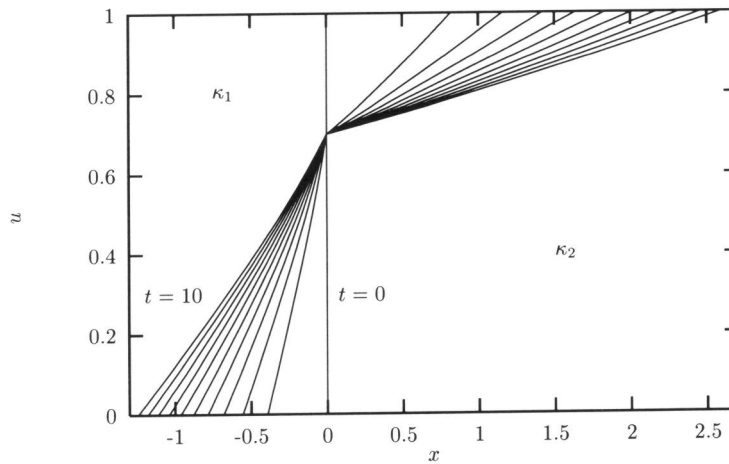
Figure 8. An example of the time evolution of an interface crossing a vertical discontinuity in permeability: the similarity solution for $\kappa_2 = 1.0$, $\kappa_1 = 0.1261$ and $f_0 = 0.7$. The time levels are $t = 0, 1, 2 \ldots 10.0$.

In Figure 9 we show the numerical solution for $\kappa_1/\kappa_2 = 0.1261$ ($f_0 = 0.7$) in terms of the similarity variable $\eta = x/\sqrt{t}$. The result clearly demonstrates the convergence of the numerical

solution towards a similarity solution. The corresponding Dupuit similarity solution is also shown in Figure 9 (the dashed line). Notice the small difference between the numerically obtained similarity solution and the approximate Dupuit solution.
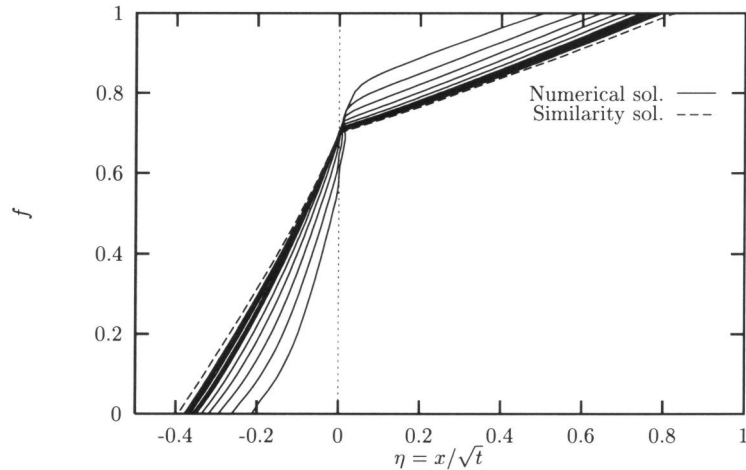

Figure 9. Convergence of the numerical solution towards a similarity solution. The dashed line represents the Dupuit similarity solution

The approximate Dupuit solution satisfies (5.5.11) for all $t > 0$, see also (5.6.4), (5.6.5). To check whether (5.5.11) is satisfied by the numerical solution we define the relative error $F = (1 - \kappa_2 \tan(\alpha_1^k)/(\kappa_1 \tan(\alpha_2^k))) \cdot 100\%$, where α_1^k and α_2^k denote the computed angles of intersection at time $t = t^k$. The time evolution of F is depicted in Figure 10. Each plot marker corresponds to a certain time level; intermediate time levels have been omitted. For short times we find large deviations between the computed results and expression (5.5.11). This is due to the singular behavior of the interface at the very short time scale of the computations, see Figure 9. As time proceeds, the relative error F tends towards a limiting value: $F \approx -0.6\%$.

The time evolution of the speed of propagation of the top and toe of the interface is shown in Figure 11. Again, we observe convergence of the numerically computed speeds towards the speeds computed with the Dupuit solution.
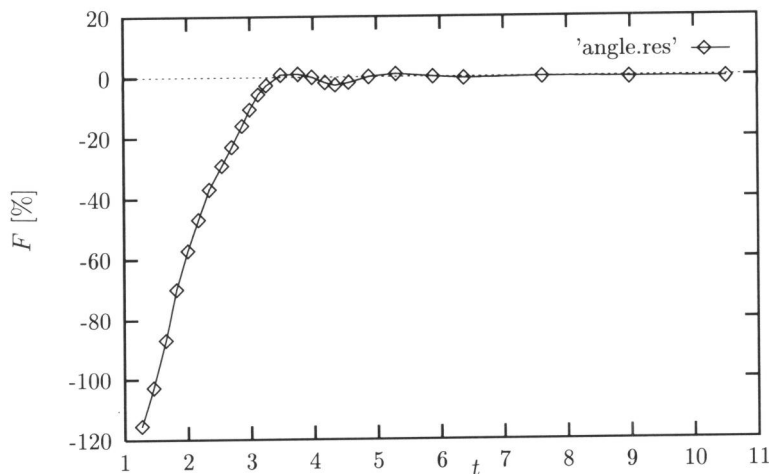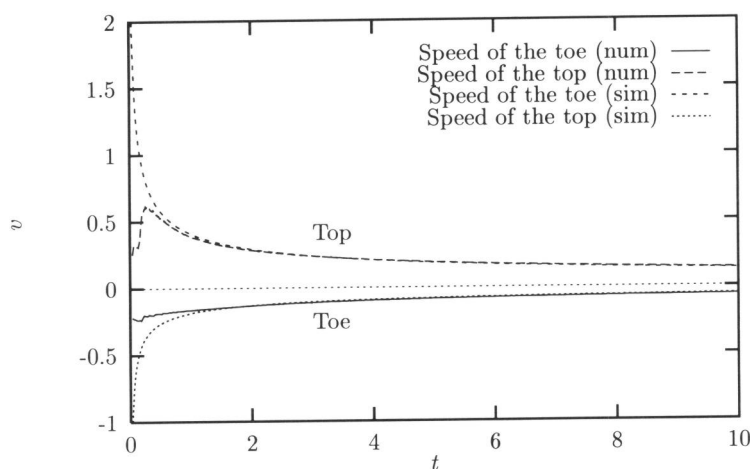
Figure 10. The relative error F as a function of time.

Figure 11. Time evolution of the speed of propagation of the top and toe of an interface: comparison of the numerical and similarity solutions.

5.7 A horizontal discontinuity in permeability

Next we consider a horizontal heterogeneity, consisting of two parallel layers of equal thickness with different permeability κ_1 (upper layer) and κ_2 (lower layer), under the assumption that $\kappa_1 < \kappa_2$. The initial interface is vertical at $x = 0$, such that the region $x < 0$ is occupied by fresh water and the region $x > 0$ by salt water. In this more complicated case it is not possible to obtain a similarity solution of a simplified problem based on the Dupuit approximation. If we assume that the two regions are separated at the plane $\{z = 1/2\}$ by an impermeable sheet, and apply the Dupuit approximation in both regions, we obtain two independent rotating line solutions. However, this is far from realistic because the exchange of fluid between the layers is disregarded.

For $t > 0$, a hydrodynamically instable zone, i.e. salt water on top of fresh water, develops in the vicinity of the discontinuity in permeability. The horizontal width of this zone grows in time. Under natural (field) conditions, small local variations in permeability perturb the interface in this zone, and fresh-salt fingers may occur. These fingers grow in time. The linear stability analysis shows that fingers of any width or 'wave length' > 0 can develop. The distribution of wave lengths in the fingering pattern depends upon the nature of the perturbation mechanism of the interface, e.g. the local (small scale) heterogeneous permeability field.

When we consider fresh and salt groundwater as miscible fluids and allow for diffusion/dispersion, stability analysis showed that there exists a (minimum) critical wave length λ_0 in the fingering pattern. The value of λ_0 is related to the value of the diffusivity/dispersivity D, see for instance List [14]. This implies that fingers with width smaller than (half) the critical wave length are dissipated by diffusion and/or dispersion and decay in time. In case of the interface approximation, i.e. in the limit $D \to 0$, we have, at least in theory, $\lambda_0 = 0$.

The computed time evolution of an initially vertical interface exhibits the development of fresh-salt fingers in the vicinity of the horizontal discontinuity in permeability, see Figure 12. To ensure numerical stability, the (variable) time step is chosen such that the condition CFL= 0.2 is satisfied at any time level. The onset of the instabilities in the physically unstable zone is caused by the discrete approximation of the interface: small numerical and discretization errors perturb the unstable interface at any time level which triggers the growth of the fresh-salt fingers.
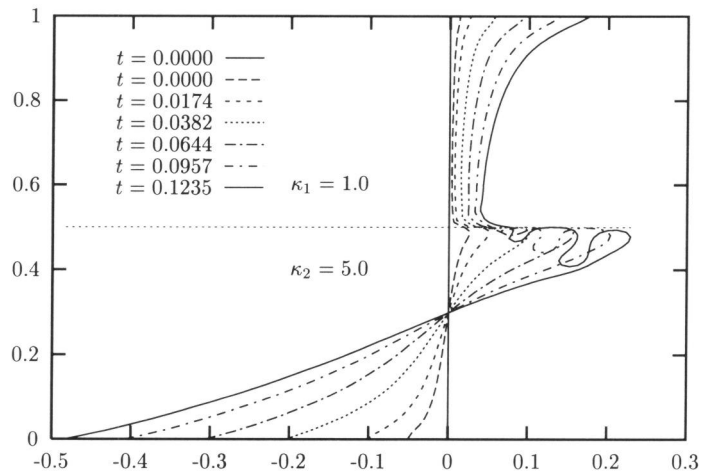

Figure 12. Time evolution of an initially vertical interface.

The width of the fingers that grow in time is directly related to the coarseness of the discretization of the interface. The minimum finger width at the onset of an instability is approximately 6 interface piecewise linears. If we refine the mesh by a factor 2, the width of the fingers that grow is also reduced by a factor 2, while the fingers start to develop earlier. In Figure 13, we compare two interfaces at $t = 0.1235$. The dashed line corresponds to the last interface shown in Figure 12, and is computed with a fine mesh. The solid line is the result of a computation with a coarse mesh, i.e. the number of nodal points at the interface is reduced by a factor 2when compared to the fine mesh. The computations break down when adjacent parts of the interface coincide. The discretization of the flow domain, i.e. two distinct regions separated by a single interface, does not allow the formation of salt or fresh water drops. The latter implies that only the short time development of instabilities can be simulated with this numerical approach.
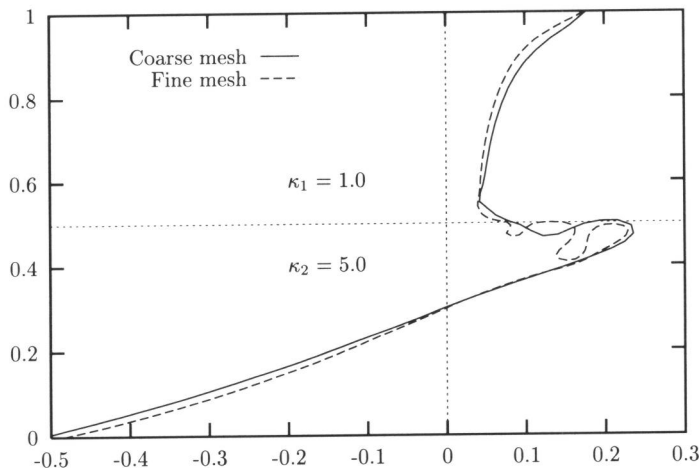
Figure 13. Interfaces at $t = 0.1235$, computed with a fine and a coarse discretization.

In Figure 14 we show the time evolution of an initially horizontal interface which coincides with the discontinuity in permeability. This interface is perturbed at $(0, 0.5)$ by -0.006. The upper part of the flow domain, i.e. the region where $\kappa_1 = 0.5$, is filled with salt water, and the lower part, i.e. the region where $\kappa_2 = 1.0$ is filled with fresh water. The computed finger shapes are not very smooth: the individual piecewise linears are clearly visible. The latter will always be that case. If we refine the mesh, the finger widths reduce accordingly. The asymmetry of the fingering pattern is caused by the asymmetry of the generated meshes with respect to the z-axis. If we do not perturb the initially horizontal interface, no growth of instabilities is observed, as to be expected. The initial interface is perfectly horizontal and the velocity field remains identically zero for all times.
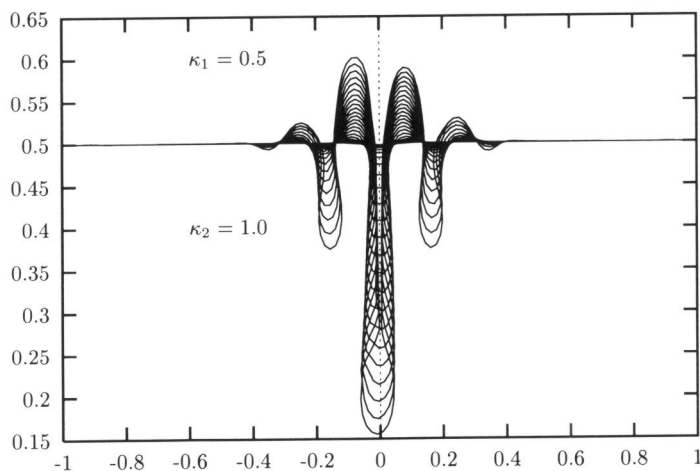

Fig 15. Time evolution of an initially horizontal interface that coincides with the discontinuity in permeability, and which is perturbed at $(0.0, 0.5)$ by -0.006.

A similar computation was carried out for the homogeneous case. The time evolution is shown in Figure 15. An example of the triangularization of the salt water domain is given in Figure 16. Notice the refinement of the discretization in the vicinity of the interface.
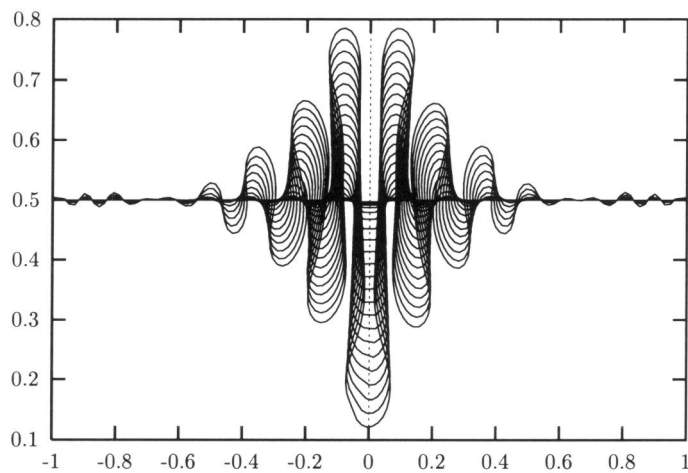
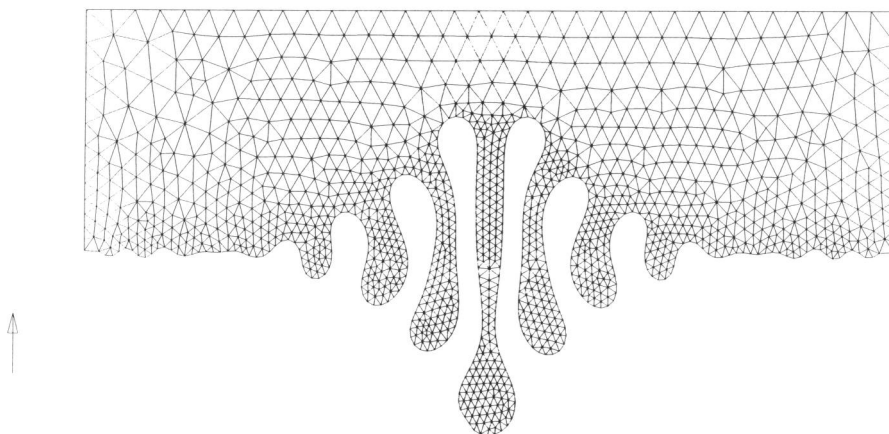Figure 15. Time evolution of an initially horizontal interface which is perturbed at $(0.0, 0.5)$ by -0.006.

Figure 16. Triangularization of the salt water region

5.8   Discussion and conclusions

The proposed front tracking procedure gives results within the same range of accuracy as the predictor-corrector scheme used by Chan Hong et. al. [6]. At least for parametrizable interfaces $(z = u(x, t))$ we are able to show this convincingly by comparison of results, generated with both methods. See for instance the rotating linear interface in a homogeneous flow domain in Section 4.1. For multivalued interfaces, no reliable test problems or related approximate Dupuit problems are available.

The bounds on the time scale of slumping brine mounds, as predicted by Van Duijn & Philip [17], could be verified and confirmed. The triangular Dupuit solution predicts the short-time behavior of the numerical solution of the full problem, while the parabolic Dupuit solution describes the large-time behavior. These results emphasize the utility of the Dupuit assumption in solving practical interface problems.

When an interface crosses a discontinuity in permeability, an exact expression can be derived, which relates the contrast in permeability to the angles of intersection at the discontinuity, see (5.5.9). If, given a permeability ratio κ_1/κ_2, the angles of intersection do not satisfy this expression, the velocities at the point of intersection will be, at least theoretically, singular. Indeed, very high velocities are encountered at the short-time scale of computations. As time proceeds, the computed interface shapes at the discontinuity in permeability converge towards the shape predicted by expression (5.5.9). In fact, the initially vertical interface, i.e. the initial condition for all heterogeneous computations, is singular itself due to the kinks at the domain boundaries. This also leads to very high initial velocities, and accordingly, due to the CFL constraint on the time step, to very small (initial) time steps.

For the case of a vertical discontinuity in permeability, a related approximate Dupuit could be solved in terms of a (semi) explicit similarity solution. The numerical solution of the full problem also converges towards a similarity profile as $t \to \infty$. The Dupuit solution gives a reasonable approximation of the large-time behavior of the numerical solution. Whereas the similarity profiles are not completely identical, the velocities of the top and toe of both solutions converge towards the same limiting values (up to small error).

The width of the fresh-salt fingers that occur in the unstable regions is selected by the numerical method, and not by any physical mechanism. This is a direct consequence of the absense of diffusion/dispersion in the interface approximation. Refinement of the mesh at the interface leads to smaller finger widths. This implies that the practical applicability of interface models for simulation of instabilities is limited. Moreover, the instabilities or fingers create a mixing zone of fresh and salt groundwater which is in some sense in contradiction with the interface approximation: strictly miscible fluids are considered to be immiscible.

Bibliography

[1]   BARENBLATT, G.I. *On some unsteady motions of a liquid and a gas in a porous medium*, Akad. Nauk. SSSR Prikl. Math. Mekh. **16**, pp 67-78.

[2]   J. BEAR. *Dynamics of fluids in porous media*, 1975, New York, American Elsevier.

[3]   BEAR, J. & SHAPIRO, A.M. *On the shape of the non-steady interface intersecting discontinuities in permeability* , Adv. Water Resources, Volume **7** (1984), pp. 106-112.

[4]   J. BEAR. *Hydraulics of groundwater*, 1979, New York, McGraw-Hill.

[5]   Bertsch, M, Esteban, J.R. & Zhang, H. *On the asymptotic behaviour of solutions of a degenerate equation in hydrology* , Nonlinear Anal., Theor. Meth. & Appl. **19** (1992), p.p. 365-374.

[6]   J.R. CHAN HONG, C.J. VAN DUIJN, D. HILHORST, J. VAN KESTER. *The interface between fresh and salt groundwater : a numerical study*, IMA J. of Appl. Math. (1989), 42, 299-316.

[7]   C. DUPAIX, D. HILHORST, J.F. SCHEID. *On a dissolution-growth problem with surface tension : a numerical study*, to appear.

[8]   ELDER, J.W. *Steady free convection in a porous medium heated from below*, J. Fluid Mech. **27** (1967), p.p. 29-48.

[9]   VAN DUIJN, C.J. & DE JOSSELIN DE JONG, G. *Free boundary problems in fresh-salt groundwater flow*, In Summer School on Flow and Transport in Porous Media, Beijing, China, 8-26 August 1988, Editor: Xiao Shutie, World Scientific.

[10]   VAN DUIJN, C.J. & HILHORST, D. *On a doubly nonlinear diffusion equation in hydrology*, Nonlinear Anal. Theory Meth. Appl. **11**, 305-333.

[11]   DE JOSSELIN DE JONG, G. *The simultaneous flow of fresh water in aquifers of large horizontal extension determined by shear flow and vortex theory*, Proceedings Euromech. **143** (1981) (eds A. Verruijt & F.B.J. Barends), Balkema Rotterdam, pp. 132-149.

[12]   DE JOSSELIN DE JONG, G. *Singularity distributions for the analysis of multiple flow through porous media*, J. Geophys. Res. **65** (1960), p.p. 3739-3758.

147

[13]   LERAT, A. & PEYRET, R *Sur le chois de schémas aux différences finies du second ordere fournissant des profiles de choc sans oscillations.* C.R. Acad. Sci. Paris **277** (1973), pp. 363-366.

[14]   LIST, E.J. *The stability and mixing of a density-stratified horizontal flow in a porous medium,* Rep. KH-R-11, Calif. Inst. of Technology, Pasadena (1965).

[15]   PATTLE, R.E. *Diffusion from an instantaneous point source with a concentration dependent coefficient,* Q.J. Mech. Appl. Mech. **12** (1959), pp. 407-409.

[16]   PHILIP, J.R. *Diffusion from an instantaneous point source with a concentration dependent coefficient ,* Q.J. Mech. Appl. Mech. 12 (1959), p.p. 407-409.

[17]   PHILIP, J.R. & VAN DUIJN, C.J. *Slumping of brine mounds: bounds on behaviour,* Journal of Hydrology **179** (1996), pp. 159-180.

[18]   SCHEID, J.F. *Etude théorique et numérique de l'évolution morphologique d'interfaces* Ph.D. thesis, Orsay 1994.

[19]   I. STAKGOLD. *Green's functions and boundary value problems,* 1979, A Wiley-Interscience Series of Texts.

[20]   WILDERS, P. *Minimization of dispersion in difference methods for hyperbolic conservation laws,* Ph.D. thesis, University of Amsterdam (1983)

[21]   WOODING, R.A. *Steady state free convection of liquid in a saturated porous medium,* J. Fluid Mech. **2** (1957), p.p. 273-285.

[22]   WOODING, R.A. *Free convection of fluid in a vertical tube filled with porous material,* J. Fluid Mech **13** (1962), p.p. 129-144.

[23]   ZHANG, H. *Nonlinear degenerate diffusion problems,* PhD thesis, Delft University of Technology, The Netherlands.

Chapter 6

Non-equilibrium crystal dissolution

6.1 Introduction

In this paper we study chemistry affected transport processes in porous media. The transported solutes are participants in a precipitation-dissolution reaction, which in general is not in equilibrium, but is kinetically controlled. In the Chapter 1 (i.e. the Introduction of this thesis) we have set up a model for spatially one-dimensional flow regimes. Throughout the rest of this paper we refer to the solid phase as 'crystal' or 'crystalline solid', which is due to the fact that we have a specific example in mind: the dissolution of a crystalline mineral phase, which occurs as a very thin layer on the grains of the porous medium, see e.g. Willis & Rubin [15]. In fact, the dissolving substance may be either crystalline or amorphous. It was assumed that water content, bulk density, pore velocity q [cm/s] and diffusion/dispersion coefficient D [cm^2/s] are constant. The unknown functions are u and v [mM/cm^3], where u is the molar concentration of one of the reacting participants in solution, v is the scaled concentration of the crystalline solid (both relative to the water volume), and a third unknown w [-], which appears to take into account the nature of the dissolution reaction. For a detailed discussion on the role of w we refer to Knabner et. al. [7]. The governing equations are

$$\frac{\partial}{\partial t}(u+v) + q\frac{\partial u}{\partial x} - D\frac{\partial^2 u}{\partial x^2} = 0 \tag{6.1.1}$$

$$\frac{\partial v}{\partial t} = k\{g(u;c) - wK\} \tag{6.1.2}$$

$$0 \le w \le 1 \quad \text{and} \quad w(x,t) = 1 \quad \text{if} \quad v(x,t) > 0 \tag{6.1.3}$$

for $-\infty < x < \infty$, $t > 0$. The positive constants K and k are the saturation constant and a rate parameter, respectively. There is a further function c in the nonlinear function g related to the precipitation reaction. It is a conserved quantity in the sense that it satisfies the linear diffusion-advection equation

$$\frac{\partial c}{\partial t} + q\frac{\partial c}{\partial x} - D\frac{\partial^2 c}{\partial x^2} = 0 \tag{6.1.4}$$

for $-\infty < x < \infty$, $t > 0$. The function c is solely determined by the stoichiometry of the precipitation-dissolution reaction. If this is given by

$$\overline{M}_{12} \rightleftharpoons nM_1 + mM_2 \tag{6.1.5}$$

149

with positive integers n, m where M_1, M_2 denote the species in solution and $\overline{M}_{12}$ the solid, then

$$c = mc_1 - nc_2 \tag{6.1.6}$$

where c_1, c_2 [mM/cm^2] are the molar concentrations of M_1, M_2. In (6.1.1)-(6.1.4), $c_1 := u$ is kept as an unknown and c_2 is substituted by means of (6.1.6). For a spatially independent batch situation the function c would be constant due to (6.1.4), i.e. all possible values of concentrations $c_1(t), c_2(t)$ lie in an affine subspace of the one-dimensional stoichiometric subspace of the reaction, defined by the condition $c = 0$. In the case of ionic species, it is also possible to consider c as the scaled total (positive) electric charge of the solution. This observation helps us in distinguishing two principal situations with respect to a specification by means of initial conditions. We will consider piecewise constant states at $t = 0$, i.e.

$$u(x,0), v(x,0), c(x,0) = \begin{cases} u^*, v^*, c^* & \text{for} \quad x < 0 \\ u_*, v_*, c_* & \text{for} \quad x > 0 \end{cases} \tag{6.1.7}$$

We can relate these solutions to solutions of a corresponding boundary value problem for $x > 0, t > 0$ by considering u_*, v_*, c_* as initial conditions and u^*, v^*, c^* as boundary conditions. Thus there are two situations

$$c^* = c_* \quad \text{and therefore} \quad c(x,t) = c = \text{constant} \tag{6.1.8}$$

or

$$c^* \neq c_* \tag{6.1.9}$$

In case (6.1.8) the boundary(/initial) conditions are <u>compatible</u> in the sense that they belong to the same affine stoichiometric subspace of the reaction or for ionic species that the injected fluid has the same ionic composition as the resident fluid. This situation is the only one which leads to travelling wave solutions being the subject of the paper by Knabner et. al. [7]. Here we concentrate on case (6.1.9), i.e. on <u>incompatible</u> boundary(/initial) conditions. In this paper we show how to obtain solutions of this problem in the presence of a dissolution front, i.e. a curve in the (x,t)-plane separating the region where $v = 0$ from the region where $v > 0$. To ensure that a dissolution front exists for all $t \geq 0$, one needs

$$v^* = 0 \quad \text{and} \quad v_* > 0. \tag{6.1.10}$$

If initially crystalline solid is everywhere present in the flow domain, i.e. $v^* > 0$ as well, then a dissolution front may occur after a certain finite time interval. Conditions for which this happens are discussed in Section 3.2.

A typical example for the function g is, assuming the thermodynamically ideal mass action law:

$$g(u; c) = u^n \left(\frac{1}{n}(mu - c) \right)^m \tag{6.1.11}$$

where (6.1.6) is used. To ensure that $c_1 \geq 0$, $c_2 \geq 0$, only the variable $u \geq (c/m)_+$ is allowed, where $a_+ = a$ for $a \geq u$, $a_+ = 0$ for $a < 0$. In general the function g has the following properties to be used later on:

$g(\cdot; c)$ is strictly monotone increasing for $u \geq (c/m)_+$,

$g(\cdot; c)$ is smooth for $u \geq (c/m)_+$ (at least Lipschitz-continuous).

We need the existence of a (unique) $u_S = u_S(c) \geq (c/m)_+$ such that

$$g(u; c) = K \tag{6.1.12}$$

i.e. u_S is the solubility for given c. Due to the properties of the function g given above, the following condition fulfilled by (6.1.11) is sufficient for (6.1.12):

$$g\left(\left(\frac{c}{m}\right)_+ ; c\right) = 0. \tag{6.1.13}$$

When we require (6.1.10), we additionally assume the initial states to be in chemical equilibrium, i.e.

$$\left(\frac{c}{m}\right)_+ \leq u^* \leq u_S(c^*) \quad \text{and} \quad u_* = u_S(c_*). \tag{6.1.14}$$

If solid is present everywhere, this would not lead to the appearance of a dissolution front, see 6.3.63),(6.3.64). Thus we allow in this case for an initial state for $x < 0$ not in equilibrium, which might be thought of as the consequence of an instantaneous removal of saturated fluid.

If dispersive transport is negligible compared to the advective transport, it is reasonable to let $D \to 0$, i.e. to cancel the corresponding terms in (6.1.1)-(6.1.4) and to obtain

$$\frac{\partial}{\partial t}(u + v) + q\frac{\partial u}{\partial x} = 0 \tag{6.1.15}$$

for $-\infty < x < \infty$, $t > 0$. The initial value problem (6.1.15),(6.1.2)-(6.1.4) and (6.1.7) is known as a Riemann problem. In this paper we consider the analytical and numerical construction of a solution of this Riemann problem. For dominating advective transport, i.e. the limit $D \to 0$ in (6.1.1), we expect a good approximation of the solutions of (6.1.1)–(6.1.4) and (6.1.7) ignoring only certain smoothing effects (see the comparison in Section 5). On the other hand, the treatment of the hyperbolic system by means of the method of characteristics allows a nearly explicit construction of the solution and thus gives detailed information about the qualitative structure of the solution. The function c is found directly, without a priori knowledge about u, v and w. It follows from (6.1.4) and (6.1.7) that for all $t \geq 0$

$$c(x,t) = \begin{cases} c^* & \text{for} \quad x < q\,t, \\ c_* & \text{for} \quad x > q\,t. \end{cases} \tag{6.1.16}$$

To be specific, we assume in the following

$$c^* > c_*. \tag{6.1.17}$$

The other case can be treated in exactly the same way or transformed to the above situation, which basically corresponds to a renumbering of the dissolved reaction participants. A further property, which holds true for the example (6.1.11), is the monotone dependence of the solubility $u_S(c)$ on c, i.e. in particular

$$u_S(c^*) > u_S(c_*). \tag{6.1.18}$$

In the analysis we will not make use of this property, but in the figures it is assumed to hold true or implied by the choice of example (6.1.11). The outline of the paper is as follows. We first construct a solution of the Riemann problem in the case of equilibrium reactions. That is, we take '$k = \infty$' in equation (6.1.2) and replace it by

$$g(u; c) = w\,K. \tag{6.1.19}$$

In Section 3.1, we use the method of characteristics, to obtain an explicit representation of the solution, which still is dependent on the dissolution front $x = s(t)$. For this free boundary, which necessarily exhibits a waiting time, we derive an integral equation, which in Section 4 is transformed to a linear Volterra equation of the second kind. This settles the existence of a solution of the integral equation, which then can be used to define a solution of the Riemann problem. In Section 3.2, this procedure is extended to the treatment of $v_*, v^* > 0, u^* \leq u_S(c^*)$. In Section 5, an algorithm for the precise approximation of solutions is presented based on the above procedure.

The analysis of multi-component reactive systems with pure advective transport by means of the corresponding hyperbolic systems has a certain tradition in the chemical engineering literature. Although the situation considered usually allows for more species and reactions then considered here, most of these papers are restricted to the case of equilibrium reactions and a constant number of phases (see e.g. Walsh et. al. [14], Dria et. al. [3], Novak et. al. [9], Bryant et. al. [2], Novak et. al. [10], Helffrich & Klein [6], Schweich et. al. [11] and the literature cited there). If the non-equilibrium case is considered most authors (see e.g. Sevougian et. al. [12] and [13]) resort to numerical methods, allowing more complex and realistic situations. The main features of the simple situation studied semi-analytically in this paper are the assumption of non-equilibrium and the appearance of a dissolution front.

6.2 Equilibrium

When studying the transport process at equilibrium we replace the first order equation (6.1.2) by the equilibrium relation (6.1.19). Thus the equations to be analyzed are equation (6.1.15),

$$g(u; c) = wK, \qquad (6.2.20)$$

subject to (6.1.3), where c is given by (6.1.16). In this section we construct a solution of this system in the domain $-\infty < x < +\infty$ for $t > 0$, which satisfies at $t = 0$ the piecewise constant initial distribution (6.1.7). We recall that the constant states in (6.1.7) fulfill conditions (6.1.14). To emphasize the role of the dissolution front we impose condition (6.1.10) as well. This simple case is treated for further comparison and introduction of the techniques to be used. In fact the result of this section is well-known in the chemical engineering literature (at least formally) and a special case of e.g. Bryant et.al. [1].

For the construction, the following two observations are essential. The first one relates to equation (6.2.20) and says that if $v(x, t) > 0$ then $w(x, t) = 1$ and by (6.2.20)

$$g(u(x, t); c(x, t)) = K \qquad (6.2.21)$$

In addition, if $x > qt$ then $u(x, t) = u_S(c_*) = u_*$ and if $x < qt$ then $u(x, t) = u_S(c^*)$.

The second one is the Rankine-Hugoniot shock condition for solutions of (6.1.15). This condition which is based on a mass-conservation argument (see for instance Whitham [16] or LeVeque [8]), says that discontinuities or shocks in solutions of equation (6.1.15) propagate with

$$\text{speed} \quad = \frac{[u]}{[u + v]} \, q. \qquad (6.2.22)$$

Here the quantities between the brackets denote the size of the jump discontinuity in u and v across the location of the shock.
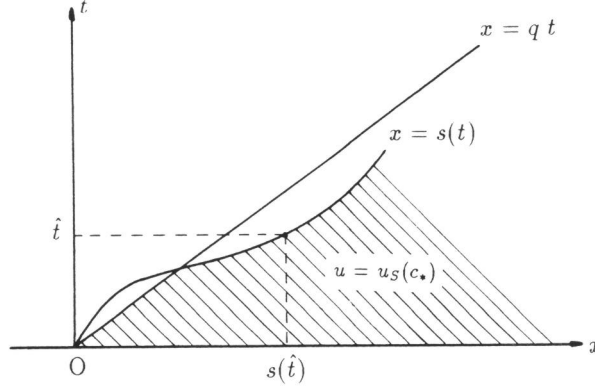
Fig 1. Dissolution front ahead of the fluid front.

Now suppose a dissolution front $x = s(t)$ exists such that

$$v(x,t) = \begin{cases} 0 & \text{for} \quad x < s(t) \\ > 0 & \text{for} \quad x > s(t). \end{cases} \tag{6.2.23}$$

On physical grounds one expects $s(t) \leq qt$ for all $t > 0$, because q denotes the averaged pore velocity of the fluid: i.e. ahead of the front $x = qt$ one expects to find the initial states $u = u_*$ and $v = v_*$.

The mathematical argument is the following. Suppose the dissolution front moves ahead of the fluid front, as in Figure 1. Since $w(x,t) = 1$ for $x > s(t)$ we find from (6.2.21) that $u = u_S(c_*)$ in the shaded region in Figure 1. Next select $\hat{t} > 0$ such that

$$s(\hat{t}) > q\hat{t} \quad \text{and} \quad \dot{s}(\hat{t}) > q, \tag{6.2.24}$$

where the dot denotes differentiation. In other words, we have selected a time $\hat{t}$ at which the speed of the dissolution front exceeds q. Then by the Rankine-Hugoniot condition (6.2.22),

$$u(s(\hat{t})^-, \hat{t}) > u_* = u_S(c_*), \tag{6.2.25}$$

as v jumps downwards from right to left or does not jump. Here $u(y^-, t) = \lim_{x \uparrow y} u(x,t)$ denotes the limit in y from the left and $u(y^+, t) = \lim_{x \downarrow y} u(x,t)$ the limit from the right. But $c(s(\hat{t}), \hat{t}) = c_*$, and thus by (6.2.20) and (6.1.3)

$$u(s(\hat{t})^-, \hat{t}) \leq u_S(c_*), \tag{6.2.26}$$

a contradiction. In other words, assumption (6.2.24) implies over-saturation for u. But this is not allowed under equilibrium conditions. We further note that if v is discontinuous at the dissolution front, i.e. $v(s(t)^+, t) > 0$ then $\dot{s}(t) = q$ cannot occur. This is a direct consequence of (6.2.22). This observation implies that $s(\hat{t}) = q\hat{t}$ and $\dot{s}(\hat{t}) = q$ for some $\hat{t} > 0$ can also not occur as $v(s(\hat{t})^+, \hat{t}) = v_* > 0$. Hence

$$s(t) < qt \quad \text{for all} \quad t > 0. \tag{6.2.27}$$

The ordering of the fronts and (6.2.20),(6.2.21) imply

$$u(x,t) = \begin{cases} \leq u_S(c^*) & -\infty < x < s(t) \\ u_S(c^*) & s(t) < x < qt \\ u_S(c_*) & qt < x < +\infty \end{cases} \tag{6.2.28}$$

Consequently by (6.2.22)

$$0 \leq \dot{s}(t) \leq q \ \text{ for all } \ t > 0 \tag{6.2.29}$$

and $\dot{s}(\hat{t}) < q$ occurs at points $\hat{t}$ where v is discontinuous. In particular this shows that all dissolution fronts are monotone in time. Since v vanishes in the region $x < s(t)$, we have there

$$\frac{\partial u}{\partial t} + q \frac{\partial u}{\partial x} = 0. \tag{6.2.30}$$

The initial condition on u for $x < 0$, the upperbound in (6.2.29) and equation (6.2.30) imply that $u = u^*$ for $x < s(t)$. To determine v in the region $x > s(t)$ we use (6.2.28) and equation (6.1.15). Combined they imply that $\partial v(x,t)/\partial t = 0$ for $x > s(t)$, $x \neq qt$. Then using the initial condition on v for $x > 0$ and the lower bound on $\dot{s}$, we find after integration $v = v_*$ for $x > s(t)$. Thus we have constructed a piecewise constant solution of (6.1.15), (6.2.20) and (6.1.3) which satisfies the initial distribution (6.1.7). The dissolution front follows from the Rankine-Hugoniot condition (6.2.22): $s(t) = at$, with

$$a = \frac{u_S(c^*) - u^*}{u_S(c^*) - u^* + v_*} \ q \ \ (< q) \tag{6.2.31}$$

Across the other shock, $x = qt$, v is constant. This is consistent with (6.2.22). In the chemical engineering literature this front is called the salinity front, see e.g. Bryant et. al. [1]). In Figure 2 we show the level set of the solution $\{u, v, w, c\}$ at equilibrium. The separating curves are shock curves at $x = at$ and $x = qt$. Figure 3 shows a sketch of the profiles of the variables for some $t > 0$. A qualitative comparison with the computations of Willis and Rubin [15] will be given in Section 5.

One may raise the question if the solution as constructed in this section is the unique solution of the initial value problem. For the following reasons we believe that it is. In the construction, inequalities (6.2.29) are crucial. They imply directly that the concentrations u and v are constant to the left and the right of a dissolution front, leading to the constant speed (6.2.31). In (6.2.29) the inequalities are a consequence of the Rankine-Hugoniot condition and the fact that over-saturation is ruled out by requiring $w \leq 1$ in (6.1.3). In other words, (6.2.29) are local properties of any dissolution front. As outlined above they lead to a piecewise constant solution as presented in this section.

6.3   Non-equilibrium

When precipitation-dissolution reactions cannot assumed to be at equilibrium, one needs to incorporate the first-order reaction equation (6.1.2) in the description. This leads to a much more involved analysis. In this section we construct solutions of the Riemann problem (6.1.15), (6.1.2)-(6.1.4) and (6.1.7) for two distinct cases. In Section 3.1 we assume (6.1.10) to be satisfied, implying that crystalline solid is present only in part of the flow domain, and in Section 3.2 we assume $v^*, v_* > 0$. In this first case a dissolution front exists for all $t \geq 0$. In the second case it may appear in finite time.
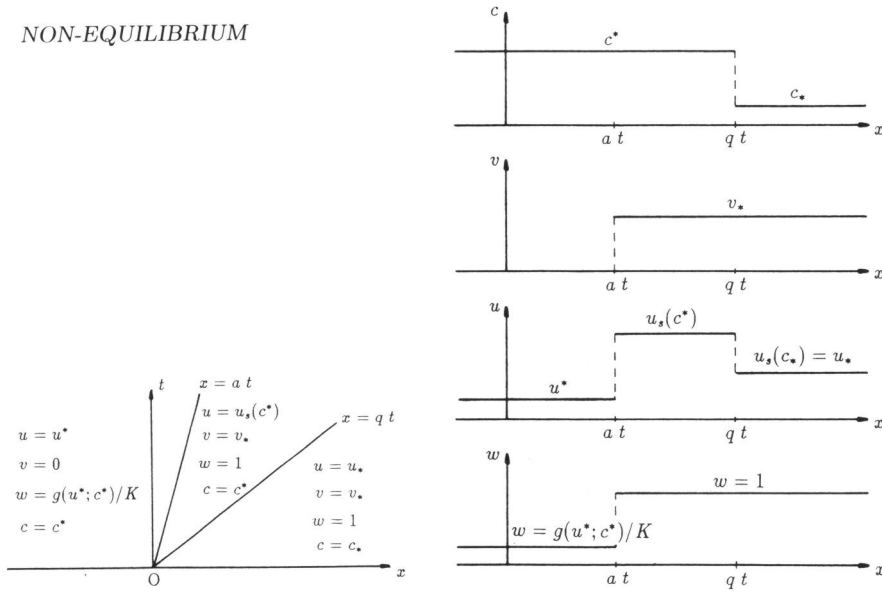
c

c^*

c_*

$a\,t$ $q\,t$ x

v

v_*

$a\,t$ $q\,t$ x

u

$u_s(c^*)$

$u_s(c_*) = u_*$

u^*

$a\,t$ $q\,t$ x

w

$w = 1$

$w = g(u^*;c^*)/K$

$a\,t$ $q\,t$ x

t $x = a\,t$

$u = u_s(c^*)$

$u = u^*$ $v = v_*$ $x = q\,t$

$v = 0$ $w = 1$ $u = u_*$

$w = g(u^*;c^*)/K$ $c = c^*$ $v = v_*$

$c = c^*$ $w = 1$

$c = c_*$

O x

Fig 2. Level sets of concentrations at equilibrium. Fig 3. Sketch of profiles at some $t > 0$.

6.3.1 Crystalline solid partly present

Inspired by the equilibrium results, i.e. '$k = \infty$', we start with the assumption that a dissolution front exists, as in (6.2.23), which satisfies inequalities (6.2.29). These inequalities are crucial for the construction of a solution. Unfortunately there are no obvious physical or mathematical arguments to support these assumptions. In contrast, the weaker statement $s(t) \leq qt$ for all $t \geq 0$, which is obviously physical, can be justified similarly as in Section 2. We return to the possibility of existence of solutions not fulfilling these assumptions when discussing the uniqueness at the end of Section 4. The main goal is to derive an equation for the location $x = s(t)$ of the dissolution front.

As in Section 2 we conclude, because of $\frac{\partial v}{\partial t} = 0$ for $x < s(t)$, that $u = \text{const} = u^*$ for $x < s(t)$ and that $w = g(u^*, c^*)/K$ there. Similarly for $x > qt$ we have $u = \text{const} = u_* = u_S(c_*)$ and thus $v = \text{const} = v_*$. With reference to Figure 4, we are going to consider the following problem:

Find a u, v and s such that

$$\frac{\partial u}{\partial t} + q\frac{\partial u}{\partial x} = k\{K - g(u;c^*)\}, \tag{6.3.32}$$

$$\frac{\partial v}{\partial t} = k\{g(u;c^*) - K\}, \tag{6.3.33}$$

for $s(t) < x < qt$ and for $t > 0$, subject to

$$u(s(t),t) = u^*, \; v(s(t),t) = 0 \tag{6.3.34}$$

and

$$v(qt,t) = v_* \tag{6.3.35}$$

Note that in the composite solution the crystalline concentration v is continuous across $x = qt$, due to (6.2.22) and then (6.3.35) holds, while the fluid concentration u possibly has a discontinuity there. Equation (6.3.33) implies continuity of v across the dissolution front $x = s(t)$, which in turn, due to (6.2.22), implies continuity of u across $x = s(t)$.
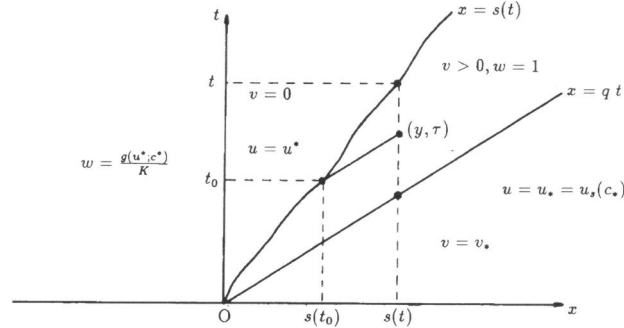

Fig 4. Dissolution front in the (x, t)-plane.

We solve equations (6.3.32), (6.3.33) by the method of characteristics. Choose any point (y, τ) in the domain $\{(x, t) : s(t) < x < qt, t > 0\}$, see also Figure 4. The characteristics of (6.3.32) are straight lines in the (x, t)-plane, having slope q with respect to the t-axis. The characteristic passing through the point (y, τ), i.e. the curve $x = y + q(t - \tau)$, intersects the dissolution front in the point $(s(t_0), t_0)$, which satisfies

$$s(t_0) = y + q(t_0 - \tau). \tag{6.3.36}$$

Due to $\dot{s}(t) \leq q$ this point is unique and thus is the same for all starting points (y, τ) satisfying (6.3.36). For a given dissolution front $s(t)$, this would determine t_0 as a function of y and τ, i.e. $t_0 = t_0(y, \tau)$. Integrating (6.3.32) along the characteristic and using (6.3.36) yields

$$\int_{u^*}^{u(y, \tau)} \frac{1}{k\{K - g(z; c^*)\}} \, dz = \tau - t_0(y, \tau) = \frac{y - s(t_0(y, \tau))}{q} \tag{6.3.37}$$

The idea is now to use equation (6.3.33) and the boundary conditions on v to determine the location of the dissolution front, i.e. to find the function $s(t)$. Before we proceed we first introduce for the case $u^* < u_S(c^*)$ the function $f : [0, +\infty) \to [u^*, u_S(c^*))$ defined implicitly by the integral

$$\int_{u^*}^{f(\delta)} \frac{1}{k\{K - g(z; c^*)\}} \, dz = \frac{\delta}{q} \quad \text{for all } \delta \geq 0, \tag{6.3.38}$$

and the function $F : [0, +\infty) \to (0, +\infty)$, defined by

$$F(\delta) = k\{K - g(f(\delta); c^*)\} \quad \text{for all } \delta \geq 0. \tag{6.3.39}$$

Here δ denotes a distance $y - s(t_0(y, \tau))$, measured along the characteristic from the dissolution front $x = s(t_0)$ to a point (y, τ), while $f(\delta) = u(y, \tau)$ denotes the fluid concentration at that point. The fluid concentration f and reaction rate F at any point of a characteristic depend only on this distance δ, which is due to the fact that convection is the only transport mechanism in this single reaction problem. Note that due to the differentiability of $g(\cdot; c^*)$ at $u = u_S(c^*)$

$$\int_{u^*}^{u} \frac{1}{k\{K - g(z; c^*)\}} \, dz \to \infty \quad \text{for} \quad u \to u_S(c^*) \tag{6.3.40}$$

and thus f and F are well defined.

Examples. Let the rate function g be given by the law of mass action (6.1.11). We can explicitly compute the cases:

n=1,m=0 (The linear case, see also Part I, equation (40)).
Then $g(u; c) = u$ and $u_S(c) = K$, independent of c. We find

$$f(\delta) = K - (K - u^*)e^{-\frac{k}{q}\delta} \tag{6.3.41}$$

and

$$F(\delta) = k(K - u^*)e^{-\frac{k}{q}\delta} \tag{6.3.42}$$

n=1,m=1. (See Figure 5).
Then $g(u; c) = u(u - c)$ and $u_S(c) = \frac{c}{2} + \frac{1}{2}\sqrt{c^2 + 4K}$. We find that f satisfies

$$\frac{f(\delta) - u_0}{u_S - f(\delta)} = \frac{u^* - u_0}{u_S - u^*}e^{\alpha\delta} \tag{6.3.43}$$

where $u_S = u_S(c), u_0 = u_0(c) = \frac{c}{2} - \frac{1}{2}\sqrt{c^2 + 4K}$ and $\alpha = \frac{k}{q}(u_S - u_0)$. Consequently

$$F(\delta) = k(u_S - u_0)^2 \frac{u^* - u_0}{u_S - u^*} \frac{e^{-\alpha\delta}}{\{e^{-\alpha\delta} + \frac{u^* - u_0}{u_S - u^*}\}^2} \tag{6.3.44}$$

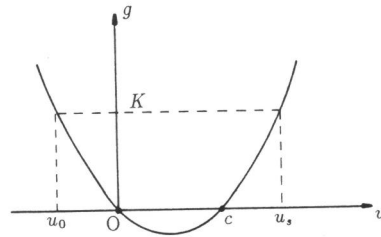When $u^* = u_S(c^*)$, which we consider as a degenerate case, we extend the definitions (6.3.38)

Fig 5. Rate function g for $n = m = 1$. Note that $u^* \geq c$.

and (6.3.39) by setting

$$f(\delta) = u_S(c^*) \quad \text{and} \quad F(\delta) = 0 \quad \text{for all} \quad \delta \geq 0. \tag{6.3.45}$$

Unless stated otherwise we avoid this degeneracy by taking $u^* < u_S(c^*)$. This implies $F(\delta) > 0$ and $F'(\delta) < 0$ for all $\delta \geq 0$.

Next we continue the analysis of (6.3.32), (6.3.33), by rewriting equation (6.3.37). Take any $t > 0$ and let $y = s(t)$. Using definitions (6.3.38),(6.3.39) we now write

$$k\{K - g(u(s(t), \tau); c^*)\} = F(s(t) - s(t_0)), \tag{6.3.46}$$

for any $s(t)/q < \tau < t$. Here we have used $\dot{s}(t) \geq 0$. In this expression, $t_0 = t_0(s(t), \tau)$ satisfies $t_0 = t$ when $\tau = t$. Substituting (6.3.46) into equation (6.3.33), integrating the result in time and applying the v-boundary condition in (6.3.34) and (6.3.35), yields

$$\int_{\frac{s(t)}{q}}^{t} F(s(t) - s(t_0)) \, d\tau = v_*. \tag{6.3.47}$$

Note that in deriving this equation we in particular assumed s to be monotone, but not to be strictly monotone. In the derivation of (6.3.47) we can allow for constant parts of s, i.e. for times $0 \leq t_1 < t_2$ such that $s(t) = s(t_1)$ for all $t_1 \leq t \leq t_2$. In such a case the definition of $t_0 = t_0(s(t), \tau)$ gives for t such that $t_1 \leq t \leq t_2$:

$$t_0(s(t), \tau) = \tau \quad \text{for} \ \ \tau \in [t_1, t] \tag{6.3.48}$$

and the whole derivation of equation (6.3.47) holds true with the following exception: If $s(t) = 0$ for $0 \leq t \leq t_2$, then the integration leading to (6.3.47) cannot be performed for $t \in [0, t_2]$ as $v(0,0)$ is not defined. But on the other hand a dissolution front as sketched in Figure 4, i.e. $s(0) = 0$ and $s(t) > 0$ for $t > 0$, would lead to a contradiction in (6.3.47). Letting $t \downarrow 0$ would make the left hand side zero while $v_* > 0$ as given. Therefore we have a <u>waiting time</u> $t_* > 0$, see Figure 6, such that

$$s(t) = \begin{cases} 0 & \text{for} \ \ 0 \leq t \leq t_*, \\ > 0 & \text{for} \ \ \ \ \ \ \ t > t_*. \end{cases} \tag{6.3.49}$$

From equation (6.3.47) for $t \downarrow t_*$ we conclude
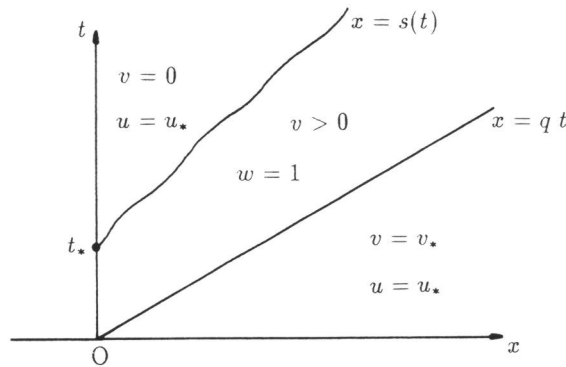

Fig 6. Waiting time in dissolution front.

$$t_* F(0) = v_*. \tag{6.3.50}$$

Using (6.3.38) and (6.3.39) we find for the waiting time the expression

$$t_* = \frac{v_*}{k\{K - g(u^*, c^*)\}}. \tag{6.3.51}$$

Note that in the degenerate case $u^* = u_S(c^*)$ expression (6.3.51) implies $t_* = \infty$. In other words, when u^* equals the solubility concentration then the dissolution front remains stagnant. Furthermore, apart from the initial waiting time, no further constant parts of s can occur: if this would be the case, say on the interval $[t_1, t_2]$, then we can conclude from (6.3.47)

$$
\begin{aligned}
v_* &= \int_{s(t_2)/q}^{t_2} F(s(t_2) - s(t_0)) \, d\tau \\
&= \int_{t_1}^{t_2} F(s(t_1) - s(t_0)) \, d\tau + \int_{s(t_1)/q}^{t_1} F(s(t_1) - s(t_0)) \, d\tau \\
&= \int_{t_1}^{t_2} F(0) \, d\tau + v_*,
\end{aligned}
\tag{6.3.52}
$$

which is a contradiction. We want to rewrite the integral in (6.3.47) in terms of t_0 and we do this by using (6.3.36). From that equality, with $y = s(t)$, we obtain due to $\dot{s}(t) \le q$ a unique correspondence of the points τ with the points t_0, where

$$
\tau : \frac{s(t)}{q} \to t \quad \text{implies} \quad t_0 : 0 \to t
\tag{6.3.53}
$$

and

$$
\frac{\partial \tau}{\partial t_0} = 1 - \frac{1}{q} \dot{s}(t_0).
\tag{6.3.54}
$$

Applying these observations to (6.3.47) yields

$$
\int_0^t F(s(t) - s(t_0)) \, dt_0 = v_* + \frac{1}{q} \int_0^t F(s(t) - s(t_0)) \dot{s}(t_0) \, dt_0
$$
$$
= v_* + \frac{1}{q} \int_0^{s(t)} F(z) \, dz,
\tag{6.3.55}
$$

where the left-hand side can be slightly rewritten by introducing the waiting time:

$$
\int_0^t F(s(t) - s(t_0)) \, dt_0 = t_* F(s(t)) + \int_{t_*}^t F(s(t) - s(t_0)) \, dt_0.
\tag{6.3.56}
$$

To summarize, we have obtained an integral equation from which the location of the dissolution front can be determined. The precise formulation is: Let t_* be given by (6.3.51). Then find the function $s(t)$, satisfying (6.3.49) and the dissolution front equation (DFE)

$$
(DFE) \begin{cases}
\int_{t_*}^t F(s(t) - s(t_0)) \, dt_0 = B(s(t)) & \text{for } t \ge t_* \text{ where} \\
B(s(t)) := t_* \{ F(0) - F(s(t)) \} + \frac{1}{q} \int_0^{s(t)} F(z) \, dz.
\end{cases}
\tag{6.3.57}
$$

The expression for B follows from (6.3.50), (6.3.55) and (6.3.56). In general we have to rely on numerical methods to solve (DFE). One such method will be discussed in Section 5. Only very special cases can be solved analytically, for instance the case $n = 1$ and $m = 0$ (the linear case) in the examples, where F is given by (6.3.42). For that form of F it is straight forward to solve (DFE) explicitly. The result is

$$
s(t) = \frac{q}{1 + kt_*} (t - t_*) \quad \text{for } t \ge t_*,
\tag{6.3.58}
$$

where

$$t_* = \frac{v_*}{k(K - u^*)}. \tag{6.3.59}$$

In Section 4 we show how to transform (DFE) into a standard integral equation, from which some characteristic properties of the front can be derived. Having found an expression or approximation for $s(t)$, one has to go back to equation (6.3.37) and definition (6.3.38) to determine u. The concentration of the crystalline solid is obtained from integrating (6.3.33).

6.3.2 Solid present everywhere

As in the previous case, the concentrations ahead of the fluid front are not affected by the displacing fluid and therefore equal to the initial concentrations. Since v is continuous across $x = qt$, the essential parameters which determine the behavior of the concentrations are u^*, v^*, c^* (rather $u_S(c^*)$) and v_*, see Figure 7. For definiteness we assume here that $v^* < v_*$. As long
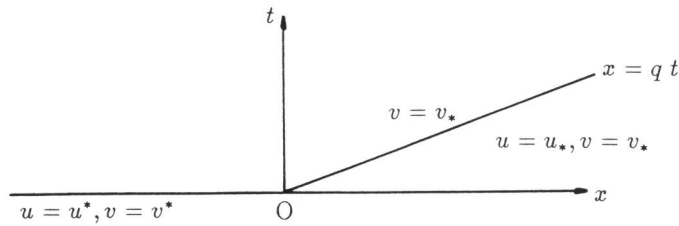

Fig 7. Initial conditions for the domain $x < qt, t > 0$.

as $v > 0$, implying $w = 1$, no dissoltion front will emerge and we need to solve equations (6.3.32),(6.3.33) subject to the conditions shown in Figure 7. From the physical point of view the initial conditions for $x < 0$ are somewhat unrealistic because u^* and v^* are not in equilibrium. This implies that in a laboratory experiment the resident fluid in the region $x < 0$ at $t = 0$ has to be instantaneously replaced by fluid with concentration u^*. The latter is, by approximation, only feasible for (very) small reaction rates.

Integrating the u-equation along the characteristic $x - qt = $ constant and the v-equation in t, we find that

$$u(x,t) = f(qt) \text{ for } x < 0 \text{ or } 0 < x < qt \text{ and } t > 0, \tag{6.3.60}$$

with f defined by (6.3.38) and

$$v(x,t) = \begin{cases} v^* + u^* - f(qt) & \text{for} & x < 0, \ t > 0 \\ v_* + f(x) - f(qt) & \text{for} & 0 < x < qt, \ t > 0 \end{cases} \tag{6.3.61}$$

The latter follows immediately from integration of

$$\frac{\partial v(x,t)}{\partial t} = -\frac{\partial u(x - qt, t)}{\partial t} \tag{6.3.62}$$

in time, see equation (6.1.15). Note that f is monotonically increasing from $f(0) = u^*$ towards $f(\infty) = u_S(c^*)$. The solid concentration for fixed $t > 0$ is sketched in Figure 8.

Obviously, expressions (6.3.60),(6.3.61) are only meaningful if $v > 0$. This leads us to consider the following cases.
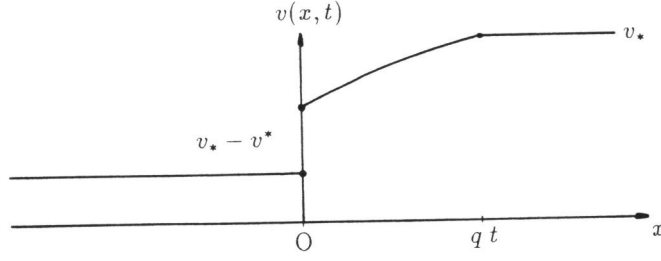
Fig 8. Crystalline solid distribution for fixed $t > 0$.

i) $u^* = u_S(c^*)$.
This choice implies $f = \text{constant} = u^*$, yielding the solution

$$u(x,t) = \begin{cases} u^* & x < qt \\ u_* & x > qt \end{cases} \qquad (6.3.63)$$

and

$$v(x,t) = \begin{cases} v^* & x < 0 \\ v_* & x > 0 \end{cases} \qquad (6.3.64)$$

ii) $u^* < u_S(c^*)$ and $v^* \geq u_S(c^*) - u^*$.
The second inequality being strict means that the concentration of crystalline solid is too high to be fully dissolved in the fluid. As a consequence (6.3.60) and (6.3.61) hold for all $t > 0$, where

$$v(x,t) > v(x,\infty) = \begin{cases} v^* + u^* - u_S(c^*) \geq 0, & x < 0 \\ v_* + f(x) - u_S(c^*) > 0, & 0 < x < qt. \end{cases} \qquad (6.3.65)$$

iii) $u^* < u_S(c^*)$ and $v^* < u_S(c^*) - u^*$.
Now the second inequality and (6.3.61) imply that there exists a finite time $T > 0$, defined by

$$f(qT) = v^* + u^*, \qquad (6.3.66)$$

such that $v(x,t) > 0$ for $0 \leq t < T$ and

$$v(x,T) = \begin{cases} 0, & x < 0 \\ v_* + f(x) - f(qT), & 0 < x < qT. \end{cases} \qquad (6.3.67)$$

The distribution of the concentrations in the (x,t)-plane is sketched in Figure 9. At the point $(0,T)$ a dissolution front emerges as explained in Section 3.1, except that the constant v_* has to be replaced by the known function $v(q(t-T),t)$. Translating the point $(0,T)$ to the origin by setting $x = x, \tau = t - T$, and writing $s = s(\tau)$ (with $s(0) = 0$, $s(\tau) \geq 0$, for $\tau > 0$) we find the waiting time τ_*

$$\tau_* \tilde{F}(0) = v_* - v^*, \qquad (6.3.68)$$
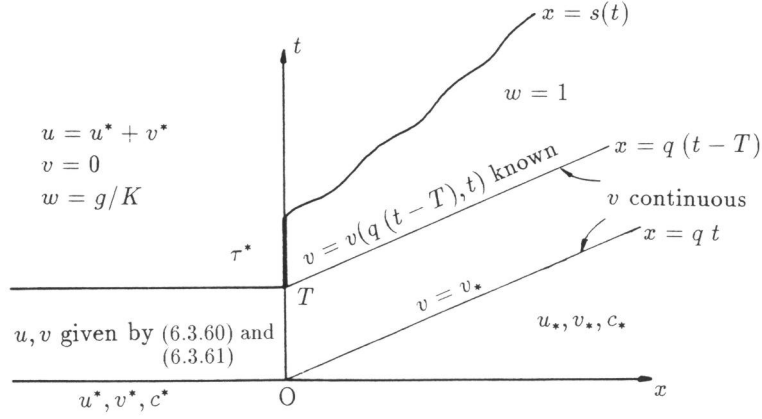
Fig 9. Concentrations in the (x, t)-plane.

and the modified dissolution front equation (MDFE)

$$(MDFE) \begin{cases} \int_{\tau_*}^{\tau} \tilde{F}(s(\tau) - s(\tau_0)) \, d\tau_0 = \tilde{B}(s(\tau)) \text{ for } \tau \geq \tau_*, \text{ where} \\ \tilde{B}(s(\tau)) = V(s(\tau)) + \tau_* \{\tilde{F}(0) - \tilde{F}(s(\tau))\} + \frac{1}{q} \int_0^{s(\tau)} \tilde{F}(z) \, dz. \end{cases} \tag{6.3.69}$$

In the expressions, the function $\tilde{F}$ differs from the function F used in (DFE): obviously u^* has to be substituted by $f(qT) = u^* + v^*$ in the definition of a function $\tilde{f}$ in (6.3.38) and F is given by (6.3.39) by substituting f by $\tilde{f}$. Furthermore, the function V in $\tilde{B}$ is related to v along $x = q(t - T)$. It is found to be

$$V(s(\tau)) = v \left(s(\tau), T + \frac{s(\tau)}{q} \right) - (v_* - v^*) \tag{6.3.70}$$

or, using (6.3.61),

$$V(s(\tau)) = v^* + f(s(\tau)) - f(qT + s(\tau)). \tag{6.3.71}$$

Note that here the original function f according to definition (6.3.38) appears in (6.3.71). Clearly $V(0) = 0$. Having determined $s(\tau)$ from (6.3.68), (MDFE) and (6.3.71), one proceeds as before to find u and v in the region $s(\tau) < x < q\tau, \tau > 0$.

In principle a discontinuity of u is possible at $x = q(t - T)$. In fact u is continuous there, which can be seen as follows: Due to (6.3.60) we have $u(q(t - T)^+, t) = f(qt) = f(x + qT)$. On the other hand the definition of $\tilde{f}(x)$ leads to $u(q(t - T)^-, t) = \tilde{f}$. We have setting $h(z) = 1/(k\{K - g(z; c^*)\})$:

$$\int_{u^*}^{\tilde{f}(\delta)} h(z) \, dz = \frac{\delta}{q} + \int_{u^*}^{u^* + v^*} h(z) \, dz = \frac{1}{q}(\delta + f^{-1}(u^* + v^*)) \tag{6.3.72}$$

as $u^* + v^* < u_S(c^*)$ and thus is in the range of f. Therefore

$$\tilde{f}(\delta) = f(\delta + f^{-1}(u^* + v^*)) = f(\delta + qT) \text{ due to (6.3.66),} \tag{6.3.73}$$

in particular we have

$$u(q(t-T)^+, t) = u(q(t-T)^-, t). \tag{6.3.74}$$

The qualitative analysis concerning dissolution fronts, as given in Section 4, is restricted to (DFE) only. This choice implies no loss of generality. All results/properties carry over to the solution of (MDFE). However, when discussing the numerical results, we do present an example in which a concentration distribution as shown in Figure 9 will arise.

6.4 Dissolution Front Equation

Before discussing the qualitative behavior of the dissolution front, i.e. the solution of integral equation (DFE), we recall here that this equation was derived by assuming the structural conditions (6.2.29). These conditions are consistent with the following results.

Property. Let $s : [t_*, \infty) \to [0, \infty)$ be differentiable and satisfy (DFE). Then

(i) $s(t_*) = 0$;

(ii) $\dot{s}(t_*) = q/(1 - \frac{F'(0)}{F(0)} t_* q) \in (0, q)$;

(iii) $0 < \dot{s}(t) < q$ for all $t \geq t_*$;

(iv) $s(\infty) = \infty$.

Proof (i) By assumption $s(t) \geq 0$ for all $t \geq t_*$. Since $F'(\delta) < 0$ for all $\delta \geq 0$, with $F(0) = k\{K - g(u^*; c^*)\} > 0$ and $F(\infty) = 0$, we observe that the expression B in (DFE) has the property $B(0) = 0$, $B(x) > 0$ for $x > 0$. Evaluating (DFE) at $t = t_*$ yields $B(s(t_*)) = 0$, implying at once $s(t_*) = 0$.
(ii) Differentiating (DFE) with respect to t and rearranging terms yields

$$\dot{s}(t) = \frac{F(0)}{\frac{1}{q}F(s(t)) - t_* F'(s(t)) - \int_{t_*}^t F'(s(t) - s(t_0))\, dt_0} \tag{6.4.75}$$

for all $t \geq t_*$. Taking $t = t_*$ in this expression and using (i) gives the desired result.
(iii) Because the right hand side in (6.4.75) is strictly positive, the lower bound is immediate. The upperbound is more involved. To show it we argue by contradiction. Thus suppose there exists $\tilde{t} > t_*$ such that

$$\dot{s}(t) < q \text{ for all } t_* \leq t < \tilde{t} \text{ and } \dot{s}(\tilde{t}) = q. \tag{6.4.76}$$

Taking $t = \tilde{t}$ in (6.4.75) and estimating

$$-\int_{t_*}^{\tilde{t}} F'(s(\tilde{t}) - s(t_0))\, dt_0 = -\int_0^{s(\tilde{t})} \frac{F'(z)}{\dot{s}}\, dz > \frac{1}{q}\{F(0) - F(s(\tilde{t}))\} \tag{6.4.77}$$

results in

$$\dot{s}(\tilde{t}) < q\left\{1 - qt_*\frac{F'(s(\tilde{t}))}{F(0)}\right\}^{-1} < q. \tag{6.4.78}$$

This contradicts (6.4.76) and therefore $\dot{s}(t) < q$ for all $t \geq t_*$.

(iv) To prove this we construct a lower bound which becomes unbounded as $t \to \infty$. Let

$$C := \max_{z \geq 0}(-F'(z)). \tag{6.4.79}$$

Using this upper bound in (6.4.75) gives for $t \geq t_*$

$$\dot{s}(t) > \frac{F(0)}{\frac{1}{q}F(s(t)) + t_*C + (t - t_*)C} \geq \frac{qF(0)}{F(0) + qCt} \tag{6.4.80}$$

and after integration

$$s(t) \geq \frac{F(0)}{C} \ln \left\{ \frac{1 + \frac{qC}{F(0)}t}{1 + \frac{qC}{F(0)}t_*} \right\} \tag{6.4.81}$$

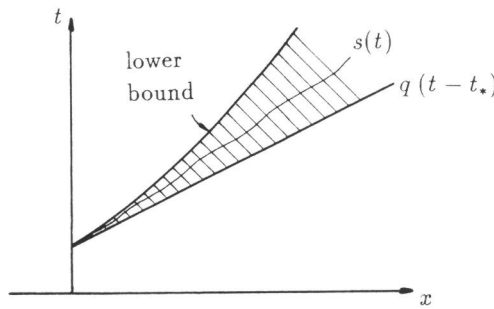This shows that $s(t)$ becomes unbounded as $t \to \infty$, see also Figure 10.

Fig 10. Estimate of location of dissolution front.

Having determined these a priori properties of the dissolution front, we now turn to the question of existence. To make use of well-known results, we transform the equation to a standard linear integral equation of the second kind for a new unknown function. Due to monotonicity Property (iii), by a change of variable (see the line below (6.4.88)) , we can rewrite (DFE) as a linear integral equation of the first kind for the derivative of the inverse of s, denoted by ϕ. By differentiation with respect to t, this equation transforms to

$$B'(x) = F(0)\phi(x) + \int_0^x F'(x - y)\phi(y)\, dy \ \text{ for } \ x \geq 0, \tag{6.4.82}$$

where the primes denote differentiation and where B and F are as in (DFE). In particular

$$B'(x) = \frac{1}{q}F(x) - t_*F'(x). \tag{6.4.83}$$

Equation (6.4.82) has been studied in the mathematics literature and it is known that if $F \in H^1_{\text{loc}}([0, \infty))$ (i.e. F and F' are locally square integrable on $[0, \infty)$) then (6.4.82) has a unique global solution ϕ on $[0, \infty)$, see Zabreyko and Mayorova [17]. Furthermore, if F is continuously

differentiable (in fact F belongs to C^∞ in many relevant examples) then ϕ is continuous (or also C^∞) in $[0, \infty)$. As in the proof of (iii), one easily finds

$$\phi(x) > \frac{1}{q} \quad \text{for all} \ x \geq 0. \tag{6.4.84}$$

Having established the existence of a smooth function ϕ satisfying (6.4.82) and (6.4.84), we are now in the position to define the function $s : [0, \infty) \to [0, \infty)$ such that $s(t) = 0$ for $0 \leq t \leq t_*$ and

$$t - t_* = \int_0^{s(t)} \phi(x) \, dx \quad \text{for all} \ t > t_*. \tag{6.4.85}$$

The smoothness of ϕ carries over to s in $[t_*, \infty)$: for instance, if ϕ is continuous in $[0, \infty)$ and satisfies (6.4.84), then s is continuously differentiable satisfying (iii). Thus s is strictly increasing for $t \geq t_*$ and also $s(\infty) = \infty$ holds true due to the absence of singularities in ϕ. In this way, there is a one-to-one correspondence of the points $x \geq 0$ and $s(t)$ for $t \geq t_*$. To verify that the function s satisfies (DFE), we integrate (6.4.82) with respect to x from $x = 0$ to $x = s(t)$. This yields for $t \geq t_*$

$$B(s(t)) = F(0)(t - t_*) + \int_0^{s(t)} \left\{ \int_0^x F'(x - y)\phi(y) \, dy \right\} dx. \tag{6.4.86}$$

Writing

$$\int_0^x F'(x - y)\phi(y) \, dy = \frac{d}{dx} \int_0^x F(x - y)\phi(y) \, dy - F(0)\phi(x), \tag{6.4.87}$$

gives

$$B(s(t)) = \int_0^{s(t)} F(s(t) - y)\phi(y) \, dy = \int_{t_*}^t F(s(t) - s(t_0)) \, dt_0. \tag{6.4.88}$$

In the last equality we used the variable transformation $s^{-1}(y) \to t_0$, as due to (6.4.85) we have $d/dy(s^{-1}(y)) = \phi(y)$. This proves the existence of a continuously differentiable dissolution front for $t \geq t_*$ which satisfies (DFE).

We conclude this section with a remark about uniqueness. Any solution of the Riemann problem (6.1.15), (6.1.2)-(6.1.4) and (6.1.7), for which a dissolution front $x = s(t)$ according to (6.2.23) exists must be of the form discussed in Section 3 with s satisfying (DFE), provided that conditions (6.2.29) are satisfied. Now suppose two solutions are possible. They would satisfy Property (iii) and thus, using (6.4.85), one could define two solutions to the integral equation (6.4.82). But (6.4.82) has only one solution which yields a contradiction. The question arises if solutions are possible with dissolution fronts violating (6.2.29). If a solution is such that the violation occurs only after some time, i.e. there is a $t_1 > 0$ such that

$$0 \leq \dot{s}(t) \leq q \quad \text{for} \ 0 \leq t \leq t_1 \ \text{and} \ \dot{s}(t_1) = 0 \ \text{or} \ \dot{s}(t_1) = q, \tag{6.4.89}$$

then s satisfies the integral equation (6.3.47) in the interval $[0, t_1]$ and the waiting time t_* according to (6.3.51) exists. Assume that $t_1 > t_*$. Then the integral equation (DFE) is valid in $[t_*, t_1]$ and Property (iii) implies $0 < \dot{s}(t_1) < q$, i.e. a contradiction. Thus the only possible further solutions we cannot exclude at the moment have the very unlikely property that there are points $\hat{t}$ arbitrary close to $t = 0$ such that $\dot{s}(\hat{t}) < 0$ or $\dot{s}(\hat{t}) > q$.

One should bear in mind that not every uniqueness condition is an entropy condition, i.e. a condition which selects from all possible solutions a physical solution. One should also understand that the differential equation describing the dissolution process, has a smoothing effect on the solution. Discontinuities do not occur at the dissolution front, but only at the known front $x = qt$. Therefore interpreting (6.2.22) in terms of 'entropy' is misleading. Van Duijn & Knabner [4] analyzed in full detail the traveling waves when diffusion is present in the model: the so called viscosity solutions. As solutions are continuous across the dissolution front, no information concerning (6.2.22) is to be gained from that analysis.

6.5 Numerical method and results

In this section we construct numerical solutions of the Riemann problem (6.1.15), (6.1.2)-(6.1.4) and (6.1.7). The numerical solution procedure is based on the method of characteristics and follows the lines of Section 3 in detail. We shall give quantitative results for two distinct non-equilibrium cases:

    i) The crystalline solid is only present in the flow domain where $x > 0$, i.e. $v^* = 0, v_* > 0$

    ii) The crystalline solid is initially present everywhere in the flow domain, i.e. $v^*, v_* > 0$

The parameters used in the computations are adopted from Willis and Rubin [15] and listed in Table 1. The differences are the following: K is slightly larger, in Willis and Rubin [15] only the equilibrium case $k = \infty$ is considered. K is determined by c_{1*} and c_{2*} and thus has to be different from Willis and Rubin [15], as we do not consider Debye-Hückel corrections in our computations. But note that also these could be handled without problems as the rate function is of general form. The value of fluid concentration c_1^* used in our computations differs from the value given in the caption of Figure 3 in Willis and Rubin [15]. The value in the caption is $c_1^* = (Sr^{2+})_f = 2.0 \text{x} 10^{-5}$ mMol/cm^3 (which we used in Part I) while Figure 3 suggests that the correct value used by Willis and Rubin [15] equals $c_1^* = 2.0 \text{ x} 10^{-4}$ mMol/cm^3. We decided to use the latter value in this paper.

$$
\begin{aligned}
\Theta &= 0.32 \\
\rho &= 1.8 & [\text{g/cm}^3] \\
q^* &= 0.3\text{x}10^{-3} & [\text{cm/s}] \\
M_1 &= \text{Sr}^{2+} \\
M_2 &= \text{SO}_4^{2-} \\
n &= 1 \\
m &= 1 \\
c^* &= 2.0\text{x}10^{-4} & [\text{mMol/cm}^3] \\
c_* &= 0.0\text{x}10^{-4} & [\text{mMol/cm}^3] \\
k_p &= 1 \\
k_d &= K = 3.8688\text{x}10^{-7} \\
k &= 0.1 & [\text{1/s}] \\
c_{12*} &= 4.9\text{x}10^{-5} & [\text{mMol/g}] \\
c_{12}^* &= 0.0\text{x}10^{-5} & [\text{mMol/g}] \\
c_1^* &= 2.0\text{x}10^{-4} & [\text{mMol/cm}^3] \\
c_{1*} &= 6.22\text{x}10^{-4} & [\text{mMol/cm}^3]
\end{aligned}
\tag{6.5.90}
$$

Table 1. Parameters used in the computations.

6.5.1 Numerical method

The numerical procedure consists of the following steps: evaluation of integral (6.3.38) to obtain a numerical approximation of the function $f(\delta)$, substitution of $f(\delta)$ in (6.3.39) to obtain $F(\delta)$, numerically solving a Volterra integral equation which follows from (DFE) to find the location of the dissolution front $s(t)$ and finally we go back to (6.3.37) and (6.3.38) to determine u. The concentration of the crystalline solid is obtained by integration of (6.3.33).

The integrand of (6.3.38) becomes singular when u^* tends to the solubility concentration $u_S(c^*)$. This singularity has to be handled with care because we need numerical approximations

of $f(\delta)$ in a wide range of δ values. We used Clenshaw-Curtis quadrature in combination with symbolic transformation techniques to remove the singularity, as implemented in the computer algebra system Maple, see Geddes [5]. The result of the numerical integration is given as a table $[\delta_i, f(\delta_i)]$, where $\delta_i = i \cdot \Delta\delta$. Only in special cases, i.e. $n = 1, m = 0$ (the linear case) and $n = m = 1$, exact evaluation of integral (6.3.38) is possible. We used the exact expressions (6.3.41),(6.3.44) to verify the accuracy of the numerical integration of (6.3.38). The discrete result of (6.3.38) is used to evaluate (6.3.39), i.e. $F(\delta_i)$ on the δ-grid.

Equations (6.4.82),(6.4.83) can be written as a standard linear Volterra integral equation of the first kind, i.e.

$$\tau(\delta) = h(\delta) - \int_0^\delta K(\delta - y)\,\tau(y)\,dy \qquad (6.5.91)$$

where

$$h(\delta) = \frac{1}{q}\frac{F(\delta)}{F(0)} - t_*\frac{F'(\delta)}{F(0)} \qquad (6.5.92)$$

and kernel

$$K(\delta - y) = \frac{F'(\delta - y)}{F(0)}. \qquad (6.5.93)$$

We solve this equation explicitly, using the trapezoidal rule to discretize the integral in (6.5.91). The approximation of the derivatives are chosen central in δ, except in the first integration step where the derivatives are discretized forward in δ. The position of the dissolution front follows from the definition of τ, hence

$$t - t_* = \int_0^{s(t)} \tau(z)\,dz. \qquad (6.5.94)$$

Because τ is computed at the location of the grid points we have $s(t) = i\Delta\delta$ and the corresponding value of t is found by approximating the right hand side of (6.5.94) using Simpson's rule. To compute a profile of the fluid concentration u at a certain time level t_1 we choose a point P(y, t_1) in the (x, t)-plane (see Figure 11). We walk backwards along the characteristic through point P and compute the coordinates of the intersection point $(s(t_0), t_0)$ of the characteristic and the free boundary curve $s(t)$. The precise procedure is as follows: start in point P, follow the characteristic in the direction of the dissolution front $s(t)$, check in every grid point if the t-coordinate of the characteristic is above the corresponding t-coordinate of $s(t)$ in that point. If this is the case we use the last and before last step to compute the intersection point of the characteristic and $s(t)$, assuming that the approximation of $s(t)$ is piecewise linear between successive coordinates. This gives the desired value $\delta_{t_1} = y - s(t_0)$, corresponding to point P. Next we use the table of discrete $[\delta_i, f(\delta_i)]$-values to compute the fluid concentration $u(y, t_1) = f(\delta_{t_1})$ in P. Because δ_{t_1} (usually) does not coincide with one of the δ_i-values in the table, we have to interpolate once more. A fluid concentration profile is constructed by repeating this procedure in the region $s(t_1) \leq y \leq q\,(t_1 - t_*)$ at a sufficiently large number of points P.

To obtain a numerical approximation of the concentration v of the crystalline solid in point P(y, t_1) we first have to obtain values of the fluid concentration in discrete points along the vertical line through (y, t_2) and (y, t_1) using the procedure given above, see line B in Figure 11. By explicit integration in time of (6.3.33) from the position of the free boundary, i.e. t_2 to the position of P, i.e. t_1, we obtain $v(y, t_1)$. Full integration from the position of the free boundary
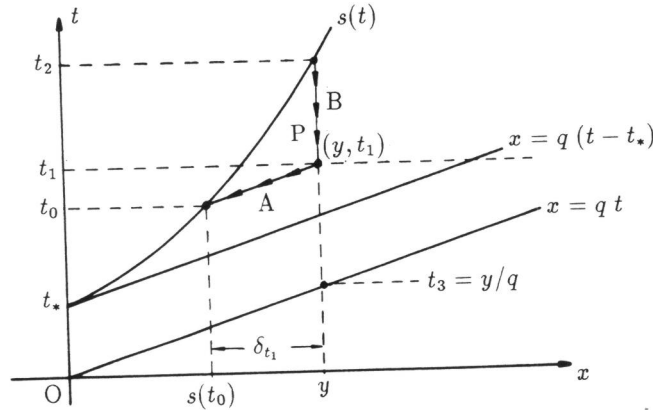
Fig 11. Construction of solutions in the (x, t)-plane.

$(s(t_2), t_2)$ to the position of the fluid front (y, t_3) has to reproduce the boundary condition v_* (up to a small error, due to the discrete numerical approximations), which follows from (6.3.47). This serves as a check for the accuracy of the numerical procedure. For the linear case $(n = 1, m = 0)$ we compared results obtained by the numerical procedure and the corresponding exact solutions and found excellent agreement.

6.5.2 Results

In this section we give computed results for the following cases:

1. The linear case $n = 1, m = 0$ for $v^* = 0$
2. A non-linear case $n = 1, m = 1$ for $v^* = 0$ and for $v^*, v_* > 0$
3. A non-linear case $n = 2, m = 2$ for $v^* = 0$.

Remark: In order to obtain comparable time, space and concentration scales for all cases considered in this section we introduce an artificial factor a that multiplies the function g and assume $K = 3.8688 \times 10^{-7}$ to be independent of the values of n and m. This implies that only the results of the computations for the case $n = m = 1$ have physical meaning. The values of a used in the computations are:

n	m	a
1	0	6.22×10^{-4}
1	1	1.0
2	2	$1.83 \times 10^{+6}$

The linear case: n=1, m=0.

Figure 12 shows the position of the crystal dissolution front in the (x, t)- plane for the linear case $(n = 1, m = 0)$. In this example we have $t_* = 10499s$. The dissolution front is a straight line which satisfies exactly expression (6.3.58). Due to the introduction of a we have to replace kt_* by akt_* in the denominator of (6.3.58). Figure 13 shows breakthrough curves of the fluid concentration at different observation points. An observation independent of this special case is: There are horizontal parts in these curves, which correspond to the fluid concentration in the region in the (x, t)-plane where $x_1/q \le t \le x_1/q + t_*$ at a given position $x = x_1$. In this region $\delta = x_1$ is constant and therefore u is constant, $u = f(x_1)$ increasing monotonically from
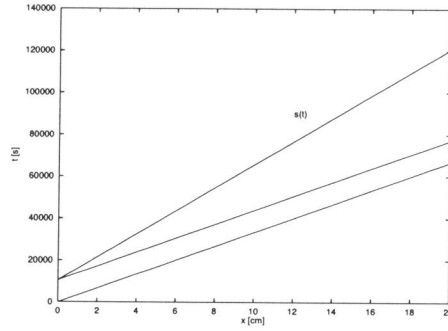
Fig 12. Dissolution front in the (x, t)-plane for the linear case.

u^* to $u_S(c^*)$ for x_1 ranging from 0 to ∞. The width of the flat region in all curves is constant and equal to the waiting time t_*. Figure 14 shows the time evolution of the crystalline solid concentration at different positions. The regions with constant slope in the v-curves correspond to the regions in the breakthrough curves for u where u is constant.

Figure 15 gives profiles of the fluid concentration at different time levels. We observe several points in the u-profiles where the derivative $u_x = \partial u / \partial x$ is discontinuous. The discontinuity in u_x at the toe of the profiles in Figure 15 travels with speed $\dot{s}(t)$. A simple computation shows that for the general case

$$\frac{\partial}{\partial x} u(s(t)^+, t) = k\{K - g(u^*; c^*)\} \frac{1}{q - s'(t^-)} \tag{6.5.95}$$

The second discontinuity (from the left) in u_x reflects the discontinuity of $\dot{s}(t)$ at $t = t_*$. Its
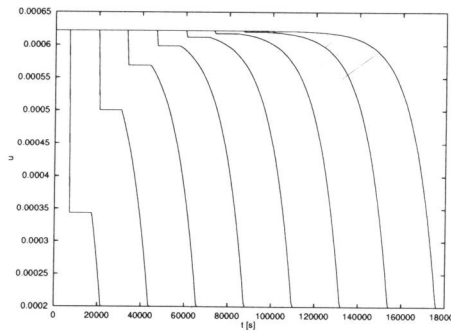
Fig 13. Breakthrough curves of the fluid concentration u at different positions for the linear case. From left to right the observation points are: $x = 2,6,10,14,18,22,26$ and 30 cm. (See Figure 12)

position is a point at the line $x = q(t - t_*)$ in the (x, t)-plane for a given time t. In fact, we have
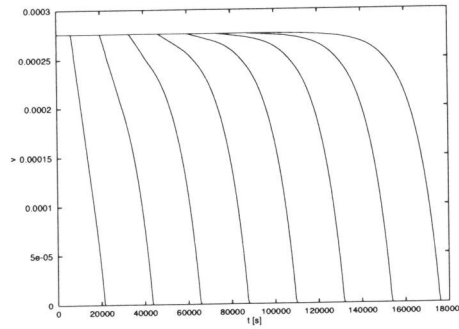
Fig 14. Time evolution of the crystalline solid concentration v at different positions for the linear case. From left to right the observation points are: $x = 2,6,10,14,18,22,26$ and 30 cm. (See Figure 12)

in general due to Property (ii) for such (x, t)

$$\frac{\partial}{\partial x} u(x^+, t) - \frac{\partial}{\partial x} u(x^-, t) = -f'(x) \frac{1}{kt_* \frac{\partial}{\partial u} g(u^*; c^*)} \tag{6.5.96}$$

At the fluid front, i.e. the top of the u-profile, we have a jump in u which is consistent with
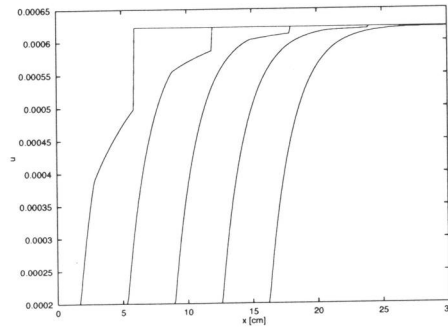
Fig 15. Fluid concentration profiles at different time levels for the linear case. From left to right the curves correspond to $t = 20000,40000,60000,80000,100000$ s. (See Figure 12)

the Rankine-Hugoniot shock condition (6.2.22), and given by

$$u(qt^+, t) - u(qt^-, t) = u_* - f(qt) \rightarrow u_* - u_S(c^*) < 0 \tag{6.5.97}$$

An exception is the linear case, as here $u_S(c^*) = u_S(c_*) = u_*$ and thus the discontinuity at $x = qt$ vanishes for $x_1 \to \infty$. Figure 16 shows the corresponding profiles of v. The derivative $v_x = \partial v / \partial x$ at the dissolution front is discontinuous, due to the discontinuity in u at the front. The constant speed is given according to (6.3.58) by

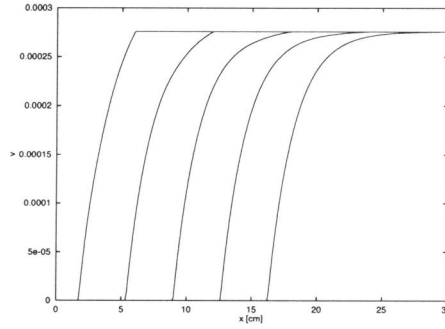$$\dot{s}(t) = \frac{q}{1 + kt_*} = \frac{u^* - u_*}{u^* - u_* + v^* - v_*} q \tag{6.5.98}$$

Fig 16. Crystalline solid concentration profiles at different time levels for the linear case. From left to right the curves correspond to $t = 20000,40000,60000,80000,100000$ s. (See Figure 12)

which corresponds to the speed of travelling waves, which exist for constant c (compare Part 1, in particular (54)). By inspection of the explicit solution given by (6.5.98), (6.3.59), (6.3.36), (6.3.41) for the Riemann problem and the explicit solution for the travelling wave problem (note that g is independent of c here, see e.g. the first example in Section 3.1) derived from Part 1, (94),(54) we see that for taking the shift $L = at_*$, where a is given by (6.5.98), the solutions coincide for $x < (t - t_*)q$. In particular there is pointwise convergence in x for $t \to \infty$ of the solution profile here to the travelling wave solution.

A non-linear case: n=1,m=1

For this case we shall distinguish between the two sets of initial and boundary conditions as discussed in Section 3.1 and Section 3.2.

Solid only partly present (See Section 3.1)

In this case the solubility concentration is given by $u_S(c) = \frac{c}{2} + \frac{1}{2}\sqrt{c^2 + 4K}$, i.e. $u_S(c^*) > u_S(c_*) = u_*$. We have chosen $c^* = u^* = 2.0 \times 10^{-4}$. Because $c_* = 0$ we now have $K = u_*(u_* - c_*) = u_*^2$, see Table 1. For the waiting time t_* we find 7108.0 s. The dissolution front $s(t)$ is now a curve with slope $\dot{s} < q$ for all $t \geq 0$. Figure 17 shows the position of the dissolution
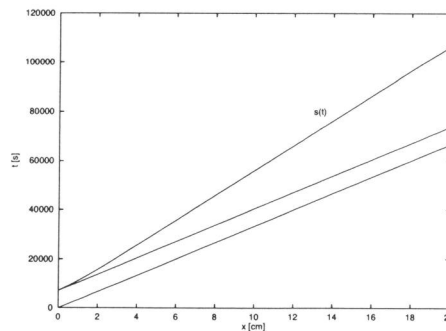

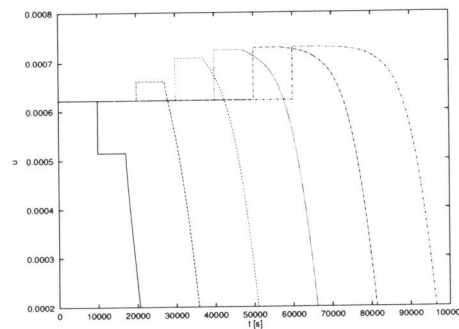Fig 17. Dissolution front in the (x, t)-plane for the non-linear case $n = m = 1$.

Fig 18. Breakthrough curves of the fluid concentration at different positions for the non-linear case $n = m = 1$. The observation points are $x = 3.0, 6.0, .., 18.0$ cm. (See Figure 17)

front in the (t, x)-plane. The curve suggests that $\dot{s}(t_*) = q$ which is not true. In fact the $\dot{s}(t_*)$ satisfies Property (ii) in Section 4 where in this example it turns out that $F'(0)/F(0)t_* q << 1$. Figure 18 shows breakthrough curves of u for different observation points. The qualitative differences as compared to the linear case are the following: i) The toe of the u-profile does not travel with constant speed but with speed $\dot{s}(t)$. ii) After a certain time the maximum concentration in the profiles exceeds u_* and increases in time to the solubility concentration $u_S(c^*)$. iii) The fluid concentration at the fluid front remains discontinuous and jumps either from below or from above to u_*. Figure 19 gives the corresponding curves for v. The properties of the time evolution of the crystalline solid concentration compare to the those in the linear case, see Figures 14 and 19. Figure 20 shows the fluid concentration profiles at different time levels for the non-linear case. The corresponding crystalline solid concentrations are given in Figure 21.

A quantitative comparison between the solutions of the Riemann problem for the non-linear case and the solutions found by Willis and Rubin [15] is not possible because they allow for diffusion in their problem and consider only equilibrium reaction. Comparing Figure 3, Figure 20 and the
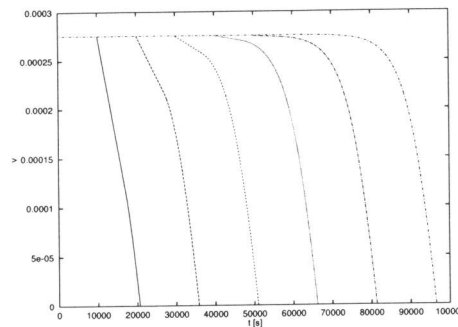

Fig 19. Time evolution of the crystalline solid concentration at different positions for the non-linear case $n = m = 1$. The observation points are $x = 3.0, 6.0, .., 18.0$ cm. (See Figure 17)
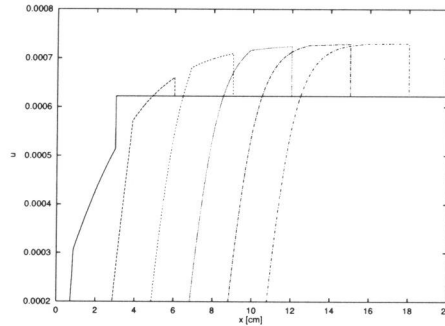
Fig 20. Fluid concentration profiles at different time levels for the non-linear case $n = m = 1$.
From left to right the curves correspond to $t = 10000.0, 20000.0, .., 60000.0$ s. (See Figure 17)

corresponding general statements mentioned and Figure 3 of Willis and Rubin [15] indicates:
The common qualitative property caused by the interplay of transport and dissolution is a
"plateau-structure", which for a fixed time t is defined by the spatial intervals $I_1 = \{x | x < s(t)\}$,
$I_2 = \{x | s(t) < x < qt\}, I_3 = \{x | x > q)\}$. In I_3 the solution is given by the "initial condition"
$u_* = u_S(c_*)$, in I_1 by the "boundary condition" $u^* = u_S(c^*)$ and in I_2 at least asymptotically,
i.e. for large t, by $u_S(c^*)$. The piece-wise constant structure of Figure 3 without dispersion
and kinetics is smeared out by the addition mechanisms in different ways. Kinetics leads to
a smoothing effect in I_2 such that the transition at $x = s(t)$ becomes continuous and the
maximum is attained at $x = qt$. Diffusion smooths more, effecting also I_1 and I_3 and leading
to overall smooth and nonconstant profiles, where the maximum in I_2 is attained at $x = s(t)$.
The solutions for other values of n and m have properties that compare to the solutions of the
non-linear example discussed in this section.

Crystalline solid present everywhere. (See Section 3.2)
Two characteristic times arise in this case: $T = 2680$ s, which is the time needed to dissolve all
initially present crystalline solid ($v^* = 1.0 \ 10^{-4}$) in the region $x < 0$ and $\tau_* = 4903$ s, which is
the waiting time for the dissolution front. For $t \geq T$ we have $u = u^* + v^* = 3.0 \times 10^{-4}$ in the
region $x < 0$. Figure 22 shows the position of the dissolution front in the (x, t)-plane. Figure
23 gives breakthrough curves of u and the time evolution of v at different positions in one graph.
The upper set of curves is u and the lower is v. The horizontal parts in the u-curves have
width τ_* and give rise to linear parts in the v-curves, while the increasing parts, which vanish
as time proceeds, have width T. The crystalline solid concentration along the line $x = q(t - T)$
in the (x, t)-plane is known and given by (6.3.61). We used this to check the accuracy of the
computations.

A non-linear case: n=2, m=2
For any combination of $n, m \geq 1$ the function $g(u; c^*)$ is monotonically increasing and convex in
the interval $c/m \leq u \leq u_S(c^*)$ and therefore we may expect similar qualitative behavior of the
solutions. The position of the dissolution front in the (x, t)-plane is shown in Figure 24. Now
the solubility concentration is given by $u_S(c) = c/4 + \sqrt{c^2 + 16\sqrt{K/a}}/4$. The factor a is chosen
such that $u_S(c) = 7.299 \times 10^{-4}$, as in the case $n = m = 1$. The breakthrough curves of u are
given in Figure 25 and the corresponding time evolution of v in Figure 26.
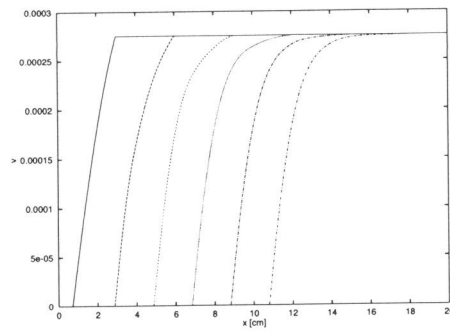
Fig 21. Crystalline solid concentration profiles at different time levels for the non-linear case $n = m = 1$. From left to right the curves correspond to $t = 10000.0, 20000.0, .., 60000.0$ s. (See Figure 17)
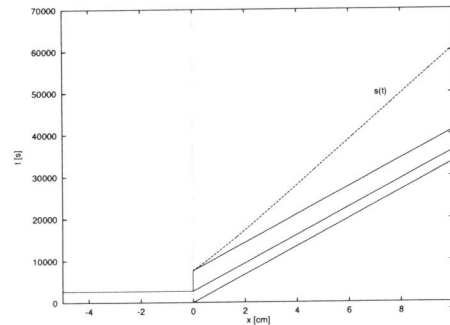

Fig 22. Dissolution front in the (x, t)-plane for the case $n = m = 1$, $v^*, v_* > 0$. (Compare with Figure 9).

6.6 Conclusions

We considered a model for transport and dissolution/precipitation, where the kinetics of the reaction is taken into account, but diffusion/dispersion is ignored. The appearance and evolution of a dissolution front from corresponding initial states, i.e. the Riemann problem of the hyperbolic system, is investigated. The initial states for the "charge distribution" c are "incompatible" in general, i.e. the "ionic composition" of the fluid changes. The method of characteristics leads to a nearly explicit representation of the solution, where only an implicitly defined function f (6.3.38) has to be evaluated numerically and based on f an integral equation (6.3.57) has to be solved numerically (or rather the transformed equation (6.4.82),(6.4.83)). The basic "plateau-structure" of the solution is revealed being characterized by the dissolution front $x = s(t)$ with speed less than q, where (for non-equilibrium) $\partial u/\partial x$ and $\partial v/\partial x$ are discontinuous and the fluid or salinity front $x = qt$, where u and $\partial v/\partial x$ are discontinuous. A comparison of solutions elucidates the role of kinetics and of diffusion/dispersion, which turns out to be similar,
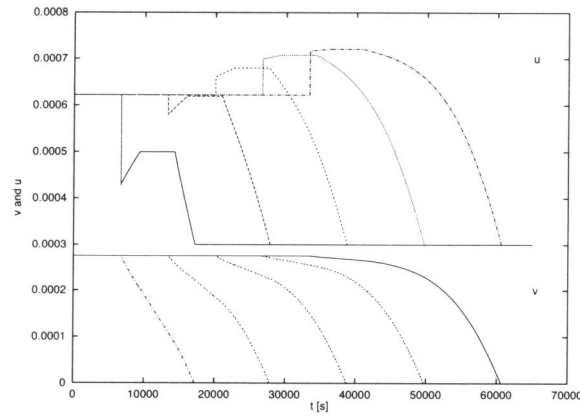
Fig 23. Breakthrough curves of u (upper curves) and time evolution of v (lower curves) at positions $x = 2, 4, 6, 8, 10$ cm for the non-linear case $n = m = 1$, $v^*, v_* > 0$.

but in detail different mechanisms. In addition, due to non-equilibrium, the dissolution front s only starts to move after a positive time t_*, with positive slope, which implies a discontinuity in $\partial u/\partial x$ at $x = q(t - t_*)$. Because of these properties the solutions are principally different from the travelling wave solutions of Part 1 for "compatible" boundary conditions and only local convergence can be expected for $t \to \infty$.
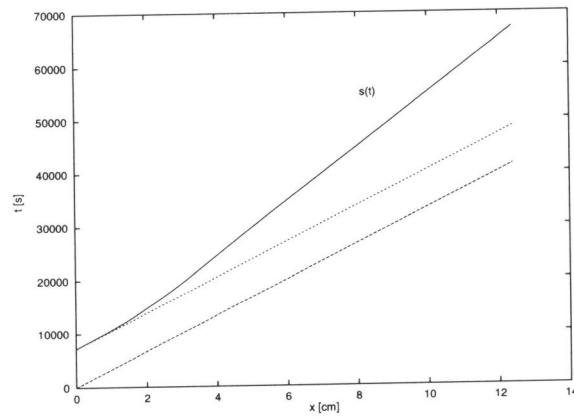
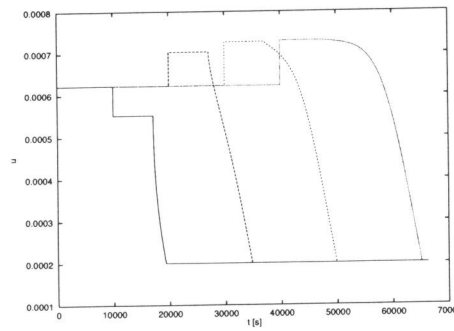Fig 24. Dissolution front in the (x,t)-plane for the case $n = m = 2$, $v^* = 0$

Fig 25. Breakthrough curves of u at $x = 3, 6, 9$ and 12 cm for the case $n = m = 2$, $v^* = 0$.
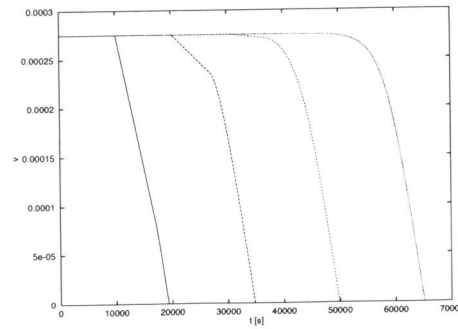

Fig 26. Time evolution of v at $x = 3, 6, 9$ and 12 cm for the case $n = m = 2$, $v^* = 0$.

Bibliography

[1] Bryant, S.L., Schechter, R.S. & Lake, L.W., Mineral Sequences in Precipitation/Dissolution Waves, *AIChE Journal* **33** (1987), pp 1271-1287.

[2] Bryant, S.L., Schechter, R.S. & Lake, L.W., Interactions of Precipitation/Dissolution Waves and Ion Exchange in Flow Through Porous Media, *AIChE Journal*, Vol **32**, No 5 (1986), pp 751-764.

[3] Dria, M.A., Bryant, L, Schechter, R.S. & Lake, L.W., Interacting Precipitation/Dissolution Waves: The Movement of Inorganic Contaminants in Groundwater, *Water Resour. Res.*, Vol **23**, No 11 (1987), pp 2076-2090.

[4] Van Duijn, C.J. & Knabner, Peter, Travelling wave behaviour of crystal dissolution in porous media flow, *Euro. Jnl of Applied Mathematics*, Vol **8** (1997), pp 49-72.

[5] Geddes, K.O., Numerical Integration in a Symbolical Context, In: B. Char (ed.), *Proceedings of SYMSAC'86*, ACM Press (1986), pp 185-191.

[6] Helfferich, F. & Klein, G., Multicomponent Chromatography, Dekker (1970).

[7] Knabner, P., Van Duijn, C.J. & Hengst, S., An analysis of crystal dissolution fronts in flows through porous media. Part 1: Compatible boundary conditions, *Advances in Water Resources*, Vol **18**, No 3 (1995), pp 171-185.

[8] LeVeque, R.J., Numerical Methods for Conservation Laws, Birkhäuser Verlag, Basel, 1992.

[9] Noval, C.F., Lake, L.W. & Schechter, R.S., Geochemical Modelling of Two-Phase Flow with Interphase Mass Transfer, —sl AIChE Journal, Vol **37**, No 11 (1991), pp 1625-1633.

[10] Novak, C.F., Schechter, R.S. & Lake, L.W., Diffusion and Solid Dissolution/Precipitation in Permeable Media, *AIChE Journal*, Vol **35**, No 7 (1989), pp 1057-1072.

[11] Schweich, D., Sardin, M. & Jauzein, M., Properties of Concentration Waves in Presence of nonlinear Sorption, Precipitation/Dissolution, and Homogeneous Reactions 1. Fundamental, *Wat. Res. Res.* **29** (1993), pp 723-733.

[12] Sevougian, S.D., Lake, L.W. & Schechter, R.S., KGEOFLOW: A New Reactive Transport Simulator for Sandstone Matrix Acidizing, Society of Petroleum Engineers, Paper (SPE 24780) Februari 1995, pp 13-19.

[13] Sevougian, S.D., Schechter, R.S. & Lake, L.W., Effect of Partial Local Equilibrium on the Propagation of Precipitation/Dissolution waves, *Ind. Eng. Chem. Res.*, Vol **32** (1993), pp 2281-2304.

179

[14] Precipitation and Dissolution of Solids Attending Flow through Porous Media, *AIChE Journal*, Vol **30** no 2 (1984), pp 317-328.

[15] Willis,C. & Rubin, J., Transport of Reacting solutes subject to a moving dissolution boundary: Numerical methods and solutions., *Water Resour. Res.* **23** (1987), pp 1561-1574.

[16] Whitham, G.B., Linear and Nonlinear Waves, Wiley, New York, 1974.

[17] Zabreyko, P.P. & Mayorova, N.L., Integral Equations-A Reference text, Noordhoff Int. Publ., Leiden, 1975.

Summary

In this thesis transport of salt in groundwater is considered. Using mathematical techniques, we study several simplified model problems in order to gain insight in both qualitative and quantitative behavior of solutions.

The thesis consists of 6 chapters: an introduction (Chapter 1) and five self-contained articles (Chapters 2 to 6). The Introduction gives an overview of the background of salt transport problems, enumerates the governing transport equations and summarizes some of the results presented in Chapters 2 to 6.

In the Chapters 2,3 and 4, we consider problems that are related to high-level radioactive waste disposal in sub-surface salt rocks or salt domes. Groundwater in the vicinity of these domes contains high salt concentrations. These high concentrations give rise to nonlinear transport phenomena such as enhanced flow due to volume (compressibility) effects and the reduction of dispersion due to gravity forces.

The enhanced flow caused by volume effects is studied in Chapters 2 and 3. The presence of high salt concentrations in groundwater leads to flow that is no longer divergence free (compressible flow). We focus on consequences of these volume effects, utilizing semi-analytical techniques: similarity transformations (Chapter 2) and a variant of the Von Mises transformation (Chapter 3). In case of the similarity transformations, the coupled set of nonlinear partial differential equations, which results from the considered model problems, reduces to a third-order ordinary differential equation. In case of the Von Mises transformation, the system reduces to a nonlinear second-order diffusion equation. Both methods yield detailed qualitative information about solutions and enable us to quantify the volume effects in an accurate and straightforward manner.

In Chapter 4 we study dispersion of salt under high concentration conditions. The stable displacement of fluids with low salt content (tracer concentrations) can be described by the fluid mass balance, the salt mass balance, Darcy's law, an equation of state and Fick's law as equation for the dispersive salt mass flux. However, if the displacing fluid has a much higher salt concentration than the resident fluid, a reduction of the salt dispersion is (experimentally) observed which cannot be modeled using linear Fick's law. An alternative nonlinear expression for the dispersive mass flux has been proposed in the hydrological literature, giving satisfactory results in both high and low concentration regimes. The combination of this nonlinear expression and the above transport equations is studied in Chapter 4 using analytical and numerical methods. Moreover, we present the results of an experimental study in order to validate the nonlinear dispersion model. The results of the mathematical analysis are used to analyze and interpret the experimental data.

Whereas in Chapters 2,3, and 4 diffusion/dispersion is considered to be one of the important salt transport mechanisms, it is disregarded in the problems studied in Chapters 5 and 6.

In Chapter 5 we consider a problem that is related to seawater intrusion in coastal aquifers. In general, the dimensions of these aquifers are large compared to the width of the diffu-

182

sive/dispersive mixing zone between the fresh and salt groundwater. This justifies the assumption of an interface between the fluids. Each fluid has a constant, but different density, which is discontinuous at the interface. In Chapter 5, we study some of the implications of an interface model numerically, using a finite element method. In particular, we are interested in the the the movement of the fresh-salt interface in heterogeneous aquifers under the action of gravity. The considered heterogeneities are discontinuities in intrinsic permeability. A front tracking method has been implemented in order to allow for non-parametrizable interfaces. Some attention is given to the implications of physically unstable situations, i.e. when fresh water is overlain by salt water.

Salt (or other chemical substances) can be present as a thin layer of crystalline (or amorphous) material on the soil particles, in general due to a precipitation reaction. When such a soil system is flushed with fresh water, the crystalline phase is going to participate in a dissolution reaction. Two fronts will emerge: the salinity or fluid front and a dissolution front, separating the region where all solid phase has been dissolved from the region where the solid is still present. In Chapter 6 we consider a binary non-equilibrium dissolution reaction in flow in a porous medium, disregarding diffusion and dispersion. In case of piecewise constant initial concentrations (in the fluid and on the soil particles), the problem leads to a Riemann problem. Using the method of characteristics, an almost explicit solution can be constructed: only a resulting Volterra integral equation for the position of the dissolution front has to be solved numerically. The advantage of this approach is that the role of the non-equilibrium reaction kinetics can be made explicit.

Chapter 2 is transcription of the article 'Brine Transport in Porous Media: Self-Similar Solutions', with L.A. Peletier (Leiden University) en C.J. van Duijn (Center for Mathematics and Computer Science (CWI)/Delft University of Technology). This paper has been accepted for publication in Advances in Water Resources.

Chapter 3 is a transcription of the article 'Brine Transport in Porous Media: On the use of Von Mises and Similarity Transformations', with C.J. van Duijn (Center for Mathematics and Computer Science (CWI)/Delft University of Technology). This paper has been submitted for publication in Computational Geosciences.

Chapter 4 is a transcription of the article 'High-Concentration-Gradient dispersion: Experiments, Analysis and Approximations, with S.M. Hassanizadeh (Delft University of Technology/National Institute of Public Health and the Environment (RIVM)) and H. Moser (Technische Universität Berlin). This paper has been submitted for publication in Water Resources Research.

Chapter 5 is a (concept) transcription of the article 'The interface between fresh-salt groundwater in heterogeneous aquifers: a numerical approach', with J.F. Scheid (CNRS Université Paris-Sud, Orsay). This article has not been submitted to a journal yet.

Chapter 6 is a transcription of the article 'An Analysis of Crystal Dissolution Fronts in Flows through Porous Media: Incompatible Boundary Conditions', with P. Knabner (Universität Erlangen) and C.J. van Duijn (Center for Mathematics and Computer Science (CWI)/Delft University of Technology). This paper has been accepted for publication in Advances in Water Resources.

Samenvatting

Dit proefschrift heeft als centraal thema het transport van zout in grondwater. Met behulp van wiskundige technieken bestuderen we een aantal vereenvoudigde modelproblemen, met als doel zowel het kwalitatieve als het kwantitatieve gedrag van oplossingen in kaart te brengen. Het proefschrift bestaat uit zes hoofdstukken: een inleiding (hoofdstuk 1) en vijf artikelen (de hoofdstukken 2 tot en met 6). De inleiding geeft een kort overzicht van de achtergrond van zouttransportproblemen in grondwater. De transportvergelijkingen worden geïntroduceerd en we bespreken de methoden en resultaten zoals die naar voren komen in de overige hoofdstukken.

De hoofdstukken 2, 3 en 4 behandelen problemen die gerelateerd zijn aan risico-analyses betreffende de opslag van hoog radio-aktief afval in ondergrondse zoutkoepels. In het grondwater dat langs deze zoutformaties stroomt worden zeer hoge zoutconcentraties aangetroffen. Deze hoge concentraties geven aanleiding tot (niet-lineaire) effecten, welke bij lage concentraties niet of nauwelijks worden waargenomen. Voorbeelden hiervan zijn stroming door volume-effecten en de reductie van zoutdispersie onder invloed van de zwaartekracht.

In de hoofdstukken 2 en 3 bestuderen we stroming ten gevolge van zogenaamde volume- of compressibiliteitseffecten. Door de aanwezigheid van grote concentratieverschillen leidt zouttransport door diffusie en dispersie tot vloeistofstroming die niet langer divergentievrij is (compressibele stroming). We bestuderen de consequenties hiervan met behulp van semi-analytische technieken: gelijkvormigheidstransformaties (hoofdstuk 2) en een variant van de Von Mises-transformatie (hoofdstuk 3). In het eerste geval wordt het stelsel gekoppelde, niet-lineaire partiële differentiaalvergelijkingen, dat voort komt uit de bestudeerde modelproblemen, gereduceerd tot een derde-orde gewone differentiaalvergelijking. In geval van de Von Mises-transformatie reduceert het stelsel tot een tweede-orde niet-lineaire diffusievergelijking. Beide methoden geven een gedetailleerd beeld van het gedrag van oplossingen en stellen ons in staat de volume-effecten nauwkeurig te kwantificeren.

In hoofdstuk 4 bestuderen we een niet-lineair model voor dispersie in geval van (zeer) hoge zoutconcentraties in grondwater. De stabiele verdringing van vloeistoffen met lage zoutconcentraties kan beschreven worden met behulp van de massabalans voor de vloeistof, de massabalans voor het zout, de wet van Darcy, een toestandsvergelijking en de wet van Fick als vergelijking voor de dispersieve massaflux. Laboratoriumexperimenten geven aan dat, indien er grote dichtheidsverschillen tussen de vloeistoffen bestaan, er een significante reductie van het dispersieve zouttransport optreedt. Dit effect is niet op een bevredigende manier te beschrijven met behulp van de bovengenoemde lineaire wet van Fick. In de literatuur is een niet-lineaire vorm voor de dispersieve massafluxvergelijking voorgesteld die wel in overeenstemming met de experimentele resultaten blijkt te zijn. De combinatie van deze niet-lineaire wet van Fick en de bovengenoemde transportvergelijkingen wordt bestudeerd in hoofdstuk 4 middels numerieke en analytische methoden. Tevens presenteren we de resultaten van uitgebreid experimenteel onderzoek die ons in staat stellen de validiteit van het niet-lineaire dispersiemodel te onderzoeken en te bevestigen. De resultaten van de wiskundige analyse zijn gebruikt bij de verwerking en interpretatie van de

184

experimentele gegevens.

De problemen die bestudeerd worden in de hoofdstukken 2,3 en 4 hebben als gemeenschappelijk kenmerk het belang van diffusie/dispersie als (zout)transportmechanisme. In de resterende hoofdstukken beschouwen we problemen waarin juist de bijdrage van dit mechanisme als verwaarloosbaar klein wordt verondersteld.

In hoofdstuk 5 bestuderen we een probleem dat gerelateerd is aan de intrusie van zout (zee)water in de watervoerende pakketten van kustgebieden. Veelal zijn de afmetingen van dergelijke pakketten groot in verhouding tot de diffusieve/dispersieve mengzone tussen het zoete water en het zeewater. Dit rechtvaardigt de aanname van een abrupte overgang in dichtheid of scheidingsvlak tussen beide vloeistoffen. De in principe mengbare vloeistoffen worden gemodelleerd als niet mengbaar. In hoofdstuk 5 geven we resultaten van een numerieke (eindige elementen) studie van een dergelijk model. In het bijzonder zijn we geïnteresseerd in de beweging van het scheidingsvlak onder invloed van de zwaartekracht in een niet-homogeen watervoerend pakket. De beschouwde heterogeniteiten zijn discontinuïteiten van de intrinsieke permeabiliteit. Een front tracking methode is geïmplementeerd om ook niet-parametriseerbare scheidingsvlakken in de tijd te kunnen volgen. Tevens wordt aandacht besteed aan het gedrag van het (numerieke) model in fysisch instabiele situaties.

Zout (of andere chemische componenten) kan ook als dun laagje kristallijn materiaal op bodemdeeltjes aanwezig zijn, bijvoorbeeld als gevolg van een precipitatie reactie. Wanneer een dergelijk bodemsysteem doorspoeld wordt met zoet water zal de kristallijne fase oplossen. Er onstaan dan twee fronten: het vloeistof (salinity) front en een (dissolution) front dat het gebied waar al het kristallijne materiaal reeds is opgelost scheidt van het gebied waar dit materiaal nog aanwezig is. In hoofdstuk 6 bestuderen we een dergelijk probleem waarbij we veronderstellen dat het zout participeert in een binaire niet-evenwichtsreaktie, onder verwaarlozing van diffusie en dispersie. In geval van stuksgewijs constante beginvoorwaarden voor de concentraties (in de vloeistof en op de bodemdeeltjes) leidt dit tot een Riemann-probleem. Met behulp van de karakteristiekenmethode kan een vrijwel expliciete oplossing geconstrueerd worden: alleen een resulterende Volterra-integraalvergelijking voor de positie van het dissolution-front moet numeriek worden opgelost. Het voordeel van deze aanpak is dat de rol van de niet-evenwichtskinetiek van de reactie op een nauwkeurige en expliciete manier tot uiting kan worden gebracht.

Hoofdstuk 2 is een transcriptie van het artikel 'Brine Transport in Porous Media: Self-Similar Solutions', met L.A. Peletier (Rijks Universiteit Leiden) en C.J. van Duijn (Centrum voor Wiskunde en Informatica/Technische Universiteit Delft). Dit artikel is geaccepteerd voor publicatie in Advances in Water Resources.

Hoofdstuk 3 is een transcriptie van het artikel 'Brine Transport in Porous Media: On the use of the Von Mises Transformation', met C.J. van Duijn (Centrum voor Wiskunde en Informatica/Technische Universiteit Delft). Dit artikel is aangeboden voor publicatie in Computational Geosciences.

Hoofdstuk 4 is een transcriptie van het artikel 'High-Concentration-Gradient dispersion: Experiments, Analysis and Approximations, met S.M. Hassanizadeh (Technische Universiteit Delft/Rijks Instituut voor Volksgezondheid en Milieuhygiëne) en H. Moser (Technische Universiteit Berlijn). Dit artikel is aangeboden voor publicatie in Water Resources Research.

Hoofdstuk 5 is de tekst van het artikel 'The interface between fresh-salt groundwater in heterogeneous aquifers: a numerical approach', met J.F. Scheid (Universiteit Paris-Sud, Orsay). Dit

artikel zal worden aangeboden ter publicatie in een nog nader te bepalen tijdschrift.

Hoofdstuk 6 is een transcriptie van het artikel 'An Analysis of Crystal Dissolution Fronts in Flows through Porous Media: Incompatible Boundary Conditions', met P. Knabner (Technische Universiteit Erlangen) en C.J. van Duijn (Centrum voor Wiskunde en Informatica/Technische Universiteit Delft). Dit artikel is geaccepteerd voor publicatie in Advances in Water Resources.

Curriculum vitae

Rudolf Johannes Schotting werd op 18 april 1957 geboren te Rotterdam. Hij behaalde in 1976 een HAVO-diploma aan de Christelijke Scholengemeenschap Melanchthon in Rotterdam-Schiebroek en vervolgde zijn opleiding aan de Hogere Technische School te Dordrecht met de studie Fysische Techniek (nu Technische Natuurkunde). In 1980 werd deze studie afgesloten met het afstudeer-werk 'Ontwerp en bouw van een N_2-laser', alwaarvoor een NIRIA 'Chemie 1980'-prijs ontvangen werd.

Van 1980 tot 1985 werkte hij bij het Laboratorium voor Grondmechanica te Delft by de afdeling Fysisch en Chemisch Onderzoek. De nadruk van zijn werkzaamheden lag op het terrein van het numeriek modelleren van grondwaterverontreinigingproblemen en het begeleiden van grondwatersaneringsprojecten voor de industrie en overheden.

Van 1985 tot 1988 was hij werkzaam als docent praktische toepassingen van de natuurkunde op de afdeling Technische Natuurkunde van de HTS te Dordrecht.

Vanaf 1988 is hij in dienst bij de Technische Universiteit Delft, Faculteit der Technische Wiskunde en Informatica, vakgroep Algemene Wiskunde. Aanvankelijk als technisch medewerker, met als taak numerieke ondersteuning van het onderzoek binnen de vakgroep en het beheer van de computerinfrastructuur. Op instigatie van prof.dr.ir. C.J. van Duijn werd hij betrokken bij het wiskundige onderzoek op het gebied van de transportverschijnselen in poreuze media. Het aandachtsgebied van de auteur bestond uit de wiskundige analyse van (grondwater)problemen waarin (grote) dichtheidsverschillen een belangrijke rol spelen. Tijdens zijn detachering van 1995 tot 1997 bij het Centrum voor Wiskunde en Informatica te Amsterdam is hij in de gelegenheid gesteld dit onderzoek af te ronden met het schrijven van dit proefschrift.

Dankwoord

Er is wel eens gezegd dat het tot standkomen van een proefschrift 10 % inspiratie vergt en 90 % transpiratie. Daar ben ik het helemaal mee eens, maar ik zou er aan willen toevoegen dat het zonder 100 % support van de omgeving ondoenlijk is. Dat ik die support heb gekregen blijkt uit het feit dat u nu mijn proefschrift in handen hebt. Ik realiseer me dat het niet mogelijk is een ieder hiervoor persoonlijk te bedanken, en daarom moet ik mij noodgedwongen beperken.

Allereerst wil ik alle leden van de vakgroep Algemene Wiskunde (AW) van de TU Delft bedanken voor de prettige, inspirerende en collegiale werkomgeving die ze mij lange tijd hebben geboden. In het bijzonder wil ik noemen Gerard van Hoorn, Jan Aarts, Philipe Clément, Juriaan Simonis en Tini van Baar. Ook ben ik de vakgroep AW en het Faculteitsbestuur van Technische Wiskunde en Informatica dankbaar voor het feit dat men mij toestond mijn onderzoek en proefschrift bij het Centrum voor Wiskunde en Informatica (CWI) te Amsterdam af te ronden.

Het was een voorrecht èn een plezier bij het CWI te mogen werken. Dankbaar heb ik gebruik gemaakt van de mogelijkheden die het CWI als professionele en goed geoliede onderzoeksorganisatie biedt. De directie van het CWI, in het bijzonder de directeur Gerard van Oortmerssen, wil ik danken voor het in mij gestelde vertrouwen. Van de collega's bij het CWI wil ik Jan Verwer, Joke Blom en Willem Hundsdorfer noemen en natuurlijk dank ik Nada Mitrovic (' Èn Ruud, nog iets meegemaakt?'.....nou reken maar!) voor het aanhoren van mijn verhalen en de vele dingen die zij voor mij gedaan heeft.

Zowel in Delft als in Amsterdam heeft Gerard de Josselin de Jong, emeritus hoogleraar Grondmechanica aan de TU Delft, mij steeds weer getoond wat het credo van het Wiskundig Genootschap 'Een Onvermoeide Arbeid Komt Alles te Boven' werkelijk betekent. Zijn inzichten zijn van fundamenteel belang voor het vakgebied gebleken en nog steeds leiden inhoudelijke discussies met hem tot prikkelende en interessante wetenschappelijke vragen. Gerard, ik dank je hartelijk voor de inspiratie die je me geboden hebt en biedt.

Joost Hulshof, Bert Peletier, Hans Bruining en Majid Hassanizadeh hebben, ieder op hun eigen wijze, bijgedragen aan mijn vorming tot wetenschappelijk onderzoeker.

Hans van Duijn is voor mij op vele gebieden van grote betekenis. Allereerst natuurlijk als promotor, want zonder zijn vertrouwen, inzet en geduld was dit proefschrift nooit gerealiseerd. Voorts als klankbord, inspirator, coördinator en nuchter referentiepunt. En als vriend. Als je wilt promoveren leer je niet alleen op wetenschappelijk gebied veel, maar je leert vooral veel over jezelf. Niemand heeft me dat zo duidelijk weten te maken als hij. Hans, je support was niet 'compact' maar wat mij betreft 'onbegrensd'!

Promoveren is geen baan van 9 tot 5, maar een zaak die zich afspeelt tussen ontbijt en het weer slapen gaan (en lange tijd alleen iets is waarover je, al dan niet onrustig, kunt dromen). Dat alles is Kitty, Sanne en David overduidelijk geworden, zeker het afgelopen jaar. Zij hebben zich heel veel ontzegd om mij de kans te geven dit tot een goed einde te brengen en nooit het vertrouwen in de goede afloop verloren. Samen staan we sterk, ik hou van jullie!

STELLINGEN

bij het proefschrift

Mathematical Aspects of Salt Transport in Porous Media

Ruud Schotting

9 februari 1998

1. Geheel ten onrechte brengen Carey et.al. de concentratieafhankelijkheid van de diffusiecoëfficient van $CuSO_4$ in verband met de reductie van NaCl-dispersie in geval van grote concentratieverschillen in een poreus medium. De metingen van Chapman tonen aan dat de diffusiecoëfficient van NaCl in water nagenoeg concentratieonafhankelijk is, en zich dus niet laat vergelijken met het gedrag van $CuSO_4$. De resultaten van de verdringingsexperimenten, zoals beschreven in Hoofdstuk 4 van dit proefschrift, waarin beide vloeistoffen een hoge zoutconcentratie bezitten maar het concentratieverschil klein is, tonen aan dat de effectieve NaCl-dispersiecoëfficient onafhankelijk is van de absolute zoutconcentratie.

   Carey, A.E., Wheatcraft,S.W., Glass, R.J. & O'Rourke, J.P., Non-Fickian ionic diffusion across high-concentration gradients, Water Resourses Research, Vol. 31, NO.9 (1995) p.p. 2213-2218.

   Chapman, T.W, Transport properties of concentrated electrolyte solutions, PhD thesis University of California (1967).

2. Aan de ontstaansgeschiedenis van de stromingsvergelijking voor zoet/zout-problemen in poreuze media zou meer recht worden gedaan indien deze wordt aangeduid als de Darcy-Lorentz[1]-vergelijking.

   Opmerkingen bij het artikel van Dr. A.H. Borgesius in "De Ingenieur" van 7 December 1912, No. 49, door Prof. Dr. H.A. Lorentz (Met afbeeldingen), De Ingenieur, No. 2 (1913), blz 24-26.

3. Voor een zoet/zout-interface $\zeta = \zeta(x,t)$ op een tijdstip $t \geq 0$ in het domein $\Omega_h = \{(x,z) : -\infty < x < +\infty, 0 < z < h\}$, kan worden aangetoond dat het bijbehorende zwaartekrachtgeïnduceerde specifieke debiet $\mathbf{q} = (q_x, q_z)$ gegeven wordt door (in complexe notatie)

$$q_x - iq_z = \frac{i\Gamma}{2h} \int_{-\infty}^{\infty} \left(\frac{e^{\tilde{x}_s + i\zeta}}{e^{\tilde{x} + i\tilde{z}} - e^{\tilde{x}_s + i\zeta}} - \frac{e^{\tilde{x}_s - i\zeta}}{e^{\tilde{x} + i\tilde{z}} - e^{\tilde{x}_s - i\zeta}} \right) \frac{\partial \zeta}{\partial x}(x_s) dx_s, \qquad (1)$$

   waarin $\tilde{x} = \pi x/h$, $\tilde{z} = \pi z/h$, etc., en waarin Γ een constante is die lineair afhangt van het dichtheidsverschil tussen het zoete en zoute grondwater. Een bewegingsvergelijking voor het interface volgt uit de massabalans voor het zoute water

$$n\frac{\partial \zeta}{\partial t} + \frac{\partial Q}{\partial x} = 0 \text{ met } Q = \int_0^{\zeta(x,t)} q_x \, dz, \qquad (2)$$

---

[1] Hendrik Antoon Lorentz (1853-1928), Nederlands theoretisch-fysicus en Nobel-prijswinnaar, die ondermeer een belangrijke rol heeft gespeeld bij de formulering van de speciale relativiteitstheorie.

waarin Q het zout-waterdebiet is, n de porositeit en q_x gegeven wordt door het reële deel van (1). Met behulp van partiële integratie van (1) en na substitutie van het resultaat in (2) kan worden aangetoond dat de bewegingsvergelijking te schrijven is in de vorm van de integro-differentiaalvergelijking

$$n\frac{\partial \zeta}{\partial t} = \frac{\Gamma}{h}\frac{\partial}{\partial x}\left\{\zeta(h-\zeta)\frac{\partial\zeta/\partial x}{1+(\partial\zeta/\partial x)^2}\right\} + \frac{\partial}{\partial x}\left\{\int_0^{\zeta(x,t)} B(x,t,\zeta)\,dz\right\}, \qquad (3)$$

waarin $B(x,t,\zeta)$ een combinatie van integralen langs de $x-$as ($-\infty < x < +\infty$) voorstelt. Voor voldoende vlakke interfaces kan de niet-lokale integraalterm worden verwaarloosd en reduceert (3) tot de Dupuit-bewegingsvergelijking voor een zoet/zout-interface, welke ook op basis van simpele fysische principes kan worden afgeleid. Dit verklaart het feit dat de Dupuit-vergelijking in veel praktische gevallen een goede benadering geeft van het exacte interfaceprobleem.

4. Indien we uitgaan van de door De Josselin de Jong afgeleide (fysisch correcte) uitdrukking

$$n\frac{\partial\zeta}{\partial t} = \frac{q_n^i}{\cos\alpha} = q_z^i - \frac{\partial\zeta}{\partial x}q_x^i, \qquad (4)$$

waarin $i =$ zoet, zout, $\alpha = \arctan(\partial\zeta/\partial x)$ en q_n^i de normaalcomponent van de discharge aan het interface, dan leidt de combinatie van (1) (na partiële integratie) en (4) tot de alternatieve integro-differentiaalvergelijking

$$n\frac{\partial\zeta}{\partial t} = \frac{\Gamma}{h}(h-2\zeta)\frac{(\partial\zeta/\partial x)^2}{1+(\partial\zeta/\partial x)^2} + A(x,t,\zeta). \qquad (5)$$

Hierin is $A(x,t,\zeta)$ weer een combinatie van integralen langs de x-as ($-\infty < x < +\infty$). Gegeven een initieel interface $\zeta(x,0) = \zeta_0(x)$ in Ω_h dan zijn oplossingen van (3) en (5) voor elke $t > 0$ identiek. Verwaarlozen we echter de niet-locale term dan reduceert (5) tot het eerste-orde deel van de Dupuit-bewegingsvergelijking. Deze eerste-orde vergelijking heeft als benadering slechts in zeer uitzonderlijke gevallen fysische betekenis. Daarom is, als uitgangspunt voor de afleiding van de bewegingsvergelijking, (2) te prefereren boven (4).

De Josselin de Jong, G., *The simultaneous flow of fresh and salt water in aquifers of large horizontal extension determined by shear flow and vor tex theory*, Proceedings Euromech. 143 (1981) (eds. A. Verruijt & F.B.J. Barends), Balkema Rotterdam, p.p. 132-149.

5. Benaderen we een interface $\zeta = \zeta(x,t)$ in Ω_h ($t \geq 0$) door middel van een stuksgewijs lineaire functie, dan leidt (5), in tegenstelling tot (3), tot een eenvoudig, doch effectief numeriek algoritme.

6. In geval van een lineair zoet/zout interface $\zeta = \zeta(x,t)$, met helling $p \geq 0$ in domein Ω_1, wordt de $x-$component van het specifieke debiet aan de zoet waterzijde van het interface gegeven door

$$q_{x_{\text{zoet}}} = \Gamma\zeta\frac{p}{1+p^2} + \frac{\Gamma}{2\pi}\ln\left(\frac{1-2e^{-\frac{\pi}{p}\zeta}\cos(\pi\zeta)+e^{-2\frac{\pi}{p}\zeta}}{1+2e^{\frac{\pi}{p}(\zeta-1)}\cos(\pi\zeta)+e^{2\frac{\pi}{p}(\zeta-1)}}\right). \qquad (6)$$

2

De limieten $\zeta \downarrow 0$ en $\zeta \uparrow 1$ van (6) leveren singuliere waarden van $q_{x_{zoet}}$ op, hetgeen een oneindige voortplantingssnelheid van het interface aan de domeinranden impliceert. Dit gedrag wordt niet waargenomen (zelfs niet in benadering) in de resultaten van eindige elementenberekeningen zoals omschreven in Hoofdstuk 5 van dit proefschrift. Dit is te verklaren uit het logaritmisch-singuliere karakter van de bovengenoemde limieten en het feit dat in de eindige elementenbenadering de discharge een stuksgewijs constante grootheid is.

7. De objectiviteit van het beoordelingsproces van wetenschappelijke artikelen kan worden verhoogd, indien editors van tijdschriften ingediende artikelen geanonimiseerd doorzenden aan de beoordelaars.

8. Als het van de Inquisitie of van Calvijn had afgehangen, zou er nu niet zo brandend om grensverleggend wetenschappelijk onderzoek worden geroepen, want het denken - of wat daarvoor doorging - zou voor eens en altijd binnen bijbelse grenzen zijn gebleven.
   Citaat van W.F. Hermans in 'Houten leeuwen en leeuwen van goud', Uitgeverij De Bezige Bij (1979)).

9. Zonder daadwerkelijke compassie voor de patiëntjes en belangstelling voor hun stoornissen zal de kinderpsychiatrie als relatief jonge wetenschap het stadium van de kinderschoenen nooit kunnen ontgroeien.

10. Het wetenschappelijke bewijsmateriaal van de werkzaamheid van homeopathische geneesmiddelen is even sterk als de bij de bereiding van deze middelen gebruikelijke verdunningen.

11. De bijdrage van vrijwilligerswerk aan de samenleving is niet in geld uit te drukken.

12. Verzekeringsmaatschappijen zijn te vergelijken met zwangere vrouwen: ze ontvangen in liefde, maar baren in pijn.
    Naar een uitspraak van mijn vader Ph. Schotting.